11-5-2004

Using Multiwavelength UV-Visible Spectroscopy for the Characterization of Red Blood Cells: An Investigation of Hypochromism

Akihisa Nonoyama
University of South Florida

Using Multiwavelength UV-Visible Spectroscopy for the Characterization of Red Blood Cells: An Investigation of Hypochromism

by

Akihisa Nonoyama

A dissertation submitted in partial fulfillment
of the requirements for the degree of
Doctor of Philosophy
Department of Chemistry
College of Arts and Sciences
University of South Florida

Co-Major Professor: Robert L. Potter, Ph.D.
Co-Major Professor: Luis H. Garcia-Rubio, Ph.D.
German F. Leparc, M.D.
Li-June Ming, Ph.D.

Date of Approval:
November 5, 2004

Keywords: multiwavelength UV-visible spectrophotometry, hypochromism, light scattering, Mie theory, red blood cell, hemoglobin

Dedication

This dissertation is dedicated to all of my family members who have supported me throughout my life and allowed me to achieve my goals: to my late father Meihan, who helped in making my educational decisions and sent me on the path to my graduate career; to my aunt, Michiko, for providing me with financial and moral support throughout my stay in graduate school; to my mother Keiko for raising me into an honest person and for providing financial and moral support; to my wife Tina for her encouragement and support since we met in 1994; to my son Jacob who gave me a more of a reason to succeed at my endeavors; and to any future child…I just don't know who you are yet.

Acknowledgements

I would like to acknowledge the guidance and support of my co-major professors, Dr. Robert L. Potter and Dr. Luis H. Garcia-Rubio. I would also like to thank Dr. German F. Leparc, Chief Medical Officer of the Florida Blood Services, for his invaluable advice in hematology and for providing us with samples and laboratory space without which this research would not have been possible. Additionally, I want to thank everyone that has offered help or encouragement in the laboratories of Dr. Potter and Dr. Garcia-Rubio. Finally, I thank University of South Florida and the Department of Chemistry for providing me with the opportunity to achieve my goal.

Table of Contents

List of Tables

List of Figures

List of Abbreviations

UV-vis	ultraviolet-visible
RBC	red blood cells
WBC	white blood cells
Hb	hemoglobin
HCT	hematocrit
HGB	total hemoglobin concentration
MCV	mean corpuscular volume
MCH	mean corpuscular hemoglobin
MCHC	mean corpuscular hemoglobin concentration
RDW	red cell distribution width
PLT	platelet
MPV	mean platelet volume
PBS	phosphate buffered saline
RPM	revolutions per minute
EDTA	ethylenediamine tetra-acetic acid
OD	optical density
HSA	human serum albumin
BSA	bovine serum albumin

2,3-BPG	2,3-bisphosphoglycerate
PSD	particle size distribution
RBD	Rayleigh-Gans-Debye
LR	leukocyte reduced
DTS	diffuse transmission spectrum
SATS	small angle transmission spectrum

List of Symbols

$A(\lambda)$	absorption at a given wavelength
$\varepsilon(\lambda)$	Beer's law extinction coefficient at a given wavelength
λ	wavelength
I_0	intensity of the incident light
I_t	intensity of the transmitted light
$m(\lambda)$	complex refractive index
$n(\lambda)$	refractive index
$\kappa(\lambda)$	absorption coefficient
τ	turbidity
N_p	number of particles
D	particle diameter
$f(D)$	particle size distribution
$Q_{ext}(\alpha,m(\lambda))$	Mie efficiency coefficient
α	size parameter
ε	approximation of errors
H	covariance matrix
γ	regularization parameter

Using Multiwavelength UV-Visible Spectroscopy for the Characterization of Red Blood Cells: An Investigation of Hypochromism

Akihisa Nonoyama

ABSTRACT

Particle analysis using multiwavelength UV-visible spectroscopy provides the potential for extracting quantitative red blood cell information, such as hemoglobin concentration, cell size, and cell count. However, if there is a significant presence of hypochromism as a result of the concentrated hemoglobin (physiological value of 33%), successful quantification of red cell values would require a correction.

Hypochromism has been traditionally defined as a decrease in absorption relative to the values expected from the Beer-Lambert Law due to electronic interactions of chromophores residing in close proximity of one another. This phenomenon has been suggested to be present in macroscopic systems composed of strong chromophores such as nucleic acids, chlorophyll, and hemoglobin. The study presented in this dissertation examines the presence of hypochromism in red blood cells as a part of a larger goal to qualitatively and quantatively characterize red blood cells using multiwavelength UV-visible spectroscopy.

The strategy of the study was three-fold: 1) to determine the instrumental configuration that would provide the most complete information in the acquired spectra,

2) to develop an experimental model system in which the hemoglobin content in red blood cells could be modified to various concentrations, and 3) to implement an interpretation model based on light scattering theory (which accounts for both the scattering and absorption components of the optical density spectrum) to provide quantitative information for the experimental system. By this process, hypochromicity was redefined into two categories with *molecular hypochromicity* representing the traditional definition and *macroscopic hypochromicity* being an attenuation of the absorption component due to a scattering-related effect. Successful simulations of experimental red cell spectra containing various amounts of hemoglobin were obtained using the theoretical model. Furthermore, successful quantitative interpretation of the red blood cell spectra was achieved in the context of corpuscular hemoglobin concentration, corpuscular volume, and cell count solely by accounting for the scattering and absorption effects of the particle, indicating that molecular hypochromicity was insignificant in this macroscopic system.

Chapter 1: Introduction

Multiwavelength ultraviolet-visible (UV-vis) spectrophotometry is a powerful tool for the characterization of particles in suspension. With the acquisition of one spectrum, it is possible to obtain information on parameters such as particle count, size, shape, and chemical composition.[1,2] Application of this technology coupled with spectral interpretation using the theory of light scattering allows for the analysis of particles in a large range of sizes (10^{-9} – 10^{-6} m). The method proves particularly useful in the examination of micron-sized particles due to their significant scattering properties, especially if they exhibit a high optical contrast (high refractive index) in relation to the background medium. For such particles, light scattering theory provides the means to interpret the combined scattering and absorption components of the spectrum to extract a wealth of information about the suspension system. Furthermore, the opportunity to examine the spectrum over a large wavelength range (190 – 1100 nm) allows for redundant analysis through mathematical corroboration of all wavelengths, providing a high level of reliability of the elucidated values.

1.1 Blood

The capabilities of multiwavelength UV-visible spectrophotometry offers the potential for the characterization of whole blood. Whole blood is a complex system with

the major components being red blood cells (RBC, or erythrocytes), white blood cells (WBC, or leukocytes), platelets, and plasma, each making a contribution to the whole blood spectrum (Figure 1.1). Each individual component exhibits unique spectral features based on their physical characteristics that impact their optical behavior. The combination of important parameters (size, shape, chemical composition) that influence the cumulative spectral attributes of the particle is referred to as the joint property distribution (JPD).[3,4]

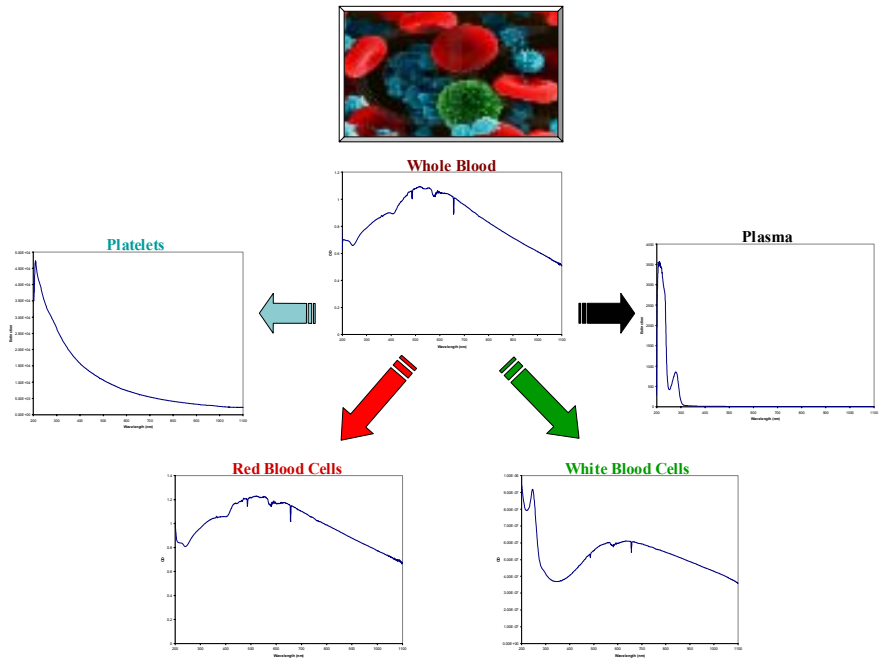

Figure 1.1: Blood components and their spectral contributions to the whole blood spectrum. The spectrum of each major component (red blood cells, platelets, plasma, and white blood cells) is unique to their individual physical properties such as size and chemical composition.

The objective of the study reported in this dissertation is to obtain a multiwavelength characterization of red blood cells. In whole blood, red cells dominate in number and in its contribution to the overall spectrum; hence it is important to achieve an accurate spectral depiction of the red cells as a necessary step to obtaining information on the other major components of whole blood such as white blood cells, platelets, and plasma. In the context of spectral analysis, the red cell suspension can be broken down into three pathlengths, each of which offers different levels of particle information as indicated in Figure 1.2. Each pathlength denotes a different type of hypochromism, with *observed hypochromism* representing the most general definition: a decrease in the optical density (and extinction coefficient) as a result of the increase in concentration of a strong chromophore relative to the value expected by the Beer-Lambert Law.[5] *Macroscopic hypochromism* is a type of observed hypochromism where a decrease in the optical density (relative to Beer-Lambert) is seen due to the combined effects of absorption and scattering of chromophores in aggregated and encapsulated systems. Moreover, *molecular hypochromism* is another category of observed hypochromism where molecular charge interaction among closely packed chromophores causes a decrease in the absorption spectrum.[5] Since red blood cells contain a highly absorbing species, hemoglobin, it is necessary to account for the possibility of hypochromicity to attain a qualitative optical characterization of RBCs. The study clearly establishes two subcategories of hypochromism and identifies the level of significance of each to the spectral analysis of red cells.

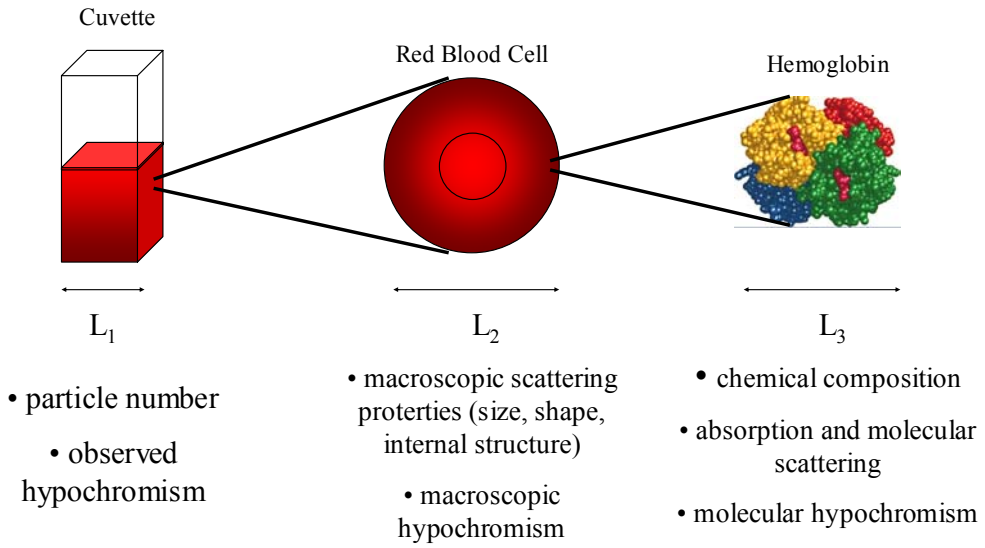

Figure 1.2: Three important pathlengths to consider in the spectral analysis of red cells. Each pathlength accounts for a different set of information reflected in the spectrum of the suspension.

The issue of hypochromism was addressed by closely examining two paradigms: measurement variables including instrumental configuration and the combined effect of the scattering and absorption components on the red cell spectrum. The instrumental configuration of the optical arrangement of commercially available spectrophotometers may reflect differences in the design of the optics, particularly in the angle of acceptance, which can result in different spectral features that can mislead the interpretation of the optical density spectrum. Some studies that have disregarded the importance of the detection angle on the spectrum have attempted to explain the observed hypochromism in ways other than to consider the instrumental configuration.[6,7]

The second method of investigating hypochromism in red cells was to examine the absorption and scattering components of the red cell spectrum in an effort to interpret the spectrum using the theory of light scattering. To this end, any hypochromic effect present in the spectrum would have to be accounted for to achieve a good interpretation of the particle parameters (eg. size, number and chemical composition). The investigation was extended beyond physiological red cell values by developing a protocol to modify the hemoglobin composition. A procedure using hypotonic shock (with varying incubation times) was developed to control the final cellular hemoglobin concentration. Observing cells with varying hemoglobin content allowed for the inspection of spectral features and trends in relation to their changing optical characteristics.

1.2 Theoretical Modeling

Theoretical modeling and interpretation of the red cells were performed using the Mie theory, which provides analysis for spherical particles.[8] This approach has already proven successful in offering good spectral interpretation for particle systems such as polymers,[1] molecular aggregates,[2] platelets,[9] and microorganisms.[10] In the case of the red cells, the capabilities of the Mie theory were extended to obtain good values for RBC number, size, and hemoglobin concentration. The success of this interpretation model helped to identify the two categories of hypochromism and their influence, if any, on the transmission spectrum of purified and modified red blood cells.

Chapter 2: Whole Blood, Red Blood Cells and Hemoglobin

2.1 Whole Blood

Whole blood is a complex system of regenerating cells and physiologically essential molecules which work to sustain life in various ways. It is responsible for transporting nutrition, oxygenating tissues, removing waste products, controlling body temperature, and maintaining hemostasis.[11,12] Whole blood is composed of four major components: plasma, thrombocytes (platelets), leukocytes (white blood cells), and erythrocytes (red blood cells). It has a viscosity approximately 1.5 times that of water, maintains a specific gravity of 1.050 – 1.060, and has a physiologic pH of 7.35 – 7.45.[12] The cell-to-plasma ratio is on the order of 45%:55% and a normal adult sustains 70 – 75 milliliters of blood per kilogram of body weight, which constitutes 7 – 8% of total body weight.[11]

The components of blood have been well characterized and baseline normal values have been established for each constituent (Table 2.1). Such accepted values are typically represented as ranges or statistical averages due to the fact that the physiological abundances of cells and proteins vary according to age, sex, race, geographic locations, and pathologies. Typically, 95% of all normal individuals fall within $\pm$ 2 standard

deviations of the reported reference values, with only the remaining 5% normal individuals being outside of this range.[11]

Blood Component	Size (μm)	Volume (fl)	Count (number/μl)	Role
Erythrocytes	7 – 8	80 – 100	Male: 4.7 - 6.1x10^6 Female: 4.2 - 5.4x10^6	O_2 and CO_2 transport
Leukocytes			4 – 11x10^3	
Granulocytes				
Neutrophils	10 – 15	--	4,420	Phagocytose small organisms
Basophils	10 – 15	--	40	Mediate inflammatory events
Eosinophils	10 – 15	--	200	Allergic inflammatory response
Monocytes	15 – 22	--	300	Phagocytose organisms
Lymphocytes	10	--	2,500	Cellular and humoral immunity
Thrombocytes	1 – 2	7.4 - 10.4	1.5 - 4.5x10^5	Maintain hemostasis
Plasma	--	--	--	Fluid medium in blood

Table 2.1:[11,13,14,15,16,17] Normal values of major blood components.

Leukocytes

Leukocytes, or white blood cells (WBC) contribute only about one percent of the total blood volume, yet plays an important role in defense against infections and phagocytosis of cell debris.[11,13] Leukocytes are classified under two major categories: granulocytes and mononuclear cells (non-granulated cells). As the name implies, the granulocytes exhibit a granular cytoplasm when stained and can be further organized into three subcategories: neutrophils, eosinophils, and basophils. The mononuclear cells include lymphocytes and monocytes.[12] The abundance of each leukocyte type in a healthy individual is illustrated in Table 2.2.

Leukocyte Type	Percent Abundance
Neutrophil	62.0%
Eosinophil	2.3%
Basophil	0.4%
Lymphocyte	30.0%
Monocyte	5.3%

Table 2.2:[12] Percent abundances of leukocyte sub-types.

Among the granulocytes, neutrophils are the primary line of defense owing to their functional characteristics and large nucleus. They will destroy foreign agents mainly by means of phagocytosis, and are a major contributor to inflammatory responses. Neutrophils are approximately 10 to 14 μm in diameter and contain a lobulated nucleus (two to five lobes) with condensed chromatin. The cytoplasm contains granules of sizes ranging from 200 to 500 nm. These granules are classified as peroxidase-positive and peroxidase-negative, with the latter typically being smaller in size (~ 200 nm diameter). An electron micrograph will show on the average, 200 to 300 granules, with approximately one third being peroxidase-positive granules (Figure 2.1).[14]

Eosinophils, which are the second most abundant of the granulocytes, have the capacity to secrete toxic granules to help eradicate invading cells. They also aid in digesting old clots. Eosinophils are usually slightly larger than neutrophils and contain a nucleus with two lobes. The granules in the cytoplasm are larger than those in the

neutrophils and are more uniform in size. Moreover, the granules contain crystalline structures that are readily seen in the electron microscope picture in Figure 2.2.

Basophils, normally low in concentration, increase in number during the healing phase of an inflammation. Furthermore, they release histamine, heparin, bradykinin and serotonin to help mediate the inflammatory response.[12] The size of the basophils are slightly smaller than the neutrophils. The nucleus is larger than those of the other granulocytes, and typically are not as segmented as they are in neutrophils. They contain large granules that are less uniform in size compared to those of the eosinophils (Figure 2.3).[14]

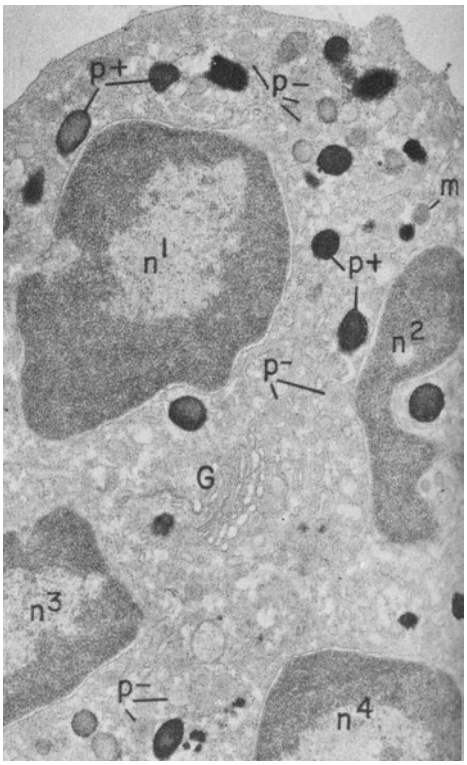

Figure 2.1:[14] An electron microscopy picture of a mature neutrophil using peroxidase staining. The picture shows multiple lobes of nuclei (n), peroxidase-positive granules (p+), and peroxidase-negative granules (p-).

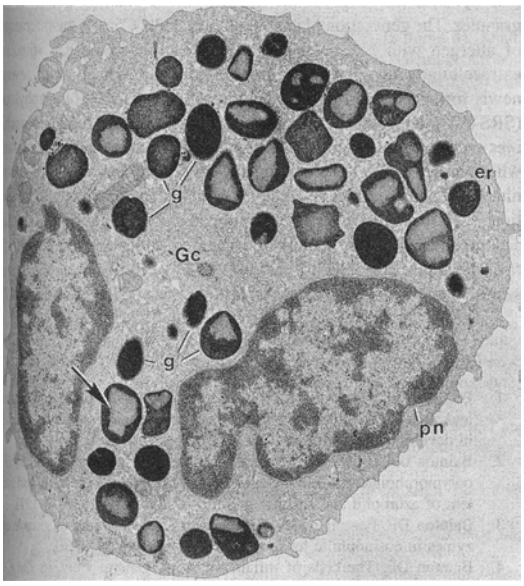

Figure 2.2:[14] An electron microscopy picture of an eosinophil using peroxidase staining. The nuclei has two lobes, and the granules (g) contains crystalline structures (arrow).

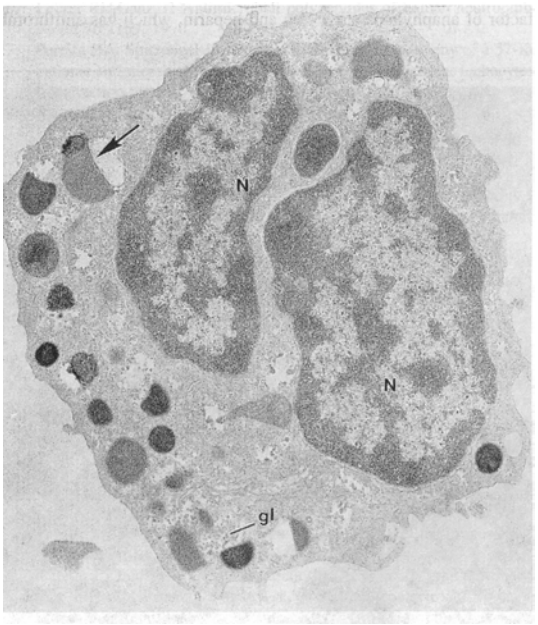

Figure 2.3:[14] An electron microscopy picture of a basophil using peroxidase staining. The granules stain lightly and are irregular in size.

Lymphocytes compose the major non-granulocyte component with a lifespan of 100-300 days and are differentiated into three types: B-lymphocytes, T-lymphocytes and natural killer (NK) cells. All are principal contributors to the immune response. The B-lymphocyte recognizes antigens that cause the cells to proliferate and release large amounts of immunoglobulins (antibodies). The T-lymphocytes aids in B-lymphocyte function as well as exhibiting cytotoxic effects such as lysing virus-infected cells.[12,13] Upon activation, T-cells (T-lymphocytes) can proliferate into one of four types of cells: memory T-cells (memory for previously encountered antigens), helper T-cells (help enhance the activities of lymphocytes and phagocytes and stimulate proliferation and maturation of B-cells), suppressor T-cells (suppress over-activity of lymphocytes and phagocytes), and cytotoxic T-cells (kill cells targeted by specific antigen).[12] The NK cells provide immunity against infectious agents and transformed cells. Morphologically,

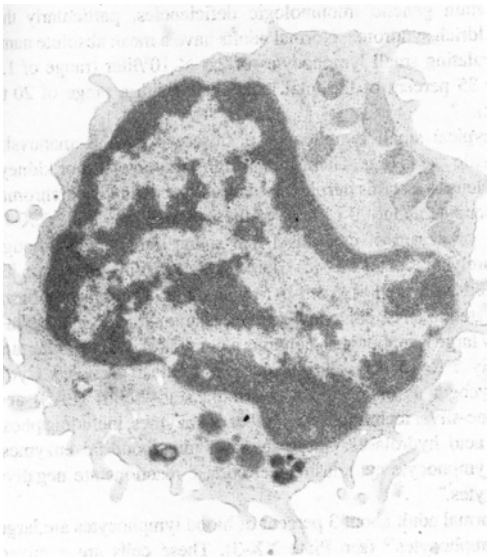

Figure 2.4:[14] An electron microscopy picture of a lymphocyte. The nucleus dominates the cellular space.

the three types of lymphocytes share similarities, with sizes ranging from 6 to 15 μm (Figure 2.4). The nucleus is round or kidney-shaped ad occupies ~ 90% of the cell.[14]

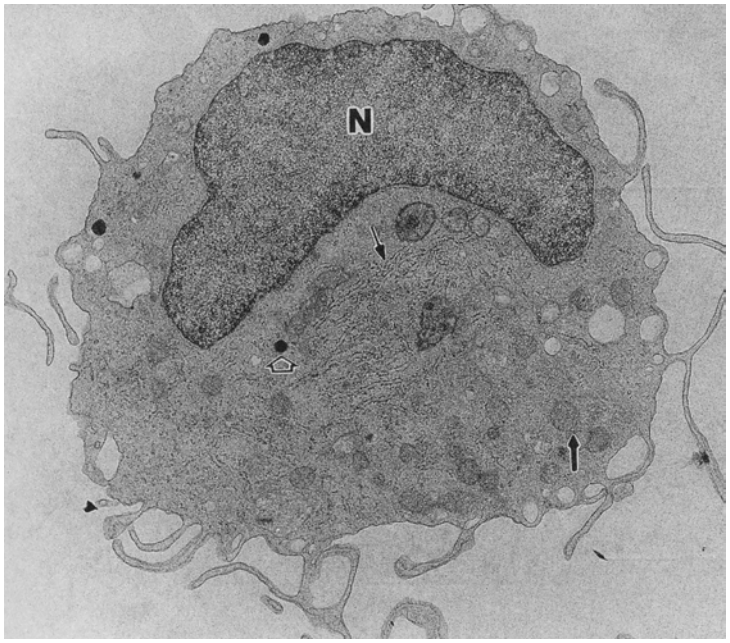

Figure 2.5:[14] An electron microscopy picture of a monocyte. It contains a relatively large nucleus (N) along with visible organelles such as the ER (thin arrow), mitochondria (thick arrow), and lysosomes (empty arrow).

Monocytes (Figure 2.5) constitute two to eight percent of whole blood cells and are released from the marrow as immature cells. Once in tissues, they differentiate into the larger macrophages to fight infections and remove debris from blood through phagocytosis. They are more resilient than neutrophils and they can also endocytose larger particles.[12] In terms of size, the monocytes large blood cells with diameters ranging from 12 to 15 μm. The shapes of the nucleus vary form round to oval and lobulated. The cytoplasm contains frequently vacuolated granules (~ 50 to 200 nm).

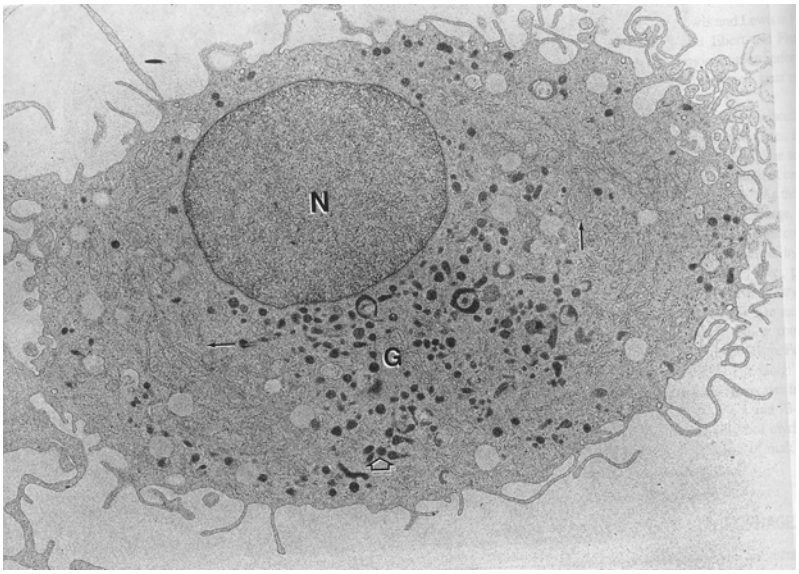

Figure 2.6:[14] An electron microscopy picture of macrophage. Internal contents include the nucleus (N), ER (thin arrow), Golgi zone (G), mitochondria (thick arrow), and lysosomes (empty arrow).

Monocytes will differentiate into macrophages in tissue, an event characterized by an increase in cellular size up to 22 μm accompanied by an increase in the granules (Figure 2.6).[14]

Thrombocytes

Thrombocytes, or platelets, are derived from megakaryocytes in the bone marrow and play a crucial role in maintaining hemostasis. Mature megakaryocytes are released from the marrow and subsequently fragment into platelets, which survive in the vasculature for approximately ten days.[12,14] Through receptor-mediated signaling, platelets converge at the site of vascular injury and activate, allowing for aggregation, which is part of the clotting process. Furthermore, they will release granules and

cytoplasmic contents containing essential hemostatic components such as clotting factors and serotonin which promote the clotting cascade.[14]

Erythrocytes

Erythrocytes (red blood cells – RBC) are biconcave discoid cells containing the protein hemoglobin. Its primary function is to transport molecular oxygen (O_2) from the lungs to the tissues and to carry carbon dioxide (CO_2) from the tissues to the lungs. The composition and functions of RBCs will be discussed in detail in section 2.2.

Plasma

Plasma is the liquid medium of whole blood through which the blood cells are circulated. While the cells make up approximately 45% of the volume of blood, plasma constitutes the complementary 55%. It is primarily composed of water and it accounts for roughly six liters of blood in a normal human body.[11] Aside from the cells, plasma also contains a multitude of proteins, ions, lipids, and carbohydrates, many of which are responsible for maintaining the integrity of the vascular system. Some major proteins include albumin, γ-globulins, and fibrinogen, with albumin being the most abundant. Important ions include H^+, Na^+, K^+, Mg^{2+}, Ca^{2+}, and Cl^-.[11,18,19]

The plasma-enabled fluidity of whole blood helps the heart deliver essential biological components to all body tissues with great efficiency. It allows for the body to maintain hemostasis, protect against infections, deliver oxygen to tissues, transport lipids via water soluble proteins, and remove catabolites, among other functions.[14] This

intricate network of components is maintained in a delicate balance of functions in the vascular system of a healthy individual. Advances in clinical and research-oriented diagnoses have helped to identify the numerous abnormalities currently seen in whole blood.

Serum Albumin

Human serum albumin (HSA) is the most abundant protein in plasma at a concentration of 42 g/L and serves several important biological functions within the vascular system.[20] Synthesized predominantly in the liver, HSA exhibits dimensions of 134 x 41 angstroms and has a molecular weight of 66,439 da. At physiological pH, the protein displays a net charge of approximately -17 and is composed of 585 amino acid residues.[20,21]

Albumin possesses the unique capacity to bind numerous endogenous and exogenous compounds, making it a vital transport protein. It binds mainly water insoluble substances, such as lipids and also potentially toxic compounds such as bilirubin, giving its transport mechanism a multi-purpose role.[20, 22] Its abundance also provides the vasculature with 80% of the osmotic pressure needed to maintain the integrity of cell structure in whole blood.

Human serum albumin is composed of the following chromophoric amino acid residues: 1 tryptophan, 1 cysteine, 17 cystines (disulfide bridges), 18 tyrosines, and 31 phenylalanines.[20] The structure consists of a series of three identical domains with each of the domains connected to each other by a hinge region and a disulfide bond. Each

domain is predominantly characterized by helices and the three domains are arranged in a trough-like tertiary structure. Bovine serum albumin has a slightly smaller number of amino acids with 583 and possesses a molecular weight of 66,267 da. It is structurally similar to the human isoform, and chromophoric residues include 19 tyrosines, 26 phenylalanines, 18 cystines and 2 tryptophans.[20,23]

Albumin is an extensively studied molecule which has been well characterized in many different aspects and it has proven to be a useful model molecule in our research (See Appendices C and H). Our studies revolve around UV-visible spectroscopy and albumin has been analyzed in terms of its optical behavior based on its size and chemical composition.[24]

2.2 The Erythrocyte

Erythrocytes, or red blood cells (RBC), are dark red, flexible, biconcave cells that carry O_2 and CO_2 to and from tissues respectively.[14] In the early 1800's, Francois Magendie did not heed colleague William Hewson's recommendation to dilute blood in

Component	Concentration (mg/ml)
Total protein	371.0
Hemoglobin	361.8
Non-hemoglobin protein	9.2
Insoluble stroma protein	6.3
Protein from enzymes	2.9

Table 2.3:[14] Protein content of human erythrocytes

serum when studying them. He instead used water, and through his microscopy studies, reported that red blood cells were air bubbles.[25] Since then, scientific knowledge of erythrocytes has soared as a result of advances in research technology.

Red blood cells generally exhibit a diameter of approximately 7.5 – 8.7 μm, (Figure 2.1) and are found at a concentration of 5 x 10^6 cells per microliter of blood.[13,14] They owe their deep red color to the presence of the iron-containing molecule hemoglobin (33% m/v).[14] In fact, roughly 97% of all total protein in erythrocytes is hemoglobin, as illustrated in Table 2.3. That is, approximately 95% of the total cell weight can be attributed to the chromophoric molecule.[12] Furthermore, mature human erythrocytes lack a nucleus and mitochondria and exhibit minimal metabolism yet maintain their existence for an average of 100-120 days.[14,26]

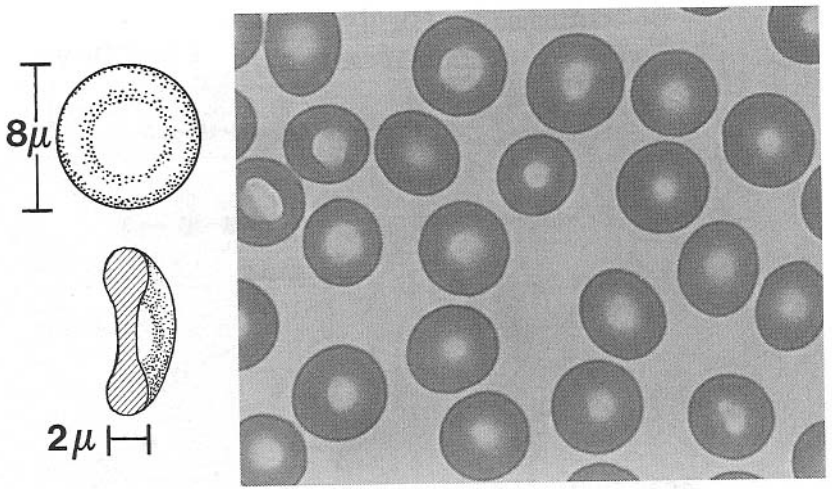

Figure 2.7:[26] A cartoon and micrograph representations of the erythrocyte.

The biconcave discoid has a thickness of approximately 2 μm (Figure 2.7), a surface area of 136 μm^2, and a volume of ~90 fl.[26] Its flat shape keeps the hemoglobin molecules closer to the membrane which allows for a more efficient transfer of oxygen. The resourceful functionality of the cell is attributed to the composition of the membrane and the underlying cytoskeleton.

The Erythrocyte Membrane and Cytoskeleton

The membrane of the red blood cell is a phospholipid bilayer (75 angstroms in thickness) in which the non-polar, hydrophobic tails orient to form the internal region of the membrane, while the polar, hydrophilic heads of the phospholipids face out into the aqueous plase.[26,27] The density of the membrane alone is reported to be 1.15 g/cm^3.[27] The contents of the red cell membrane can be broken down by mass into the following: 52% protein, 40% lipid and 8% carbohydrate.[27]

The major types phospholipids present in the membrane include phosphatidylcholine (28% of total phospholipids), phosphatidylserine (13%), phosphatidylethanolamine (27%), and sphingomyelin (26%).[14] Known generally as glycerophospholipids or phosphoglycerides, phosphatidylcholine, phosphatidylserine, and phosphatidylethanolamine are derivatives of glycerol-3-phosphate, with the R_1 and R_2 groups being fatty acids which are associated with the first two carbons of the 3-carbon backbone via an ester linkage (Figure 2.8). The R_1 group typically represents C_{16} and C_{18} fatty acids while R_2 is often C_{16}-C_{20} unsaturated fatty acids.[28] The third carbon is linked

to the R_3 group by a phosphodiester bond with the variations of R_3 defining the type of phosphoglyceride (Figure 2.9).

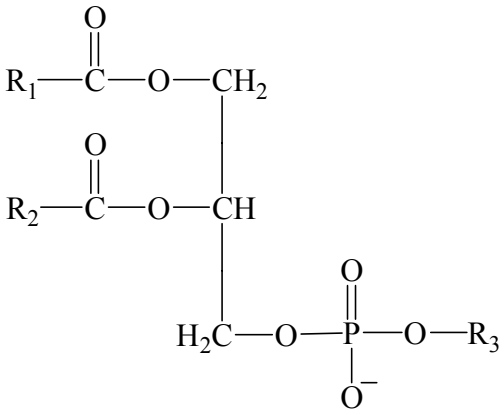

Figure 2.8: The general chemical structure of a phosphoglyceride. R_1 and R_2 represent hydrophobic fatty acid chains and R_3 defines the specific type of phospholipid.

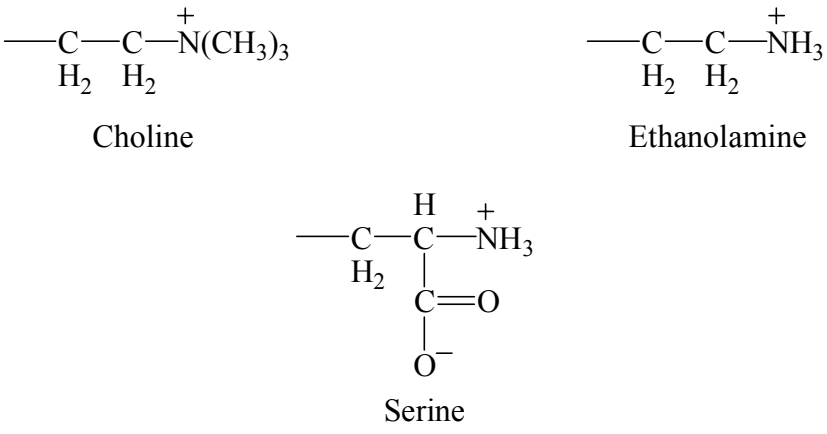

Figure 2.9: R_3 groups for major types of phosphoglycerides: phosphatidylcholine, phosphatidylethanolomine, and phosphatidylserine.

Sphingomyelin is derived from a long chain amino alcohol sphingosine and is classified as a sphingolipid. The derivative contains a ceramide group which is characterized by a fatty acid linked to the second carbon by an amide bond. The head carbon is attached to a phosphocholine (Figure 2.10).

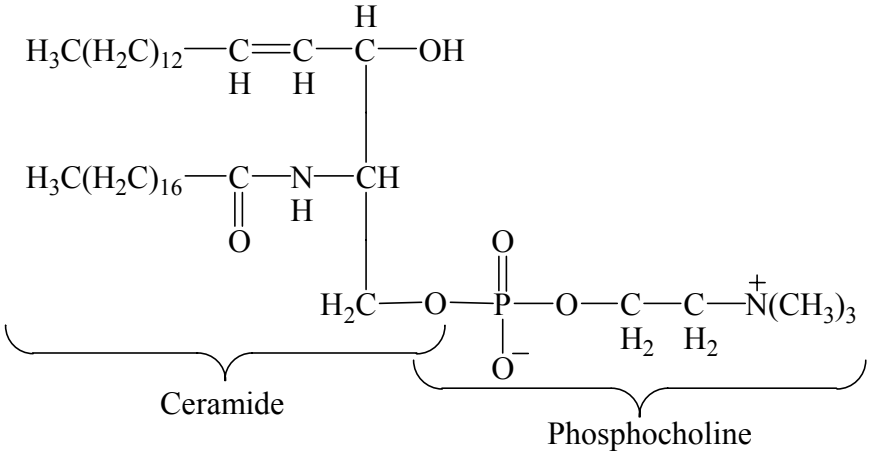

Figure 2.10: A structural formula of sphingomyelin showing the ceremide and phosphocholine moieties.

Unesterified cholesterol is also found in the membrane in a 1:1 molar ratio with the phospholipids. Cholesterol (Figure 2.11) is a bulky ring system that modulates the membrane by hindering the movements of the fatty acid side chains and decreasing their fluidity. The presence of the cholesterol also obstructs the potential crystallization of the phospholipids if they become packed too closely.[28] Furthermore, it creates openings in the membrane which allow for the passive transport of certain cations.[11] Hence, the diet of an individual can influence the lipid and cholesterol concentrations in the blood stream which in turn could affect the quality of the erythrocyte membranes.

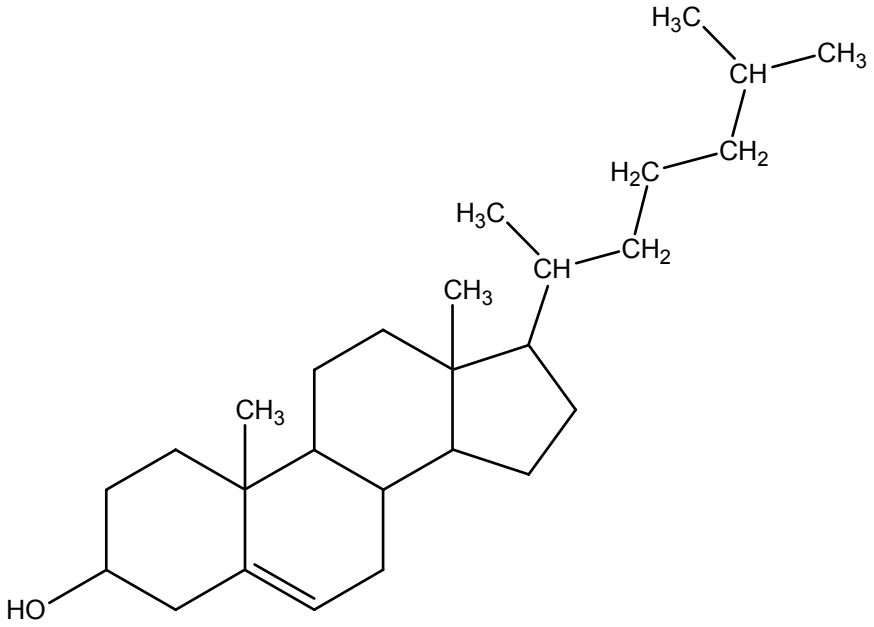

Figure 2.11: The structural formula of cholesterol.

The membrane phospholipid contents exhibit a characteristic asymmetry. Phosphatidylserine and phosphatidylethanolamine are found in larger quantities in the inner leaflet of the bilayer whereas phosphatidylcholine and sphingomyelin are mostly located in the outer layer. An enzyme, aminophospholipid translocase (flipase), has been identified to execute an ATP-dependent translocation of phosphatidylserine and phosphatidylethanolamine from the outside to the inner layer. The asymmetry can be maintained on the most part due to the slow fluidity of the membrane, and the electrostatic attractions of skeletal proteins to the phosphatidylserine. Alterations in the phospholipids distributions may have a significant effect on vascular normalcy. For

example, a substantial amount of phosphatidylserine on the external layer may incite the activation of blood clotting.[14]

The characteristic and functional shape of the red blood cell is maintained by a network of proteins in the skeletal matrix. The erythrocyte also owes its deformability to this intricate matrix and internal viscosity, allowing the cell (~8 μm in diameter) to squeeze through capillary openings as small as 3 μm, or increase its volume from 90 fl up to 150 fl.[11,14]

The supporting network of proteins (Figure 2.12) in the membrane skeleton consists of spectrin and actin, among others. Spectrin, the most abundant protein of the skeleton, is a heterodimer composed of two non-identical subunits (α and β) with molecular weights of 240 kD and 220 kD respectively.[29] The two subunits are intertwined in a linear fashion, measuring approximately 1000 angstroms. Furthermore, the heterodimer will interact head-to-head to form a heterotetramer, which will be the core of the meshwork in the membrane skeleton.[28,30] Five to eight spectrin heteromer tails come together at a junctional complex composed of a combination of actin, protein 4.1 (band 4.1), tropomyosin, adducin, and protein 4.9 (dematin).[11,31,32] The spectrin tails are directly associated with actin and protein 4.1. The junctional complex itself is anchored down via protein 4.1 to the membrane by its association to glycophorin C, an integral membrane glycoprotein which carries an antigen on its extracellular domain.[11] A deficiency in glycophorin C shows a deficit of protein 4.1 and a disruption in membrane stability that leads to a mild case of elliptocytosis.[33] In between two junctional complexes, ankyrin (protein 2.1) attaches to the spectrin tetramer, and through the aid of

protein 4.2 (pallidin), the complex is anchored to the integral membrane protein, band 3 (protein 3).[33] This elaborate meshwork of the membrane skeleton maintains the erythrocyte's biconcave discoid shape as well as its flexibility which allows it to pass through small openings.

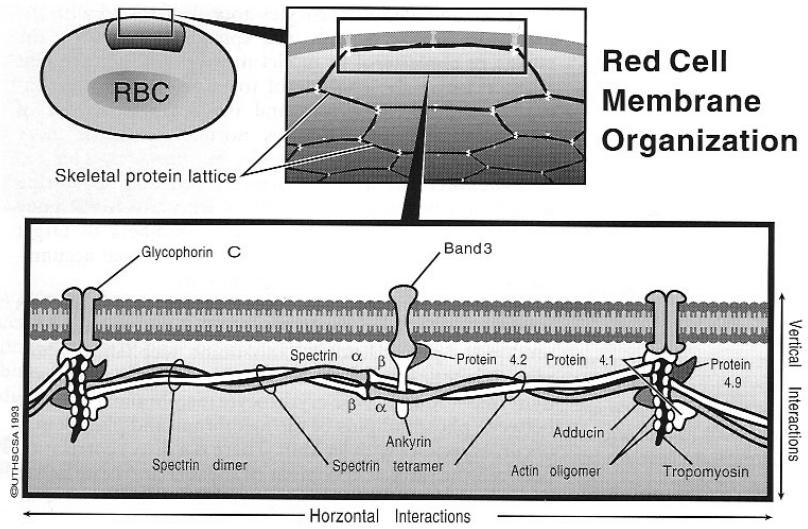

Figure 2.12:[11] The figure depicts the organization of the membrane and membrane skeleton. The spectrin heterotetramer attaches to both the junctional complex (actin, tropomyosin, adducing, protein 4.9 and protein 4.1) and the ankyrin/protein 4.2 complex. The junctional complex is attached to the membrane by way of glycophorin C and the ankyrin/protein 4.2 is attached via band 3.

The Erythrocyte Surface

The outer surface of the red blood cell has an overall negative charge due to its richness in neuraminic acid residues primarily located on the glycophorin A transmembrane protein.[14] More importantly, it is the different blood group determinants on the surface that comprise about 22 different blood group systems. Two systems, the ABO and rhesus (Rh) blood groups have the largest clinical implications.[28]

The antigenic determinants for the ABO blood group system are oligosaccharides of type A, B, and H attached on surface sphingoglycolipids. The three subtypes differ in sugar residues at their non-reducing ends with all three sharing the same base polysaccharide sequence. The A and B variants each exhibit a unique sugar residue attached to the base whereas the H antigen has none. The H antigen is therefore considered to the precursor to the A and B types, and in the absence of A or B antigens, the individual is deemed type O. A type A individual bears A antigens on the red cell surface while the blood plasma contains antibodies to the B antigen. A type B person would show the opposite phenotype. If anti-A serum is introduced to type A red cells, the antibodies would cause the cells to agglutinate, illustrating the importance of matching up blood types for clinical transfusions.[28] AB individuals carry both types of antigens on the cell surface but do not express either antibody in their plasma.

The Life of an Erythrocyte

Hematopoiesis is the formation of cells in the vascular system, and erythropoiesis is specifically the process by which red blood cells are developed. In post-birth individuals, cells are generated from the bone marrow, where all blood cells are differentiated from a pool of common stem cells.[11,12,14,15] Although less than five percent of the stem cells are dividing at one time, approximately $1x10^{11}$ cells are generated per day from a stem cell pool of around $2x10^{6}$ by constant division and proliferation.[11]

Figure 2.13 shows the lineage of the different blood cells. The stem cell (CFU-S), deemed "pluripotential" due to its capacity to differentiate, can be stimulated into

becoming CFU-GEMM (colony-forming unit-granulocyte, erythrocyte, monocyte, megakaryocyte) or CFU-L (colony-forming unit-lymphocyte). The CFU-GEMM will then be differentiated into one of the committed progenitor cells (with the aid of specific hematopoietic growth factors) for neutrophils, eosinophils, basophils, monocytes, platelets, or erythrocytes. The CFU-L will either become the B- or the T-lymphocyte.[11]

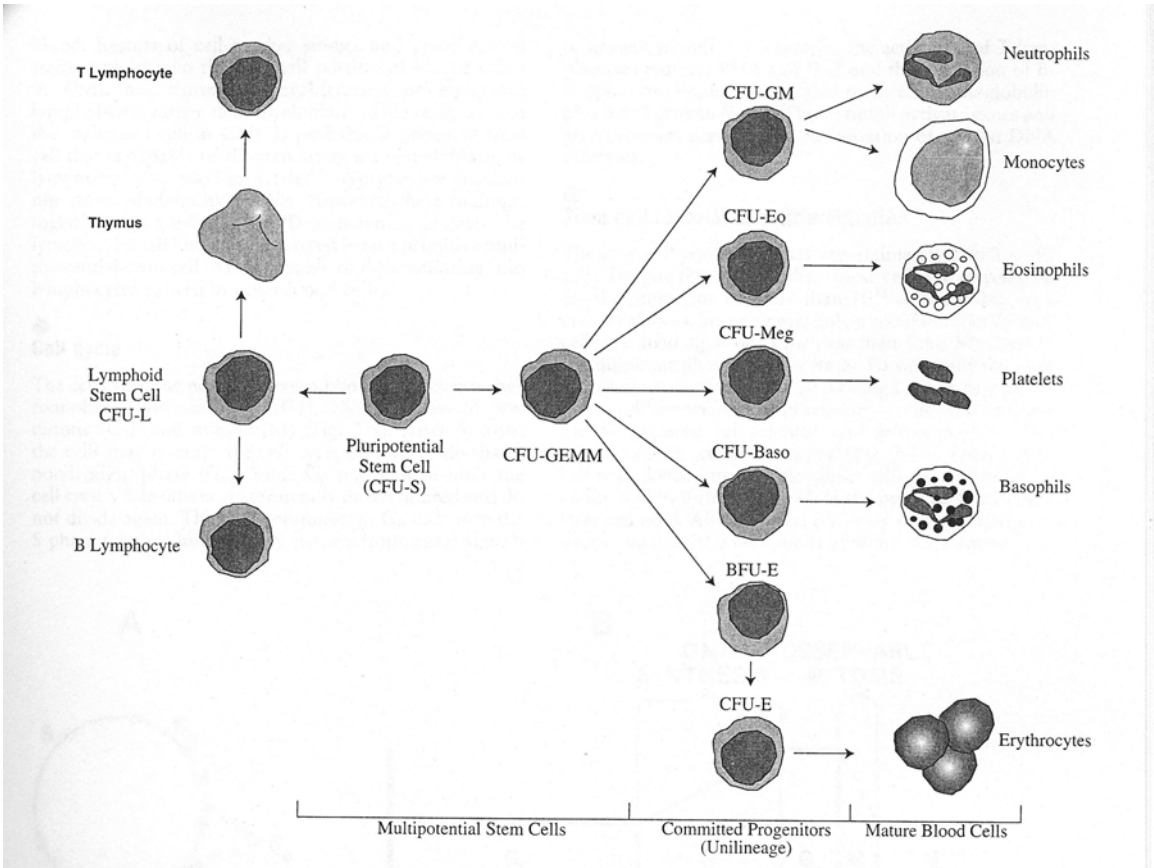

Figure 2.13:[11] The figure illustrates the cell lineage of each of the blood cells generated from the pluripotential stem cell (CFU-S). The CFU-GEMM (colony-forming unit-granylocyte, erythrocyte, monocyte, megakaryocyte) will differentiate into committed progenitor cells, eventually producing neutrophils, monocytes, eosinophils, basophils, platelets, and erythrocytes. The CFU-L (colony-forming unit-lymphocyte) will differentiate into T- and B-lymphocytes.

As indicated in figure 2.13, erythropoiesis shares the CFU-S to CFU-GEMM lineage with the granulocytes, monocytes, and platelets. From the CFU-GEMM stage, however, differentiation into the early progenitor cell blast-forming unit-erythrocyte (BFU-E), the late progenitor cell colony-forming unit-erythrocyte (CFU-E) and subsequent proliferation are initiated by combinations of the granulocyte-macrophage colony-stimulating factor (GM-CSF), interleukin-3 (IL-3), interleukin-4 (IL-4), and erythropoietin.[11] Proliferation of CFU-E leads to maturation stages in the following order: pronormoblast (rubriblast), basophilic normoblast (prorubricyte), polychromatophilic normoblast (rubricyte), orthochromatic normoblast (metarubricyte), reticulocyte, and erythrocyte.[11,15,26] The pronormoblasts and basophilic normoblasts are large in size and volumes (up to 20 μm and 300-800 fl respectively) and have clumped nuclear chromatin. Polychromatophilic normoblasts show early signs of hemoglobin production (blue-green in color) and a smaller size (10-12 μm). The hemoglobin content is visibly increased in the orthochromatic normoblast as demonstrated by the cell's pink color and it contains 2/3 of the total erythrocyte hemoglobin. The nucleus is gradually pushed out of the cell for it to become a marrow reticulocyte. Residual mitochondria and RNA will help synthesize the remaining hemoglobin before they are eliminated. The size of the reticulocyte continues to decrease in size and lose RNA for approximately 24 hours post release into circulation. Once the reticulocytes are released via the sinuses, they will mature within a day into erythrocytes.[11,26] One CFU-E will produce 16-32 adult erythrocytes.[26]

Metabolic Pathways in the Erythrocyte

Although the red cell is devoid of many common cellular activities, it still exhibits metabolic pathways essential to maintaining its viability for its lifetime in circulation. Briefly, the Embdon-Meyerhof pathway, or glycolysis, accounts for 90-95% of the cell's glucose consumption. The glucose, which is harvested externally (due to the fact that erythrocytes lack glycogen reserves), is converted to lactate producing two moles of adenosine triphosphate (ATP) for every mole of glucose reacted. The ATP is then used to maintain everything from membrane integrity to active ion pumps (Na^+ and Ca^{2+} out; K^+ and Mg^{2+} in). Two subsidiaries of the glycolysis pathway are the methemoglobin reductase pathway and the Rapoport-Leubering shunt. The methemoglobin reductase keeps hemoglobin iron in a reduced state (Fe^{2+}) and maintains the oxidized form, methemoglobin (Fe^{3+}) to about two percent. The Rapoport-Leubering shunt takes the 1,3-bisphosphoglycerate (1,3-BPG) from the glycolysis pathway and catalyzes it to 2,3-bisphosphoglycerate (2,3-BPG). 2,3-BPG is important for the release of oxygen by the hemoglobin molecule. The hexose-monophosphate shunt produces nicotinamide adenine dinucleotidephosphate (NADPH) and glutathione (GSH) both in their reduced forms. When the sulfhydryl groups (-SH) of hemoglobin become oxidized, GSH will work to reduce these groups, and in turn will become oxidized (GSSG). GSSG will then be reduced to back GSH with the aid of NADPH. Deterring the oxidation of the hemoglobin –SH groups is important since such an event would lead to denaturation and precipitation of the oxygen-carrier. Furthermore, GSH/NADPH are responsible for maintaining reduced sulfhydryl groups on the membrane.[11,34]

Morphology of the Red Cell

The characteristic biconcave shape of an erythrocyte is referred to as a discocyte.[14] There have been many speculations as to why and how the cell is able to maintain this unique shape. One hypothetical model showed that the discocyte shape has lowest bending energy due to the reduced surface curvature.[35] From a biochemical standpoint, the shape could be explained as an effect due to the interactions between the molecules which make up the membrane and membrane skeleton. Regardless of the cause of the shape, it cannot be argued that it is an efficient design to carry out its task.

Aside from its discocyte shape, erythrocytes may take on alternate shapes, usually due to an abnormality. Such variant forms include, but are not limited to, echinocyte, elliptocyte, and drepanocyte.[14] The echinocytes are spherical, crenated cells characterized by spicule projections, not unlike a sea urchin (Figure 2.14). The echinocytes will form under circumstances such as prolonged storage or uremia. Elliptocytes are oval-shaped red cells and are commonly seen in types of anemias and thallassemias. Finally, the drepanocyte (Figure 2.15) is the sickling of the cell as seen in sickle cell anemia patients.[14,35]

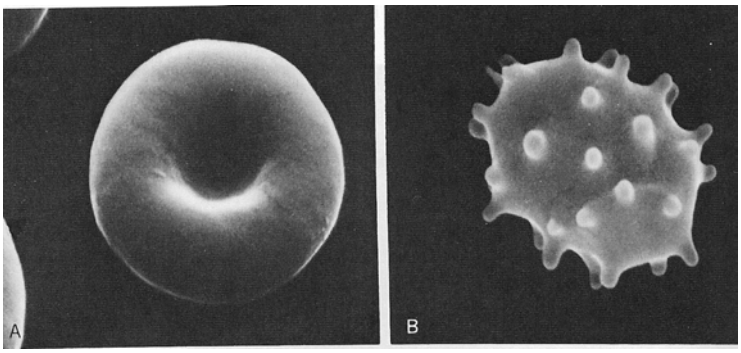

Figure 2.14:[35] An electron micrograph of a discocyte (A) and an echinocyte (B).

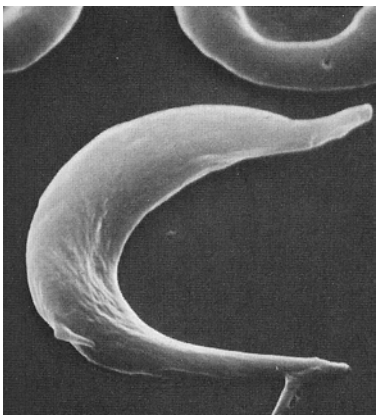

Figure 2.15:[35] An electron micrograph of a drepanocyte.

2.3 Hemoglobin

Erythrocytes can generally be considered as sacks of hemoglobin, the oxygen carrying molecule which gives the cell its red color. As previously mentioned, approximately 97% of the total red cell protein is hemoglobin with a cell mass fraction of approximately 0.33.[14] The protein is found in different subtypes such as A_1 (most common, ~95%), A_2 (~2-4%), and F (fetal).[36,37] It is one of the most well-studied proteins due to its elegant complexities as well as its availability. It can also exhibit a multitude of abnormalities, leading to various clinical pathologies. Moreover, its optical characteristics provide a means for the spectrophotometric analysis of blood quality.

Hemoglobin Structure and Function:

Simple organisms can sustain life by depending on the diffusion or oxygen, but with tissues thicker than ~1 mm, the rate is too slow to support life. Additionally, oxygen

solubility in blood plasma is around 1 x 10^{-4} M, which is too low for the metabolic needs of animals. Whole blood, which contains 150 g Hb/L can carry O_2 at concentrations up to 0.01 M.[36]

With the average man containing approximately 1 kg of hemoglobin, its major functions aside from O_2 transport include CO_2 transport and buffering the blood to maintain its homeostatic environment.[38] It has a molecular weight of 64,458 kD and overall dimensions of 64 x 55 x 50 Å.[28,38] Its tetrameric nature allows for its complex yet efficient oxygen binding properties.

Hemoglobin (Hb) contains two distinct entities: the globular portion of the protein and the heme group. The apoprotein of adult hemoglobin A_1 consists of two α- and two β-subunits ($\alpha_2\beta_2$), whereas subtype A_2 is designated $\alpha_2\delta_2$ and F is $\alpha_2\gamma_2$.[38] The heme group consists of the reduced form of iron (Fe^{2+}) which binds to the molecular oxygen for transport. The discussion on Hb characteristics will focus on the most common subtype, A_1.

The α-chain contains 141 amino acid residues and the β-chain has 146 residues, with approximately 70 – 75% of both chains arranged as a series of α-helices (7 in the α-chain and 8 in the β-chain with the helices named A-H and A-G respectively starting from the amino-terminus).[14,38,39] A heme (ferroprotoporphyrin IX) is noncovalently associated with each subunit in the space created between helices E and F (Figure 2.16). The heme is tucked into a hydrophobic pocket, which acts as the stabilizer to the binding of the molecule to the protein subunit. That is, specific hydrophobic amino acid residues are within proximity of the heme for van der Waals contact. The hydrophobicity also

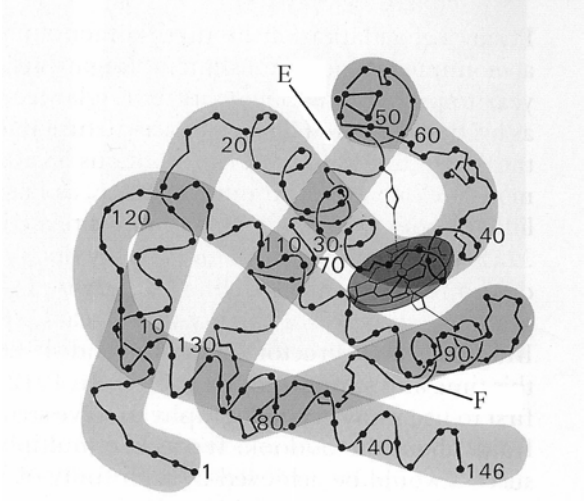

Figure 2.16:[40] The β chain of hemoglobin shows the globular tertiary structure consisting of eight α-helices. The heme group is tucked in the crevice between helices E and F.

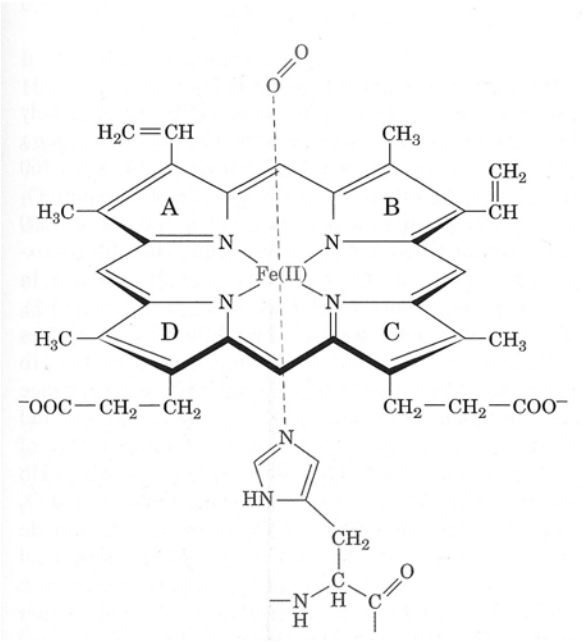

Figure 2.17:[28] A structural depiction of the heme molecule. The protoporphyrin IX consists of four pyrrole rings linked in a heterocyclic ring system. The Fe(II) center is chelated to the four nitrogen groups. The proximal histidine (F8) can be seen coordinated to the iron from the bottom of the plane and the molecular oxygen binds to the iron on the opposite side.

repels any small polar molecules away from the ligand binding site. Furthermore, a nonpolar crevice makes the oxidation of Fe^{2+} to Fe^{3+} more difficult.[14]

The heme consists of an iron (II) coordinated to the nitrogens of four pyrrole rings in a heterocyclic ring system named protoporphyrin IX (Figure 2.17). When the heme is situated in a hemoglobin subunit, the iron is also coordinated covalently to the imidazole

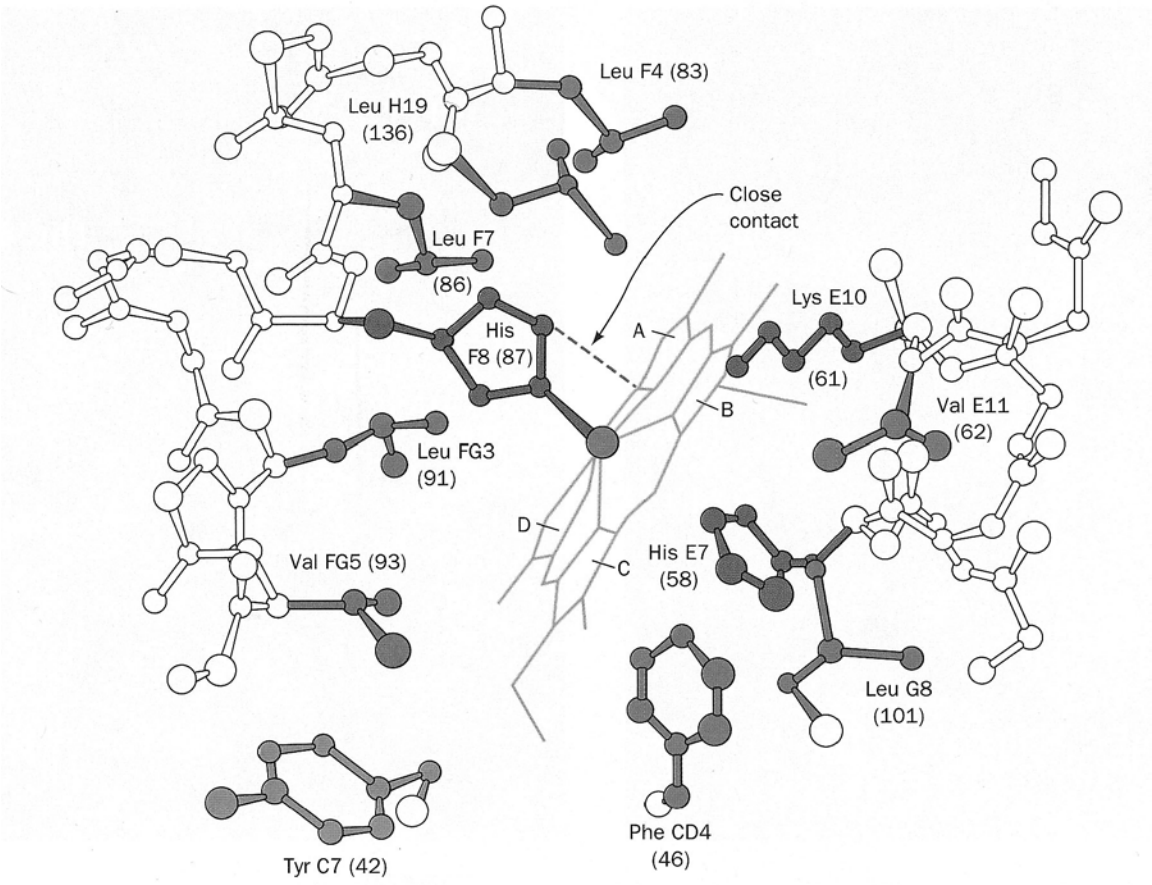

Figure 2.18:[28] An illustration of the heme pocket in the deoxygenated state. The proximal histidine (F8) is coordinated to the iron center as a part of a square pyramidal geometry. In the pocket, the heme is surrounded by mostly hydrophobic residues, which keeps out small polar molecules. The distal histidine (E7) stabilized the ligand in the oxygenated state. In the absence of a ligand, the heme adopts a domed shape.

nitrogen of the proximal histidine (histidine F8) to form a square pyramidal geometry in the deoxygenated state (Figure 2.18). When a molecular oxygen associates to the Fe in an octahedral geometry, a distal histidine (E7) will hydrogen-bond to the ligand to stabilize it.[36,38] Moreover, in the deoxygenated form, the iron center is pulled by the proximal histidine approximately 0.6Å out of the plane of the heme (Figure 2.19) to form a slightly domed structure. However, when an oxygen binds, the iron is pulled back into the heme plane, causing strain in the ring structure. The movement of the iron center repositions the proximal histidine and alters the distance between certain residues, such as Val FG5, and the heme (they become closer). Additionally, the proximal histidine is tilted with respect to the heme plane in the deoxygenated state, but becomes more

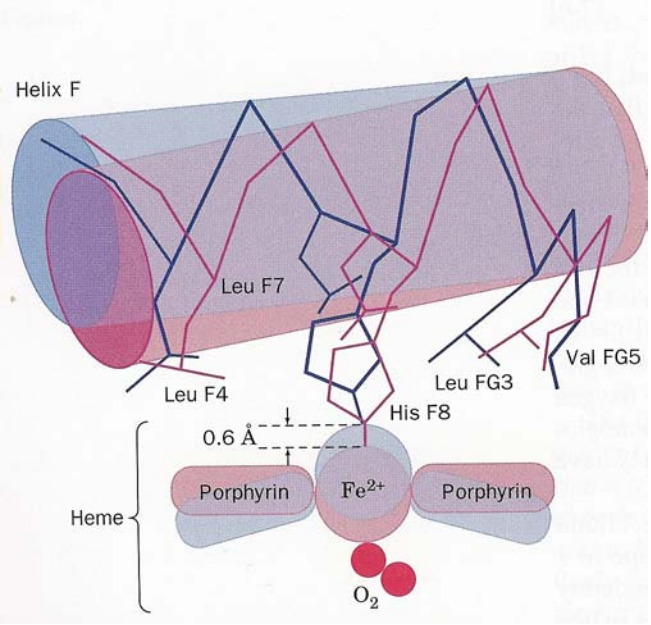

Figure 2.19:[36] When deoxygenated, the iron is pulled out of the heme plane ~0.6Å whereas the iron resides in the plane in the presence of a ligand. The shift affects the tertiary structure, and ultimately, the quarternary structure of the tetrameric hemoglobin molecule.

perpendicular when the iron is retracted into the plane (in the oxygenated state), subsequently affecting the positioning of certain neighboring residues.[41] Such shifts within the subunit will cause the globular structure to reorganize, resulting in a conformational change.[36,41] A shift in one subunit will affect the conformation of the juxtaposed hemoglobin subunits, and such is the basis for its cooperative properties (discussed later in this chapter).

The quarternary structure involves the subunits of the tetramer being held together by a combination of direct hydrogen bonds, solvent mediated hydrogen bonds, hydrophobic contacts and salt bridges.[14] The deoxygenated form is typically known as the T (tense) state and the oxygenated form is considered the R (relaxed) state.[36,38,41] While the R state is stabilized by ligand binding, the T state is a more rigid form and it is stabilized by a series of salt bridges that involve the C-terminal residues of each subunit; residues which are otherwise free.[38] Furthermore, the T state has a Val E11 in the β subunits positioned on the distal side of the heme, hindering ligand binding.[41] The α-β interface also shows two stable positions that switch between the states. In the T state, Tyr αC7 hydrogen bonds with Asp βG1, but upon oxygenation, the R state causes a shift in the interface, which is now stabilized by a hydrogen bond between Asp αG1 and Asn βG4 (Figure 2.20). In both conformations, the hills and valleys on the surfaces of subunits complement each other well, such that any intermediate positioning is not energetically favorable.[36]

Another factor that favors the deoxygenated state of hemoglobin is the presence of the compound 2,3-diphosphoglycerate (2,3-DPG) (Figure 2.21). 2,3-DPG binds

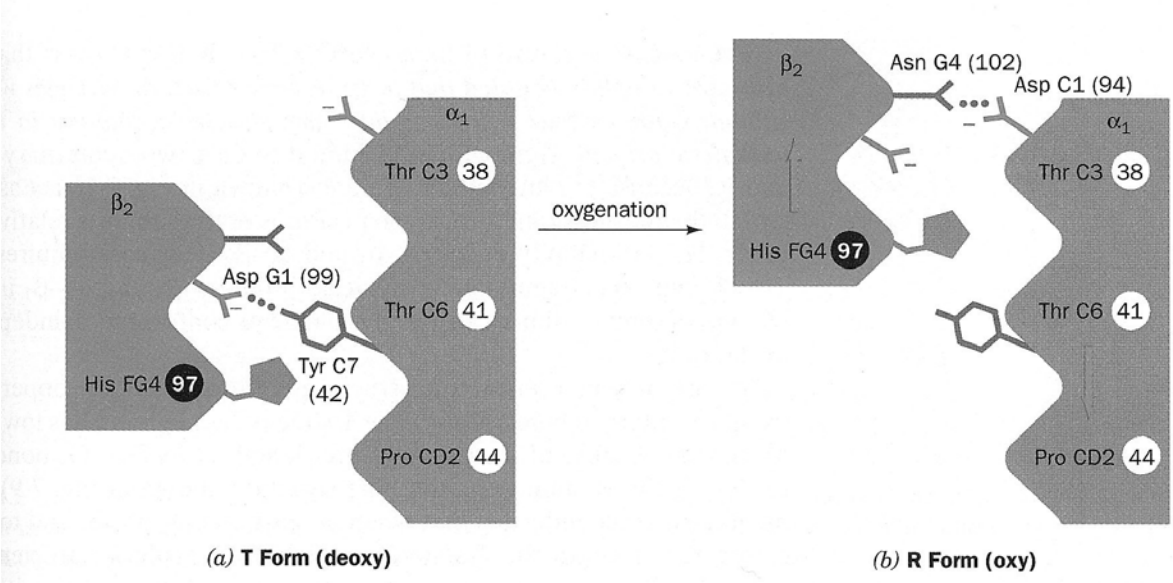

Figure 2.20:[36] This figure illustrates the dynamics in the α-β interface between the T and R forms of hemoglobin. In the T form, Tyr αC7 hydrogen bonds with Asp βG1. The R form sees a shift in the interface and a new interaction between Asp αC1 and Asn βG4. The hills and valleys of the surfaces complement each other in both conformations such that any intermediate would be unstable.

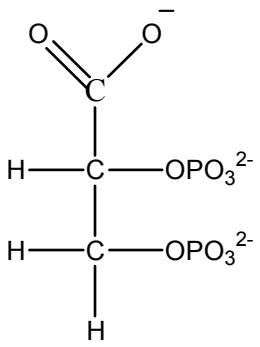

Figure 2.21: Structural formula for 2,3-diphosphoglycerate (2,3-DPG).

tightly to the central cavity created by the four subunits by way of electrostatic attractions and hydrogen bonding. The molecule has an important function for the following reason.

In arterial blood, where oxygen is abundant (pO_2 ~100 torr), approximately 95% of the hemoglobin is saturated with oxygen. As it circulates, the red cells release ~40% of the oxygen. Due to hemoglobin's high affinity for O_2, it is the presence of 2,3-DPG that allows for the efficient delivery of oxygen.[28]

Hemoglobin Cooperativity

The complex series of conformational dynamics that stems from the interaction of O_2 to the heme and ultimately affecting the quarternary structure plays an important role in the hemoglobin's ability to effectively deliver oxygen. This allosteric behavior of hemoglobin can be seen in an oxygen dissociation curve of fractional oxygen saturation (Y) as a function of partial pressure of oxygen (pO_2). Figure 2.22 shows a sigmoidal curve for hemoglobin compared with myoglobin (a single subunit oxygen carrier similar in structure to one of Hb's subunits) which shows a hyperbolic curve reflecting its lack of allostericity. The myoglobin curve suggests that it will not release its bound oxygen until the partial pressure of O_2 in the surrounding environment drops below 20 torr. Although a single hemoglobin subunit has similar affinity to oxygen as myoglobin, the cooperative feature of the tetrameric structure of hemoglobin helps lower its attraction to O_2 with every subsequent O_2 it loses. As noted before, this is due to the conformational change experienced by each subunit from the loss (or gain) of a ligand.[36] The sigmoidal curve of isolated hemoglobin in itself is a significant reflection of the regulatory feature of oxygen delivery. However, in its native environment (in erythrocytes), the presence of such

factors as 2,3-BPG further modifies the profile of the oxygen dissociation curve. Hence, red cells show a more reduced oxygen-binding capacity than hemoglobin by itself.

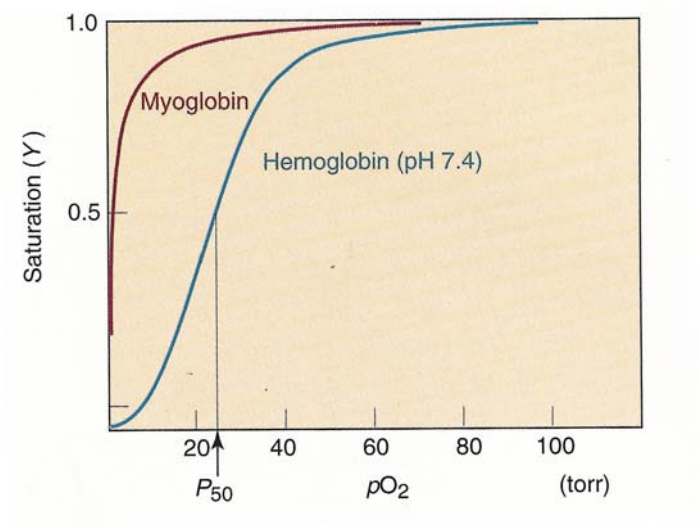

Figure 2.22:[28] Oxygen binding curves of hemoglobin and myoglobin, with the hemoglobin curve showing a sigmoidal shape denoting its allosteric behavior.

Hemoglobin Derivatives

In its primary function as an effective oxygen-carrier, hemoglobin houses its iron atoms in the reduced state. The molecule, however, can exist in small quantities with the iron in an altered oxidation state. Additionally, hemoglobin exhibits the capacity to bind to ligands other than molecular oxygen.

Methemoglobin is the form of hemoglobin that exists with oxidized irons.[14] In this state, the molecule loses its ability to reversibly bind molecular oxygen, hence it is not the preferred physiological form. As oxyhemoglobin is converted to methemoglobin, the color changes from bright red to a dark brown color, corresponding to shifts in the

absorption peaks at ~410 nm and 500-600 nm.[14,42] Although the mostly hydrophobic pocket in which the heme resides prevents the oxidation of the iron to a degree, it cannot prevent it completely. In vivo, methemoglobin reductase (also known as cytochrome B_5 reductase) is present to reduce the methemoglobin in order to maintain normal concentrations at <1.5% of the total hemoglobin.[43,44] Methemoglobin's affinity for cyanide (CN) has been exploited in the development of a standard assay for total hemoglobin quantification. All forms of hemoglobin with the exception of sulfhemoglobin is converted into the stable cyanohemoglobin form and assayed at 540 nm with respect to a standard curve.[45,46,47]

Hemoglobin in its reduced state also has potential ligand alternatives beyond O_2. Carboxyhemoglobin involves carbon monoxide (CO) binding to the heme center with an affinity that is approximately 200 times stronger than that of oxygen. This is due to the fact that the rate of dissociation of CO is significantly slower that O_2.[14] The presence of 0.1% atmopheric CO would convert 50% of the hemoglobin into its carboxy derivative and prove to be fatal within one hour as a result of oxygen deprivation to the body.[48] Sulfhemoglobin is a form in which sulfur is bound to the porphyrin group of the heme and lowers the iron's affinity to oxygen ~100 times.[14] It is typically caused by, but not limited to, the ingestion of drugs, such as sulfonamides and phenacetin.[14]

2.4 Current Methods of Red Cell Analysis

Red cells are typically analyzed for transfusion viability at blood banks by monitoring such parameters as cell counts and hemoglobin concentrations. A common

automated method for obtaining such values is electric impedance-based hematologic analyzers like the Coulter counters.[49] In these instruments, the cells are passed into an aperture and through a constant electric current. The impedance caused by the cells as they pass through the current results in a voltage spike which is converted into the volume of the cell. Thus, the volume of the cell is proportional to its induction of current change as it travels through the aperture.[49,50]

Cell types (erythrocytes, leukocytes, platelets) are identified based on size cutoffs of their known physiological distributions, hence the counts and mean cell volume are obtained. Knowing these two values, the % hematocrit, or the packed red cell volume can be calculated by the relationship:

$$\text{Mean corpuscular volume (MCV)}^{51} = \frac{\%\ \text{hematocrit (HCT)}}{\text{erythrocyte count } (\times 10^6/\mu l)} \times 10 \quad \text{(Eq 2.1)}$$

The erythrocytes are then lysed and the hemoglobin is allowed to disperse in free solution. Quantification of the hemoglobin involves the standard Drabkin's method where all forms of hemoglobin are converted to the cyanomethemoglobin derivative and compared against standards. The resulting concentration of the diluted hemoglobin (Hb) is reported in g/dL. The mean corpuscular hemoglobin concentration (MCHC) is calculated by the following equation.

$$\text{MCHC (\%)}^{51} = \frac{\text{hemoglobin (g/dl)}}{\%\ \text{packed cell volume}} \times 100 \quad \text{(Eq 2.2)}$$

Mean corpuscular hemoglobin (MCH) is another interpretation of MCHC and is expressed in picograms of Hb/cell. The above parameters, as the names imply, are all average values and they may or may not reflect an abnormality in the donor unit.

2.5 Erythrocytes and Multiwavelength UV-Visible Analysis

In the context of clinical settings, the need for quality red cells for transfusion purposes is immeasurable. For this reason, blood banks must adopt the latest technology in quality control for donated blood to insure that transfusion recipients are getting viable blood units and not ones that are infected or incompatible. The current blood banking system implements multiple methods and instrumentations for different analyses including cell counts, blood typing, and screening of infections, among others. Efforts to improve upon current technologies in the area of efficiency, accuracy and cost are constantly underway.

Our proposed entry into clinical whole blood analysis revolves around multiwavelength ultraviolet-visible (uv-vis) spectroscopic analysis. Based on the knowledge of the optical properties of whole blood components (erythrocytes, leukocytes, thrombocytes, plasma), it is possible to obtain size, shape, number, and chemical composition information from a single scan. The spectrograph can be modeled as a mathematical representation based on the Mie theory to corroborate with the experimental data. This method has been demonstrated with certain types of blood analyses. The first was a blood typing method in which blood groups were determined by changes seen in the spectra when red cells were introduced to agglutinating

antibodies.[52,53] That is, the spectra showed their sensitivity to changes in particle size and number. Secondly, uv-vis spectroscopy was used for the quantitative analysis for platelet quality.[9] The multiwavelength analysis successfully estimated the particle size distribution (PSD) for platelets and also showed the potential for monitoring platelet activation.

In terms of erythrocyte analysis, the implications of this technology span from the routine screening of whole blood to diagnosis of certain types of diseases to online monitoring of blood oxygenation during surgeries. It is important to establish a spectral baseline for normal erythrocytes so that any anomalous conditions could be immediately detected. A simple scan of a patient's whole blood could produce information about his or her cell counts, MCV, MCH, MCHC, and the ability to detect any morphology variations associated with red blood cells, such as sickle cell anemia (which produces sickle-shaped red cells as a result of hemoglobin polymerization).[14] Infections may potentially be revealed as it has been suggested by data (Garcia-Rubio, L. H. *et al.*, unpublished) that blood from individuals infected with the malaria parasite show characteristic spectrophotometric features. Furthermore, the ability to screen transfusable units for proper leuko-depletion, or the capacity to confirm the viability of 5-day-old blood could enhance the effectiveness of quality control in blood banks.[54,55] In this quest to spectrally characterize the norm in whole blood, it is necessary to separate the optical behavior of each component. An accurate depiction and the defining of the spectral limits of normal erythrocytes are particularly important for a few reasons: 1) it is the most abundant cell in the vascular system, 2) it contains hemoglobin, a protein with a

high absorptivity (extinction) coefficient, and 3) the majority of the spectral fingerprint of whole blood is due to the contribution of red cells.

In order to use this technology as a multifunctional analytical tool for red blood cell quality, it is necessary to establish the optical properties of normal red cells and how they affect the absorption and scattering of light. It is well known that erythrocytes contain hemoglobin at a physiologic concentration of 33%. At such elevated concentrations, it has been suggested by using similarly chromophoric compounds (chlorophyll, nucleic acids) that the absorbance component experiences an observed hypochromism. In this context, hypochromism refers to a decrease in the absorbance (and hence the absorption coefficient) due to an increase in the concentration of a strongly absorbing species.[56] The phenomenon has been documented in free solution as well as the absorbing species being stacked in the form of micelles.[57,58] It is proposed in this study that the UV-visible characterization of red blood cells be approached from the context of a combined scattering and absorption effect based on light scattering theory. In the process of using this technology to solve the optical behavior red cells, the problem of hypochromism will be addressed.

Chapter 3: Multiwavelength Spectrophotometry and Its Application for the Characterization of Red Blood Cells

3.1 Features of Spectrophotometry

Spectrophotometry is widely used for various types of chemical and biological analysis, and by its nature spans a broad range of wavelengths. This dissertation focuses on applying the significant potential of multiwavelength ultraviolet-visible (UV-vis) spectrophotometry to characterize erythrocytes. The spectrophotometer used for experiments, the Hewlett Packard/Agilent 8453, outputs data in the wavelength range of 190 – 1100 nm, which covers the near UV (200 – 380 nm), the visible (380 – 780 nm), and part of the near infrared (IR) region (780 – 1100 nm) (Figure 3.1).[59,60]

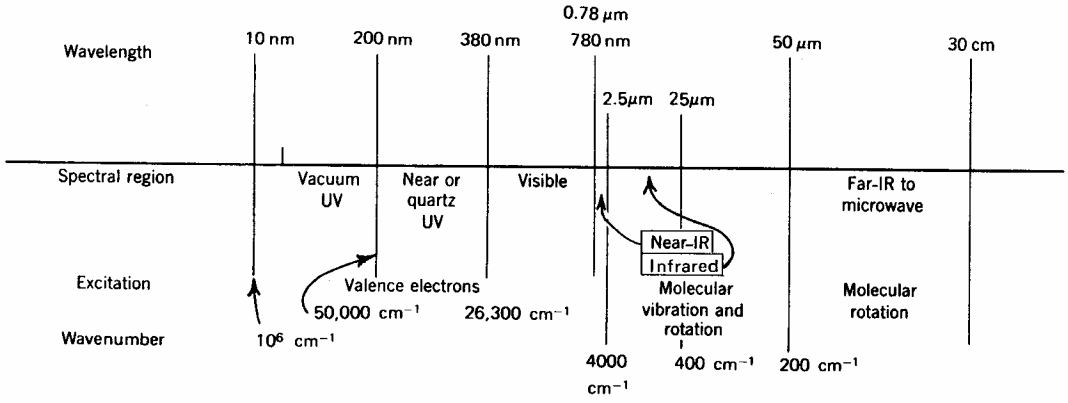

Figure 3.1:[59] Diagram of electromagnetic radiation in the UV, visible, and IR regions.

Particle analysis requires both the acquisition of spectral data and the ability to understand and interpret the absorption and scattering components of the optical density spectrum. The optical density is often referred to as absorbance; however this is typically under the assumption that the absorption dominates and that the molecule under analysis is small in size on the order of proteins (usually < 10 nm) with negligible scattering. Even in this size range, light scattering occurs in the Rayleigh regime and must be accounted for interpretation purposes.[24] While the absorption component dominates in solutions or pure liquids and solids, light scattering still makes a contribution.[8] Hence a more specific terminology will be established where all raw spectra will be referred to as optical density (OD) in this dissertation.

Absorption Component

Electromagnetic radiation is a two-component field consisting of an electric (E) and magnetic (B) fields (Figure 3.2). Both constituents are oscillating waves and are oriented perpendicular to each other as well as to the direction of propagation. The rate of propagation of the radiation in a vacuum, more commonly referred to as the speed of light (c) is equal to 3×10^8 m/s. The unit energy of the emitted radiation is a wavelength-dependent function

$$E = hc/\lambda \qquad \text{(Eq 3.1)}$$

where h is Planck's constant (6.62×10^{-34} J-s) and λ is the wavelength. When the radiation travels through a medium and interacts with a chromophoric molecule, the

energy is absorbed in a quantized manner. That is, the light energy must equal the energy required to allow for a specific electronic transition.[60]

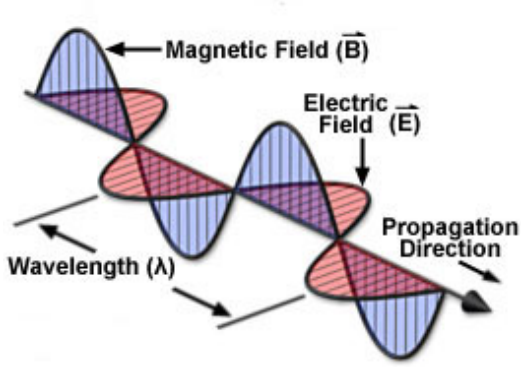

Figure 3.2:[61] A depiction of a wave of electromagnetic radiation where the magnetic field (B) and electric field (E) are perpendicular to each other as well as to the direction of propagation. The wavelength is the distance of one full wave oscillation.

As inferred above, the energies of UV and visible light absorbed by a molecule result in electrons changing energy levels. Not all electrons can make such transitions as is the case with σ-bonds, which requires too high an excitation energy to effectively be transitioned. The allowed transitions that arise as absorbances are n→σ*, n→π*, and π→π*, where n is a non-bonding orbital and π are orbitals found in double and triple bonds. The asterisks denote anti-bonding energy levels. The n→σ* occurs with non-bonding electrons adjacent to saturated bonds and require energies of short wavelengths typically below 200 nm. The n→π* occurs when a non-bonding electron is elevated to a low lying π anti-bonding orbital, such as in the case of the carbonyl moiety in Figure 3.3, and it is characterized by relatively a low absorptivity coefficient. The π→π* transitions (Figure 3.4) are usually seen in conjugated systems and show the highest absorptivity

coefficients. In the context of absorbance spectroscopy in the UV and visible wavelength range, the n→π* and π→π* transitions are the most relevant.[59,60]

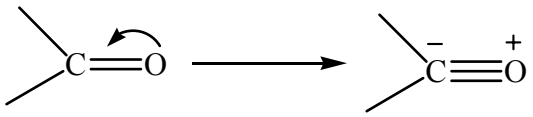

Figure 3.3:[60] A representation of an n→π* electronic transition in a carbonyl moiety.

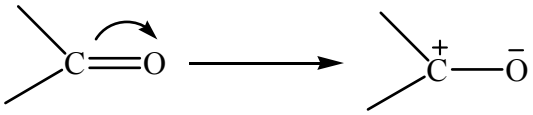

Figure 3.4:[60] A representation of an π→π* electronic transition in a carbonyl moiety.

Inorganic chelates, such as the heme group of hemoglobin, are sources of high absorption. Metals are strongly chelated by moieties like nitrogen that possesses an unshared pair of electrons. Hence there is the possibility for the excitation of these unshared pairs of electrons. The metal atoms themselves typically have high lying energy shells and orbitals and they have the capacity for electronic transitions. Finally, the chelate is capable of a charge transfer, or the movement of electrons from the ligand to the metal, or vice versa. These transfers show intense absorbance, owing to the ability of the electrons to transition to unoccupied orbitals of the metal ions.[60]

When light travels through a vessel (cuvette) containing a solution of an optically absorbing substance, the incident, or source light is attenuated as it exits the vessel. In a particle suspension, the transmitted radiation is a combination of non-absorbed incident

light and forward scattered light. In a solution, where the absorbing species are sufficiently smaller than the wavelength and the refractive index of the species compared to that of the medium is close to unity, it is categorized in the Rayleigh scattering regime, where the contribution of the absorption dominates over that of the scattering.[8]

Considering the above assumption, the Beer-Lambert law is a limit of the Mie theory as the particles become infinitely small and the medium-to-particle refractive index ratio approaches one.[62] Under these conditions, the scattering is negligible and the transmitted light exclusively describes absorbance. The Beer-Lambert relationship, typically used for solutions, can be used to calculate a wavelength-dependant absorptivity (extinction) coefficient

$$A(\lambda) = \varepsilon(\lambda)lc \qquad \text{(Eq 3.2)}$$

where $A(\lambda)$ is the absorbance value at a given wavelength, l is the pathlength of the cuvette (typically 1 cm or 0.1 cm), c is the concentration of the solution (moles/L or g/ml), and $\varepsilon(\lambda)$ is the extinction coefficient at the given wavelength.[63] The extinction coefficient is defined by Bouger's Law,

$$\varepsilon(\lambda) = \frac{4\pi\kappa(\lambda)}{\lambda} \qquad \text{(Eq 3.3)}$$

where $\kappa(\lambda)$ is the imaginary part of the complex refractive index representing the chromophore's absorptive characteristics (complex refractive index is defined in the *Optical Properties* section of this chapter). Absorbance in this context can be further defined as

$$A = \log (I_0/I_t) \qquad \text{(Eq 3.4)}$$

where I_0 is the incident light from the radiation source and I_t is the transmitted light seen by the detector of the spectrophotometer.

The measured data obtained by the spectrophotometer is collected first as percent (%) transmission. The relationship between absorbance and transmission is[63]

$$A = -\log (1/T) \qquad \text{(Eq 3.5)}$$

where T is transmission, and when converted in terms of % transmission,

$$A = 2 - \log (\%T) \qquad \text{(Eq 3.6)}$$

Absorption in Proteins

Biological systems contain proteins, many of which possess multiwavelength UV-visible fingerprints from their chemical composition. This is due to the presence of chromophoric amino acids. The major contributing amino acids are: aromatic residues tyrosine, tryptopan, and phenylalanine, thiol containing cysteine, and its derivative cystine (Figure 3.5).[64,65,66]

Tryptophan, phenylalanine and tyrosine are all relatively hydrophobic residues that have conjugated ring systems and their absorption peaks correspond to the $\pi \rightarrow \pi^*$ transition. Tryptophan's high level of conjugation in its indole side chain results in the most intensely absorbing bands. It is a bulky residue that occurs less frequently in proteins than other residues. Phenylalanine is a chemically non-reactive aromatic residue that can participate in hydrophobic pockets. Tyrosine is slightly more polar due to the hydroxyl (-OH) group and has the capability of hydrogen bonding for stability. Furthermore, the hydroxyl group can ionize at a basic pH and change its

spectrophotometric profile from its protonated state. Cysteine contains a polar thiol (-SH) group and is able to undergo a redox reaction to form a disulfide bond with the sulfur of another cysteine residue to forming cystine. This bond is integral in the folding of proteins as it stabilizes tertiary and quarternary structures.[67]

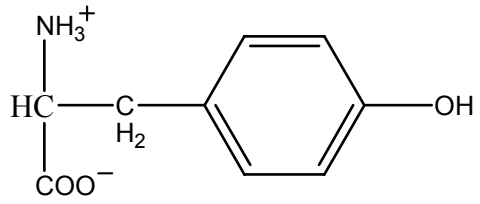

Tyrosine

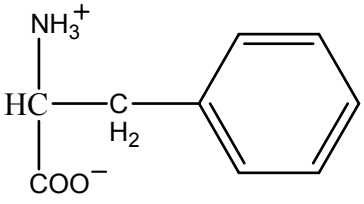

Phenylalanine

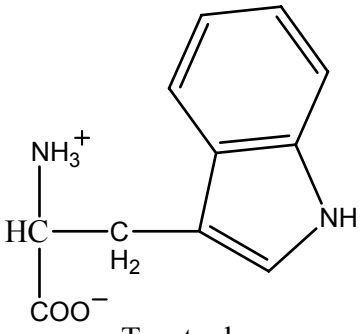

Tryptophan

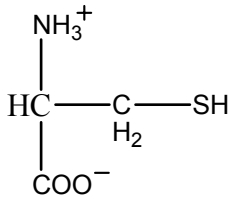

Cysteine

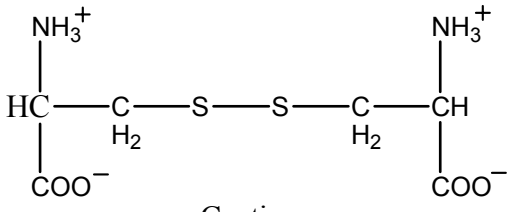

Cystine

Figure 3.5: Chemical structures of the chromophoric amino acids that contribute to the absorbances of proteins.

Scattering Component

In a complex heterogeneous mixture such as whole blood, the scattering component has a significant presence in the optical density spectra. This is because of the abundance of particles with diameters on the order of micrometers and having refractive indices greater than that of the medium. When incident light encounters one of these scattering bodies, the electric component of the electromagnetic radiation induces dipole moments within different regions of the particles, exciting them into an oscillatory motion. These accelerated charges reradiate the energy in all directions and it is this radiation that is referred to as scattered light.[8]

Although all media scatter light to some extent through events such as density fluctuations, the scattering caused by particles in suspension is the most profound. Understanding how to translate the data will allow the investigator to obtain size, shape, and orientation information on the particles, given that the chemical composition of the particles is known.

3.2 Light Scattering Theory

Scattering Trends

When the particle is small compared to the wavelength of analysis, the scattered waves are approximately in phase. This will scatter the light in a relatively uniform manner in all directions (Figure 3.6). However, as the particle increases in size, the

scattered waves tend to dominate in the forward direction. The shape and the orientation

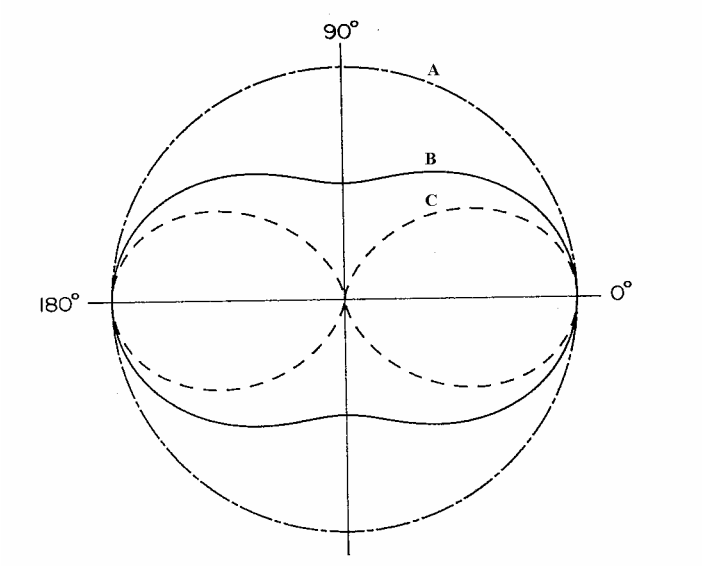

Figure 3.6:[8] Scattering patterns for a spherical particle that is small relative to the wavelength (Rayleigh scattering) where A is scattering due to a polarized incident light perpendicular to the scattering plane, B is unpolarized incident light, and C is polarized incident light parallel to the scattering plane. The source beam originates from the left (180^o) and the detector resides at 0^o.

of the particle with respect to the incident beam will further determine the scattering pattern. Figure 3.7 shows scattering models of a few representative shapes and orientations. The top left is a sphere of significant diameter (~1.24 μm) and it is easy to see the dissymmetry of the profile along the plane perpendicular to the unpolarized incident beam. An elliptical particle of equivalent volume (top right) maintains its axis of symmetry parallel to the beam similar to the sphere, but the scattering lobes contain more oscillations. When the spheroids are oriented in various angles with respect to the incident light, the dissymmetry is evident on all planes.[68] To add to the complexity, the

chemical composition of the particle will determine its refractive index which will have a bearing on the magnitude of reradiation.[8]

Another important parameter that affects the direction and magnitude of scattered light is the size of the particle. It has previously been discussed that particles small compared to the wavelength exhibit Rayleigh scattering and produce symmetrical scattering patterns in the forward and backward directions. As the size of the particle increases to be larger than the wavelength of the incident light, the profile becomes biased in the direction of forward scattering.[8]

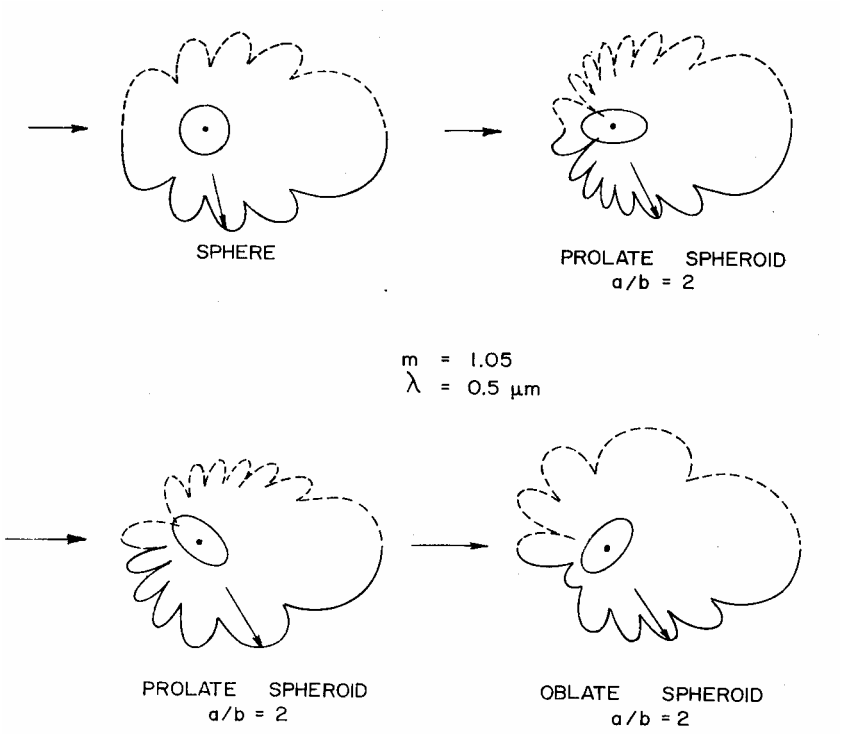

Figure 3.7:[8,68] Scattering profiles of large particles (~1.24 μm) as a sphere, and ellipses in various orientations. The refractive index (m) of the particles is 1.05 and the wavelength is 500 nm.

A simulation model based on angular formulations of the Mie theory was used to predict angular scattering profiles of large particles. The model accepted wavelength, diameter of sphere, the real and imaginary part of the refractive index of the particle, and the refractive index of the medium as inputs. Holding all parameters constant except for size, Figure 3.8 shows the predicted scattering profile for the optical properties of

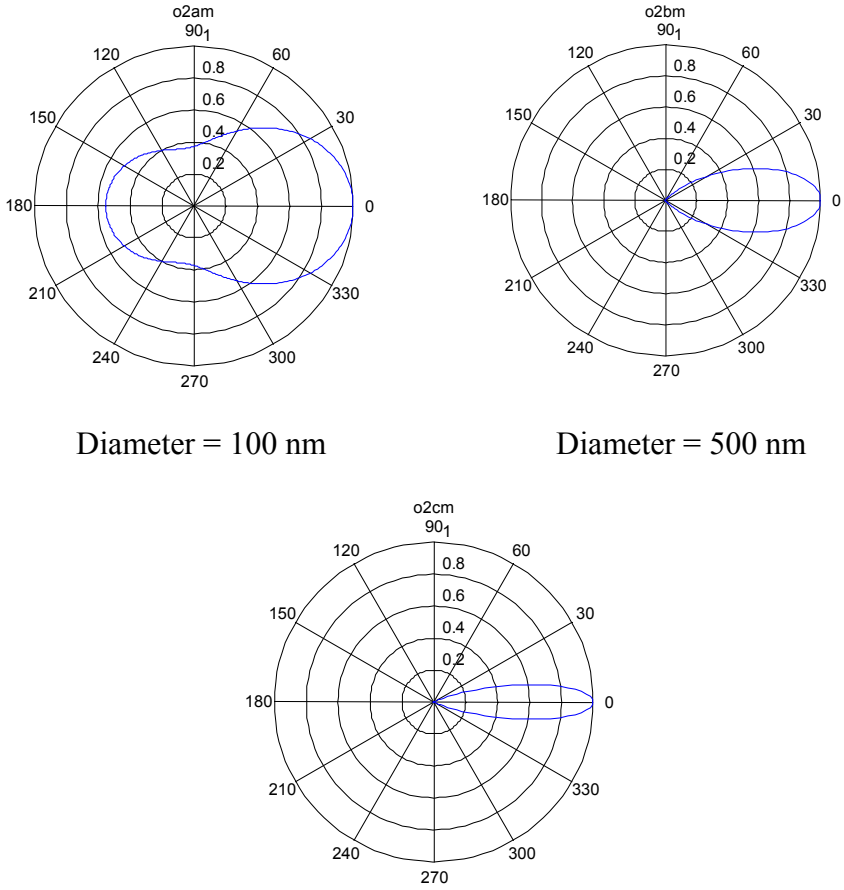

Figure 3.8: Calculated scattering patterns of spherical particles increasing in size generated using the Mie theory, where λ = 500 nm, the medium is water, and the optical properties are that of bacteria.[69] With increasing size, the scattering shifts in the forward direction.

bacteria at $\lambda = 500$ nm. A bacterium is considered a "soft particle" that exhibits a small refractive index close to that of the medium compared to particles like erythrocytes that show a larger refractive index and a higher visual contrast to the medium. Results show that with an increase in size, there is a noticeable change in favor of forward scattering. Analysis of particles with larger refractive indices, polystyrene and alumina, yield a similar trend.

Understanding this phenomenon is advantageous to our work with erythrocytes which are approximately 8 μm in diameter, or ~5.5 μm in diameter in terms of an equivalent sphere. Reynolds (1975) showed the forward scattering trend to be true for erythrocytes using the Rayleigh-Gans-Debye approximation which accounts for the shape of the scattering particle.[70] A log polar plot of the scattering intensities (at 800 nm) predicts the strong forward scattering of the erythrocytes.[70] Our calculations based on the Mie theory yields similar results (Figure 3.9). The figure suggests that approximately 97% of the total scattered light is scattered in the forward direction within a 5^{o} angle. The inset shows a semi-logarithmic plot elucidating the oscillatory features of the scattering at larger angles. It is evident by the inset that at an angle of approximately 4^{o}, there is an intensity decrease of nearly three orders of magnitude. Thus we can take advantage of the forward scattering property of macroscopic particles to effectively interpret data captured by varying acceptance angles.

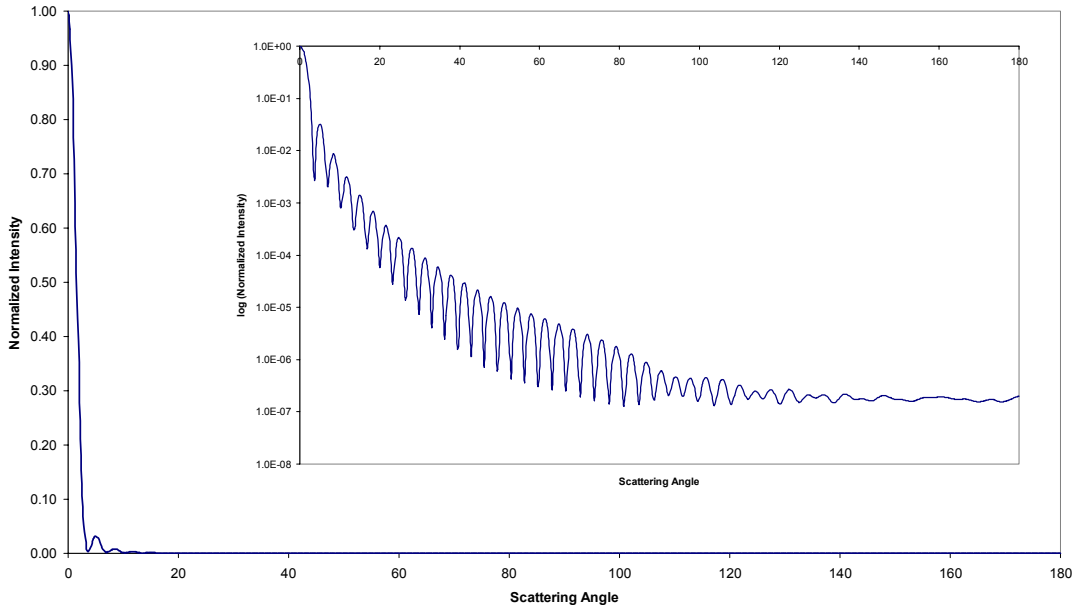

Figure 3.9: Angular scattering prediction for an equivalent sphere red cell. The large plot is a linear plot and the inset is represented as a semi-logarithmic scale. A majority of the scattered light is directed in the forward direction within five degrees.

Mie Theory

First published in 1907, Mie theory provides an exact solution to Maxwell's equations for spherical particles and contains information on the refractive index and the absorption coefficient of the materials constituting the particles, as well as, on the absorption and scattering components of the transmitted light.[8,71,72] The optical density (OD), sometimes referred to as turbidity, contains various information about the particulate system being characterized. Given enough information about the system, Mie theory can provide a general solution for its extinction properties with the assumption that the particles in question are isotropic spheres. Mie theory is widely used because of its lack of limitations in two important areas: 1) it is applicable for any size and 2) there are no refractive index constraints.[8,72] The same cannot be said for related

approximations although they are simpler in execution. For example, Rayleigh scattering is limited to particles with diameter (D) << λ (more specifically, it is typically defined as being effective for particles < λ/20) and the refractive index of the particle to be close to that of the medium ($n/n_0 \sim 1$).[8] The Rayleigh-Debye-Gans (RDG) approximation perceives the particle as a body containing multiple scattering centers and allows for the implementation of particle form factors. However, this theory limits analysis to particles where $D \geq \lambda$ and $n/n_0 \sim 1$.[8]

The turbidity (τ) is defined by the equation

$$\tau = N_p \int_0^\infty \frac{\pi}{4} D^2 Q_{ext}(\alpha, m(\lambda)) f(D) dD \qquad \text{(Eq 3.7)}$$

where N_p is particle number per unit volume, D is the particle diameter, $Q_{ext}(\alpha,m)$ is the extinction efficiency which can be evaluated using the appropriate approximation (in our case, Mie theory), α is the size parameter, m is the complex refractive index, and f(D) is the particle size distribution (PSD). The size parameter is a function of wavelength (λ) and is defined as

$$\alpha = \frac{\pi D}{\lambda} \qquad \text{(Eq 3.8)}$$

and the complex refractive index (m(λ)) is

$$m(\lambda) = \frac{n(\lambda) + i\kappa(\lambda)}{n_0(\lambda)} \qquad \text{(Eq 3.9)}$$

where $n(\lambda)$ is the refractive index of the particle, $n_0(\lambda)$ is the refractive index of the medium, and κ is the absorption coefficient of the particle. (See Appendix A for further details of the Mie equations.)

The Mie extinction coefficient (Q_{ext}) is an important term that defines the sum effect of the scattering and absorption components of the particle. Hence,

$$Q_{ext} = Q_{sca} + Q_{abs} \qquad \text{(Eq 3.10)}$$

where Q_{sca} and Q_{abs} represent the scattering and absorption constituents respectively. Thus Equation 3.8 can be separated into two independent terms:

$$\tau = N_p \int_0^\infty \frac{\pi}{4} D^2 Q_{sca}(\alpha, m(\lambda)) f(D) dD + N_p \int_0^\infty \frac{\pi}{4} D^2 Q_{abs}(\alpha, m(\lambda)) f(D) dD \quad \text{(Eq 3.11)}$$

Furthermore, the absorption coefficient of chromophores in solution $\varepsilon(\lambda)$, or Beer-Lambert absorption coefficient is directly related to the Mie absorption coefficient $\kappa(\lambda)$ through Bouger's law

$$\varepsilon(\lambda) = \frac{4\pi\kappa(\lambda)}{\lambda} \qquad \text{(Eq 3.12)}$$

enabling direct comparison of the magnitude of the absorption coefficients for encapsulated chromophores and chromophores in solution.[8]

Through the understanding of the turbidity equation, it is possible to use it in a constructive manner depending on the available information. If an experimental spectrum of a single population particle system is available and the optical properties are known, the size of the particles could be calculated. Conversely, if enough information about the system is obtained through an alternative analysis, it would be feasible to construct a spectrum that would correspond closely with the experimental. The latter

case is considered the "direct problem", where if the particle size, shape, PSD, and composition are given, it is possible to predict the intensity of the irradiance in a given direction. The opposite predicament or the "inverse problem" is far more complex as it demands the elucidation of particle parameters in an experimental spectrum.[8]

Optical Properties

The complex refractive index (Eq 3.9) of a particle is also referred to as its optical properties. The real part of the refractive index, $n(\lambda)$, is the component which describes the scattering capacity of the particle. In order for it to be meaningful, it must be observed against a reference, which in this case is the refractive index of the medium ($n_0(\lambda)$). The imaginary part of $m(\lambda)$, $\kappa(\lambda)$, is the absorption coefficient and is prominent in strong chromophores such as hemoglobin. Consideration of the two parts in combination with complementary parameters helps paint an optical picture of the particle. For example, small spheres absorb proportionally to their volume, whereas large metallic spheres absorb only about half of the radiation striking their surface implying that it is a strong scatterer.[72]

Furthermore, the ratio of the refractive index to that of the medium dictates the sensitivity of the measurement. A high ratio of $n(\lambda)/n_0(\lambda)$ implies a high level of visual contrast of the particle. Erythrocytes contain a significant physiological concentration of highly chromophoric hemoglobin (33%) that account for its prominent visibility under the microscope and also its intense spectra. Additionally, the medium itself is instrumental in the outcome of the spectral data of a suspension. It has been

demonstrated by Garcia-Rubio (1992) that a change in the refractive index of the solvent will cause shifts in optical density peaks, a phenomenon that can be readily corrected for.[73]

As the notation indicates, the complex refractive index is a function of wavelength, thus it is not the same throughout when dealing with multiwavelength spectrographs. Obtaining a full frequency range of reliable optical properties dictates the accuracy of the mathematical estimations. One way is to acquire dependable optical density data on the particle being characterized. In the case of hemoglobin, absorbance spectrum over the entire wavelength (190 – 1100 nm) is obtained experimentally and the extinction coefficient ($\varepsilon(\lambda)$) is generated. Through Bouger's Law (Eq 3.12), $\kappa(\lambda)$ can be calculated. Using the Kramers-Kronig transform, the full multiwavelength complex refractive index can be obtained. In this relationship, if either $n(\lambda)$ or $\kappa(\lambda)$ are known, the unknown parameter may be calculated.[8]

Mie Theory Considerations

Although the Mie theory is a versatile and widely used approximation, it is important to understand that it is not the definitive solution to all particle optics. It may, however, be a powerful tool if used within its constraints and great care is taken in making certain assumptions. One case is the seemingly limited use of the theory on particles which are strictly isotropic spheres. It has been shown, however, that when working with particle sizes in the micron range, the forward scattering becomes dominant (Figure 3.9). Various studies with protein aggregates, platelets, and microorganisms,

have demonstrated that using equivalent-volume spheres produces reliable estimations of the transmission spectra.[9,74,75] The biconcave shape of red blood cells proves to be no different as the studies in this dissertation suggest that the equivalent sphere approximation yields dependable calculations.

Another consideration is the relationship between particle concentration and the light interaction among multiple particles. In theory, it would be easiest to examine the optical behavior of a single particle, but in reality, this is not the case as the particles are suspended in media in numbers. The problem posed by a concentrated particle suspension is presence of the multiple scattering phenomenon. Given that the system is crowded enough, the scattered light will be reradiated by numerous particles, complicating the interpretation of the spectrum. In the case of erythrocytes, it has been determined that diluting whole blood or a red cell suspension to approximately 4000 cells/μl provides enough separation of the cells in the media that it does not give rise to the multiple scattering problem. The value of ~4000 cells/μl is not an arbitrary number. It is a concentration that produces an optical density value nearing the upper limit (1.2) of the linear range of the spectrophotometer. (See Appendix B for details of multiple scattering and instrumental limits in the context of our methods.)

3.3 Spectroscopy of Blood and Erythrocytes

Spectroscopy of Whole Blood

Since blood is one of the most important biological fluids dealt with in clinical settings, much is known about its properties as well as methods of its evaluation. In

terms of optics, Angstrom was the first to use spectroscopic methods to study blood characteristics in 1855, and the spectroscopy of hemoglobin came soon after in 1862.[76] Since this time, advancements in this field of research have brought about various ways of depicting the optical properties of blood components. In terms of optical contributions by cells, erythrocytes which compose approximately 99% of all blood cells, is the major contributor of spectral features. This is further compounded by the fact that the hemoglobin is a strong chromophore. It is not to say, however, that other cells such as leukocytes and platelets are spectrally invisible. The sensitivity of multiwavelength UV-visible spectroscopy allow for the detection of more subtle changes such as leukocyte-depletion. Changes in spectral features as a result of platelet activation can be detected as well, with calculations reflecting the alterations in the platelet count and size due to aggregation.[9] Moreover, the plasma, which is approximately 55% of the total whole blood volume, will contribute absorbance bands in the UV range owing to its protein content.

Spectroscopy of Erythrocytes

The topic of interest in this dissertation is the erythrocyte and its behavior in a field of light. The spectroscopic study of red cells is facilitated by some important properties of red cells: 1) it contains hemoglobin, a strong chromophore, 2) it exists free in a suspension unlike tissue cells hence it can be diluted into the realm of single scattering 3) it can be isolated with relative ease due to its density, 4) there are seemingly no complex internal structures (although the formation of transient structures of

aggregated hemoglobin cannot be completely discounted), and 5) its properties fit within the acceptable limits of the Mie theory. In order to intelligently scrutinize red cells and to be able to make certain well-informed assumptions in relation to spectral characterization, several important parameters must be considered: the hematocrit (i.e. concentration), hemolysis, osmolarity, aggregation, orientation, sedimentation, and deformation of the cells.[76] Hemolysis in the red cell suspension would be evident as a significant hemoglobin band (417 nm) band in the red cell spectra and the investigator must be alert to noticing such changes. Sensitivity to hemolysis would be valuable to the quality control of whole blood in blood banks. Changes in osmolarity would modify both the size and the shape of the cell. Red cells placed in hypotonic media will expand into an ellipsoid and cells in hypertonic media will shrink. A suspension of red cells has been suggested to adopt some degree of organized orientation and a complete optical characterization of red cells would require the interpretation of these orientation effects with respect to the spectral features.[77] For this reason, applying mechanical force to the system in an effort to orient the cells in some uniform fashion should manifest changes in the spectra. Additionally, the density of the cells will cause erythrocytes to sediment to the bottom of the suspension over time. The rate of sedimentation, however, is low and settling takes place over a course of hours.[78] Finally, the flexible membrane of the red cells allows them to deform as they flow through blood vessels. In a relatively static experimental system (suspended in a medium inside of a cuvette), no such force is present to deform the shape of the cell to any significant extent. However, Brownian

bombardment of the membrane cause flickers in the cells that may play a role in its orientation and sedimentation rates.[77]

Erythrocyte modeling has been shown to fit within the framework of the Mie theory. One reason for this success is that red cells do not contain any organelles hence they may be generally treated as homogeneous scatterers. Steinke and Shepherd showed by using single wavelength scattering that the calculated scattering cross section of the RBC can predict experimental values of the cells.[79] The merit of using the Mie theory has been independently confirmed, and the theory has also been applied to two-angle light-scattering measurements for the determinations of hemoglobin concentration and erythrocyte volume.[80,81]

The difference in our approach stems primarily from the analysis of multi-wavelength spectra in the UV, visible, and near-infrared regions. Our efforts exist on a grand scale as we attempt to examine particle characterization across the entire wavelength range of 190 – 1100 nm. In doing so, we hope to gain the knowledge to recognize qualitative spectral features related to hematologic parameters as well as developing the ability to reliably quantify values such as cell volume, cell number, and hemoglobin concentration.

Generally in particle suspension analysis, the optical density of a particle suspension is directly affected by changes in the medium, the shape of the particle, or the chemical composition of the particle.[82] The result may be a shift in maxima, an increase or a decrease in the overall elevation of the spectrum, or the masking or unmasking of absorption peaks by the scattering component. Red cells fall into the regime of

macroscopic particles where scattering eclipses much of its absorptive features, rendering its analysis to be more complex than simply taking the sum of its parts. An important contributor to the large-particle effect of erythrocytes is the hemoglobin encapsulated within the cells. Its strongly chromophoric quality gives rise to whole particle scattering which in turn is related to its high physiological concentrations.

Spectroscopy of Hemoglobin

In order to spectroscopically characterize red blood cells, it is important to first examine the extinction spectrum of hemoglobin. Figure 3.10 shows the multiwavelength extinction spectra of two common hemoglobin derivatives, oxyhemoglobin and methemoglobin. The spectrum of oxyhemoglobin was obtained experimentally by members of our group, using commercially available human hemoglobin A_0 (Sigma-Aldrich). The spectrum of methemoglobin was mathematically acquired.[69] Both spectra agree well with previously published data.[83] The oxyhemoglobin derivative exhibits characteristic bands at 270, 337, 417, 547, and 575 nm. The methemoglobin shows a larger peak around 400 nm that is shifted compared to that of the 417 nm oxyhemoglobin peak. Moreover, the methemoglobin no longer shows that 547/575 nm doublet, characteristic of the oxyhemoglobin. This work uses oxyhemoglobin as the primary derivative in the modeling of red cell spectra. This assumption is accurate since red cells exposed to the atmosphere become almost completely oxygenated. A small amount of the oxyhemoglobin may become oxidized to methemoglobin and this will be examined

briefly by a version of our interpretation model (for the quantification of hemoglobin) in Appendix G.

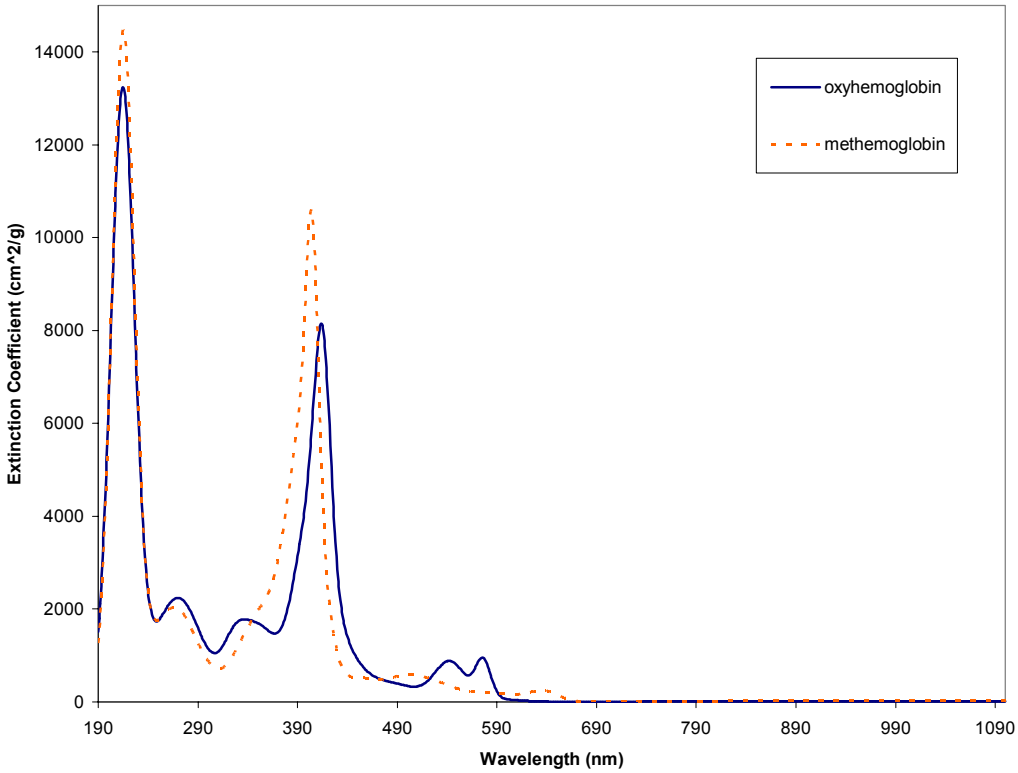

Figure 3.10: Extinction spectra of oxyhemoglobin and methemoglobin. Each has unique features that reflect the characteristics of the heme group.

Hypochromism

Although erythrocytes can be described as translucent biconcave 'bags' containing a homogenous distribution of hemoglobin, this simplicity is deceptive when considering its light scattering properties. Successful characterization and modeling of red cell spectra begins with the acquisition of reliable optical properties for hemoglobin and knowledge of the constraints of our model system. Moreover, when dealing with a strongly absorbing protein such as hemoglobin at high concentrations, we cannot ignore

the possibility of the significance of a hypochromic effect reported in similarly chromophoric biomolecules like chlorophyll and deoxyribonucleic acid (DNA).[84,85,86,87] Hence, *observed hypochromism* is defined as any decrease in the observed absorption coefficient relative to the solution spectrum of the same chromophore (Beer-Lambert). Bear in mind, that this is a specific usage of the term and is different from the decrease in absorbance seen with a proportional decrease in the chromophore concentration.

Early perceptions of the hypochromic effect of biomolecules surfaced in the 1950s and 1960s which largely dealt with the stacking behavior of polynucleotides with respect to optical density.[86,88] Moreover, chlorophyll in chloroplasts was reported to cause permutations in transmission spectra.[85] M*olecular hypochromism* was defined by these studies to be a decrease in absorption (and extinction) due to changes in electronic interactions from altered proximity between chromophores.[5] The studies typically dealt with chromophores in polymeric structures where one absorbing center would shield an adjacent absorbing center such that the second molecule is seeing a local field produced by the neighboring molecule, not the field from the incident light. Although more than one type of interaction influence the change in optical density, the predominant effect is thought to be the Coulombic interaction between the dipoles of the molecules. Lawley (1956) showed this phenomenon with DNA when he compared two different arrangements of the polynucleotides (Figure 3.11).[88] The band of greater amplitude represents DNA in its denatured state. When the nucleotides are stacked in a more ordered double-helix, however, the extinction coefficient decreases by up to 35%.

Vekshin (1999) showed a similar effect by the empirical stacking of adenines into an oliginucleotide.[89] The result is illustrated in Figure 3.12 where the X-axis is the adenine count of poly(A) and the Y-axis is the optical density. As the oligonucleotide chain was increased in length, the optical density at wavelengths of 210 nm and 260 nm

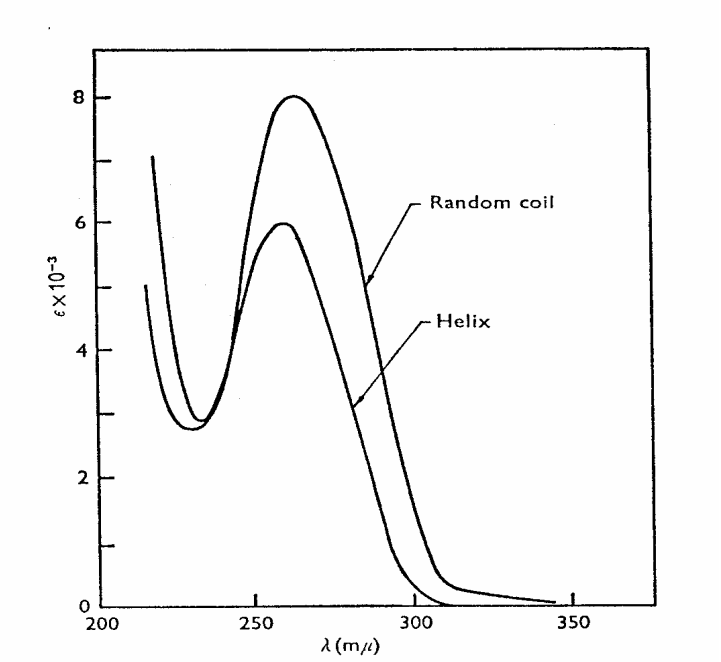

Figure 3.11:[88] An example of molecular hypochromism exhibited by DNA in a double helical configuration. When denatured into a random coil, the DNA shows a higher extinction band.

decreased by as much as 28%. Vekshin proposed a model that accounts for the hypochromic phenomenon not in terms of dipolar interactions but as a probability function describing the likelihood of the k-th chromophore in a stack seeing and absorbing the light that is not shielded by an adjacent chromophore.[90] The probability of absorption of the first chromophore of the stack as a function of wavelength (P1(λ)) is defined as

$$P_1(\lambda) = \sigma(\lambda)/S_1$$

where $\sigma(\lambda)$ is the absorption cross-section and S_1 is the effective geometric area of the chromophore. The probability of light absorption by the k-th chromophore is defined as

$$P_k(\lambda) = [1-P_1(\lambda)]^{k-1}P_1(\lambda)$$

and the probability of light absorption by the whole stack is

$$P_0 = P_1(\lambda) + P_2(\lambda) + \ldots\ldots P_k(\lambda)$$

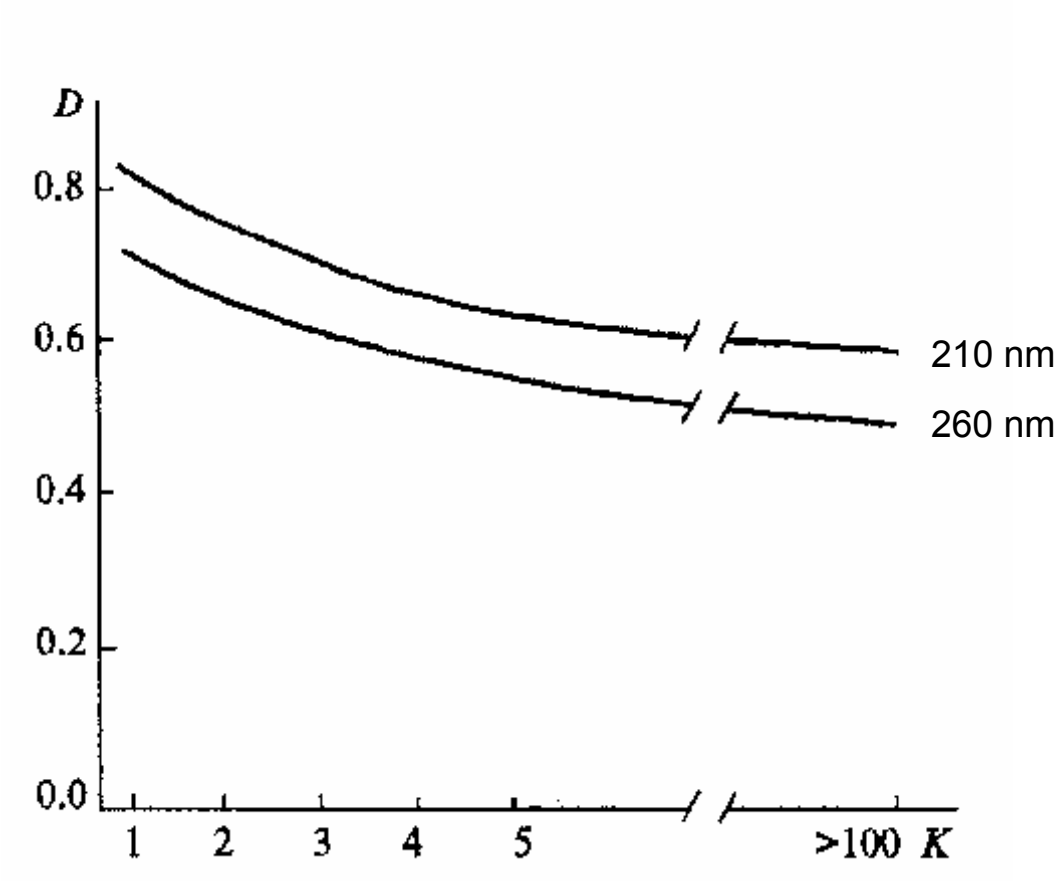

Figure 3.12:[6] The effect of chain length of a polyadenine oligonucleotide on optical density, where the x-axis is the chain length and the y-axis is the optical density. With increased stacking, a molecular hypochromic effect is seen, decreasing the optical density by up to 28%.

In Figure 3.13, Vekshin showed that his model was able to account for the molecular hypochromism of stacked poly(A) oligonucleotides.[6] Curve 1 shows the extinction spectrum for of adenosine and curve 2 is the spectrum for penta-adenosine phosphate. The stacked nature of the penta-adenosine properly shows the expected hypochromism. Furthermore, the calculated prediction of the penta-adenosine (curve 3) fits the experimental data fairly well.

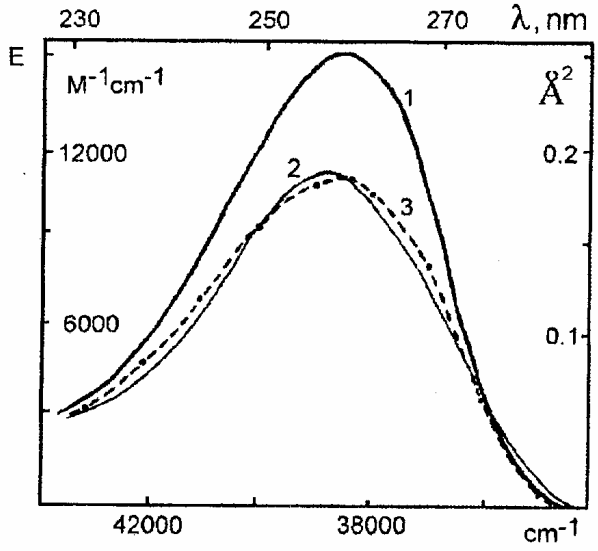

Figure 3.13:[6] Theoretical vs. experimental spectra of poly-adenosine stacks. Curve 1 is experimental data of single adenines and curve 2 is that of penta-adenosine stacks. The molecular hypochromism is evident in the stacks. Curve 3 is a theoretical calculation of the penta-adenosine spectrum using Vekshin's model.

In terms of hemoglobin, its high extinction coefficient raises the question of potential molecular hypochromism. At low concentrations of hemoglobin on the order of spectral dilutions (< 15 mg/ml), the molecules are dispersed enough so that no significant stacking or dipolar interactions are present. With increasing concentrations approaching the physiological value of ~33% (330 mg/ml), the molecules reside significantly close to

one another. Nonetheless, contrary to the fixed nucleotides of a helix where the partially stacked bases are in Van der Waals contact, hemoglobin encapsulated in red blood cells presumably exist as independent proteins with their intermolecular distance estimated to be 62 – 75 Å[36,91] (compare to hemoglobin dimensions of 64 x 55 x 50 Å).[28,38] Under such conditions, random collisions are prevalent, however, the effect of organized molecular hypochromism is questionable.

Studies based on the Mie theory done by our group predicted a decrease in the absorption component of hemoglobin when encapsulated in erythrocytes, an event that can be accounted for by a second classification of observed hypochromism: *macroscopic hypochromism*. This is defined as a phenomenological decrease in the absorption due to the combined effects of absorption and scattering of chromophores in aggregated and encapsulated systems. The effect is directly related to the size of the particle and the refractive index of the particle both of which describes whole particle scattering. Such effects could be implicated in erythrocytes, given their size and chemical composition. Mie theory converges to the Beer-Lambert law under the conditions that the molecular size approaches zero and the particle-to-medium refractive index ratio (n/n_0) approaches one.[73,92] This means that the optical density of the system is a direct result of the absorption component, with the scattering component becoming negligible. However, as the encapsulated hemoglobin concentration is increased, our Mie-based simulations suggest that a scattering-related decrease in absorption transpires.

Historically, spectroscopic work has been done on red blood cells with mixed results due to conflicting interpretations of models and/or experimental systems. Kramer

et al. (1951)[93] suggested that non-hemolysed blood does not follow the Beer-Lambert Law due to its scattering properties and "by the magnified absorption of light by intracellular hemoglobin due to the refraction of light between and within erythrocytes." The paper attributed part of the attenuation of the transmitted light to an increase in light absorption. Anderson and Sekelj (1967) observed undiluted blood in an integrating sphere spectrophotometer.[94] By implementing a model correcting for the multiple scattering effects of the concentrated particulate system, Anderson and Sekelj showed that the absorption of light was the same in both an erythrocyte and a hemoglobin solution. In contrast, our studies using the Mie theory suggested that the high refractive index difference between the erythrocyte and the medium resulted in the dominant contribution of the scattering component with very little chromophore sampling by the light. The deconvolution of spectra by means of light scattering theory supports this idea. The question of hypochromicity bears multiple layers:

1. In an encapsulated system such as red blood cells, do the internal chromophores exhibit molecular hypochromism as suggested by other studies or can it be explained by the scattering theory as macroscopic hypochromism (or a combination of the two)?
2. In studies examining the hypochromism of red cells and related macroscopic particle systems, many fail to detail the instrumental configuration of their experiments. That is, the angle of acceptance of the detector is not properly defined, hence what has been perceived as molecular hypochromism may be an

issue of improper interpretation of data in the context of instrumental configuration.

Considerations of Instrumental Configuration

The interaction of light with particles results in absorption and scattering phenomena; particles scatter light in all directions and, depending on the experimental set-up, changes in the properties of the scattered light relative to the incident light may be measured as a function of the observation angle. For finite aperture detectors, the angular resolution of the scattered light depends on the acceptance angle (γ) of the detector. Therefore the detector response is proportional to a weighted average of the scattered intensity over the angles defined by its aperture; a limiting case being measurements with an integrating sphere where essentially all scattered light is measured and subtracted from the transmitted light to obtain estimates of the attenuation due to absorption. The angle of acceptance is defined in Figure 3.14 and it is related to the radius of the detector and the distance of the sample to the detector, where 0^o is the direction of the incident light. The importance of the acceptance angle stems from the inherently pronounced light scattering properties of macroscopic particles as they change in size and refractive index. Associated with such change is the angular dependence of scattering and the effectiveness of the data interpretation would be a direct correlation to the awareness of photometer design. Latimer (1975)[95] detailed the importance of considering the angle of acceptance of the detector, however his work has been largely ignored.

Optical scattering analyses of erythrocytes have typically been limited to a single wavelength[79] or to a small number of select wavelengths,[80,81,96] while multiwavelength representations have been reported as diffuse spectra.[6,7] Diffuse transmission spectra (DTS) results from the acquisition of a large amount of scattered light at wide

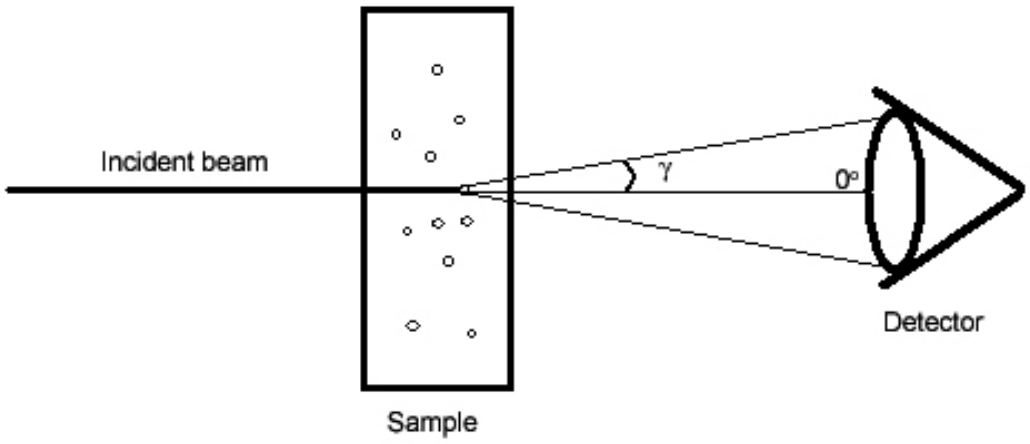

Figure 3.14: Schematic representation of the angle of acceptance. The size of the detector radius determines the amount of scattered light captured by the spectrophotometer.

angles and is typically defined by the angle of acceptance of the detector.[82] The collection of diffuse scattering plays an important role in the features of an optical density spectrum of a macro-particle system. Light collected by a small acceptance angle shows a general increase in the OD and a larger addition of the scattering component compared to that obtained with a larger detector angle.[97] In contrast, data for red cells reported as a DTS shows an overall decrease in the intensity of the spectrum. This is because as scattered light is collected at more angles, the light is averaged out and is subtracted out of the transmission spectrum. Since a small angle transmission spectrum (SATS) collects

less of the scattered light, the weighted average of the uncollected scattered light is not subtracted from the transmission spectrum. Therefore, it is possible to infer the amount of light scattered at angles greater than γ and to successfully deconvolute the spectrum into its absorption and scattering components.

A misconception in the use of OD data of suspensions is that the scattering component is a confounding constituent devoid of any significant information, and thus eliminated by a simplified scattering correction, such as in the case of Leach and Sheraga (1960).[98] Spectra of particle suspensions corrected in this manner typically reveal absorption bands of decreased magnitudes and introduce a need for an empirical correction factor to provide relevant quantitative information. By accounting for both the absorption and scattering components of the spectrum using the light scattering theory, apparent alterations in absorption can be justified.

Defining the Problems

Although the task of spectroscopically characterizing red blood cells seems quite straight-forward, there are a number of confounding issues associated with fact that the cells are significant scatterers of light. These issues are detailed here.

1. It is necessary to determine the best instrumental configuration for the examination of our particle suspension. Since red cells scatter light, it is important to know the acceptance angle of the spectrophotometer, and at what acceptance angle the OD spectrum contains the most complete absorption and scattering information.

2. The examination of molecular hypochromism in a hemoglobin solution is not possible due to the limitations of the instrument and the high extinction values (see figure 3.10). The upper concentration limit for the small doublet peaks (500 – 600 nm) using a 1 mm pathlength cuvette is ~14 mg/ml. The upper limit for the larger 417 nm band is even lower at ~1.5 mg/ml (1 mm pathlength). This is not close to the physiological concentrations of ~330 mg/ml.
3. Obtaining spectra of free hemoglobin is not a good representation of its optical behavior when encapsulated within red cells. Hemoglobin molecules free in solution are small, Rayleigh scatterers and their spectra are represented by their dominant absorption features. However, when they are encapsulated, they affect the refractive index of the cell, contributing to the macroscopic whole particle scattering properties of the cell.
4. An effective experimental model system needs to be implemented in order to optically characterize the red blood cell and to allow for the evaluation of hypochromism. Corroborative methods for important particle parameters such as cell count, hemoglobin concentration, and cell size must be established to complement the experimental system.
5. A dependable theoretical model relying on light scattering theory is necessary to evaluate the experimental data. Mie theory, based on spherical particles of equivalent volume, has been successfully tested on particles of smaller refractive indices (platelets, microorganisms). The theory must be tested on red blood cells for compatibility.

Experimental and Theoretical Approach

With the problems clearly defined, a multi-pronged approach was devised employing experimental methods in combination with theoretical interpretation. This approach is outlined as follows:

1. Red blood cell samples were examined in commercially available spectrophotometers bearing different acceptance angles to demonstrate the importance of optical configuration on spectral features.
2. Red blood cells were permeabilized and resealed to obtain modified hemoglobin concentrations.
3. Lipid vesicles (liposomes) were used to encapsulate varying concentrations of hemoglobin or other model protein. (See Appendix C)
4. A mathematical model based on the light scattering theory was used to simulate and interpret spectra of the experimental model systems.

An examination of the significance of instrumental design was performed using three spectrophotometers with different angles of acceptance. Purified red cells diluted to the same concentration under the same conditions were analyzed on all three spectrophotometers and compared. Each spectrum was also compared to a spectrum of free hemoglobin in solution with the mass held constant. The results obtained from this study allowed us to determine the optimal photometer design for red cell characterization and to verify the reliability of previously published studies.

The next proposed experimental approach was to isolate red cells and manipulate the hemoglobin concentration across various ranges to examine its spectral manifestations. A modified protocol was established for this purpose. The red blood cells were permeabilized in a hypotonic buffer solution to cause the cells to spill out hemoglobin in different amounts. The partially drained cells were then forced to reseal by restoring the tonicity of the solution. The result was red cells containing modified amounts of hemoglobin.

It may appear that the characterization of unmodified erythrocytes alone is enough to answer most questions, but it will not present the complete picture. If our knowledge is limited to normal physiological parameters, applications of this analysis cannot be extended into abnormal values. It is also in the interest of pure science to broaden the limits of the study as wide as possible. Hence the target of the red cell modifications was to achieve encapsulated hemoglobin concentrations in the medium range (MCHC ~ 15-20% w/v) and in the low range (MCHC ~ 5-10% w/v) to characterize a trend, if any, in the absorption and scattering components of the optical density spectra.

A theoretical model based on the Mie theory was used to analyze the spectra acquired from the modified red cells. Using the particle parameters obtained from a hematology analyzer (see Chapter 4), the model was used to simulate features and trends seen in the experimental data. Moreover, the Mie theory was extended to interpret the spectral data to elucidate values for particle parameters such as particle count, particle size, and hemoglobin concentration.

Finally, the possibility of using a liposome model to encapsulate hemoglobin and model proteins was explored (Appendix C). Results showed, however, that the liposomes were hard to characterize optically due to their multi-lamellar nature and small size (10^{-9} m diameter). Although extended work on the liposome model would have resolved such issues, the modified red cell approach in combination with the theoretical model offered conclusive answers to the problems defined in the previous section.

Chapter 4: Spectrophotometry of Purified and Modified Red Blood Cells

4.1 Hypotonic Modification of Erythrocytes

Hypotonic modification of red cells has been used for various purposes including loading the cells with isotope-labeled hemoglobin, hemoglobin S and C, dextran, ferritin and enzymes.[99,100,101,102,103] The biological tool has demonstrated its usefulness in different ways, ranging from model systems of membrane behavior to delivery devices for enzyme therapy. The manipulable characteristics of the red cell membrane proved to be advantageous in modifying the encapsulated hemoglobin concentrations thus we have developed a protocol exclusively for the purpose of our investigation.

The erythrocyte membrane under native conditions is normally not permeable to large proteins such as hemoglobin. Upon addition of a hypotonic buffer, however, the change in the osmotic pressure on the outside environment will cause water to enter through the semi-permeable membrane and instigate cell swelling. The osmotic pressure (π) can be defined by the equation π=MRT where M is the molarity of the solution, R is the ideal gas constant (0.0821 L-atm/mole-K), and T is temperature in Kelvin.[63] Thus in a hypotonic medium, the internal osmotic pressure of the cell will become greater than that of the medium ($\pi_{int} > \pi_{ext}$), initiating the flow of water into the cell (Figure 4.1). When the internal pressure is great enough, the membrane produces holes of roughly 200

- 500 Å allowing the passage of large molecules.[101] Seeman (1967) reported that the holes were transient and exist only for 15 – 20 seconds following the hypotonic shock.[104] During this time, a chemical gradient generates the flow of material in and out of the cell. Tonicity is then restored to isotonicity (0.9% ionic strength) to assist in the resealing of the cell.[100,101,113]

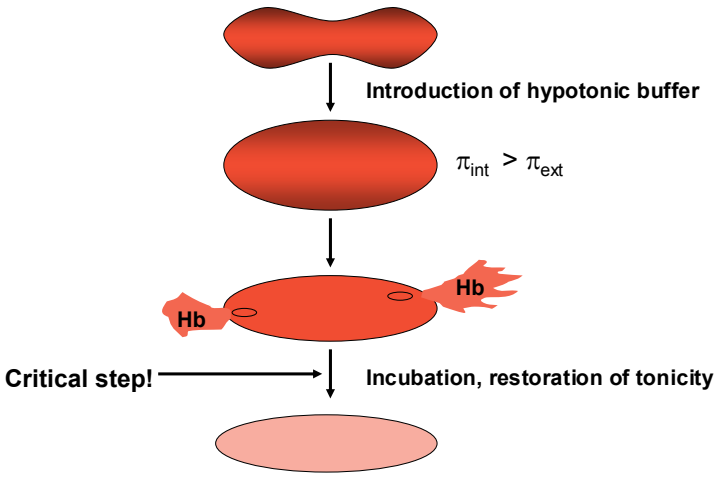

Figure 4.1: Illustrated representation of the hypotonic permeabilization of red blood cells. The final hemoglobin concentration in the restored cells is controlled by the time of incubation after the cells are permeabilized.

According to a study by Bodemann and Passow (1971), the hypotonic shock procedure produces three types of cells: type I are cells that reseal relatively quickly following hemolysis, type II cells reseal after restoration of the media to its original ionic strength, and type III are cells that remain lysed and never reseal.[113] Temperature conditions during the experiment affect cell resealing as well. At 0 ^{o}C, there are virtually

no type I cells but mostly type II whereas experiments done at 37 ^{o}C show that the proportion shifts in favor of type I cells. Furthermore, the permeabilization step performed at 0 ^{o}C and 25 ^{o}C show the presence of approximately 38% type III cells, but cells modified at 37 ^{o}C show that 75% of the cells are type III.

The purpose of our red cell modification was not to load the cells with foreign molecules, but to reduce the internal hemoglobin concentration for spectral interpretation (i.e., hemoglobin out, H_2O in). Thus a modified protocol was established. The method had three distinct steps: 1) hypotonic shock, 2) incubation, and 3) restoration of tonicity for resealing (Figure 4.1). It was found that the resulting hemoglobin concentration of the restored cells could be controlled by managing the volume of hypotonic buffer, and the incubation time. For a desired MCHC in the low range (~ 0.05 – 0.15 mass fraction), a relatively large volume of buffer was used for permeabilization and the sample was incubated for 30 minutes on ice prior to the resealing step. In this case, the hemoglobin concentration gradient is large and the low temperature maintains the membrane holes while the gradient is allowed to equilibrate. If a higher MCHC was intended, smaller volumes of hypotonic buffer and shorter incubation times were used (such as a 1:1 volume ratio of packed red cell to hypotonic buffer). (See Materials & Methods section for details.) The ability to obtain encapsulated hemoglobin concentrations from physiological values (~ 0.33 mass fraction) down to very low mass fractions of ~ 0.05 provides a valuable opportunity for the fundamental investigation of hypochromism.

4.2 Materials and Methods

The UV-Visible Spectrophotometer

The spectral measurements represented in this dissertation were performed predominantly on a Hewlett Packard/Agilent 8453 diode array spectrophotometer. The unit houses a single levered cuvette slot (Figures 4.2 and 4.3) and generates optical density values across a wavelength range from 190 nm to 1100 nm. The spectrophotometer is interfaced to a personal computer loaded with the Agilent Chemstation software which is capable of customizable spectral processing.

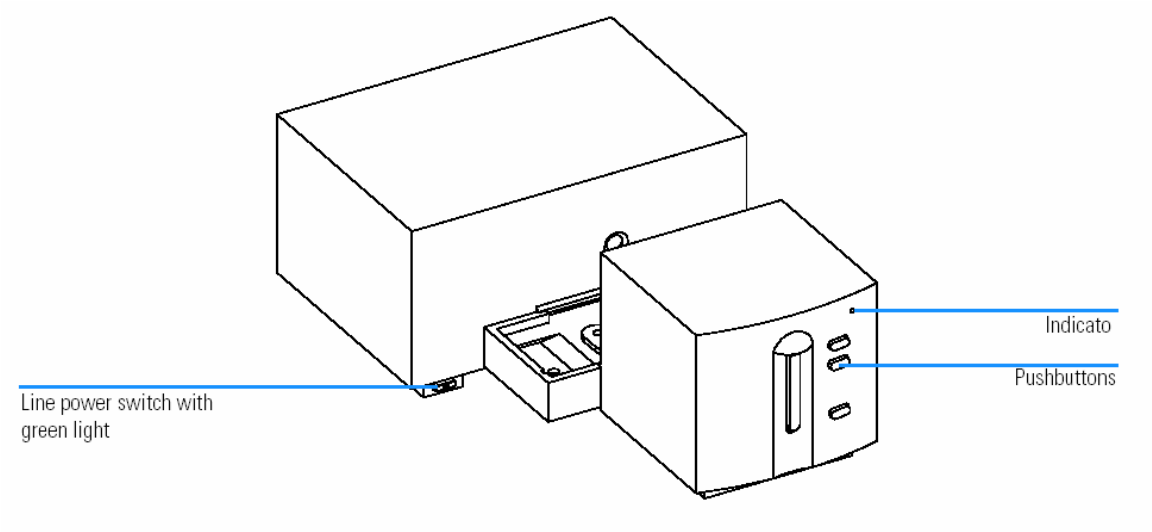

Figure 4.2:[105] The front view of a Hewlett Packard/Agilent 8453 Spectrophotometer

Figure 4.4 illustrates the optical arrangement of the spectrophotometer. The radiation emissions come from two sources: a deuterium lamp and a tungsten lamp. The deuterium lamp emits light radiation over a wavelength range of 190 nm to 800 nm and the tungsten lamp contributes radiation in the higher wavelengths from 370 nm to 1100

nm. The wavelength range of the deuterium lamp corresponds to the ultraviolet and visible regions whereas that of the tungsten represents the visible and the near-infrared regions.

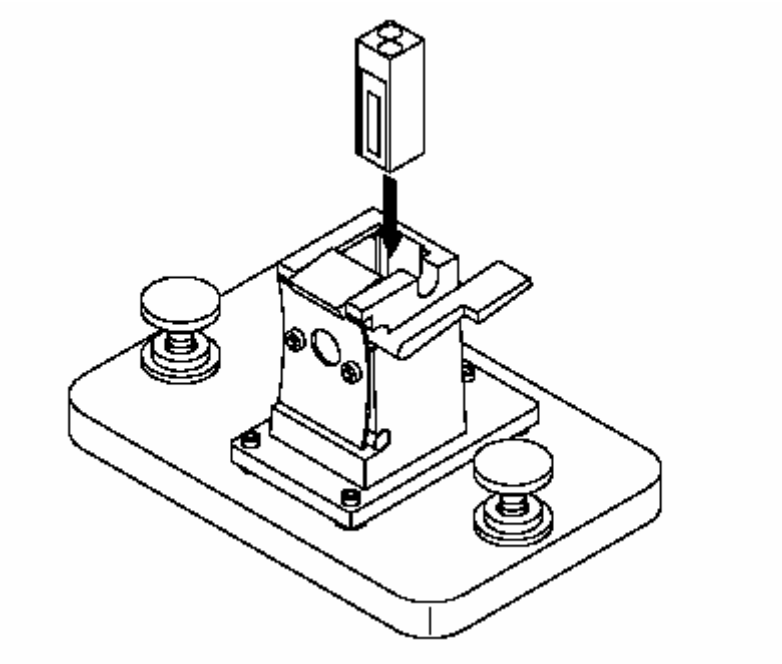

Figure 4.3:[105] Cuvette slot of an HP/Agilent 8452 spectrophotometer with a levered locking mechanism.

As the source radiation is emitted, the source lens collimates the light aimed to pass through the sample. The shutter opens to allow the light to propagate towards the sample and close as soon as the measurement is finished. Once the incident light passes through the sample, the transmitted light is passed through a spectrograph source lens which refocuses the light towards the slit. The slit is a small aperture which

limits the size of the incoming beam and prepares it for the grating, which in turn separates the light into its full array of wavelengths. The diode array detects the full spectrum of wavelengths and transmits the information to the interfaced computer where it can then be manipulated for analysis.

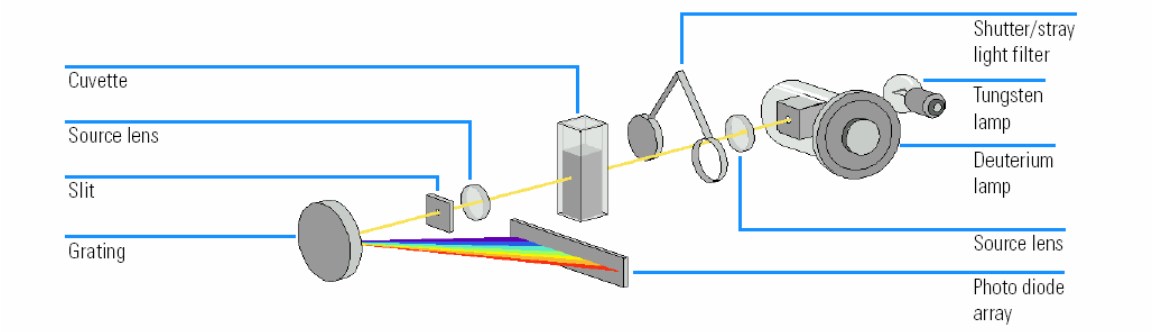

Figure 4.4:[105] The optical machinery of the HP/Agilent 8453 spectrophotometer.

Types of Spectrophotometers Used

The Agilent 8453 spectrophotometer with a 2^{o} angle of acceptance was the primary instrument used for data acquisition and analysis. However, an important aspect of our investigation related to apparent hypochromism was suspected to be a result of instrumental configuration. We therefore employed two alternate spectrophotometers with varying setups. Diffuse transmission spectra were obtained using the Perkin-Elmer Lambda 900 (Perkin-Elmer, CT) spectrophotometer. The sample cuvette was placed in front of an integrating sphere module and the diffuse spectra was acquired by the light being transmitted across the sphere (acceptance angle > 2^{o}). The Perkin-Elmer Lamda

18 fitted with an integrating sphere module (RSA-PE-18, Labsphere, NH) was used to collect essentially all of the light scattered by the suspension.

Care and Preparation of the Cuvette

The cuvettes used in this project are quartz cuvettes (Starna Cells Inc, CA) which allows for sample reading in the ultraviolet, visible, and near-infrared wavelength ranges. Cuvette capacities are typically 3 ml and 1 ml, both with a 1 cm pathlength. The cuvettes are handled and stored with care, cleaning as often as necessary to prevent build-up of protein deposits on the walls. An effective cleaning method is sonication in dilute soap water for approximately 30 minutes followed by a methanol wash to eliminate any water-insoluble contaminants. To ensure that this method does not lead to surfactant build-up, an occasional and brief (1 minute) treatment with chromic acid is recommended. In between experiments, the cuvettes are routinely filled and stored with deionized water to prevent any residual proteins and other contaminants from drying and adhering strongly to the walls. Such a preventative measure facilitates the cleaning process prior to each experiment.

Preparation for Spectrophotometry

Prior to experiments, the spectrophotometer was switched on and allowed to warm up for approximately 20-30 minutes, which is a conservative time frame compared to the manual's suggestion of 15 minutes. This allowed the lamps to reach their full intensity and provide reliable spectra. Once the lamps were ready, a blank was taken

without a cuvette inserted into the compartment to provide the spectrophotometer with a point of reference. A good blank should show a relatively uniform baseline throughout the spectrum (Figure 4.5).

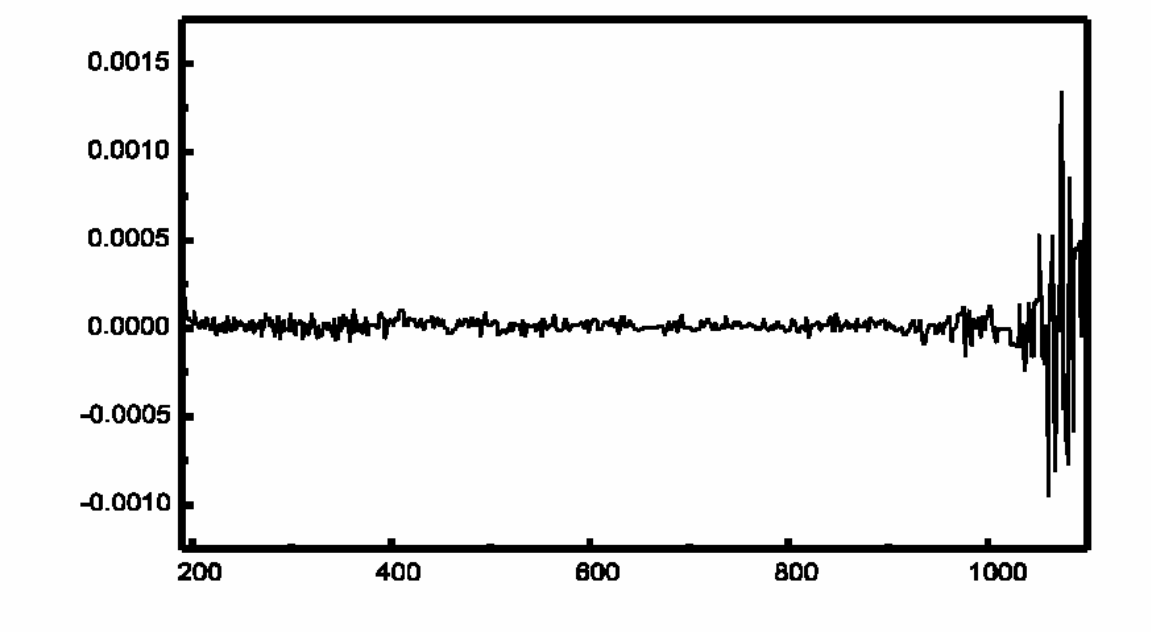

Figure 4.5:[105] A representative blank spectrum used to correct for ambient conditions prior to sample measurement, where the X-axis is the wavelength in nanometers, and the Y-axis represents optical density units.

Spectrum of Deionized Water

Prior to taking the first sample spectrum of the day, a clean cuvette was rinsed repeatedly with deionized water and then was filled to approximately two-thirds of its capacity with the deionized water (the level must be high enough for the incident beam to go through the sample).

The spectrophotometer was configured to an integration time of 15 seconds. Since the HP 8453 spectrophotometer takes ten complete multiwavelength scans over one second, a 15 second integration time produces a spectrum which is an average of 150 consecutive scans. The output file provides the mean and standard deviation of the total number of scans per wavelength.

The deionized water was scanned in the spectrophotometer and the resulting spectrum served two purposes. The first was to guarantee the proper functionality of the instrument by ascertaining the consistency of the background water spectrum from experiment to experiment. The second purpose was to evaluate the cleanliness of the cuvette. Figure 4.6 shows a representative spectrum of deionized water in a clean cuvette. The optical density value at 190 nm should typically be below 0.25 AU. The peak located at approximately 980 nm is characteristic of water and is seen in spectra taken with a 1 cm pathlength cuvette. A 1 mm pathlength cuvette is not sufficient to show a prominent peak. Evidence of impurities would usually show in the absorption range roughly between 200 and 500 nm. This is not to say that absorptions do not occur past 500 nm, however, Soret bands of chromophoric proteins are more commonly in the UV and low visible wavelength range, and slight contamination on the walls of the cuvette would show up as small bumps or elevations of the baseline in that region.

Background Correction

Once the cuvette was verified to be clean, the spectrum for the solvent background was established so that the background correction could be implemented to

the spectral analysis. The cuvette was washed a few times with the solvent which is most commonly isotonic (0.9%, pH 7.0-7.2) blood bank phosphate buffered saline (PBS) obtained from Nerl Diagnostics, RI. The PBS was composed of 0.150 M sodium chloride, 0.006 M sodium diphosphate, and 0.002 M potassium phosphate. The PBS was

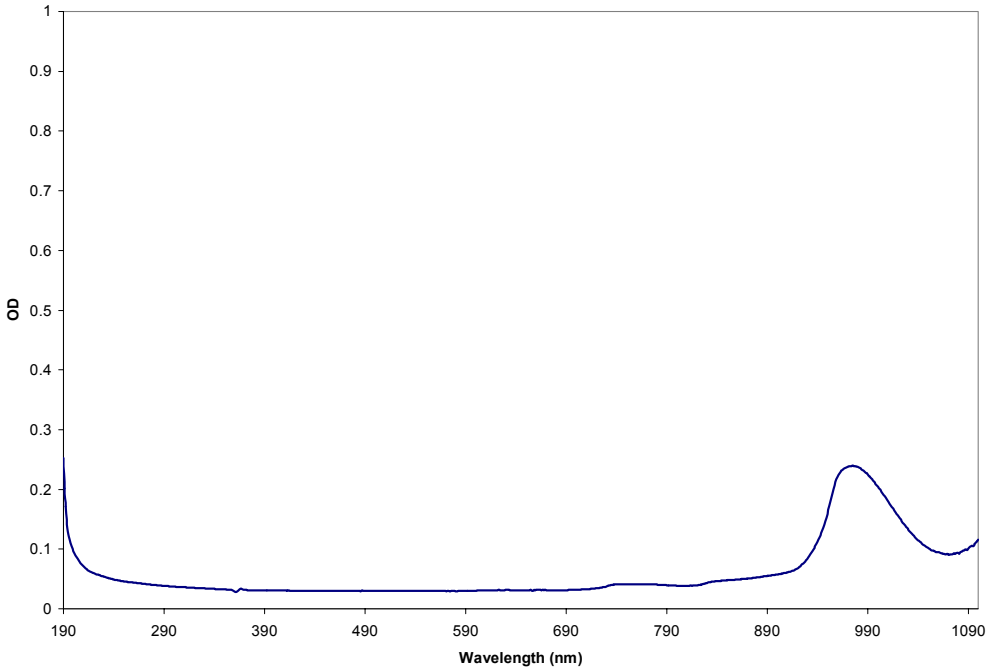

Figure 4.6: Representative spectrum of deionized water. This is an important step taken prior to any experimentation to ensure the cleanliness of the cuvette. Any contamination will show up as slight peaks, typically in the UV and low visible wavelengths.

scanned for 15 seconds in the spectrophotometer and obtained a spectrum represented by Figure 4.7. The water peak at around 980 nm was still evident. The ionic interactions of the sodium chloride (NaCl) produced an intense, saturated peak below 210 nm. The saturation occurred when the absorption intensity exceeded the linear range of the

instrument (upper limit: 1.2 OD), hence this region lacks reliable information about the system (see Appendix B for explanation of instrumental linearity).

The saline spectrum was saved as an auxiliary file in the Hewlett Packard Chemstation software. The software was customized so that this background (auxiliary) spectrum is automatically subtracted from each scanned sample. The auxiliary spectrum was updated three or four times during the experiment to account for any unforeseen changes in the instrument (i.e. lamp intensity), the cuvette, or ambient lighting in the room. The most common sign for the spectrum to be updated was when parts of the

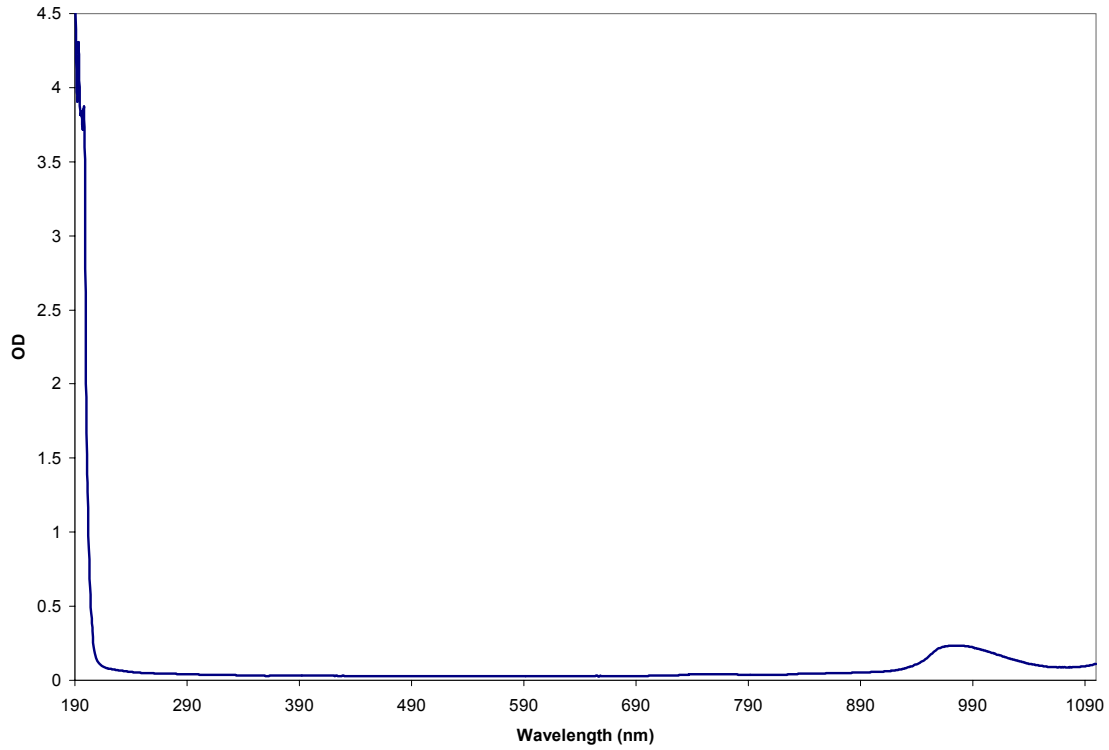

Figure 4.7: Representative spectrum of isotonic (0.9%) PBS (pH 7.0-7.2). Features include the water peak around 980 nm and a saturated peak below 210 nm.

baseline of the processed spectrum dipped below zero. Visual examination of the solvent in the cuvette was also conducted consistently to ensure that any scatterers such as dust particles were not present to elevate the baseline of the auxiliary spectrum.

Hematology Analyzer

The major method of experimental corroboration was performed with the hematology analyzer model 9110+ (Serono-Baker, PA). The instrument is primarily a cell counter, giving cell number and cell volumes by means of electrical impedence. Reagent flows through an aperture between electrodes that conduct a constant electrical current. The homogeneity of the reagent (free of contaminations) keeps the current consistent and establishes a baseline. As biological cells are introduced into the system and flow through the electrical field, they act as partial insulators and temporarily increase the electrical potential. The magnitude of the circuit resistance is directly proportional to the cell volume and is compared against a calibration to give the mean cell volume. The number of cells passing through the aperture per unit sample volume is also quantified to yield the cell counts. A discriminating threshold system for size ranges is used to categorize the results into red cells, white cells, and platelets, and eliminate any possible detection of debris.[106]

A modified Drabkin's solution is used for quantification of hemoglobin.[106] The red cells are lysed and the hemoglobin is converted to cyanomethemoglobin by the solution. An optical density reading is taken at 540 nm and compared against a

calibration, where the absorbance value is directly proportional to the concentration of hemoglobin in the blood sample.

The readout of the Serono-Baker provides the following information (Figure 4.8):

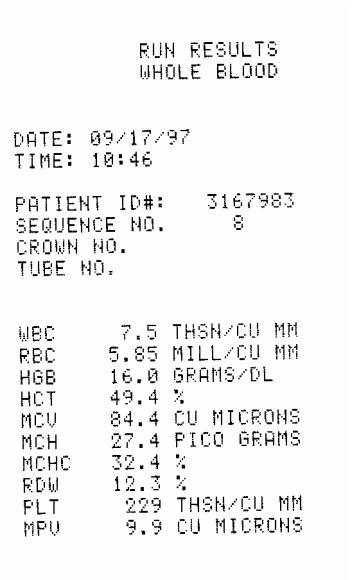

```
                RUN RESULTS
                WHOLE BLOOD

DATE: 09/17/97
TIME: 10:46

PATIENT ID#:    3167983
SEQUENCE NO.       8
CROWN NO.
TUBE NO.


WBC      7.5 THSN/CU MM
RBC     5.85 MILL/CU MM
HGB     16.0 GRAMS/DL
HCT     49.4 %
MCV     84.4 CU MICRONS
MCH     27.4 PICO GRAMS
MCHC    32.4 %
RDW     12.3 %
PLT      229 THSN/CU MM
MPV      9.9 CU MICRONS
```

Figure 4.8: A sample readout obtained from the Serono-Baker hematology analyzer.

where WBC is white blood cell count, RBC is red blood cell count, HGB is hemoglobin concentration in solution once the cell is lysed, HCT is hematocrit, MCV is mean corpuscular volume, MCH is mean corpuscular hemoglobin, MCHC is mean corpuscular hemoglobin concentration, RDW is red cell distribution width, PLT is platelet count, and MPV is mean platelet volume.

Although the instrument is typically used to analyze physiological values in clinical settings, it can reliably detect values beyond normal ranges. The linear ranges of the analyzer for some important parameters are defined in Table 4.1. The error of the instrument is defined per parameter in the brochure of the Para 12 Multi-parameter

Assayed Hematology Control (Streck Laboratories, La Vista, NE) and are shown in Table 4.2 in the context of normal physiological values. In Table 4.3, a six- replicate analysis of the same whole blood sample was obtained from the Serono-Baker system.

	Linearity Range
RBC	0.45 – 7.26 mill/µl
HGB	0.1 – 30.0 g/dl
PLT	20 – 1071 thsn/µl

Table 4.1: Linearity ranges for some important parameters of the Serono-Baker hematology analyzer.

	Mean ± error
RBC	4.17 ± 0.020 mill/µl
MCV	85.6 ± 4.0 fl
MCHC	33.9 ± 2.3 % (w/v)
HGB	12.1 ± 0.4 g/dl
PLT	237 ± 30 thsn/µl

Table 4.2: Error of the parameters of Serono-Baker hematology analyzer outputs as defined by the Para 12 Multi-parameter Assayed Hematology Control. The control represents normal physiological values.

	Mean ± error
RBC	4.99 ± 0.077 mill/µl
MCV	91.9 ± 0.4 fl
MCHC	32.3 ± 0.4 % (w/v)
HGB	14.8 ± 0.1 g/dl
PLT	216 ± 3 thsn/µl

Table 4.3: Error of the parameters of Serono-Baker hematology analyzer outputs calculated from 6 replicates of the same sample.

The manual analysis typically showed smaller error compared to those reported by the control manufacturers, with the exception of the RBC count. It should be noted, however, that six replicates of one patient sample does not necessarily represent larger test batches.

Drabkin's Hemoglobin Determination Assay

A manual assay was employed throughout the experimentation for two reasons. The first was to supplement and verify the hemoglobin concentrations obtained by the Serono-Baker hematology analyzer. The second was to acquire hemoglobin concentrations for steps in which use of the hematology analyzer was not feasible. For example, the hematology analyzer only accepted samples in the form of a particle suspension. Therefore, free hemoglobin solutions not encapsulated in cells could only be analyzed using the manual Drabkin's assay.

The kit used for the manual Drabkin's hemoglobin assay (HG980) was obtained from Randox Laboratories Ltd, UK. The method used a colorimetric assay that was standardized by the International Committee for Standardization in Haematology.[46,47] The principle of this assay is based on the fact that all derivatives of hemoglobin with the exception of sulfhemoglobin are capable of being converted to a stable form of cyanomethemoglobin. Since in most cases, the sulfhemoglobin content is negligible, the method is effective in quantifying the total hemoglobin concentration, typically in percent (%), or grams of hemoglobin per deciliter of solution (g/dL).

The kit included concentrated Drabkin's reagent (52 mmol/L potassium phosphate, 30.4 mmol/L potassium ferricyanide, and 38.4 mmol/L potassium cyanide), Brij-35 solution (detergent, 25%), and methemoglobin standard (18 g/dL). The standard was used to generate a calibration curve to which the unknown data can be compared for quantification. The working Drabkin's solution was mixed by adding the contents of one 20 ml bottle of concentrated Drabkin's reagent to 980 ml of deionized water and 0.5 ml of Brij-35 solution.

For the calibration curve, four tubes were prepared and the standard solution was mixed with Drabkin's solution according to the specifications indicated in the table below (Table 4.4):

Tube NO.	Standard Solution (ml)	Drabkin's Solution (ml)	Blood Hemoglobin (g/dl)
1	0.0	6.0	0.0
2	2.0	4.0	6.0
3	4.0	2.0	12.0
4	6.0	0.0	18.0

Table 4.4: Recipes for the mixing proportions of each tube to obtain the concentrations in the Blood Hemoglobin column. The absorbance measurements obtained from each tube will be used to generate the standard curve.

Each of the tubes was mixed well by inversion and was allowed to stand at room temperature for approximately 15 minutes to ensure total conversion of the methemoglobin to cyanomethemoglobin. The samples were then scanned in the spectrophotometer, using the Drabkin's solution as the auxiliary spectrum for background correction. The optical density values at a wavelength of 540 nm were collected and

these values were plotted as a function of concentration. The resulting extrapolated line was expected to pass through the origin. The equation of the line served to evaluate the concentrations of unknown solutions by obtaining the optical density value at 540 nm.

The unknown samples being assayed could either be free hemoglobin or hemoglobin encapsulated in red cells. The latter is feasible because of the presence of the detergent (Brij-35) in the reagent. The amphiphilic detergent molecules will disrupt the membrane, forming detergent-lipid-protein micelles and bursting the cells.[107] The cells spill their hemoglobin content in solution where it will be first oxidized to methemoglobin, then converted to cyanomethemoglobin. For the assay, suggested volume ratios for Drabkin's to sample are 5.00 ml : 0.02 ml, or 2.50 ml : 0.01ml. The former ratio was used because larger quantities will render small errors negligible. Once mixed, the sample was allowed to stand in room temperature for approximately 20 minutes and then a spectrum was obtained and background-corrected with the Drabkin's reagent. The OD value at 540 nm was converted to a concentration using the equation for the standard curve.

It was important to note that the concentration obtained from a suspension of red cells using this assay did not directly reflect the mean corpuscular hemoglobin concentration. The acquired value represented the hemoglobin concentration in the original sample if the cells were completely lysed and the hemoglobin was diluted in the media. This value was the same as the HGB parameter obtained by the hematology analyzer. Calculation of the MCHC required the relationship

$$MCHC = (HGB \times 100)/HCT \text{ (L/L volume fraction)}$$

where HGB is g/dl and MCHC will be reported as g/ml. The hematocrit (HCT) was acquired by the hematology analyzer, hence may introduce instrumental bias into the calculated MCHC.

Calibration of Conductivity Meter for Ionic Strength Measurements

For the purpose of determining the ionic strength of prepared saline solutions, Conductivity Monitor Model #1670440 (BioRad, CA) was used to prepare a calibration curve using carefully prepared dilutions of stock 0.9% (determined by the company for the particular lot used) isotonic phosphate buffered saline at room temperature. The stock

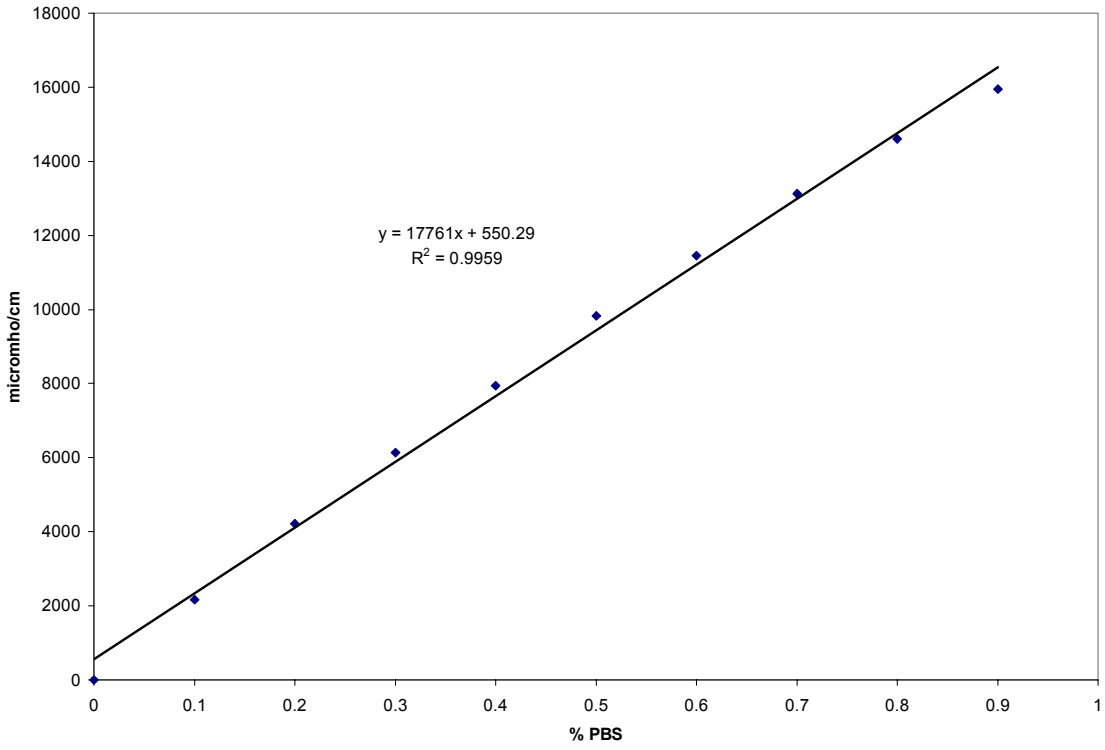

Figure 4.9: A stardard curve of conductivity vs. PBS concentration (%). The dilutions were carefully prepared from a stock 0.9% PBS and each sample was measured with the conductivity meter. They obtained values were converted to micromho/cm by multiplying by a factor of 35.46.

PBS was diluted accordingly at 0.1% intervals from 0.9% to 0.1% and each sample was measured for conductivity. For each measurement, the value obtained by the meter was multiplied by a factor of 35.46 to get conductivity units of micromho/cm. The unit mho represents inverse ohms which is a unit of electrical resistance. Figure 4.9 illustrates the standard curve of conductivity as a function of PBS concentration. The equation of the line y = 17761x + 550.29 was used to calculate the concentration of an unknown saline sample, where y is the conductivity value in micromho/cm and x is the % PBS. The error limits of the isotonic saline were reported to be approximately 0.88 $\pm$ 0.02 and each batch was tested by Nerl on red cells to ensure their viability (personal communication with a Nerl technical director). Hence using the isotonic value of 0.9% for the stock solution kept us within reasonable limits of the calibration curve.

Sample Preparation for Resealing Experiments

Cells were obtained from the Florida Blood Services in two forms. The first was a 5 ml whole blood sample stored in EDTA tubes and kept for screening purposes. The cells were refrigerated at -4^{o} C. Typical samples used for the spectroscopic experiments were no older than two days unless otherwise specified. The age of the cells have been shown to have significant effect on morphology (i.e. crenation) as demonstrated by another member of this project (unpublished data).[108] The second type of sample was packed cells suspended in Adsol^{TM} (Fenwal Division, Baxter Healthcare Corp, IL). Adsol^{TM} is used as a stabilizer for blood cell units and can extend the storage period for red blood cells. As a common blood banking practice, a large number of transfusable

units were packed and the plasma was replaced by Adsol™ for prolonged viability of the cells for up to 42 days. The age of the packed cells was also no more than two days old unless otherwise noted. The packed cells typically came in transfusable volumes of one pint and were used for the preparation of isolated erythrocytes via leukocyte-depletion and washing.

Initial exploratory studies were done using the 5 ml whole blood samples. The whole blood was analyzed for cell counts and hemoglobin content on the Serono-Baker hematology analyzer. This allowed for the verification of the parameters to be within the normal range of human physiology. The obtained red blood cell count is also helpful in obtaining the proper dilution of the whole blood sample for spectral purposes. That is, it has been previously determined that diluting the erythrocyte count to ~4000 (cells/micron) will give an optical density of approximately one.[109] As noted previously, the upper linear limit of the instrument is an optical density value of 1.2. (see Appendix B)

The dilution calculation is performed as follows, using a red cell count from data obtained on March 1, 1999:

RBC count obtained from Serono-Baker: 5,130,000 cells/mm^3

where cubic millimeters is equivalent to the volume unit of microliters (μl). Due to the large number of cells, it is not accurate to dilute down to ~4000 cells/μl in one dilution. The routine protocol calls for a series of two dilutions, with the first being a 1:50 dilution, or 0.050 ml of whole blood suspension (mixed well by inversion) in 2.45 ml of isotonic

0.9% phosphate buffered saline. Further calculation is done for the second dilution, which is contingent upon the concentration from the first dilution:

First Dilution:

$M_1V_1=M_2V_2$

$(5.13 \times 10^6 \text{ cells/}\mu\text{l})(0.050 \text{ ml}) = M_2(2.50 \text{ ml})$

$M_2 = 1.03 \times 10^5$

Second Dilution:

$(1.03 \times 10^5)V_1 = (4000 \text{ cells/}\mu\text{l})(3.00 \text{ ml})$

$V_1 = 0.117$ ml of the 1:50 whole blood dilution (total dilution factor = 1:1250)

Hence, 0.117 ml of the 1:50 dilution was pipetted into 2.883 ml of isotonic PBS for a final volume of three milliliters. The 3 ml volume was the capacity used in 3.5 ml cuvettes so that the suspension may be mixed directly into the vessel.

The whole blood suspension was then transferred into a 15 ml conical tube with a cap for washing. The tube was filled to the top with isotonic PBS, capped, and carefully inverted several times to homogenize the suspension of cells. The tubes were placed evenly in a table top centrifuge (Allegra 6, Beckman Coulter, Inc.) with a swinging bucket rotor (GH-3.8A) and spun for approximately five minutes at 3500 RPMs (1500 x *g*). The spin packed the cells at the bottom of the tube and the supernatant left above the packed cells was carefully extracted with a transfer pipet. The cells were resuspended in PBS and washed for a total of three times at which point the cells were relatively free of platelets and plasma protein, and the leukocytes were dramatically reduced in number.

After the third wash, the packed cells were suspended to a rough 1:1 volume ratio with PBS and examined in the Serono-Baker for platelet and leukocyte reduction, and to verify that the red cell volume and corpuscular hemoglobin have been maintained (i.e. that the erythrocytes had not been generally disrupted). The RBC counts are also used to determine the proper dilution (previously described) for a spectrograph. A spectrum of the washed cells will provide a qualitative assessment of the plasma reduction as well as any unforeseen changes that may have ensued following the preparations, such as morphological alterations or significant lysing of the red cells.

The Adsol^{TM} units were obtained as whole donor units held in 450 ml (~ 1 pint) collection pouches. The Adsol^{TM} contained 2000 mg/dl of dextrose, 750 mg/dl of mannitol, 27 of mg/dl adenine, and 900 mg/dl of sodium chloride.[110] A spectral evaluation of Adsol^{TM} was performed and is presented in the results section. The isolation of red cells from these donor units was more elegant. The bag of red cells was subjected to a leukocyte reduction by physically linking the bag to a leuko-reducing filter (Sepacell Pre-Storage R-500 II Leukocyte Reduction Set for Red Cells, Baxter Healthcare Corp., Fenwal Division, IL). The leukocyte reduction efficiency was reported to give residual WBC counts of $< 1.1 \times 10^5$ cells per unit with a 91% RBC recovery.[111] The common clinical use for these filters is to reduce leukocytes for transfusion purposes. The advantages of leukocyte reduction are 1) to prevent nonhemolytic febrile reactions as a result of antibodies to leukocytes in a recipient previously exposed to transfusions or pregnancy and 2) to minimize transmission of viral disease such as cytomegalovirus.[14,112]

The filtration was performed in a cold room (4° C), using gravity to pass the sample through the filter and into a collection bag. The filtered blood cells were then placed in an automated cell washer where they were packed by centrifugation and the Adsol™ was replaced with isotonic saline. The cells were used within 24 hours after preparation. Samples from each step were kept so that it was possible to spectrophotometrically monitor the changes.

Spectrophotometry of Leuko-Reduced Red Cells

Counts were performed on the Serono-Baker hematology analyzer to obtain RBC counts, hemoglobin concentration, and also to monitor the effectiveness of the leuko-reduction. The RBC cell counts were used to make the necessary dilutions to acquire the proper cell concentrations for spectrophotometry as previously described.

The spectra were collected from each step of the red cell isolation process to show the sensitivity of UV-visible spectroscopy to detect the changes in the system. After the spectra were taken, each sample was retrieved from the cuvette and spun down for approximately 8 minutes at 1500 x *g*. This pelleted the suspended cells in the sample. The resulting supernatants were scanned in the spectrophotometer to detect any free hemoglobin in solution which may have resulted from cell lysis. The Drabkin's assay was performed on the post-leuko-reduced, post-washed (PLR/PW) sample to verify the values obtained by the Serono-Baker for further quantifications and calculations.

Calculations for Resealing Experiments

The following is an example of the calculations performed in preparation for a typical resealing experiment. Numbers differed from experiment to experiment depending on the desired corpuscular hemoglobin concentration contained within the resealed cells.

Two types of buffer were needed for the permeabilization experiments (low salt and high salt phosphate buffers). The low salt (hypotonic) phosphate buffer (7mM, pH 7.2) was prepared by combining 1.44 g Na_2HPO_4 and 0.24 g KH_2PO_4. Isotonic (0.9%) phosphate buffered saline (PBS) (pH 7.0-7.2) (Nerl Diagnostics, RI) was obtained from Florida Blood Services. When a higher ionic strength PBS was necessary (eg. 2.0% PBS), NaCl was added to the isotonic PBS and the tonicity was determined by conductivity.

The cells to be permeabilized were packed by centrifugation and mixed in a 1:1 volume ratio with the hypotonic phosphate buffer. Exact quantities were 1 ml of packed cells in 1 ml of hypotonic buffer. The resealing process required the determination of concentrated PBS to bring the permeabilized system back to isotonicity. The concentration of this restoration buffer was calculated by the following process:

The cells were assumed to contain the salt concentration equivalent of 0.9%, or 0.009 g/ml. Hence,

1 ml packed cells x 0.009 g/ml = 0.009 g equivalent

For the 7 mM PB, approximately 1.7 g of salt was dissolved into one liter of water, hence the w/v concentration was 0.0017 g/ml.

1 ml PB x 0.0017 g/ml = 0.0017 g salt

So 1 ml of PB contributed 0.0017 g salt to the mixture. Summing up the two values gave a total of 0.0107 g salts in the 2 ml mixture.

Since the reaction tube held up to approximately 6 ml, it was arbitrarily determined that the total reaction volume would be 4 ml (although any other volume up to 6 ml would have been viable alternatives). Thus the final volume of 4 ml needed to be restored to 0.9%, or

0.009 g/ml x 4 ml = 0.036 g salt needed in final mixture.

The difference between the final weight needed (0.036 g) and the current weight contained in the original 2 ml mixture (0.0107 g) was 0.0253 g. That is, 2 ml of solution containing 0.0253 g of salt was needed to restore the mixture back to isotonicity.

(0.0253g/2ml)*100 = 1.3% PBS

So 2 ml of 1.3% PBS was needed to bring the reaction mixture to a 4 ml volume of isotonic condition.

The 1.3% PBS was prepared by adding NaCl to the isotonic blood bank saline and checking the tonicity with a calibrated conductivity meter. Typically, a stock solution of approximately 2.0% was made and diluted to 20 ml of the desired PBS concentration as demonstrated below:

$$M_1V_1 = M_2V_2$$

$$(2.0\%)V_1 = (1.3\%)(20\text{ ml})$$

$$V_1 = 13\text{ ml of } 2.0\%\text{ PBS}$$

Add 7 ml of deionized water for final volume of 20 ml

Red Cell Resealing Experiment

The procedures for hypotonic modification of red cells have been taken and modified from a number of published methods.[99,100,101,102,103,113,114] The goal was to be able to vary the hemoglobin concentration in the resealed cells and successfully reproduce the data in high, medium and low concentration ranges for further analysis. As previously mentioned, the cells to be modified were prepared either by washing a 5 ml sample of whole blood by centrifugation, or a large adsol-red cell unit was leuko-reduced and subjected to an automated wash. The Drabkin's assay was administered to the prepared red cell suspension for hemoglobin quantification, and counts were obtained from the Serono-Baker hematology analyzer.

The cells were permeabilized under different conditions depending on the desired outcome. For low concentrations of final MCHC, relatively large amounts of hypotonic buffer (7 mM phosphate buffer) were used in relation to the packed cell volume. For example, the ratio of packed cell volume to hypotonic buffer volume might be 1:5. The suspension was mixed carefully by inversion and incubated on ice for approximately 30 minutes. At the conclusion of the incubation, the appropriate amount of hypertonic phosphate buffered saline would be added to restore the tonicity of the suspension to 0.9%. The mixture was then incubated for 45 minutes at 37^{o} C to ensure proper resealing for a majority of the cells. The result was resealed red cells containing low amounts of hemoglobin.

For medium to large concentrations of hemoglobin in the resealed cells, the proportion of hypotonic buffer was varied. In one representative experiment, the packed

cell to hypotonic buffer volume ratio was set to 1:1. The incubation conditions were also modified to 1 minute at room temperature. The suspension was immediately restored to isotonicity and incubated at 37^{o} C for 45 minutes. The resealed cells contained higher amounts of hemoglobin.

Once the cell restoration was complete, the suspension was spun down by centrifugation to sediment the cells and isolate the supernatant. The supernatant was evaluated for hemoglobin concentration using the Drabkin's assay so that all of the hemoglobin in the sample suspension can be accounted for. The rest of the supernatant was carefully extracted using a transfer pipet and isotonic PBS was added for washing. The packed cells were carefully resuspended via multiple vessel inversions and packed again by centrifugation. The washes were performed three times, or until the supernatant exhibited a minimal or no noticeable red tint of hemoglobin. After the final wash, the packed cells were resuspended with approximately an equal volume of PBS. The mixture was analyzed in the Serono-Baker and with the Drabkin's assay. Using the obtained counts, the spectral dilution of approximately 4000 cells/μl was determined and spectra were taken of the samples. Each sample being prepared in the cuvette was carefully inverted three times for consistency and the cuvette was placed in the holder in the same orientation for each scan. In between samples, the cuvette was carefully rinsed several times with deionized water via squirt bottle, and then with saline (since saline is the sample medium). The saline spectrum for the background correction was renewed a few times during each experiment to ensure that any deviations in the light source or slight contaminations on the cuvette walls were accounted for. Such errors were minor,

however, and should not affect the spectra significantly, especially at large optical densities.

The samples prepared for spectra were transferred to centrifuge tubes and sedimented for the collection of the supernatants. The spectra of the supernatants were taken to detect any free hemoglobin which may have been present to affect the overall spectra of the samples.

4.3 Results and Discussion

Effects of Instrumental Setup on the Spectra of Erythrocytes and Hemoglobin

As an important step to achieving a meaningful interpretation of the erythrocyte suspension, it was necessary to examine the effects of instrumental arrangements that captured different amounts of scattered light. Three instrumental constructs were examined: 1) the Agilent 8453 diode array spectrophotometer captured the transmitted light at a small (2^o) acceptance angle (small angle transmission spectra), 2) the Perkin-Elmer Lambda 900 spectrophotometer was arranged to acquire data at larger ($> 2^o$) angles (referred to as diffuse transmission spectra), and 3) the Perkin-Elmer Lambda 18 spectrophotometer was fitted with an integrating sphere module to collect light scattered at all angles by the sample. Figure 4.10 shows a solid curve representing a spectrum of purified, diluted red cells (4000 cells/μl) containing a physiological hemoglobin concentration (33% w/v) taken with a small angle Agilent spectrophotometer. The dashed curve shows the spectrum of a free hemoglobin solution obtained by lysing the same concentration of red cells in a hypotonic buffer (7mM phosphate buffer), thus the

total mass of the hemoglobin was constant between the two samples. All the spectra presented in this section were obtained in replicates of three with good reproducibility. The spectrum of the encapsulated hemoglobin exhibits a significantly greater OD throughout the entire wavelength range compared to the spectrum of the hemoglobin solution, however it lacks the prominent absorption peaks that define free hemoglobin (characteristic hemoglobin peaks at 270, 337, 417, 547, and 575 nm).

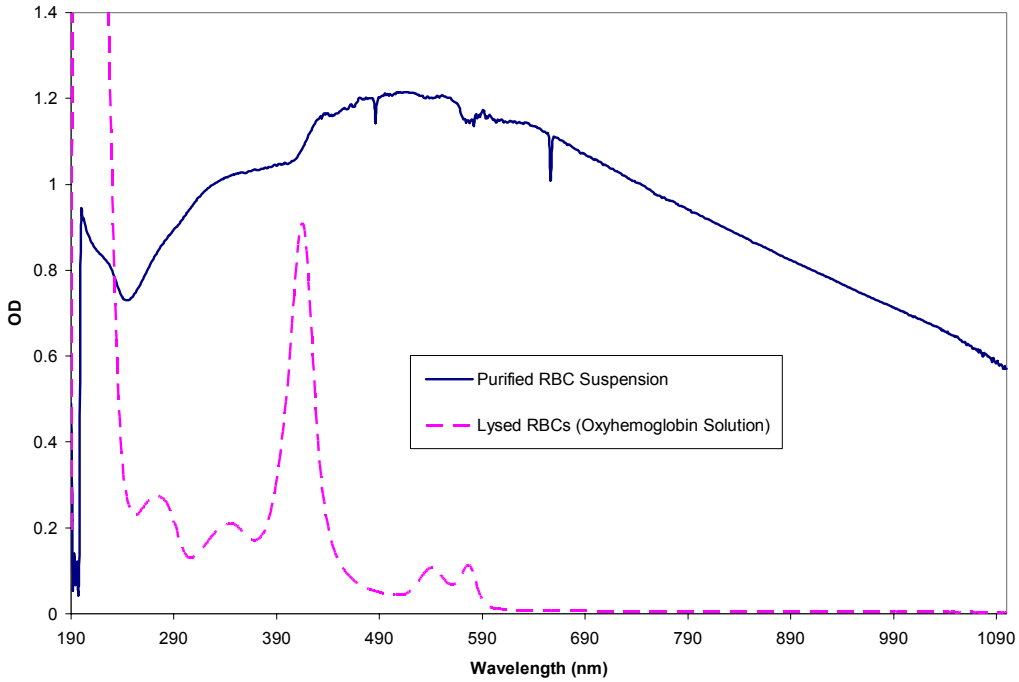

Figure 4.10: Representative comparison spectra of purified red cells and hemoglobin in solution acquired from an Agilent 8453 spectrophotometer with an acceptance angle of 2^{o}. The RBCs were purified by washing whole blood by centrifugation and passing the suspension through a leuko-reduction filter. The RBC concentration is approximately 4000 cells/µl. The spectrum of the hemoglobin solution represents a concentration of ~0.12 mg/ml.

Figure 4.11 illustrates spectra of the same samples prepared in the same manner as Figure 4.10 but captured as a diffuse transmission spectrum (DTS) on a Perkin-Elmer Lambda 900 spectrophotometer with a larger acceptance angle. Two features are immediately apparent compared to the spectra in the previous figure. First is the presence of hemoglobin peaks in the DTS, whereas these peaks in the small angle transmission spectrum (SATS) were masked. Second, the DTS of the suspension showed an overall lower spectral intensity across the entire wavelength range compared to the red cell spectrum taken with the smaller, 2^{o} acceptance angle (Figure 4.10), although it was

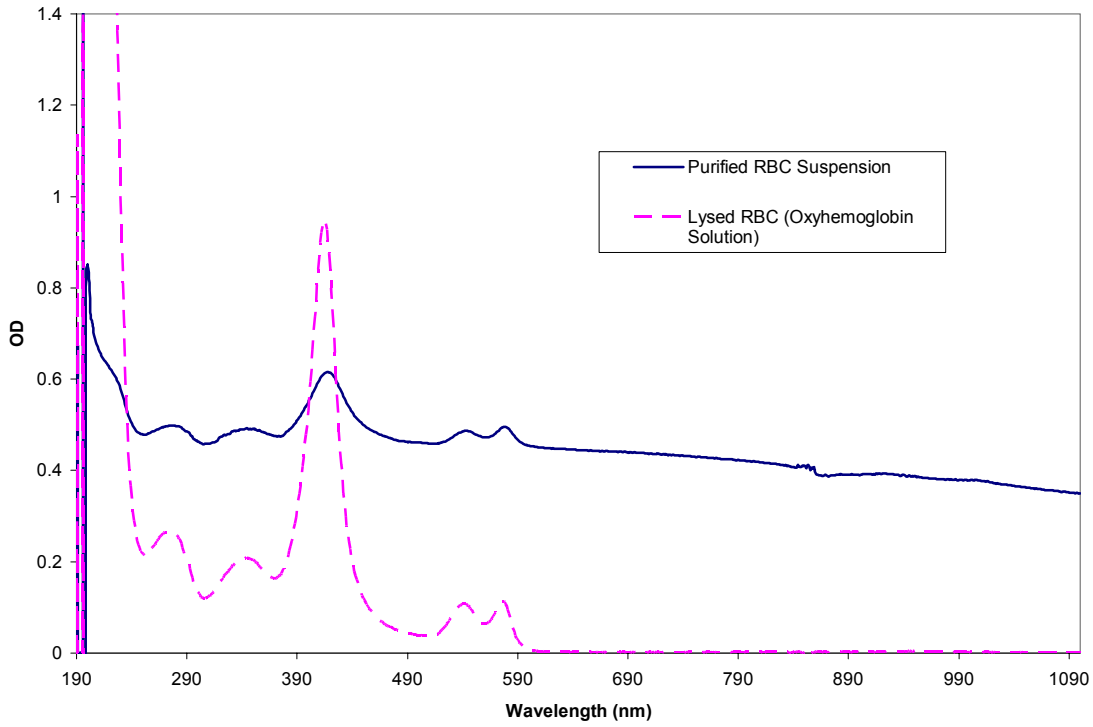

Figure 4.11: Representative comparison spectra of purified red cells and hemoglobin in solution acquired from a Perkin-Elmer Lambda 900 spectrophotometer with an acceptance angle $>2^{o}$. The RBC concentration is approximately 4000 cells/µl and the concentration for the hemoglobin in solution is ~0.12 mg/ml.

still elevated compared to the free hemoglobin spectrum. The lowered OD for the DTS was attributed to the loss of scattering information as the wider angle collected scattered light from more particles.

Figure 4.12 represents spectra acquired by an integrating sphere. In this arrangement, all of the scattered light was collected, hence the resulting transmission spectrum reflected solely the absorption component (hence it can be referred to as an

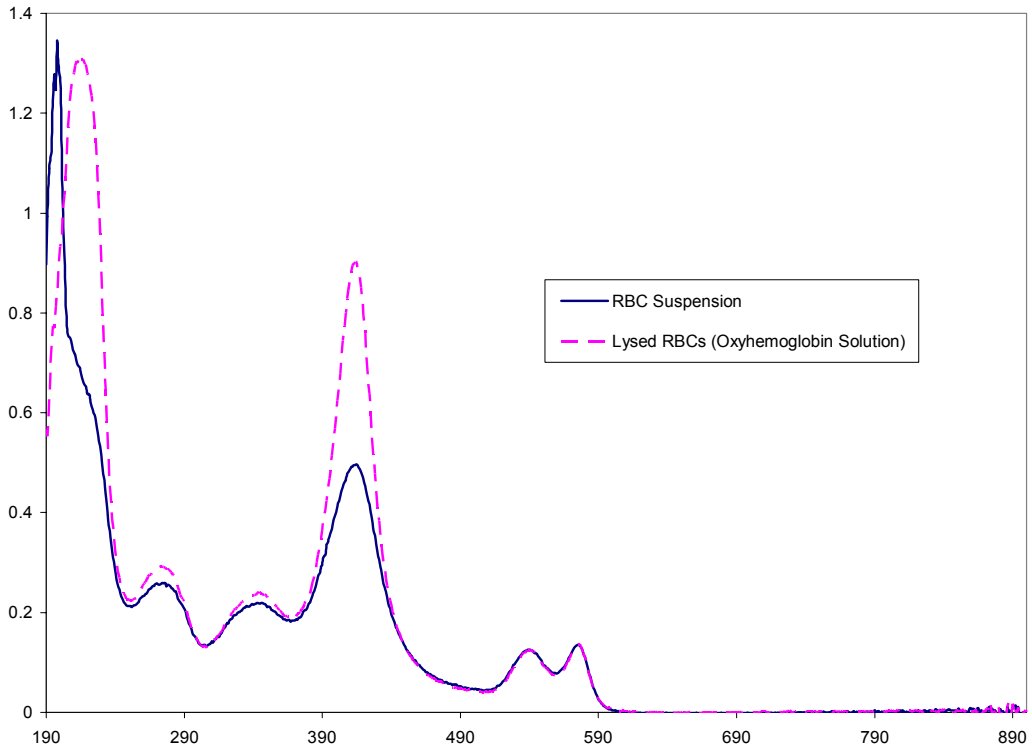

Figure 4.12: Representative comparison spectra of purified red cells and hemoglobin in solution acquired from a Perkin-Elmer Lambda 18 spectrophotometer fitted with an integrating sphere. The RBC concentration is approximately 4000 cells/µl and the concentration for the hemoglobin in solution is ~0.12 mg/ml.

absorption spectrum). The baseline of the absorption spectrum per particle of the red cells overlapped that of the spectrum of the hemoglobin solution, contrary to the elevated nature of the diffuse transmission spectrum in Figure 4.11. The hemoglobin peaks of the red cell absorption spectrum were more pronounced in comparison to the peaks of the DTS, however, the peaks at 270, 337 and 417 nm were less intense than the peaks of the hemoglobin solution. The doublet at 547 and 575 nm showed good overlap between the whole and lysed red cell spectra.

Examination of the red cell spectra in Figures 4.10 and 4.12 revealed clear differences in the presence and absence of the scattering component, respectively. The integrating sphere data demonstrated similarities to the hemoglobin solution absorption albeit the sphere showed decreases in select peaks at the lower wavelengths. With a small acceptance angle, the scattering component masked the hemoglobin absorption peaks and caused an overall elevation in the optical density spectrum. It can be inferred that the small amount of light scattered at wide angles not captured by the detector provides the differences in features and information content of the three instrumental configurations presented here. Moreover, for a DTS, the instrument collects more scattered light than a small angle detector, lowering the overall optical density and elucidating the characteristic hemoglobin peaks. By capturing more scattered light, the DTS reflects less scattering information in the OD data. To summarize, a configuration that collects a large amount of scattered light loses scattering information in the transmission spectrum because the intensities of the scattered light are averaged over the

angles accepted by the detector. In contrast, small acceptance angle transmission spectra contain a better balance of absorption and scattering information.

It is interesting to note that the spectra of the hemoglobin solution does not change across the three varying instrumental constructs, verifying that the differences in the red cell spectra are strictly related to scattering from large particles. Using the free hemoglobin spectrum as a reference, it is clear that the intensity of the SATS at 417 nm is higher than the hemoglobin Soret band whereas the DTS and integrating sphere data show smaller peaks. The reduction of select hemoglobin peaks (270, 337 and 417 nm) particularly with the DTS, had been previously attributed to a molecular hypochromic effect.[6,84,115] Our studies have clearly shown, however, that this apparent hypochromism is a matter of instrumental perspective. A smaller acceptance angle captured forward scattered light from the macroparticles without diluting the information content by capturing too much scattered light from wider angles. It was also obvious, that with a smaller acceptance angle, the spectrum of the encapsulated system showed no "hypochromism" compared to the free hemoglobin solution since this type of spectrum contains both absorbance (Q_{abs}) and scattering (Q_{sca}) information. When the scattering component is eliminated from the spectrum (Figure 4.12), the attenuation of the absorption component (compared to the absorption spectrum of free hemoglobin) describes macroscopic hypochromism. Recall that Q_{abs} and Q_{sca} are additive constituents of Q_{ext}.[8] Therefore, as the relative contribution of the scattering component increases, a concomitant decrease in the absorption component will be observed.

Comparing the three instruments, the small angle Agilent spectrophotometer yielded spectra that contained the most complete information about the scattering and absorption components of the red cell suspension. For this reason, Agilent instrument was used exclusively for the qualitative and quantitative characterization of red cells in their native and modified forms.

Spectral Evaluation of Adsol™

Since a significant number of blood units used in the experiments were stored in Adsol™ for prolonged transfusion viability, it was necessary to evaluate the spectral implications of the effect of Adsol™. Two spectra were taken: Adsol™ in its undiluted state, and "Adsol" diluted in the same manner as whole blood. The latter was prepared by first diluting the Adsol™ to 1:50 with isotonic PBS (0.050 ml Adsol™, 2.45 ml PBS), and then following with a second dilution of proportions which are similar to that of whole blood being diluted to 4000 cells/μl (0.200 ml 1:50 Adsol, 2.800 ml PBS). Figure 4.13 illustrates the outcome. Concentrated Adsol™ clearly showed prominent absorption at the wavelengths below 300 nm, a possible problem if the whole blood was spectrally processed without dilution. The peak can most likely be attributed to adenine. However, since the blood cells need to be diluted to give reliable data, such a dilution was simulated with the Adsol™ alone. The result was a spectrum that was essentially devoid of any features. The small peak close to 200 nm is a typical artifact of subtracting a large background peak from an even larger sample peak. Since both of these peaks are well beyond the linear range of the instrument, they are usually saturated (as seen in the

concentrated Adsol™ peak) and contain little information. Hence the difference between such peaks produced a peak containing unreliable information. The water peak at approximately 980 nm in the concentrated Adsol™ spectrum is present because no background correction was employed. A correction with

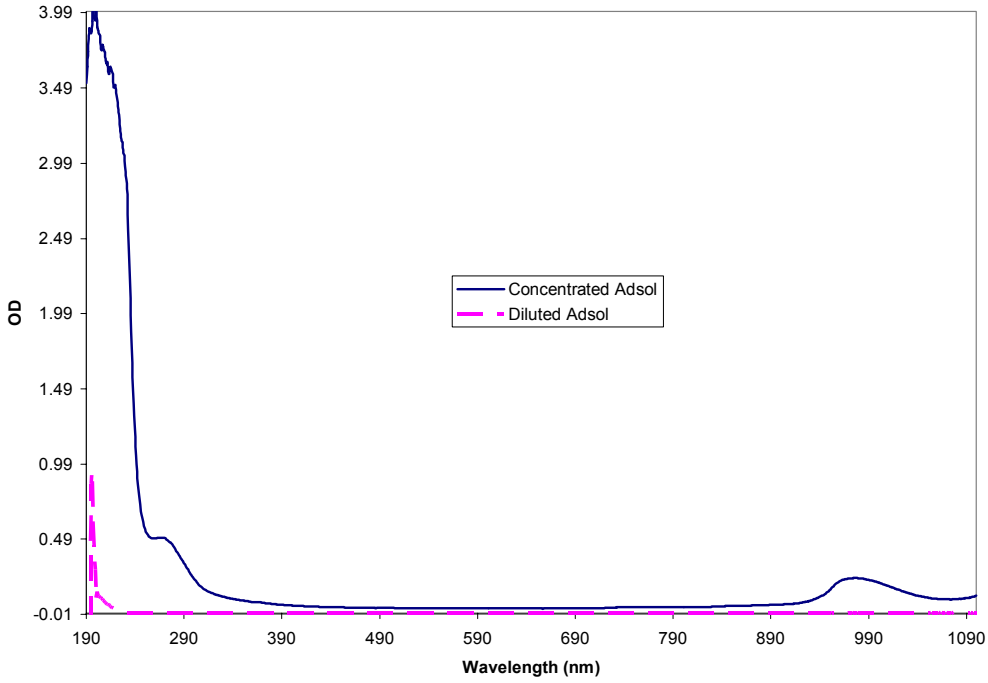

Figure 4.13: Optical density spectra of Adsol. The solid-line spectrum represents undiluted Adsol directly from the bag. The dashed-line spectrum represents Adsol when diluted in the same manner as a red cell suspension would for spectral purposes.

water would produce essentially the same spectrum without the 980 peak. The diluted spectrum was background corrected with PBS (since the dilution was prepared with PBS), thus the absence of the 980 peak.

The issue with Adsol was whether its absorption bands were prominent enough to interfere with the spectrum of red cells prior to washing and leuko-reduction. At high

concentrations, it did in fact show high absorption in the lower wavelengths (190-400 nm). However, when it was diluted in the same manner as the red cell suspension, the Adsol was optically transparent at wavelengths greater than ~220 nm, eliminating the need to correct for its effects in the background (under red cell measurement conditions).

Washed and Leuko-Reduced Cells

Before the cells were modified, they were prepared from either whole blood or Adsol-suspended blood. The whole blood samples were prepared with manual washings by centrifugation to rid the suspension of plasma, platelets, and some white cells. A combination of spectra and Serono-Baker counts show the degree of success of this method. Figure 4.14 is a representative normalized sample spectra showing both whole blood and washed cells. Normalization eliminates any concentration effects of the samples and provides a better visual comparison of the spectral changes caused by other parameters such as the removal of certain blood components, or changes in cell size. Whole blood showed an elevated optical density throughout the entire wavelength range encompassing the optical effects of each major component in this complex mixture. The most striking difference between the washed and unwashed samples is the large peak at 202 nm and the small but relatively broad peak at 280 – 290 nm, an effect accounted for by the removal of the plasma components.

When spun down and the red cells were sufficiently packed, the remaining supernatant was a clear liquid with a slight yellow tint. Shifting viewing angles of the supernate against the light revealed a shimmer due to the suspended platelets which were

less dense than the red and white cells. Directly above the bottom layer of red cells was a white layer commonly referred to as the buffy coat that consisted mostly of leukocytes. The clear plasma containing platelets were easily extracted and removed using a transfer

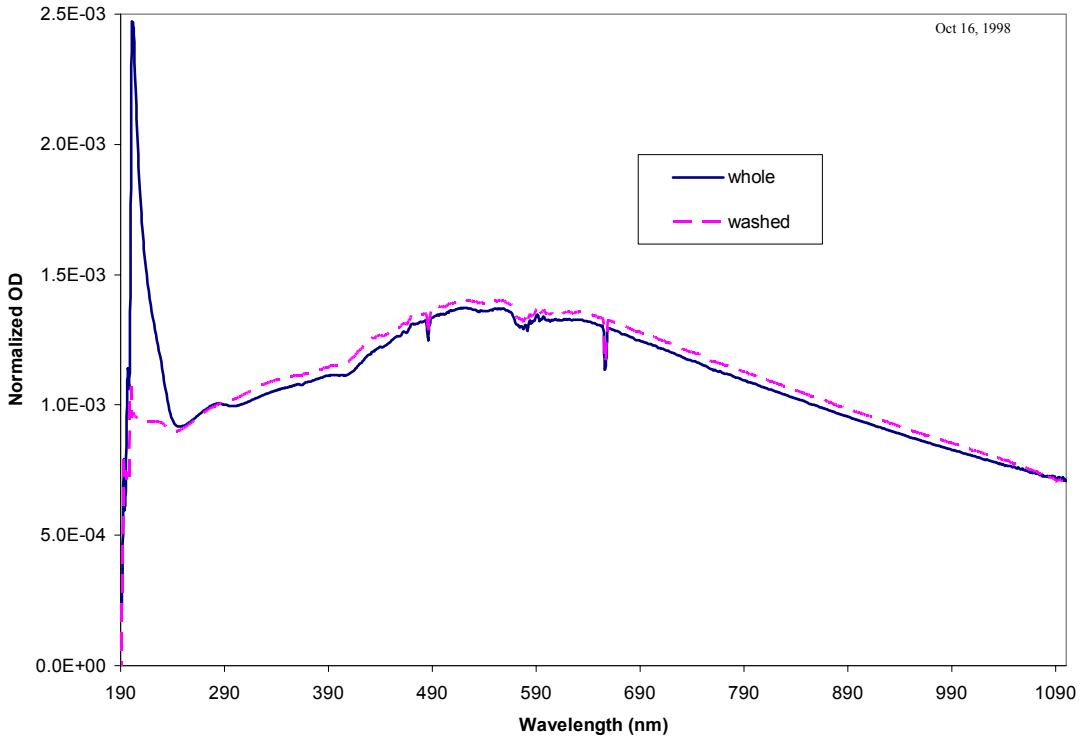

Figure 4.14: Normalized (by area under curve) optical density spectra of whole blood and washed cells. The cells were washed manually three times by centrifugation to reduce the amount of white cells, platelets, and plasma proteins.

pipet. However, removal of the layer of white cells proved to be trickier and the effective elimination of the leukocytes meant taking with it some red cells from the bottom layer. After three washes, the packed red cells were resuspended in PBS at an approximate volume ratio of 1:1.

Table 4.5 shows the values obtained by the Serono-Baker hematology analyzer to corroborate with the changes in the spectra. Consistent with the objective of the washes, there was a significant reduction seen in the white blood cell (WBC) and platelet (PLT) numbers, albeit the removal was not complete. Due to the estimated volume of the resuspension of the packed cells (approximate 1:1 volume ratio), the result of the red cell

	Whole blood	Washed cells
WBC(thsn/cu mm)	6.4	1.6
RBC (mill/cu mm)	4.29	3.81
HGB (grams/dl)	13.5	12.3
HCT (%)	43.7	38.3
MCV (cu microns)	101.9	100.6
MCH (pg)	31.5	32.3
MCHC (%)	30.9	32.1
PLT(thsn/cu mm)	276	38
MPV (cu microns)	10.1	10.8

Table 4.5: Values obtained by the Serono-Baker hematology analyzer of whole blood and washed cells.

counts (RBC) varied but always on the order of $10^6/mm^3$ ($10^6/\mu l$). In this case, the cell count decreased slightly with a corresponding decrease in the hematocrit value (HCT). Reduced RBC also meant a decrease in the overall hemoglobin count (HGB) as manifested in the results. The mean corpuscular volume (MCV) values showed, however, that the washings did not disturb the size of the red cells although it is not possible to determine how the morphology may have been affected. The hemoglobin concentration within the red cells (MCH, MCHC) were also undisturbed, as well as the platelet volume.

The Adsol-suspended cells were prepared by automated washing and leuko-reduction via filtration. Figure 4.15 shows the different stages of red blood cell purification with the washing step done first. The wash eliminated the plasma and the most significant spectral difference is the peak at approximately 200-230 nm. With the removal of the leukocytes, however, a change in the overall spectral profile is evident. In corroboration with the spectral data, hematology analyzer counts showed values that correspond with each step (Table 4.6).

For corroborative purposes, it was important to evaluate every aspect of the

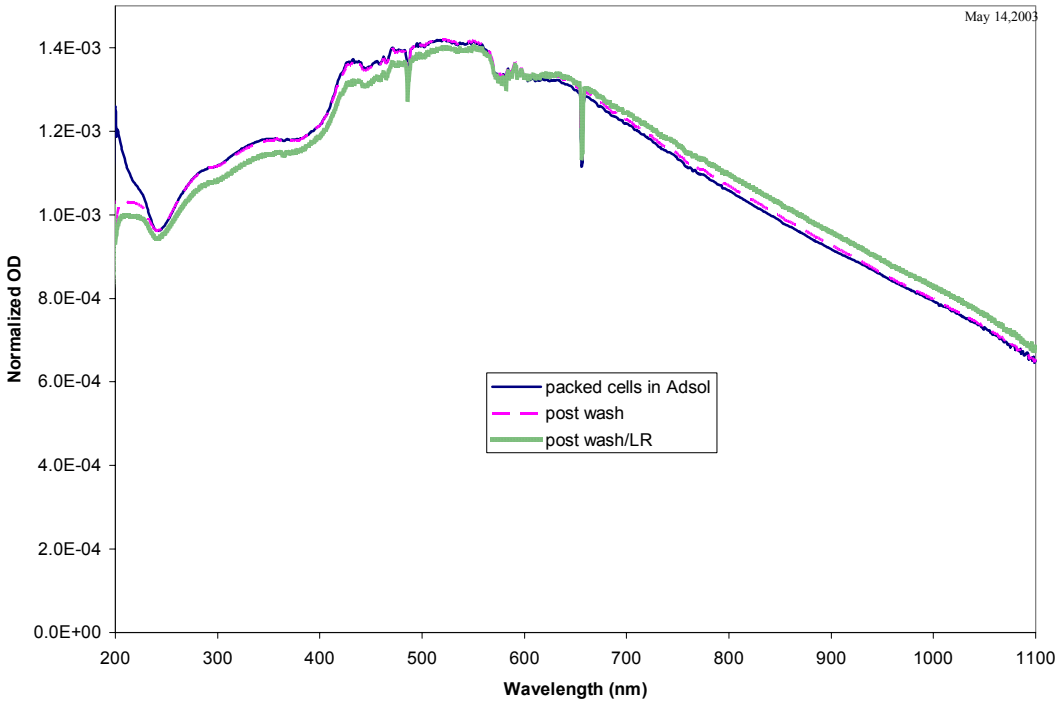

Figure 4.15: Stages in the purification of red cells. The samples were first washed with isotonic phosphate buffered saline and then passed through a leukocyte filter.

	Pre-wash/LR	Post-wash	Post-wash/LR
WBC(thsn/cu mm)	10.6	3.3	*****
RBC (mill/cu mm)	5.53	6.54	6.47
HGB (grams/dl)	18.4	21.3	21.0
HCT (%)	55.3	64.0	63.3
MCV (cu microns)	100.0	97.9	97.8
MCH (pg)	33.3	32.6	32.5
MCHC (%)	33.3	33.3	33.2
PLT(thsn/cu mm)	72	0	0
MPV (cu microns)	14.4	---	---

Table 4.6: Values obtained from the hematology analyzer for the different stages of red cell purification.

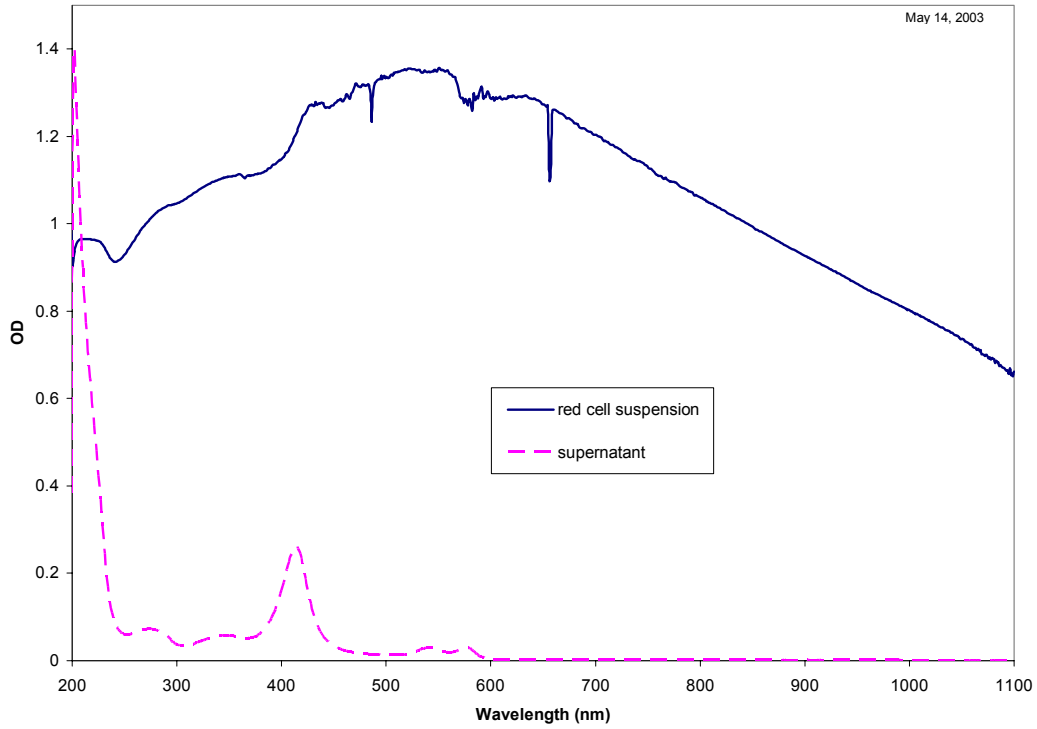

Figure 4.16: Comparison of red cell suspension and supernatant (I). The blue spectrum represents a red cell suspension post wash/LR. The pink spectrum of lesser magnitude is the supernatant after the cells were spun down by centrifugation.

system. Hence it was necessary to determine whether the hemoglobin was all encapsulated or if some were free in solution. In Figure 4.16, the solid line spectrum represents the raw data of the suspended red cells after the washing and leuko-reduction. The sample was then poured out of the cuvette and into a centrifuge tube. The sample was centrifuged for approximately 8 minutes at 1500 x *g* to pellet the cells. The pink dashed-line spectrum that looks more like a spectrum of hemoglobin reflects the supernatant obtained post-centrifugation. The amount of free hemoglobin seen in the supernatant depends on the quality of the washes. Typically, three washes were sufficient for elimination of a majority of the free hemoglobin. Visual inspection of the

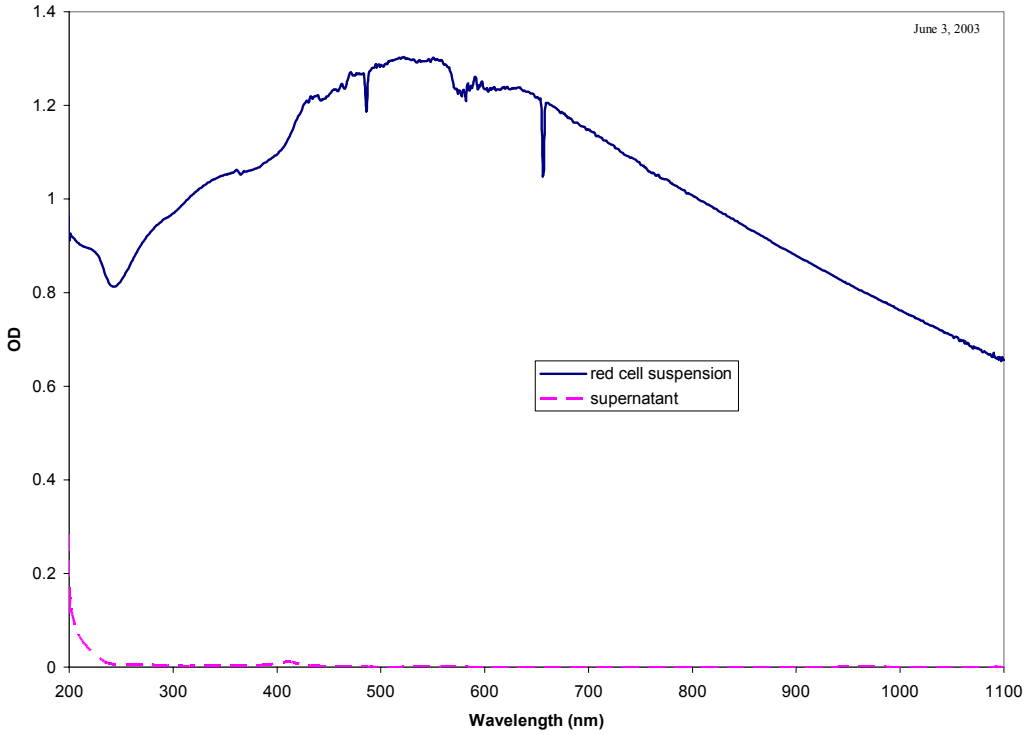

Figure 4.17: Comparison of red cell suspension and supernatant (II). The blue spectrum represents a red cell suspension post wash/LR. The pink spectrum of lesser magnitude is the supernatant after the cells were spun down by centrifugation.

supernatant should yield a colorless medium. Washing excessively, however, was not necessarily advantageous since repeated shear between cells may cause some to lyse, increasing the free hemoglobin in solution. Figure 4.17 shows a different trial with a more thorough wash. The supernatant spectrum reflected a minute amount of hemoglobin compared to that seen in Figure 4.16. Typical washes more often yielded results similar to that of Figure 4.16. Estimated quantification of free hemoglobin Figures 4.16 and 4.17 using the extinction coefficient at 417 nm (7786 cm^2/g) are 0.032 mg/ml and 0.0013 mg/ml respectively. However, the presence of any amount of free hemoglobin should not be a concern as long as a reliable spectrum is obtained for quantification.

Spectrum of Resealed Red Cells

The desired outcome of the resealing experiments was to obtain, at the very least, mean corpuscular hemoglobin concentrations in the medium (~ 0.15 – 0.20 mass frac) and low range (~ 0.05 – 0.10 mass frac), since physiological concentrations were established in the previous section. Figure 4.18 represents a resealed cell suspension with an MCHC of 0.084 (mass fraction), or 8.4% w/v. A striking change in the feature compared to the spectrum of physiological MCHC (Figures 4.16, 4.17) is the decrease in overall scattering, revealing more of the prominent hemoglobin peak at 417 nm along with the slight emergence of the doublet between 500 and 600 nm. The supernatant spectrum shows a relatively small amount of hemoglobin.

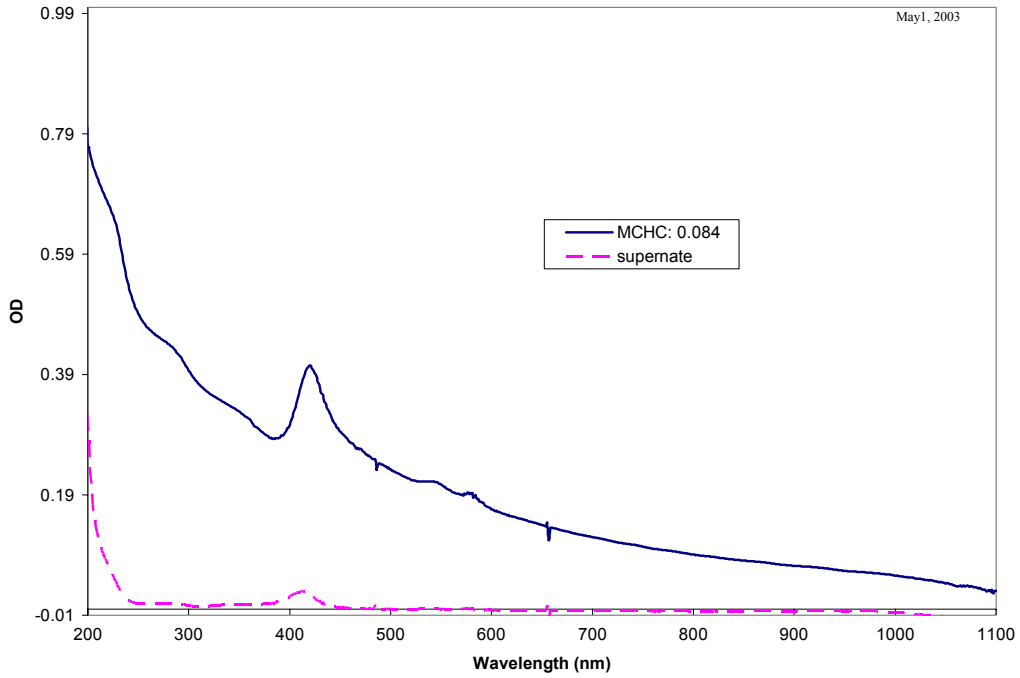

Figure 4.18: Optical density spectra of a resealed red cell suspension (MCHC: 0.084) and the supernatant. There is less scattering and a more pronounced hemoglobin peak in the cell spectrum compared to that of the high MCHC (Figure 4.12). There is a small amount of free hemoglobin in the supernatant as indicated by the supernate spectrum.

Figure 4.19 illustrates resealed red cells with MCHCs in the medium range (0.218, 0.186 mass fractions). There is a more prominent scattering seen throughout these spectra compared to that of the lower MCHC (Figure 4.18), resulting in an increased masking of the hemoglobin peaks. However, the overall scattering is less than the physiological spectrum (Figure 4.17) and the hemoglobin absorption features are not completely hidden. Between the mass fractions of 0.218 and 0.186, clear differences are seen to fit the scattering trend. The supernatant spectra again show little free hemoglobin contamination.

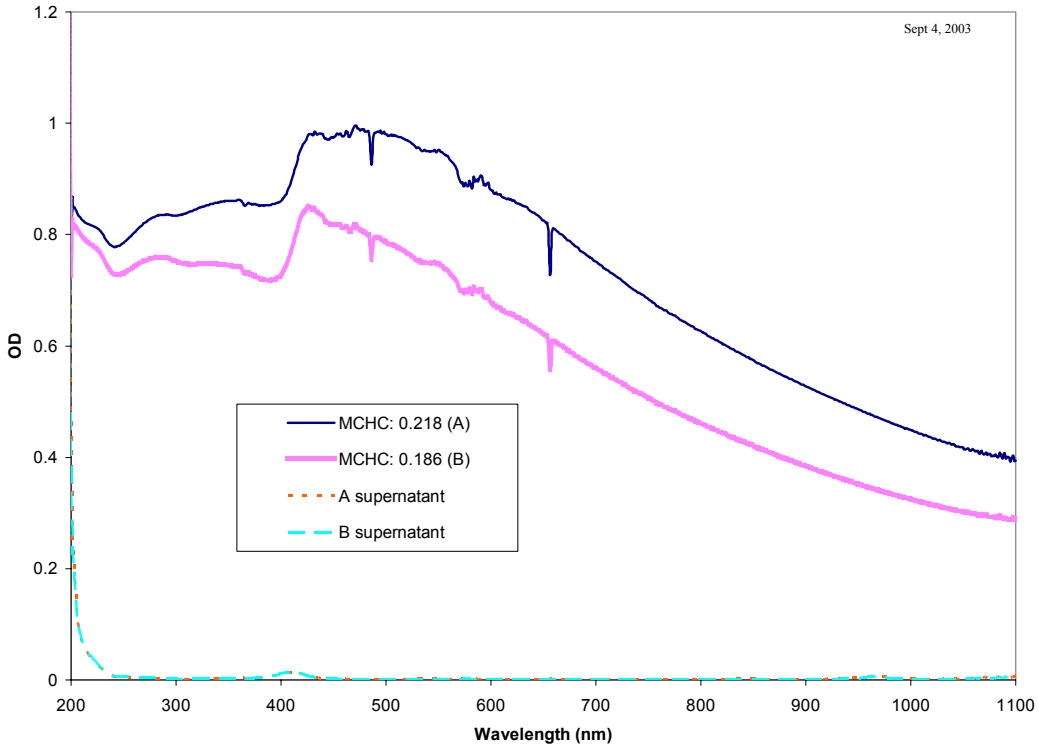

Figure 4.19: Optical density spectra of a resealed red cell suspension (MCHC: 0.218, 0.186) and the supernatant. The degree of masking of the 417 nm hemoglobin peak by scattering is somewhere between those of the high and low MCHC ranges (Figures 4.12, 4.13). The supernatants show small amounts of hemoglobin.

Figure 4.20 shows a more complete compilation of the spectra of resealed red cell data spanning a broad range of mean corpuscular hemoglobin concentrations. Every sample spectrum represents a cell suspension diluted to approximately 4000 cells/μl. Hence, the intensities of the optical densities roughly correspond to a constant cell count. As the encapsulated hemoglobin concentration decreases, the scattering effect decreases, effectively reducing the amplitude of the overall spectrum. As previously emphasized, the reduction of scattering unmasks more of the features of hemoglobin. The less the encapsulated hemoglobin, the more the spectrum looks like free hemoglobin in solution.

These changes in the features are magnified when the spectra are normalized by dividing through by the calculated area under the curve (Figure 4.21). This type or normalization eliminates concentration effects and amplifies effects caused by only the properties of the particle.[75] Here, it is abundantly evident that with decreasing MCHC, the 417:383 nm peak-to-trough ratio increases. Though this is not necessarily a linear effect, the trend is intuitive and is readily recognized.

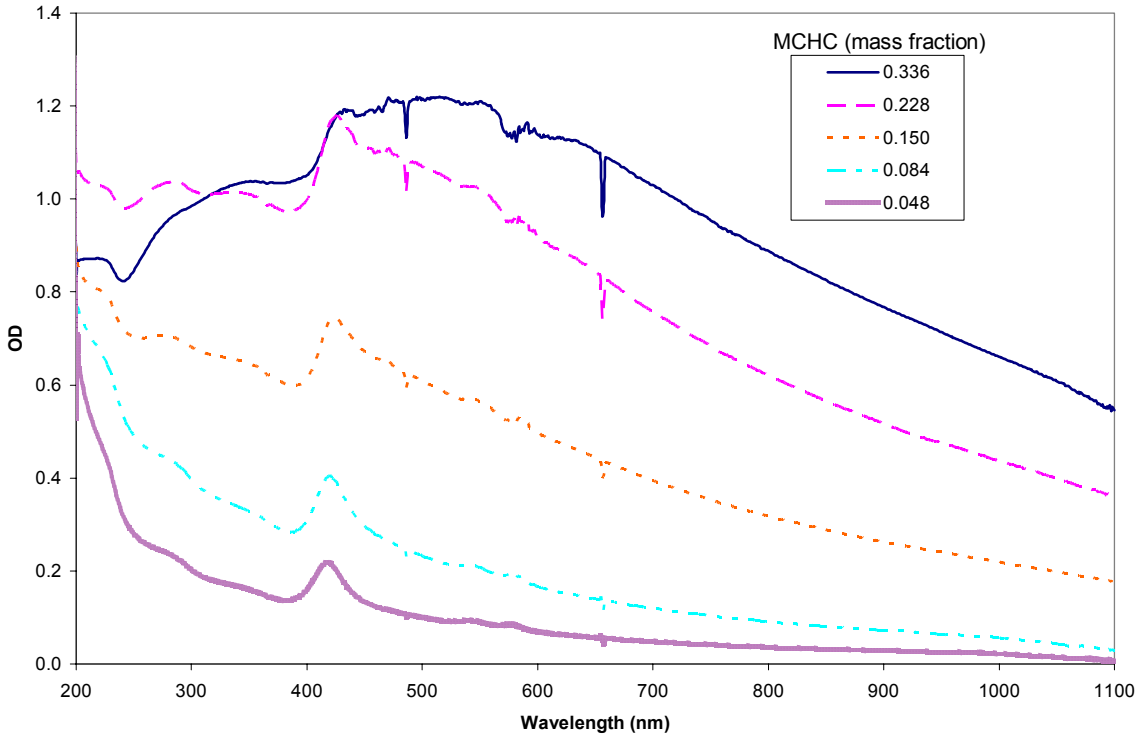

Figure 4.20: A compilation of raw spectral data of resealed cells with different encapsulated hemoglobin concentrations.

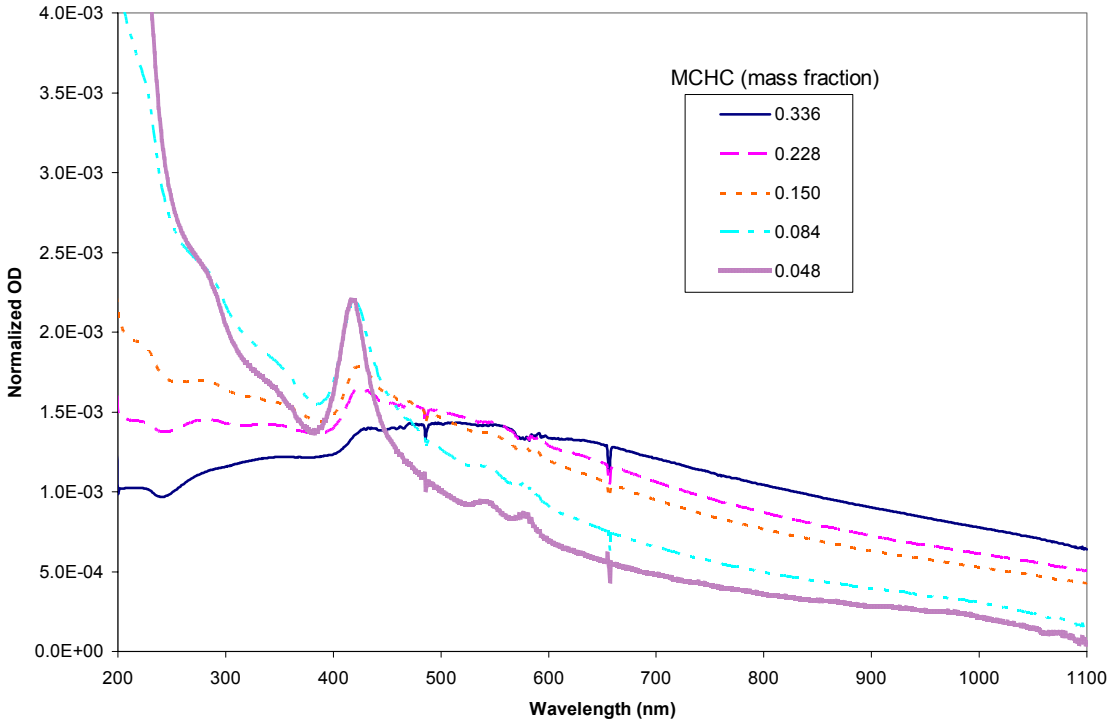

Figure 4.21: Compilation spectra normalized using the area under the curve method. This normalization eliminates concentration effects to amplify the effects due to the optical properties of the particle.

Reproducibility of the Resealed Cells

The hypotonic modification of the red cells was shown to be reproducible by performing the experiment in five parallel reaction vessels under the same conditions, using red cells taken from the same stock sample. Figure 4.22 show the spectra for the five samples, normalized to eliminate any concentration differences as a result of pipetting errors. Table 4.7 lists the values obtained from the hematology analyzer for the HGB, MCHC, and MCV. The spectra of the five replicates show strong similarities in the features across the entire wavelength range. The reported values in the table further

support the reproducibility of the experimental method. The small differences among the replicates can be attributed to experimental error (such as pipetting errors) and the error of the hematology analyzer. A comparison of experiments done under the same conditions but with different samples (not pictured) did not always yield high reproducibility because in this case, new variables are being introduced by varying the blood sample (i.e., patient genetics, how often patient donates blood, etc).

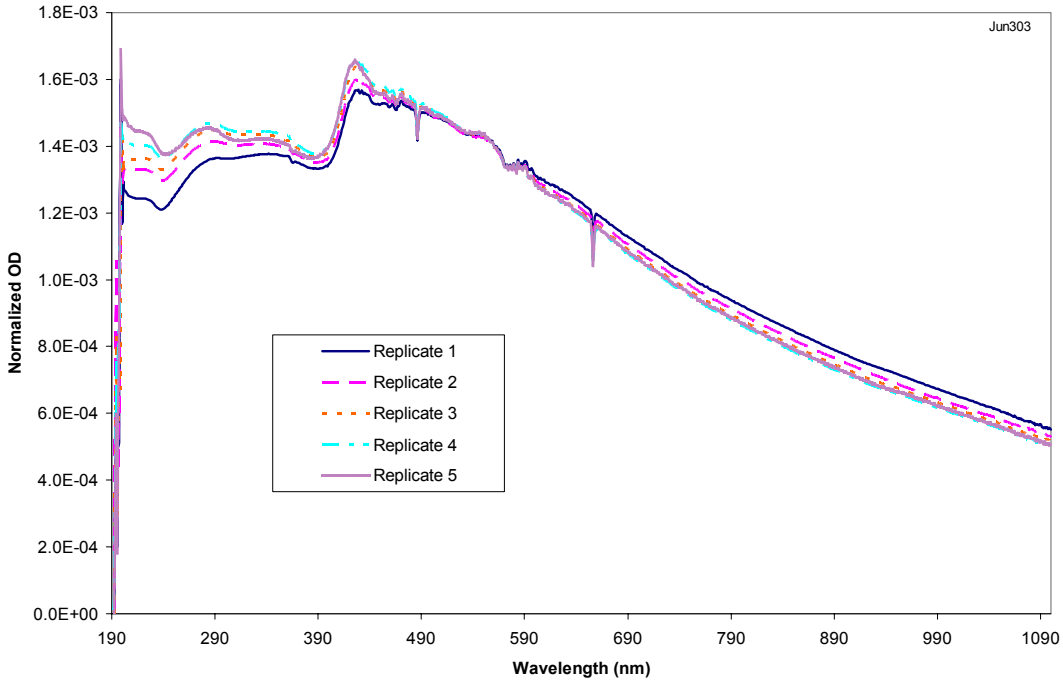

Figure 4.22: Normalized resealed cell spectra of five replicates. The modified cells are in the range of 23% MCHC. The spectra generally reflect good reproducibility with the spectra sharing common features across the entire wavelength range.

	HGB (g/dl)	MCHC (mass frac)	MCV (fl)
Replicate 1	7.4	23.8	86.2
Replicate 2	6.3	22.8	89.1
Replicate 3	7.2	23.9	86.8
Replicate 4	6.8	22.0	88.0
Replicate 5	6.1	22.8	87.8

Table 4.7: Values obtained for five experimental replicates of resealed cells for the parameters HGB, MCHC, and MCV. The values show good agreement indicating high reproducibility of the hypotonic modification experiments.

Microscopy

With each experiment, visual corroboration of the red cells was established by observing smears of the samples under the microscope. On a few occasions, we gained access to a camera-mounted phase contrast microscope (Nikon Diaphot, Department of Biology, University of South Florida) to document photographs of the cells. Both microscopes used were equipped with a 10x ocular lens with objective lenses of 10x, 40x, and 100x (oil immersion) where the total magnification was the product of the ocular and the objective magnifications. Typically, 400x and 1000x magnifications were used to assess the morphologies of the cells.

A quick microscopic inspection of the whole and washed cells was useful in evaluating the quality of the cells. Although the scope of the field of vision is small, examining a large number of random areas of the blood smear on the microscope slide gave an idea of whether or not there were any obvious morphological abnormalities in a particular sample. A high quality red cell suspension should look like Figure 4.23 where a majority of the erythrocytes assume a biconcave shape with the dimple clearly visible in the center of the donut shape. The hash marks at the bottom of the photograph give a

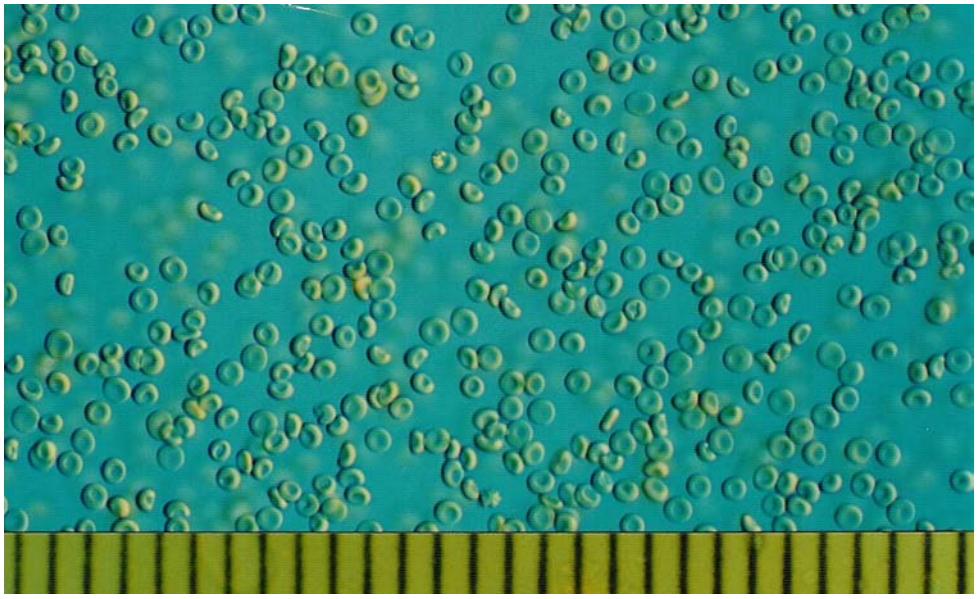

Figure 4.23: A phase contrast microscopy picture of erythrocytes in their native state magnified 400x. The sample was prepared by smearing a small drop of the cell suspension on a glass microscope slide. The hash marks at the bottom represent 10 μm per interval. The cells show their characteristic biconcave shape with a noticeable dimple in the center.

good estimation of the overall sizes of the cells, where one interval represents 10 μm. An alternate sample suspended in PBS at room temperature for a few hours is illustrated in Figure 4.24. This photograph shows crenation in which the cells have adopted a spherical conformation with spiculated protrusions. If this phenomenon is seen in whole blood samples, it could be a result of aging, contaminated medium, or improper storage (temperature). It has been demonstrated that over time, stored red cells will lose their membrane integrity and begin to crenate. Red cells suspended in isotonic PBS will adopt the speculated morphology sooner than its whole blood counterpart (matter of hours for a dilute suspension). The non-crenated cells in the picture show a flatter

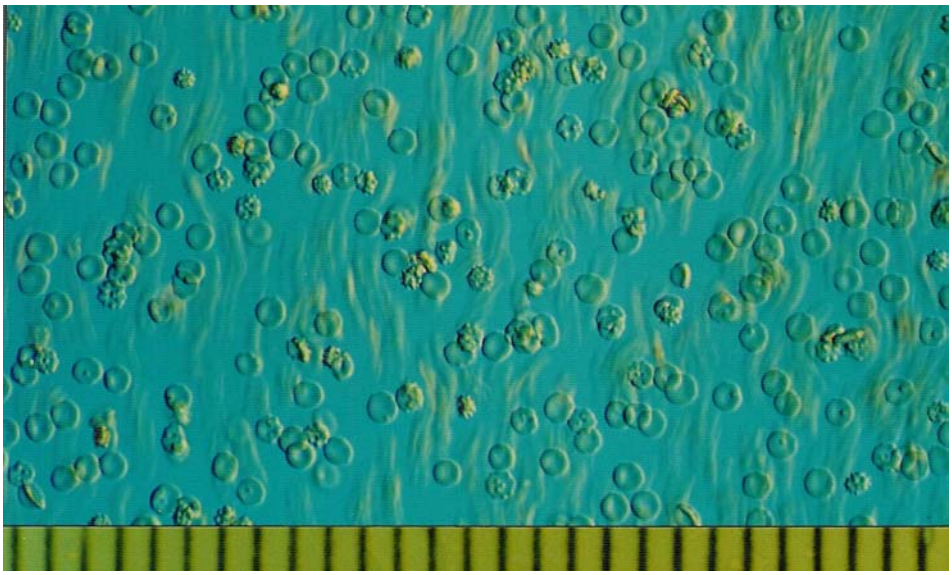

Figure 4.24: A phase contrast microscope image of non-viable red cells. Some of the cells show a crenated conformation in which they take on a spherical shape with protruding spicules. Other cells show a less defined dimple. Each interval at the bottom of the picture represents 10 μm.

discoid shape with a less apparent center dimple. In this case, the cells may have acquired excess water to become more elliptical, or indicate imminent crenation.

Likewise with the washed and leuko-reduced cells, observing the cells was a quick and easy assessment of quality. Since the washes were performed with isotonic PBS, if the ionic strength buffer was inaccurate, it would have affected the cells in ways such as crenation and swelling. Moreover, both washing and leuko-depleting filtration posed the possibility of disrupting the native membrane shape due to shear force.

Figure 4.25 shows an oil immersion (1000x magnification) picture of resealed red cells representing an estimated mean corpuscular hemoglobin concentration of 21.4% (compared to a physiological concentration of 33%). In the act of permeabilizing and resealing, the cells have lost their biconcave conformation and seemed to have adopted

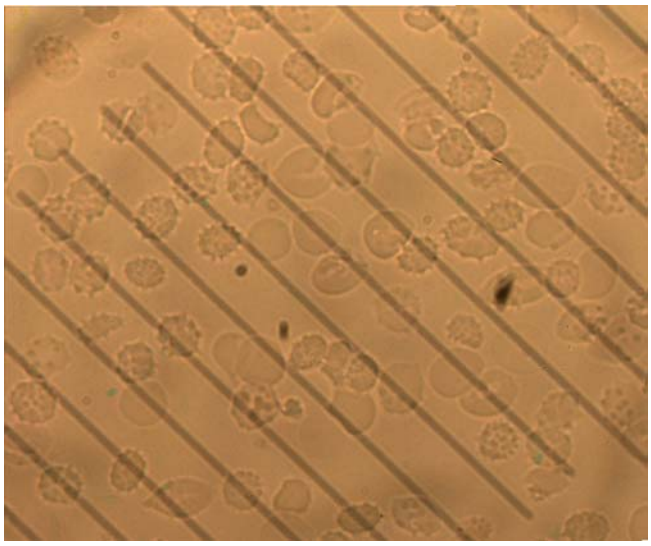

Figure 4.25: A phase contrast microscope image (1000x, oil immersion) of hypotonically resealed red cells containing 21.4% (w/v) hemoglobin. The variation in sizes has increased and the morphology has changed significantly to distorted shapes (crenated and elliptical cells). Each interval of hash marks represents 10 μm.

more distorted shapes (crenated or elliptical). The approximate diameters of the cells look to be slightly larger than their unmodified counterparts with a slightly broader distribution of sizes. Figure 4.26 is an oil immersion picture of a sample with a reported MCHC of 5.6%. Due to the low hemoglobin concentration, the contrast of the cells with respect to the background medium is greatly reduced (n/n_0 is approaching 1). The sizes seem a bit more uniform at approximately 5 μm compared to the cells containing 21.4% (Figure 4.25). This may be due to the fact that with the low MCHC samples, the samples are equilibrated for 30 minutes on ice after being subjected to hypotonic shock. In contrast, the medium range MCHC samples are exposed to the shock for approximately a minute before being restored. Thus these latter samples do not have time to equilibrate

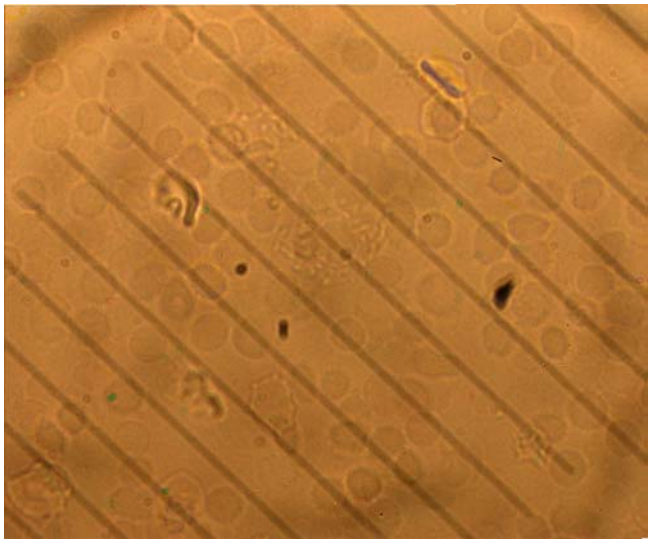

Figure 4.26: A phase contrast microscope image (1000x, oil immersion) of hypotonically resealed red cells containing 5.6% (w/v) hemoglobin. The reduction in the corpuscular hemoglobin concentrations has significantly reduced the contrast between the cell and the background medium. The cell diameters seem to be typically in the 5 μm range. The shapes seem to be spherical, however, it is impossible to assess accurately the 3-dimensional shape. Each interval of hash marks represents 10 μm.

and depending on the age of the cells present, it is possible to get more of a mixed population of resealed cells.

The sizes of the resealed cell samples were difficult to visually estimate. The diameters of the cells seemed to typically be 5 – 10 μm in all the samples evaluated (3 samples documented per low, medium and high MCHC ranges). The shapes were mostly perceived to be elliptical or crenated (more spherical). However, since light microscopy did not provide a good estimate of the three dimensional morphology, it is not a good method to corroborate the sizes (volumes) of the cells to the values obtained by the hematology analyzer.

Comments on the Acquired Experimental Data

The first significant assertion made in this dissertation is that perceived hypochromism can often be accounted for by understanding the manner in which the spectrophotometer collects the light. There are clear differences in the spectral features of the same sample taken with a small angle detector and an integrating sphere. Studies that have reported spectra of macroscopic particles with high refractive indices have presented diffuse scattering data and have maintained that any OD decreases of the encapsulated system compared to that of the free chromophore in solution are a result of molecular hypochromicity.[6,7] We have shown here that this is not the case, but instead the OD decrease can be attributed to a scattering-related effect. In this effect, the increase in the scattering component resulted in the attenuation of the absorption component and was defined above as macroscopic hypochromism. Moreover, it was determined that a small angle spectrophotometer contained the most complete scattering information useful in the qualitative and quantitative analysis of particle suspensions. Thus to summarize, observed hypochromicity has been redefined on two levels:

- Macroscopic hypochromicity which is due to changes in scattered light and as consequence is proportional to the size and refractive index of the scattering elements.
- Microscopic or molecular hypochromicity which is due to the electronic interactions resulting from close proximity of chromophoric groups and therefore a function of the chromophore concentration within the particle.

Preliminary assessment of the red cell purification and resealed red cell data indicates the proficiency of a small angle spectrophotometer to detect changes in the composition of the suspension (purification of erythrocytes) and changes in encapsulated hemoglobin concentrations. For the purification of red cells, the removal of the plasma components and white blood cells reflected small changes in the spectrum. The post-washed/post-LR spectrum (Figure 4.15) showed the largest difference in the spectral features that could be a result of the leukocyte removal, or a change in morphology of the cells after being suspended in PBS (or a combination of the two).

Resealed cells in the high, medium, and low MCHC ranges all showed clear differences in the spectral features. High hemoglobin concentration increased the contrast of the cells with respect to the medium by increasing its complex refractive index. The resulting increase in scattered light was represented by an elevation of optical density across the entire wavelength range.

Light microscopy proved to be a useful tool in evaluating the quality of the cells prior to and after the resealing experiments. Each experiment was visually monitored at select steps to ensure consistency the results. It was also possible to make rough estimates of the sizes of the cells. However, such approximations were too vague to make accurate quantifications of the cell volumes.

The data acquired by red cell purification and hypotonic modification amounted to over 50 samples. The data was assessed in terms of important parameters such as the mean corpuscular volume (MCV) and the mean corpuscular hemoglobin concentration (MCHC) to identify spectral trends and features. This analysis was necessary in our

efforts to corroborate the experimental data with spectra modeled mathematically based on the Mie theory.

As previously mentioned, a sample spectrum is represented by a set of parameters, each unique to the particular sample being examined. It is important to pay particular attention to the experimental conditions and corroborative outcomes to accurately explain the different features being manifested in the spectra. It should be noted that changes in key parameters of the particulate systems (i.e. MCHC, MCV, etc.) are not reflected spectrally in a linear fashion and therefore are often not intuitive. This complexity stems from the fact that the spectral changes arise from a combination of the absorption and scattering effects and it is this synergy that we are striving to understand by using a combination of wet chemistry and mathematical modeling.

Chapter 5: Implementation and Validation of the Mie Theory

As described in Chapter 3, the model for the mathematical construction of spectra is based on Mie theory, which represents the spectra as the combined effect of the absorption and the scattering components of the cell suspension. An effective implementation of modeling has proven to be a valuable tool in providing guidance in experimental direction. Where there are instrumental limitations in obtaining empirical data, theoretical modeling sees no such restrictions. Through modeling, it is possible to quickly generate a series of spectra allowing for the exploration of trends and manipulations of variables. Using modeled spectra as a guide may help raise a red flag when an unexpected feature is seen experimentally. Ultimately, these simulations help the scientist make an educated decision about the direction of their experimentation and also be used for verification post data-collection.

5.1 Sensitivity Analysis of Mie Theory: A test of the model

Given enough knowledge of the parameters of a cell suspension, it was possible to calculate a mathematical representation of the spectrum where the qualitative features were similar to those of the experimental spectrum. The current working implementation of the model was used to simulate the combined effect of cellular and plasma components of whole blood.[69] The flexibility of this model allowed for the exploration of isolated

effects of single blood components, and hence the program was used for the interpretation of red blood cells.

Since the model is based on Mie theory, the cells are represented by spheres of equivalent volume. Though this may be initially be construed as a restriction, the model was demonstrated to give good estimations of experimental values, and effectively predicted trends with changing parameters.

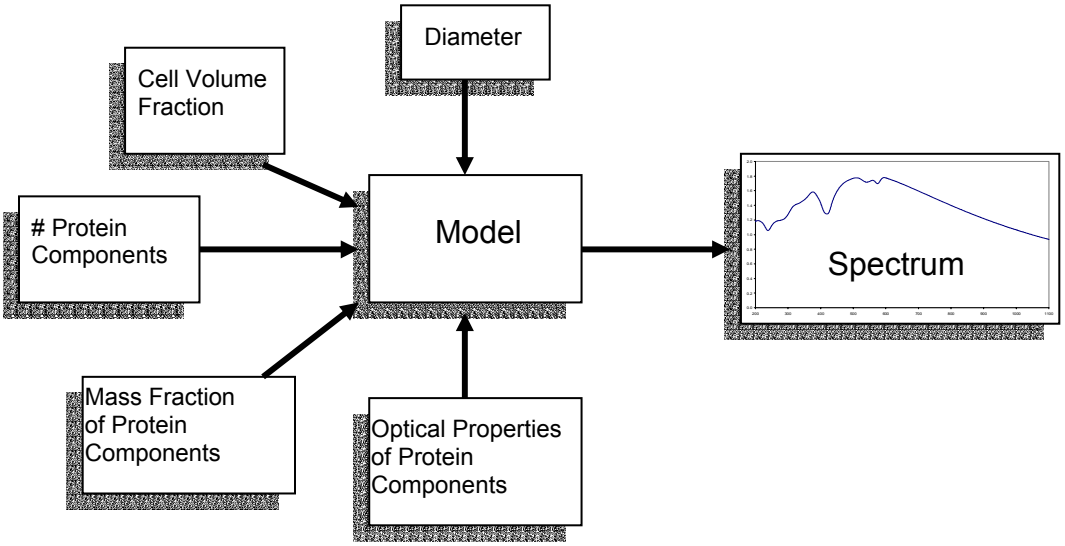

$$\tau = N_p \int_0^\infty \frac{\pi}{4} D^2 Q_{ext}(\alpha, m(\lambda)) f(D) dD$$

$$m(\lambda) = \frac{n(\lambda) + i\kappa(\lambda)}{n_0(\lambda)}$$

Figure 5.1: Diagram of the model used to calculate spectra and its inputs. The model is based on the turbidity (τ) equation and the optical properties of the suspended cells ($m(\lambda)$).

Figure 5.1 shows a block diagram of the inputs of the model. Each of the parameters serves an important purpose in describing the joint property distribution and it is their cohesion that gives rise to the qualitative and quantitative features of the calculated spectrum. The diameter, as mentioned above, is that of a sphere of equivalent volume (often referred to as the equivalent sphere). The cell volume fraction is a variable representing the hematocrit (HCT) value. The model is capable of predicting the effects of multiple chromophores within the cells. Hence the number of protein components must be specified. In the case of red cells, hemoglobin is the sole protein component, although there is the capability of including multiple derivatives of the protein (deoxyhemoglobin, methemoglobin, etc). The mass fraction or the concentration of the protein is a particularly important parameter due to the strong absorptivity of hemoglobin. The complex refractive index ($m(\lambda)$) of hemoglobin is defined by an optical properties file representing the absorption coefficient (κ) and refractive index (n) as well as the refractive index of the medium, water. Figure 5.2 depicts the components of the optical properties file of oxygenated hemoglobin. The shape of the absorption component of hemoglobin resembles that of a typical hemoglobin absorption spectrum and was derived from experimental optical density spectra of hemoglobin in solution. The real part of the complex refractive index of hemoglobin ($n(\lambda)$)[69] was then generated from $\kappa(\lambda)$ using the Kramers-Kronig transform mentioned previously in Chaper 3. The refractive index of the medium (water) was obtained from values reported by Thormaehlen et al. (1985).[116]

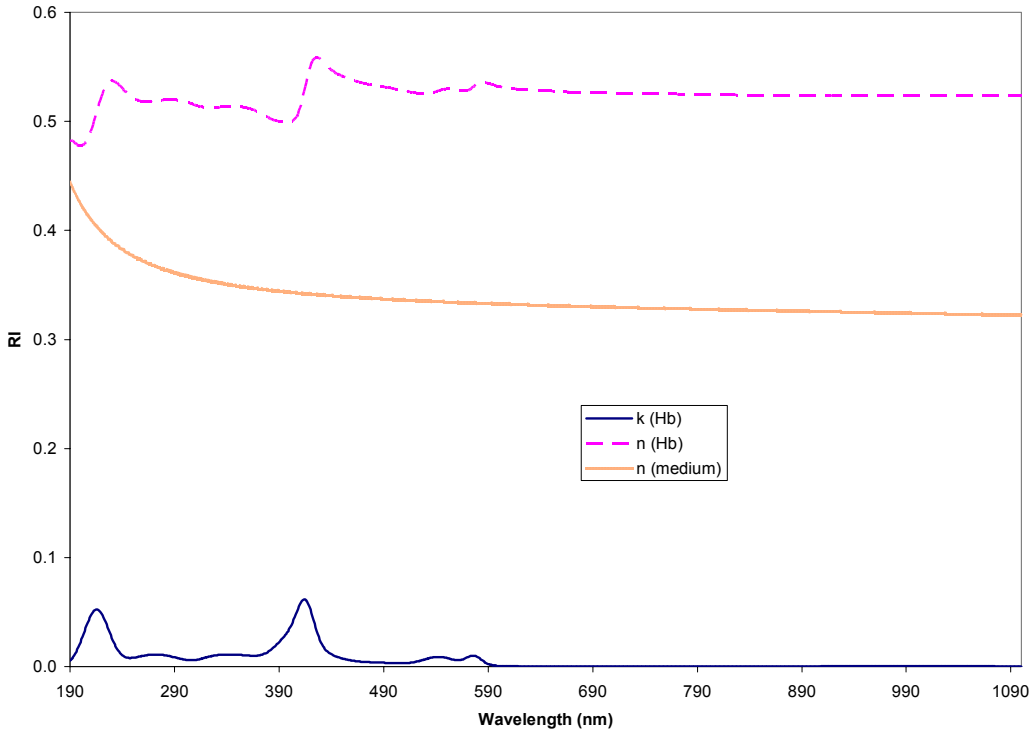

Figure 5.2: Plot of the contents of an optical properties file for oxyhemoglobin over the wavelength range of 190-1100 nm. Plots include the absorption coefficient and refractive index of hemoglobin and the refractive index of water.

Although the model is strictly used in this case for the modeling of red blood cells, its flexibility of usage extends beyond the scope of this study. The Mie theory was adapted to build a complete spectrum of whole blood or spectra of their individual components, given that reliable optical properties existed for each component. Aside from the erythrocytes, the major components of interest included leukocytes, platelets, and plasma proteins. Spectral features of platelets were successfully calculated to look like those obtained experimentally.[9] Conversely, information such as particle size distribution (PSD) and platelet activation states were extracted from the features of the

experimental spectra.[9,117] Narayanan (1999) was able to accurately model the spectrum of albumin, the major plasma protein.[118]

Simulation of Erythrocytes

The initial stage in the modeling required the program (Bldgen08) to demonstrate its ability to calculate a spectrum of a red cell suspension at physiological parameters. The inputs of the simulation were as follows:

Wavelength range for analysis: 190 1100
Spectral resolution in nm: 1
Blood concentration (g/ml) in cuvette: 1e-3
Cell pathlength in cm: 1
Erythrocyte volume fraction: 0.45
Erythrocyte average diameter (cm): 5.56e-4
Erythrocyte density (g/ml): 1
Number protein components: 1
Mass fraction for component #1: 0.33
Property filename for component #1: ophbo2.01
Leukocyte volume fraction: 0
Platelet volume fraction: 0
Plasma volume fraction: 0

This analysis was done for the entire spectral wavelength range of 190-1100 nm at 1 nm intervals (911 total points). The blood concentration in the cuvette (1e-3 g/ml) is an arbitrary number which is typically held constant. Since this is a weight-based concentration, one must be conscious of the fact that holding this number constant and varying the size of the cell would change the number-based concentration. Physiological values were maintained for the erythrocyte volume fraction (hematocrit), the mass fraction of hemoglobin, and the diameter of the equivalent sphere (calculated from a volume of 90 fl). Figure 5.3 represents the generated spectrum. The overall shape of the

spectrum closely resembles that of the experimental data of red cells (see Figures 4.8, 4.10). The 190-600 nm range includes all of the absorption peaks; hence the spectrum is rich with features resulting from the absorptive effects of hemoglobin. The 600-1100 nm range is largely considered the "scattering range" due the lack of any strong absorbance peaks. However, it would be a misconception to assume that features in the 190-600 nm range are devoid of any scattering effects. In fact the scattering is typically more prominent from 190 to 600 nm than in the "scattering range". The model typically does a good job fitting the scattering portion above 600 nm. However, as both the absorption and scattering effects both become important below 600 nm, the model may not

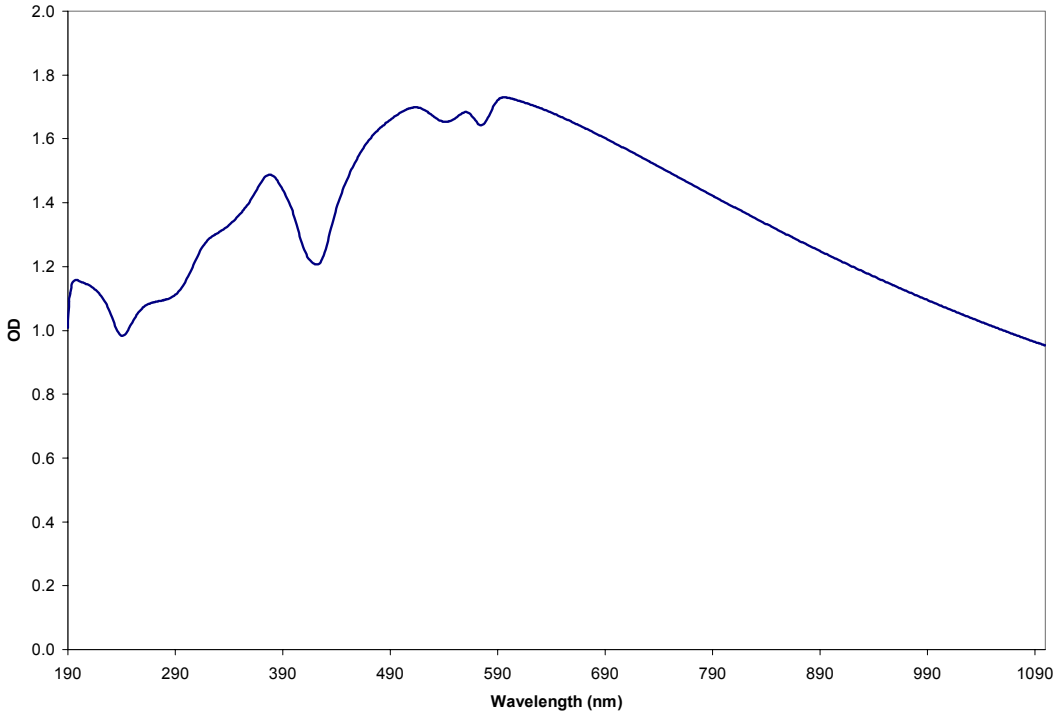

Figure 5.3: Simulated spectrum of red blood cells under physiological conditions. The simulation was calculated by the model based on the Mie theory.

necessarily provide a perfect reproduction of the features of the experimental spectrum. This may be due to the spherical approximation of Mie theory. The spherical assumption eliminates potentially important particle suspension characteristics such as particle shape and orientation which may be necessary for improved fits.

Effect of Size on Erythrocyte Spectra

One of the important parameters of the spectral characterization or erythrocytes is size. Physiologically, the reported volume limits of red cells range between 80 – 100 fl (see Chapter 2). The simulations serve as a sensitivity analysis for the qualitative features of the red cell spectra in relation to size. Since the model takes the size input as the diameter of a sphere of equivalent volume, the volume values were converted using the equation of a sphere and are reported in Table 5.1.

Volume (fl)	Diameter (cm)
80	5.35e-4
85	5.46e-4
90	5.56e-4
95	5.66e-4
100	5.76e-4

Table 5.1: Physiological volume range of red cells in 5 fl increments and their equivalent sphere diameters.

The simulations held the following parameters constant:

Wavelength range for analysis: 190 1100
Spectral resolution in nm: 1
Blood concentration (g/ml) in cuvette: 1e-3
Cell pathlength in cm: 1
Erythrocyte volume fraction: 0.45

Erythrocyte density (g/ml): 1
Number protein components: 1
Property filename for component #1: ophbo2.01
Leukocyte volume fraction: 0
Platelet volume fraction: 0
Plasma volume fraction: 0

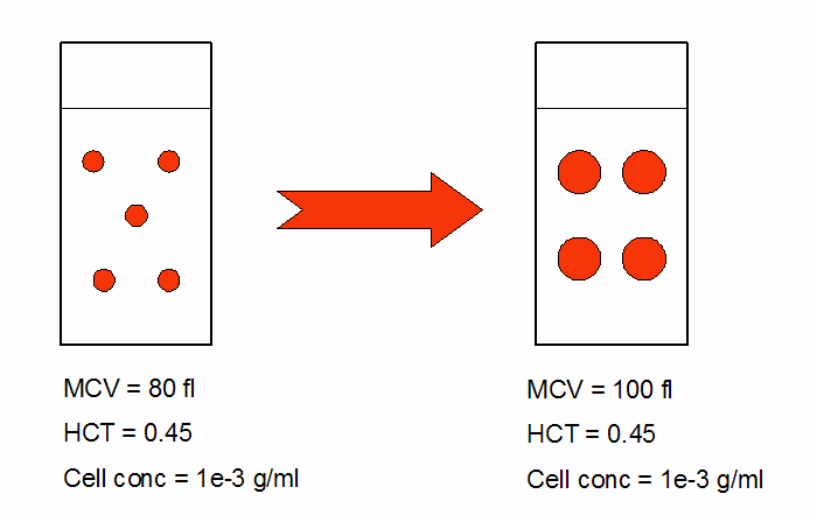

Figure 5.4: Illustration of cell suspension where the size is increased by the hematocrit and weight-based cell concentration remains constant. Under these conditions, the cell number changes, hence the need for further corrections for a comparison on a per cell basis.

The five sizes from Table 5.1 were repeated with hemoglobin mass fractions of 0.33, 0.20, and 0.05 (high, medium and low MCHC values respectively). Figure 5.4 illustrates physical implications of the system in terms of varying cell size. The simulation was initially done by keeping the hematocrit and the weight-based cell concentration (g/ml) constant while varying only the mean corpuscular volume. The problem however, is that this changed the number of cells in the system. Thus the concentration effects must be eliminated to isolate the comparison to changes in volume. One solution was to adjust the hematocrit and weight-based cell concentration values accordingly so that the cell

number was kept constant. The second solution was to correct the discrepancy by normalizing each of the spectra by the area under the curve. The latter method was employed.

Figure 5.5 shows the effect of size on cells with a low mean corpuscular hemoglobin concentration of 0.05. Slight differences in intensities are seen in the two prominent peaks at 225 nm and 417 nm. The peak at 417 nm and the doublet between 500 – 600 nm represent the characteristic peaks of hemoglobin. Observing the peaks, one can notice that the smaller sizes have higher optical densities. This trend is counterintuitive when considering the absorption component alone. The larger the particle, the more hemoglobin in the pathlength of the light hence it would seem that the larger cell should adopt the higher absorption peak. But in reality, the opposite is true and this is consistent with the theory and the observations of Garcia-Rubio (1987) on the effect of particle size on the absorption spectra.[92]

Across the entire wavelength range (at low MCHC), there is a minimal change of features as size increases. This is a direct result of the low hemoglobin concentration within the cells. A low MCHC implies a low contrast between the refractive indices of the cell and the medium and under such conditions, the scattering component is relatively small compared to cells containing hemoglobin at a physiological level.

Figure 5.6 illustrates the effect of size on cells at a medium hemoglobin concentration (mass fraction of 0.20). The hemoglobin bands are present but to a lesser degree, as scattering across the entire wavelength range is more prominent. The difference in the spectra due to the increase in cell size is more noticeable as well. As

seen with the previous simulation, the intensity in the absorption region (190 ~ 500 nm) decreases with an increase in size. The larger refractive index ratio of cell/medium (n/n_0) accounts for a more significant contribution of the scattering component which explains the more pronounced spectral differences between the cell sizes. Furthermore, the medium MCHC is beginning to show signs of the flattening of the spectra, a phenomenon previously seen with size increases due to swelling or aggregation.[118] This flattening is typically marked by the reduction of the optical density in the absorption region with the increase in size and also the decrease in the slope of the scattering region (600 – 1100 nm). The spectra shows an isosbestic point at approximately 480 nm and the trend of intensity vs. size inverts as this point is crossed coming from either direction.

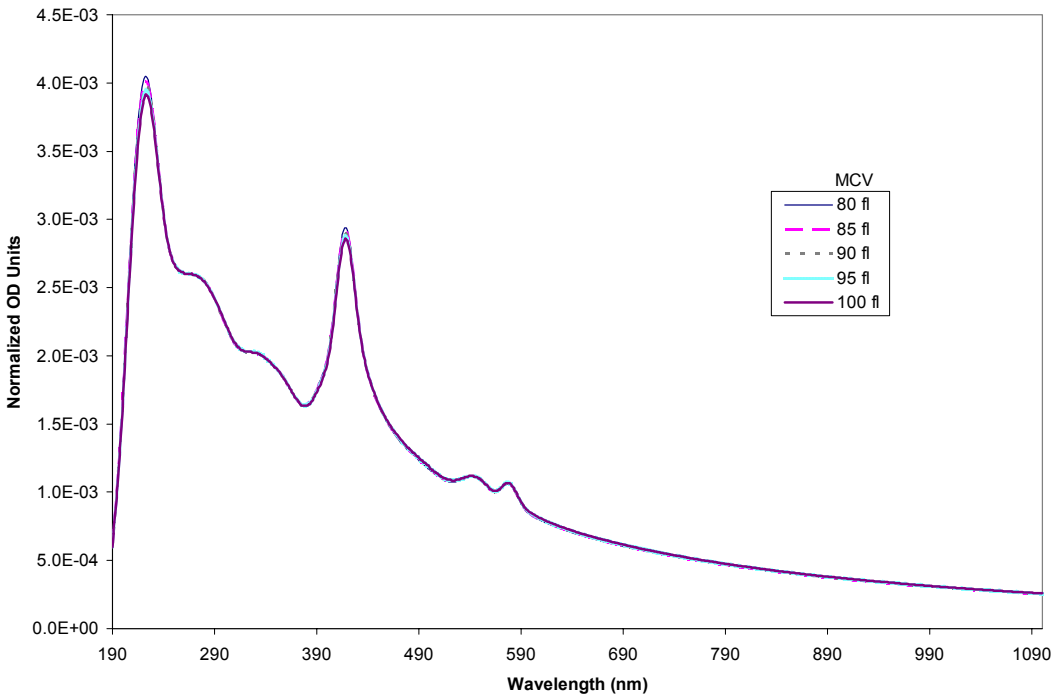

Figure 5.5: Simulated spectra of varying MCV at constant MCHC (0.05 mass fraction).

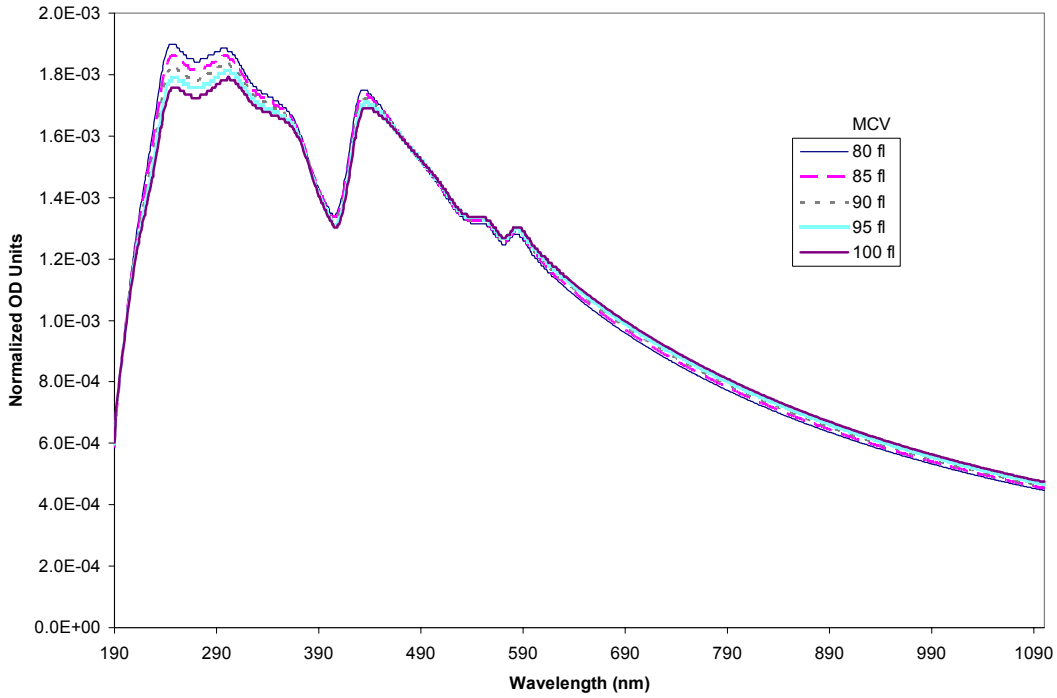

Figure 5.6: Simulated spectra of varying MCV at constant MCHC (0.20 mass fraction).

Figure 5.7 is a simulation in which both the size range (80 – 100 fl) and the MCHC (0.33 mass fraction held constant) are within relevant physiological parameters. The first striking feature to notice is that the overall shape of the spectra looks similar to experimental spectra of red cells. The n/n_0 has increased to the point to where the whole particle scattering dominates the spectra. This also accounts for the fact that the effect of the size change is dominant compared to the spectra in the previous two simulations. The spectral flattening is evident on a larger scale as well.

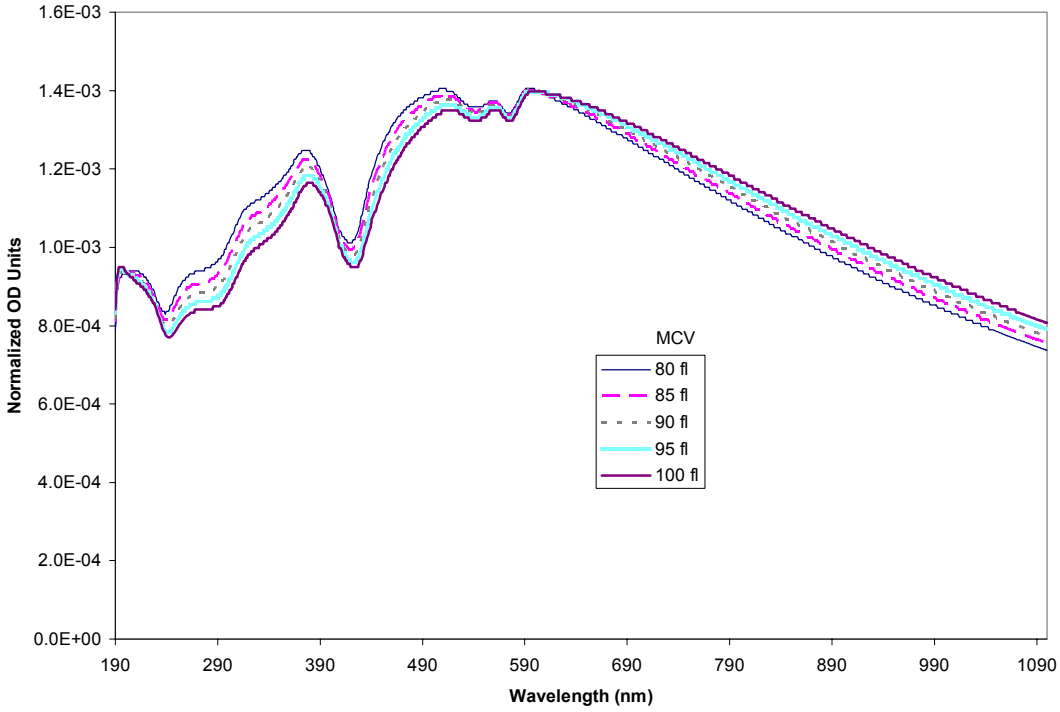

Figure 5.7: Simulated spectra of erythrocytes at varying MCV at constant MCHC (0.33 mass fraction).

Effect of Varying MCHCs on Red Cell Spectra

The simulation analysis of erythrocytes naturally progressed to the examination of trends due to varying mean corpuscular hemoglobin concentrations while holding the size constant. In this case, the interdependent parameters such as size and hematocrit were not changing therefore an adjustment for particle number was not necessary. Certain parameters were held constant as follows:

Wavelength range for analysis: 190 1100
Spectral resolution in nm: 1
Blood concentration (g/ml) in cuvette: 1e-3
Cell pathlength in cm: 1
Erythrocyte volume fraction: 0.45

Erythrocyte average diameter (cm): 5.35e-4
Erythrocyte density (g/ml): 1
Number protein components: 1
Property filename for component #1: ophbo2.01
Leukocyte volume fraction: 0
Platelet volume fraction: 0
Plasma volume fraction: 0

The sole varying parameter was the MCHC (in mass fractions) which was examined at 0.33, 0.20, 0.09, 0.5. Figure 5.8 shows the result with the MCV set at 80 fl. The most compelling trend to be noticed is that as the MCHC increases, there is an overall elevation of the spectra across the entire wavelength range due to the increase in light scattering. At the low MCHC values (0.05 and 0.09), the characteristic hemoglobin singlet (417 nm) and the doublet (500~600 nm) are visible. Even a small difference in mass fractions between 0.05 and 0.09 demonstrates a substantial scattering increase for the higher MCHC (evidenced by the elevation of the 0.09 spectrum). At a hemoglobin mass fraction of 0.20, the shape of the spectrum is significantly different from that of 0.09 with the hemoglobin peaks becoming less prominent due to the peaks being somewhat masked by the elevation of the scattering component. A physiological MCHC (0.33 mass fraction) shows the absence of the hemoglobin peaks as they are completely masked by the scattered light. The increase in the internal hemoglobin content increases the n/n_0 contrast which contributes to the increase in whole particle scattering. Furthermore, the increase in hemoglobin density suggests that less of the chromophores are being sampled by the incident light, a phenomenon that would be less profound if the hemoglobin were free in solution. Similar simulations done at constant sizes of 90 and 100 fl yielded the same trend across the four MCHCs shown in Figure 5.8.

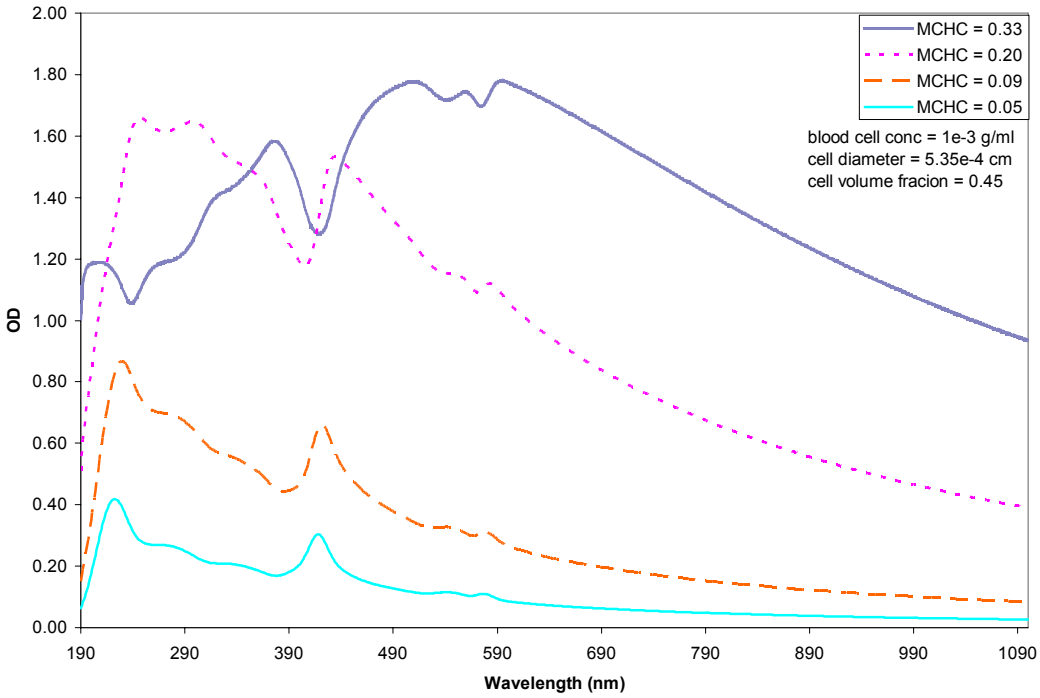

Figure 5.8: Simulated spectra of erythrocytes at varying MCHC and constant MCV.

Combined Effect of MCHC and MCV Changes

Once the individual effects of MCHC and MCV variations had been determined by the model, it was important to examine concomitant changes in both parameters. The following simulation mimics a probable physiological event where the red cells are altered in size due to changes in the osmotic environment. Associated with this change is a size-dependent alteration in concentration of the internal hemoglobin depending upon whether the cell is swelling or shrinking. If the cells swell, the influx of water will dilute the hemoglobin concentration and vice versa. As the cell volume (size) changed, the MCHC adjustments were calculated as follows:

Given: MCHC = 33% at MCV = 90 fl
33% = 33 g/dl = 0.33 g/ml

so, 0.33 g/ml x 90 x 10^{-12} ml = 2.97 x 10^{-11} g Hb

Adjusting the MCHC in a cell volume of 95 fl:
2.97 x 10^{-11} g Hb/95 x 10^{-12} ml = 0.31 g/ml

Thus the diluted MCHC mass fraction is 0.31.

The table included in Figure 5.9 shows the MCV changes and the corresponding MCHCs. The hematocrit was held constant at 0.45 and the weight-based cell concentration in the cuvette was held at 1e-3 g/ml. Similar to a previous simulation, the result was normalized (area under the curve method) to eliminate any cell number variation so that each spectra was expressed on a per cell basis. The result was a direct comparison between cells of different sizes and their corresponding hemoglobin concentrations.

The swelling and shrinking of red cells even within physiological size constraints produced significant qualitative changes in the spectra. The cell with the largest volume (100 fl) contained the most dilute hemoglobin (mass of hemoglobin held constant) and vice versa for the smallest volume cell. Referring back to a previous simulation (Figure 5.7) that examined only changes in the MCV, the trend in this current simulation (Figure 5.9) shows an opposite effect. That is, when changing only the MCV (Figure 5.7), the particle with the largest size (100 fl) but with the same hemoglobin content experienced the largest flattening of the spectrum. However, in the case of swelling cells, the spectrum flattens when the MCV decreases and the MCHC increases. This can be explained by the dominant spectral manifestation of increasing MCHC. The effect of

increasing the MCHC (increase in n/n_0) is evident in the dramatic changes in the spectra in Figure 5.8 and this is also responsible for the differences seen in Figure 5.9. Hence, the effects of the hemoglobin concentration override the effects of size.

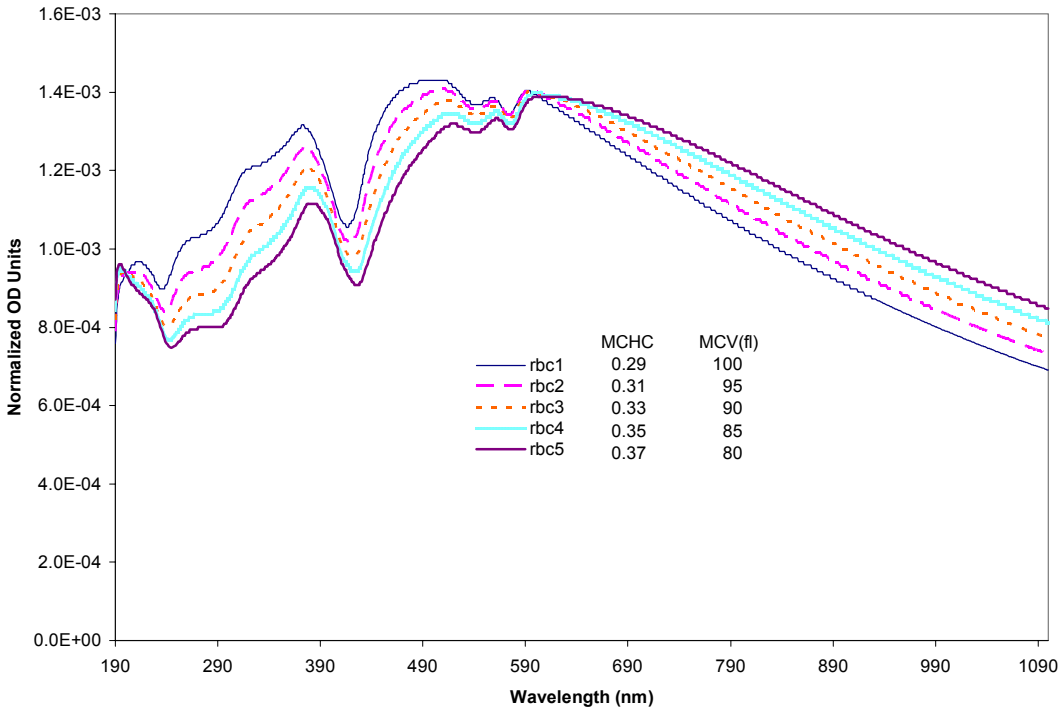

Figure 5.9: Combined spectral effect of changes in RBC hemoglobin concentration and volume.

5.2 Qualitative Analysis of Experimental Spectra

In light of the theoretical studies presented in the previous section, the next step was to examine the outcome in an experimental system to see if the predicted trends shown by Mie theory hold true when compared to experimental values. The concentration of hemoglobin in red blood cells was systematically altered by osmotic permeabilization, followed by restoration of the cells under physiologic osmolarity. A variety of

concentrations and sizes were obtained by controlling the incubation time following the permeabilization step. The sizes and concentrations were confirmed by using a Serono-Baker hematology analyzer. Each of these experimental sets was normalized using the area under the curve method from 230 – 900 nm. All of the spectra were subjected to solvent (isotonic phosphate buffered saline) correction, thus subtracting the large, saturated saline peak below 230 nm renders this region unreliable for data extraction. The wavelength range of 900 – 1100 nm also occasionally showed errors in the way that the typically straight scattering region might tail downward due to instrumental uncertainty. Hence, the 230 – 900 nm range encompassed the most consistent data.

The following figures test the ability of the model to accurately simulate combinations of varying MCHC and MCV. Figure 5.10 represents a group of experimental data selected over a range of MCHCs (0.048 – 0.336 mass fraction) each accompanied by varying MCV quantities. The inset shows raw data with each sample diluted to a concentration of approximately 4000 cells/μl. The large plot is normalized data designed to amplify the features of the spectra to facilitate visual qualitative comparisons. As the MCHC increased, the overall optical density increased (inset). The differences in the MCV provided a more subtle contribution to the spectra. The normalized plot helped to show the emergence of the hemoglobin peaks as the encapsulated hemoglobin concentrations decrease. The lowest MCHC sample (C4) showed the highest, most pronounced hemoglobin peaks whereas the highest MCHC sample (C1) exhibited a near absence of the characteristic peaks. The observed behavior is expected and consistent with the scattering theory; as the concentration of hemoglobin

within the cell is decreased, so is the contrast of the particle relative to the suspending medium, which results in a decrease of the scattering contribution the.

Figure 5.11 presents the simulations of the experimental spectra using the same MCHC and MCV values. The empirical trends are evident in the simulated spectra: 1) there is a flattening in the curve with increasing MCHC, 2) the hemoglobin peaks become more apparent with decreasing MCHC, and 3) the inset plots show that with a constant cell count, the increase in MCHC generates a dramatic increase in the intensity of the

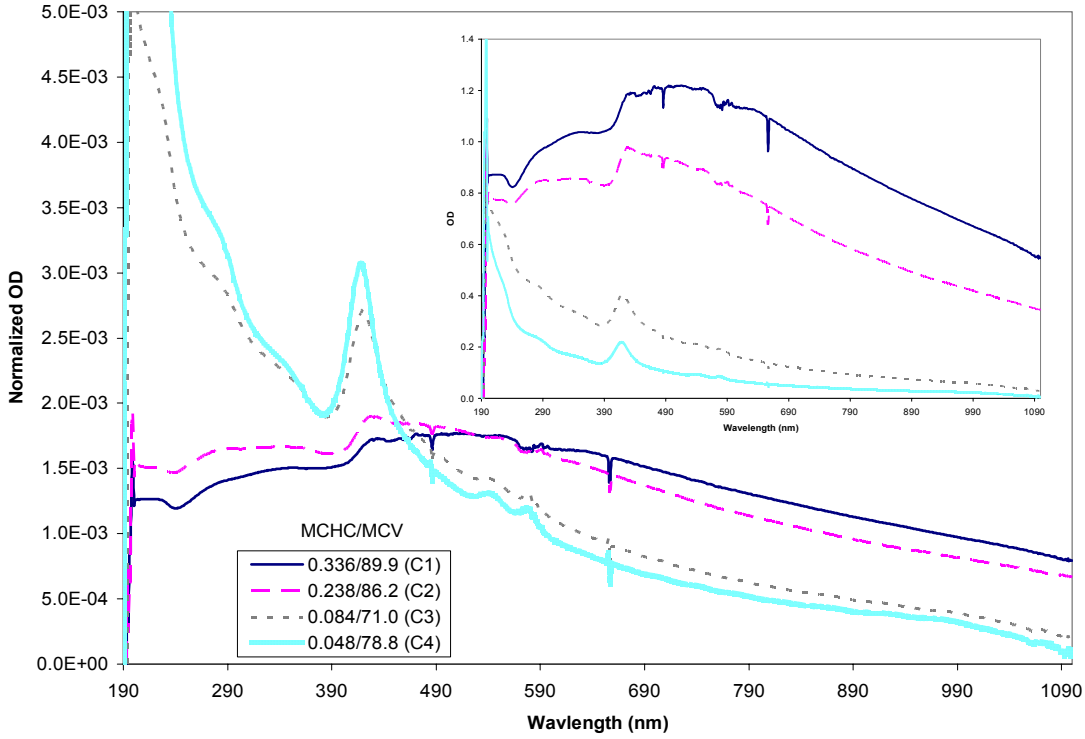

Figure 5.10: Experimental spectra of resealed cells with varying MCHC and MCV values. The MCHC is expressed in mass fractions and the MCV in fl. The inset represents the raw experimental data with each sample adjusted to a concentration of approximately 4000 cells/µl. The large plot represents the normalized data where each raw data was divided through by the area under their respective curve. The normalized plot amplifies the features of the curves to facilitate visual comparison.

overall spectrum. The good agreements seen between the experimental and simulated spectra of the unmodified and hypotonically modified erythrocytes indicate the effectiveness of the scattering theory in describing the spectral features as functions of the size and the hemoglobin concentration.

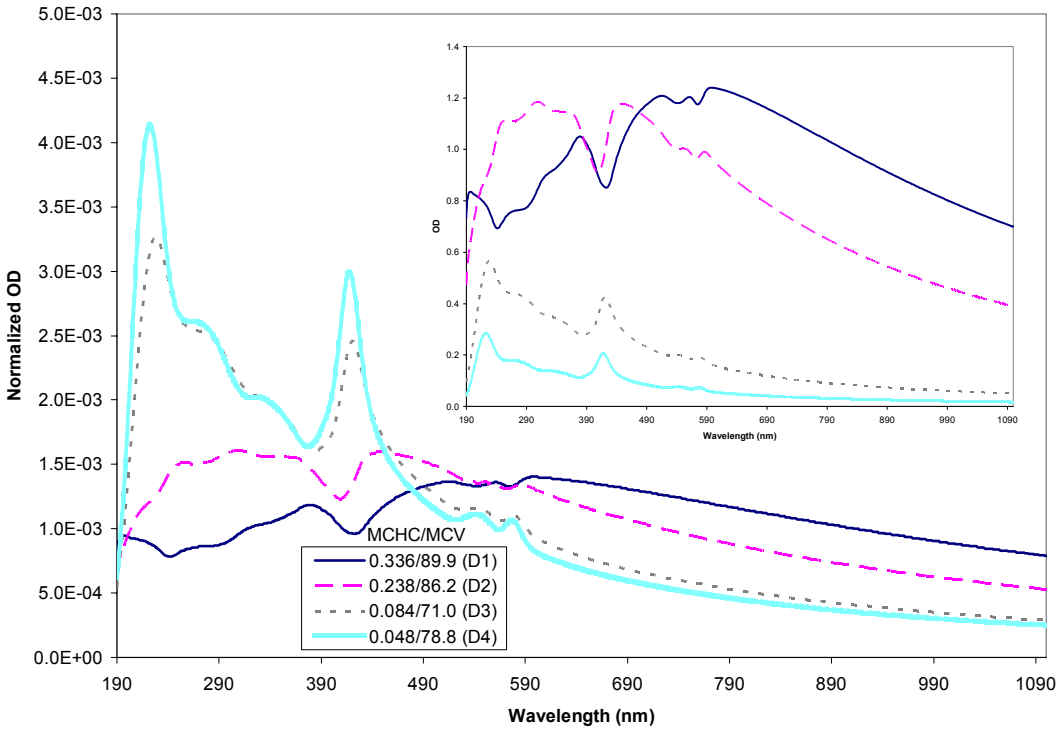

Figure 5.11: Simulated spectra of resealed cells using the experimental MCHC and MCV values in Figure 5.20. The MCHC is expressed in mass fractions and the MCV in fl. The inset represents simulations of the raw experimental data. The large plot represents the normalized data where each raw data was divided through by the area under the respective curves. The normalized plot amplifies the features of the curves to facilitate visual comparison.

5.3 Conclusions

This chapter examined the effectiveness of the Mie theory based model to simulate the spectral features and trends of purified and hypotonically modified erythrocytes. The acquisition of the experimental data of red cells possessing various MCHC and MCV values revealed features that were similar to the predictions made in the previous chapter. Furthermore, simulations of experimental data using corresponding values of hematologic parameters obtained from the hematology analyzer provided good agreement of the overall features. As two major parameters, MCHC and MCV, were changed, the trends of the spectra were modeled successfully to parallel those of the experimental spectra. Increasing MCV (at constant MCHC) showed a slight decrease in the absorption region (<600 nm), however this effect was not as dramatic as changing MCHC at constant MCV. In this latter case, increasing the MCHC drastically increased the whole particle scattering of the cell and this resulted in an elevation of the entire OD spectrum accompanied by the masking of the characteristic hemoglobin absorption peaks. Moreover, as the MCHC and MCV were both varied, the dominant parameter proved to be the MCHC in dictating the spectral trends. Also, normalized spectra showed that as the cellular hemoglobin content increased, the absorption peak decreased, strongly indicating the presence of macroscopic hypochromism at higher hemoglobin concentrations. This successful attempt to qualitatively simulate the purified and modified red cells allowed us to take the next step in our investigation: to implement a Mie interpretation model for the quantification red cell suspensions.

Chapter 6: Application of the Interpretation Model for the Quantitative Analysis of Erythrocytes

To this point, we have identified the presence of macroscopic hypochromicity as a scattering-related effect in the red cell spectra. Moreover, the features and trends of experimentally modified red blood cells were successfully simulated using the mathematical model. This chapter describes how the method was further extended to an interpretation model that permits the extraction of particle information from experimental spectrum including chemical composition, particle size, and particle number. The quality of results from the interpretation provide strong evidence that molecular hypochromicity is negligible in the UV-visible spectrum of a red blood cell system.

In Chapter 3 the concept of molecular hypochromicity was introduced. Previous studies[6,7] suggested the possibility of hypochromicity in red blood cells because of its high hemoglobin content. Considering that hemoglobin is a strong chromophore and it exists in large concentration inside the red cell, testing for molecular hypochromicity is not a trivial issue. If it exists, a hypochromicity correction would be required in addition to the implementation of a scattering and absorption model for the quantification of total hemoglobin in a red cell suspension. This test for molecular hypochromicity was to determine whether the interpretation model that accounts for scattering can provide good

estimates of the total hemoglobin concentration. The scattering model based on Mie theory simultaneously provides estimates of MCHC, MCV, and RBC counts, all parameters that can be measured independently. The good agreement found herein between the spectroscopy-based estimates and the measured values provide further support to our conclusion that molecular hypochromicity is not significant for red blood cells.

6.1 The Interpretation Model

The kernel of the interpretation model is the turbidity equation based on Mie theory (as described extensively in Chapter 3) and it provides adequate estimations of the above-mentioned parameters for a given sample spectrum. One of the big advantages to this method is its capability to efficiently analyze the spectrum across a broad wavelength range, providing a redundant mathematical check that increases the reliability of the estimated parameters. This is in contrast to many other studies using one or only a few selected wavelengths for their estimations.[79,80,81]

The general input-output format for the model is illustrated in the schematic diagram in Figure 6.1. The two major inputs are the optical properties of the chromophore (hemoglobin) and the measured spectrum. The computation consists of an iterative process to determine the best solution set for the output parameters which correspond to a good statistical fit of the spectrum. The wavelength range used for analysis was 240 – 900 nm. The range from 190 nm to 239 nm was omitted due to the solvent peak interfering with the sample spectra. Figure 4.6 (Chapter 4) showed a

spectrum of the solvent (0.9% PBS) that showed a large saturated peak < 240 nm. A background correction (subtraction of solvent spectrum from sample spectrum) of the sample spectrum would render this region unreliable for spectral interpretation. The wavelength range of 901 – 1100 nm was omitted due to spectral perturbations seen in this range resulting from an inconsistent instrumental light source. Although the diagnostics indicated that the lamp was producing intensities in this wavelength range within acceptable limits, some of the spectra showed dips below the baseline after background correction. It should be noted, however, that this omission did not alter the estimated values for the following reason. The "scattering only" region extends from approximately 620 nm to 1100 nm, a range that is largely linear. Hence, analyzing 620 – 900 nm is a good representation of the entire scattering wavelength range.

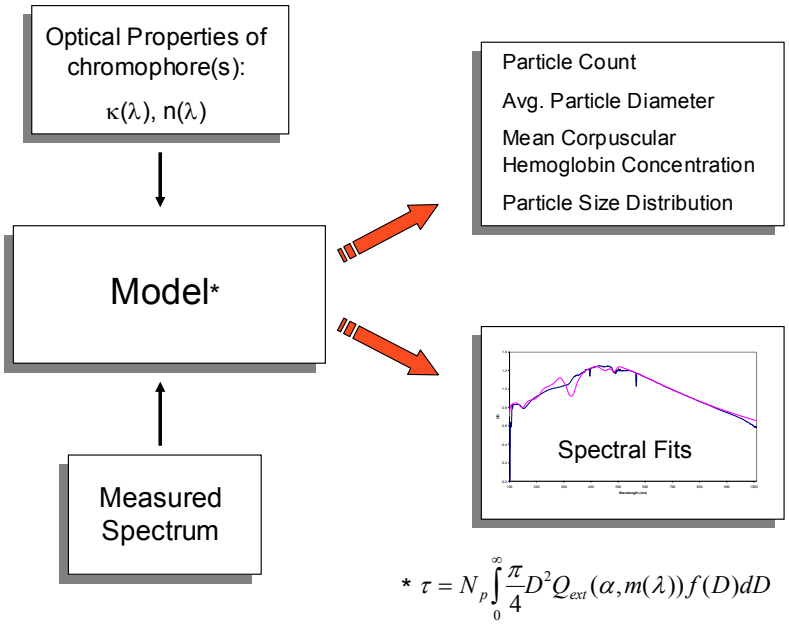

Figure 6.1: Schematic diagram of the interpretation model. Inputs consist of the optical properties of the chromophore and the experimentally measured spectrum. The outputs include the particle count, average particle diameter (of an equivalent sphere), the mean corpuscular hemoglobin concentration, particle size distribution, and the spectral fit.

Due to the multiple parameters composed in a solution set, regularization methods were implemented to confine the possible estimates and arrive at a reasonable solution while also limiting solutions to a statistically good fit of the spectrum.[119] To achieve this, the discretization of the integrand of the turbidity equation can be written in a matrix form as a quadrature approximation

$$\underline{\tau} = A\underline{f} + \underline{\varepsilon} \qquad \text{(Eq. 6.1)}$$

where ε represents the sum of the measurement error (ε_m) and the quadrature error introduced in the discretization (ε_c).[119,120] The least squares solution to the discretized model in terms of the particle size distribution (PSD) is defined as

$$\hat{f}_{ls} = (A^T A)^{-1} A^T \tau \qquad \text{(Eq. 6.2)}$$

However, small errors in the quadrature or experimental measurements can translate into large errors for $\hat{f}_{ls}$. Regularization of this equation leads to a constrained solution defined by

$$\hat{f}_{ls} = (A^T A + \gamma H)^{-1} A^T \tau \qquad \text{(Eq. 6.3)}$$

where γ is a regularization parameter and H is a covariance matrix that helps to narrow the possible solution sets that arise from the propagation of error. There exists an acceptable value for γ such that the error of $\hat{f}_{ls}$ is minimized. This value is estimated using the Generalized Cross Validation (GCV) technique described by the equation

$$V(\gamma) = m\frac{\left|[I - Z(\gamma)]\underline{\tau}\right|^2}{\{trace[I - Z(\gamma)]\}^2} \qquad \text{(Eq. 6.4)}$$

where $Z(\gamma)=A(A^TA+\gamma I)^{-1}A^T$.[120] The variable m represents the number of turbidity measurements with respect to wavelength.[117,121] The result of these equations is a reliable equivalent sphere particle size distribution for use with the turbidity equation in the interpretation model.

Variants of the Interpretation Model

The interpretation model was modified in three ways to provide slightly different approaches to the interpretation of the resealed red cell system.[69] Table 6.1 identifies and describes the three versions.

Version Name	Description
RBCHb01a	Choice of one encapsulated chromophore (oxyhemoglobin)
RBCHb01b	Choice of two encapsulated chromophores (oxy- and another hemoglobin derivative such as methemoglobin)
RBCHb02a	Choice of one chromophore but with the option to put a fraction of the chromophore outside of the cell in the medium

Table 6.1: The three versions of the interpretation models and the variations in their functions.

Version 01a is the simplest of the three with 01b and 02a introducing additional parameters for the prospect of elucidating the better solution set. However, increasing the number of parameters adds more complexity to the calculations as well as amplifying the potential error in the solution set such that the ideal situation would be if RBCHb01a proved to be an adequate model for a majority of the measured data. Therefore, the data was first analyzed with 01a while implementing the subsequent versions on an as-needed basis.

Corroboration of the Estimated Parameters

While the interpretation model is a powerful tool for extracting particle information from a single spectrum, its development requires validation of the observed parameters using separate analytical methods. These methods were previously described in the Chapter 4. Briefly, the hematology analyzer (Serono-Baker system) gives impedence-based values for the cell counts and the cell volume, with the volume being readily calculated to the equivalent sphere diameter using the equation for the volume of a sphere ($v=4\pi r^3/3$).

The hemoglobin concentration can be calculated in two independent manners albeit both are based on the same Drabkin's principle (discussed in Chapter 4).[46,47] The first is the modified Drabkin's assay automated by the hematology analyzer. The second is the manual Drabkin's assay, used as a verification tool for the values obtained via instrumental analysis. Although the two methods share the same principle, their executions bring about a systematic offset that needs to be addressed. Figure 6.2 is a scatter plot comparison of hemoglobin concentrations (HGB in g/dl) acquired from the two methods using an array of data points obtained throughout this study. The solid line represents a 45 degree reference line where a perfect correlation between the two methods of measurement would put the data points on the reference line. It is evident, however, that there is a relatively consistent bias in the data. The offset shows the Drabkin's values being slightly greater than the hematology analyzer values. Using the Serono numbers as the reference, the calculated percent (%) offset for the large (~20 g/dl) and medium (~10 g/dl) hemoglobin concentrations are within 10%. Although the best fit

line tapers towards the juxtaposed reference line at the lower values as expected, the numerical value for the % offset increases due to the decrease in the numerical values. Furthermore, the data points at the larger values (>20 g/dl) show a more pronounced deviation from the reference line. The discrepancy in the two techniques can be

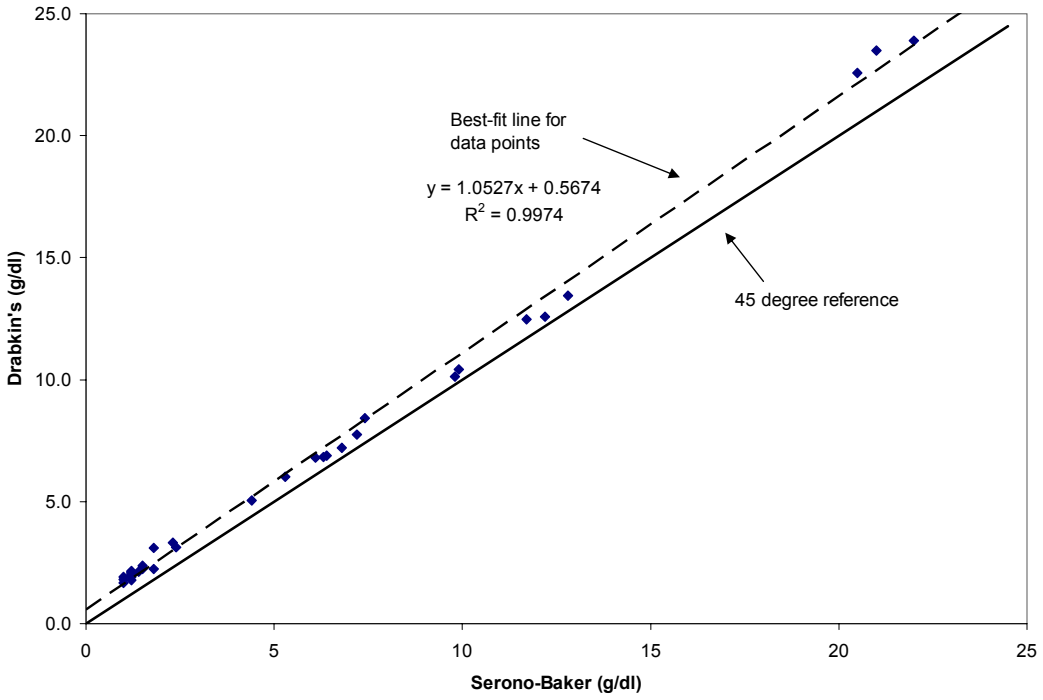

Figure 6.2: Comparison of hemoglobin concentration (HGB) values (g/dl) measured by the Serono-Baker and the Drabkin's assay. The solid line is a 45 degree reference line, the scattered points represent the data points, and the dotted line is a linear regression of the data points.

attributed to a systematic error which is not uncommon when comparing two such methods.[122,123] As long as the bias is considered, the Drabkin's method can still be used as a validation for the Serono-Baker and the estimated values from the interpretation model.

The hemoglobin concentration values compared in Figure 6.2 are raw numbers obtained directly from the measured spectra. In the case of both methods, the red cells are lysed, the optical density is taken at a predetermined wavelength and then translated into the hemoglobin concentration using a calibration curve. Since the Serono-Baker is an automated system, the error associated with the HGB reading is minimized. This is in contrast to the manual Drabkin's method in which one must take into account the human

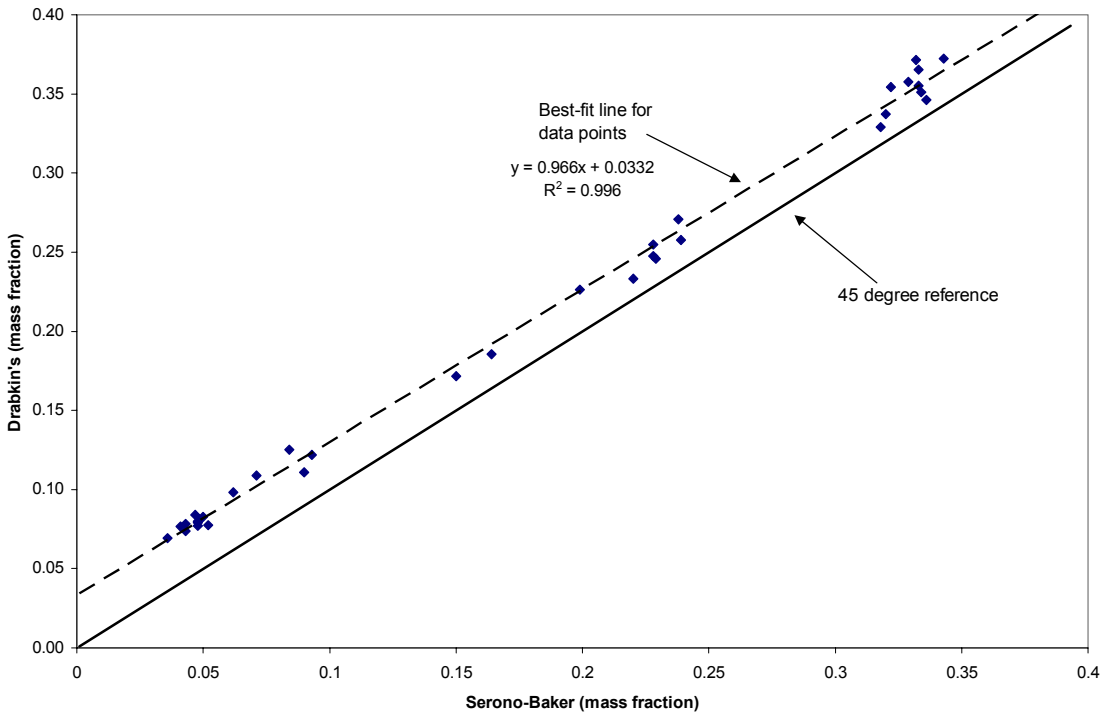

Figure 6.3: Comparison of the mean corpuscular hemoglobin concentration (MCHC) values (mass fraction) measured by the Serono-Baker and the Drabkin's assay. The solid line is a 45 degree reference line, the scattered points represent the data points, and the dotted line is a linear regression of the data points.

pipetting error as well as instrumental errors. The difference is illustrated in an analysis where six replicates of the same sample gave an error of 0.7% (standard deviation). Replicates of the Drabkin's assay showed a higher error of 1.4%.

The offset of the two methods can be further represented as a comparison of MCHC in Figure 6.3. It must be considered, however, that the MCHC is a calculated value instead of a raw number like the HGB. In the equation MCHC = HGB/HCT, it is evident that the computation introduces the hematocrit (HCT) value that is obtained by the Serono-Baker, an additional source of error. Thus this error is introduced into the MCHC obtained via both analytical formats. The plot shows that the data points at the lower MCHCs have a relatively tight fit to the linear regression whereas the higher MCHC values become slightly more scattered.

Testing the Interpretation Model

Thirty-four samples of purified and resealed red blood cells were analyzed to give good estimates red cell parameters. This section presents analyzed results for representative samples in the high, medium and low MCHC ranges. In order to explain the inputs and outputs of the model, a specific example of a resealed red cell sample in the low range MCHC (sample ID: r41603g) will be used. The program inputs for the RBCHb01a interpretation model with respect to this sample are as follows:

Problem number: 1
Cell pathlength (cm): 1
Particle density (g/ml): 1
Sample filename: r41603g.dat
Wavelength range for analysis (nm): 240 900
Optical properties file or particles and suspending medium: ophbo2.01

Enter filename for estimation results: r41603g.txt
Number of particle populations: 1
Fraction of chromophores in particles: 0.05
Estimate of D_n (nm): 4500
Estimate of sigma: 0.1
Enter filename for calculated PSD: r41603g.psd
Enter filename for calculated spectrum: r41603g.clc

Some of the parameters are self-explanatory. The optical properties file contains the absorption coefficient and the refractive index of oxyhemoglobin, and also the refractive index of the suspending medium (water). The "particle population" refers to the particle size population defined by the mean, where up to three distributions are allowed by the program. The majority of our analyses kept the population at one since this provided successful outcomes. The fraction of chromophores field is an estimation of the hemoglobin mass fraction that provides a starting point for the model to facilitate convergence. The value 0.05 was chosen as a round number close the Serono-Baker output (0.062). D_n is the estimated number based diameter of the sphere which was chosen to be 4500 nm, slightly smaller than the equivalent sphere diameter of a cell of volume 80 fl (5350 nm). The breadth of the variance (σ) for an equivalent lognormal size distribution was estimated to be 0.1.

The spectral output file is illustrated in Figure 6.4 along with some of the key estimated parameters. The data includes the measured spectrum fitted to the calculated spectrum. The residuals indicate the difference between the measured and calculated. The Beer-Lambert spectrum of the chromophore shows the absorption spectrum of oxyhemoglobin if the total mass of the encapsulated protein remained constant but existed free in solution in the same sample volume. An important feature to note in the

calculated spectrum is its close fit to the measured data. The scattering region (>600 nm), devoid of any absorption effects, shows a near-perfect overlay. Slight differences in the absorbing region of the spectrum may be attributed to either assumptions made in the modeling, or perhaps there are aspects of the biological system not being considered. Such issues will be discussed later in the chapter.

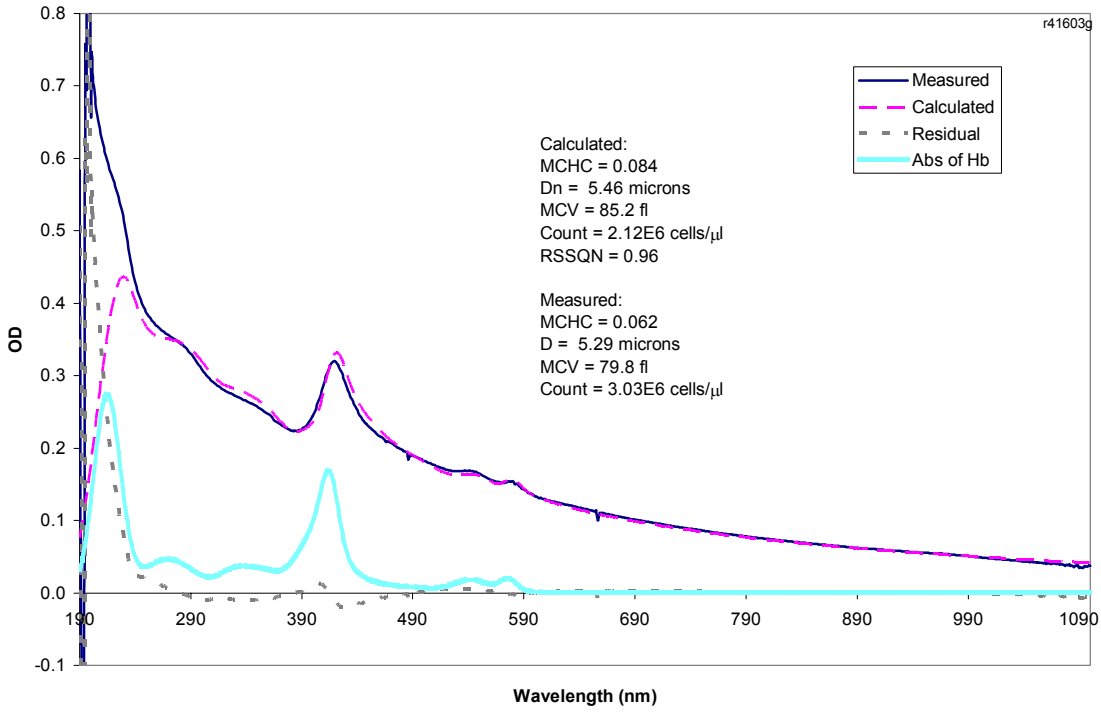

Figure 6.4: Output of the spectral estimate by the RBCHb01a interpretation model for low range MCHC. The measured and calculated spectra closely overlay each other. The residuals represent the difference between the calculated and measured spectra, and the absorption of hemoglobin illustrates the absorption spectrum if the hemoglobin resided free in solution while keeping the protein mass and sample volume constant.

Figure 6.4 is representative of successful interpretations achieved for resealed cells with the MCHC in the low range (< 0.10 mass fraction). In the case of the MCHC

value for this sample (r41603g), the measured quantity is reported to be 0.062 by the Serono-Baker (as shown in the figure) and 0.098 by the Drabkin's assay. The estimated value of 0.084 falls in the range between the two measured numbers. The MCV value itself is estimated to be 85.2 fl, slightly different from the measured quantity of 79.8 fl. The difference could be related to the instrumental error of the measured value and/or the flexibility of the numerical solutions within the statistical tolerance of the interpretation model. To elaborate this latter point, a few requirements need to be met to arrive at a reasonable solution: 1) the solution must provide a good fit to the empirical spectrum across the entire wavelength range of analysis, and 2) the values assigned to each of the important parameters (diameter, cell count, hemoglobin concentration, etc) must all make

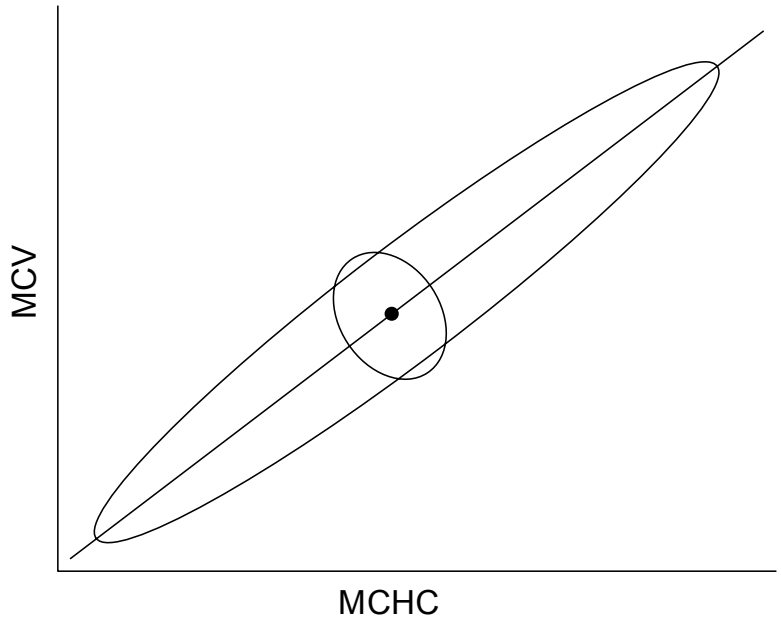

Figure 6.5: A representation of the algorithmic process of the interpretation model.

sense within physiologic constraints. Figure 6.5 illustrates a simplified example where statistically viable solutions exist within the limits of the oblong ellipse defining the error tolerance along a reference line. However, relevant solution sets reside within the smaller oval and the regularization technique narrows the possible solutions within these limits.

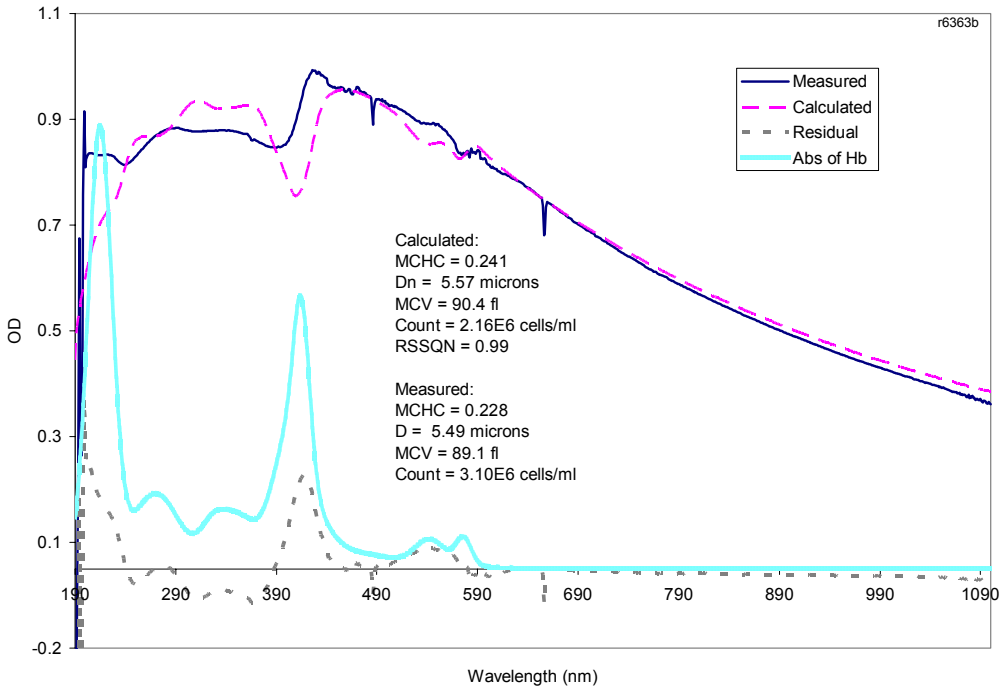

Figure 6.6: Output of the spectral estimate by the RBCHb01a interpretation model for medium range MCHC. The measured and calculated spectra resemble one another, particularly in the scattering region > 600 nm. The residuals represent the difference between the calculated and measured spectra, and the absorption of hemoglobin illustrates the absorption spectrum if the hemoglobin resided free in solution while keeping the protein mass and sample volume constant. The outputs for the hemoglobin concentration, size, and number parameters match well with the measured values.

Figure 6.6 is a representative result of a spectral interpretation by RBCHb01a for a resealed red cell population in the medium range of hemoglobin concentrations. In

terms of protocol, the length of time the cells were subject to permeabilization in the hypotonic buffer was reduced to approximately one minute so that less hemoglobin was released. The result was a higher encapsulated hemoglobin concentration compared to the data set represented by Figure 6.4. Higher hemoglobin content raised the overall refractive index of the particle, hence increasing the scattering component of the particle.

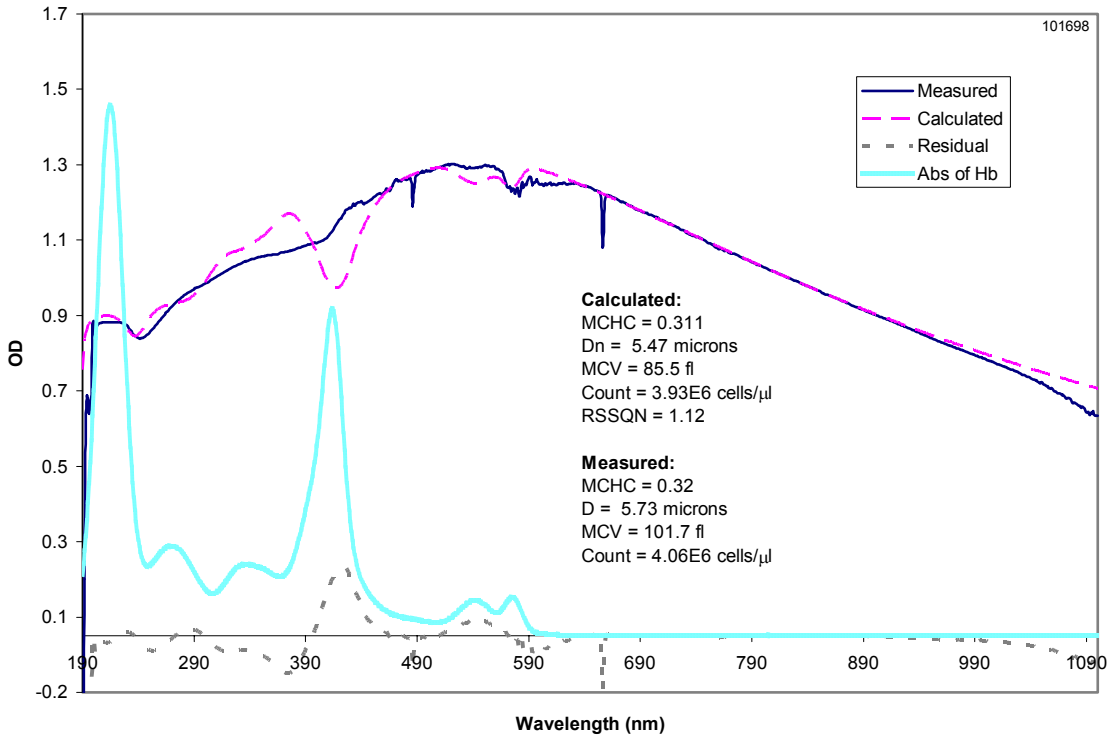

Figure 6.7: Output of the spectral estimate by the RBCHb01a interpretation model for physiological range MCHC. The measured and calculated spectra resemble one another, particularly in the scattering region > 600 nm. The residuals represent the difference between the calculated and measured spectra, and the absorption of hemoglobin illustrates the absorption spectrum if the hemoglobin resided free in solution while keeping the protein mass and sample volume constant. The outputs for the hemoglobin concentration, size, and number parameters match well with the measured values.

Increase in the scattering pattern adds to the complexity of modeling the total spectrum, particularly in the wavelength range < 600 nm that contains significant absorption information. This is reflected in the model's difficulty in closely reproducing all of the detailed features of the experimental spectrum, especially at the lower wavelengths. From a quantitative perspective, however, the three major parameters, MCHC, diameter/volume, and cell count all yield good results. Similar results were seen in samples with MCHC values in the physiological range (Figure 6.7). Experimentally, these erythrocytes were isolated from the major components of whole blood with no modification to the erythrocytes themselves. The interpreted spectral fit shows excellent correlation in the scattering-only region at wavelengths above 600 nm. The estimated MCHC and the cell counts show remarkable correspondence. The size values obtained from the experimental and calculated spectra were less similar, however, the calculated volume still falls within the physiological range (80 – 100 fl) and is a plausible value.

6.2 Quantitative Results of the Interpretation Model

As mentioned previously, the turbidity equation depends on not only the optical properties of the erythrocytes, but also a number of important parameters describing the particles: the cell size (equivalent sphere diameter/volume), the hemoglobin content, and the cell count. Provided that the refractive index of the medium is properly accounted for,[73] the interpretive results of the model generally showed satisfactory values for each of the parameters compared to their corroborative experimental values.

The three different versions of the interpretation model listed in Table 6.1 offered varying options in the way the data was evaluated. Program version RBCHb01a simulated the simplest case, assuming that all of the hemoglobin was encapsulated inside the cells in the form of oxyhemoglobin. We found that this version of the program converged to the most physiologically consistent solutions (43 of 59 samples analyzed converged to adequate values). The other two versions of the interpretation model only

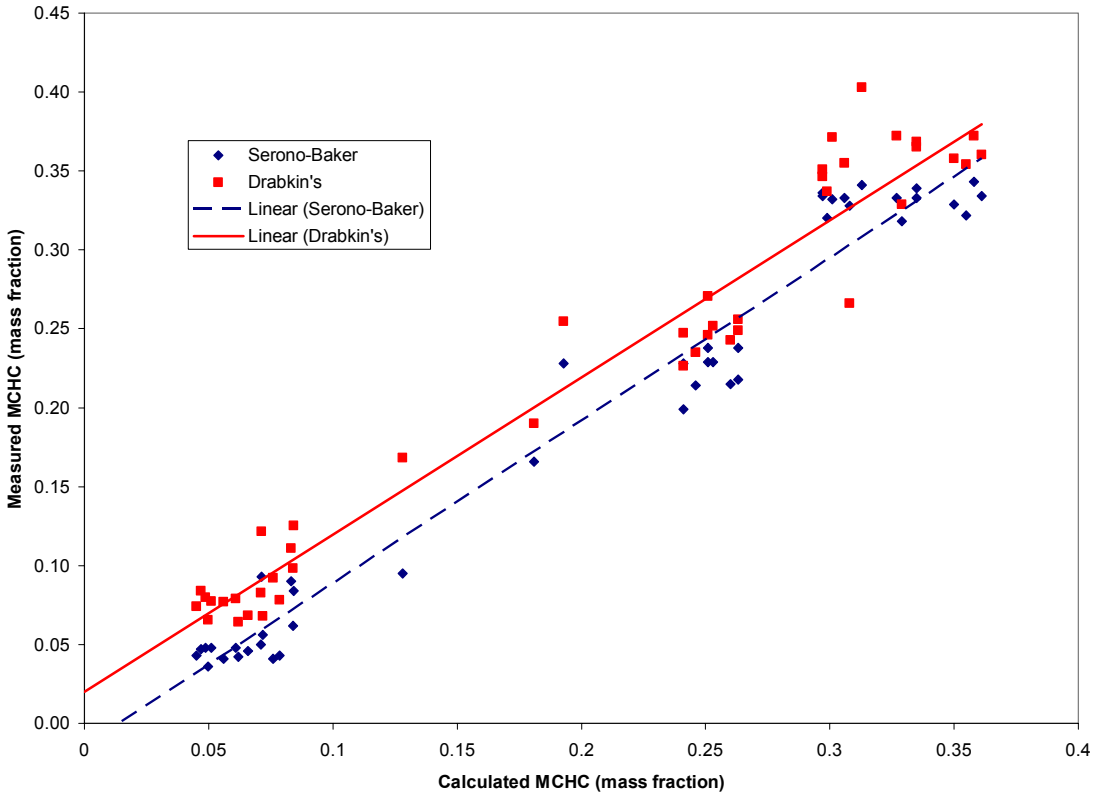

Figure 6.8: Comparison of the calculated MCHC to the MCHC values measured by the hematology analyzer and the manual Drabkin's assay. The scatter plots were fitted with a linear regression curve. Both methods show a high level of corroboration to the estimated data. The separation of the two lines is attributed to the systematic offset inherent between the two methods of measurement.

improved the estimations in isolated cases. The bulk of the results represented herein were obtained from RBCHb01a.

Quantitative Results Obtained with RBCHb01a

The mean corpuscular hemoglobin concentration (MCHC) value was reported by the Serono-Baker hematology analyzer and estimated by the interpretation model. Additionally, the MCHC was calculated from the hemoglobin concentration value obtained from the Drabkin's assay. Figure 6.8 shows a comparison of the estimated MCHC to those acquired from the two independent experimental procedures.

Sample	Serono-Baker	Estimated	Drabkin's
6399a	0.036	0.050	0.065
6399b	0.041	0.056	0.077
6399c	0.043	0.045	0.074
6399d	0.047	0.047	0.084
6999a	0.048	0.051	0.077
r5103d	0.084	0.084	0.125
r5103e	0.090	0.083	0.111
r41703d	0.095	0.128	0.168
r51403c	0.199	0.241	0.226
r6303b	0.228	0.241	0.247
r51403d	0.229	0.251	0.246
r6303a	0.238	0.251	0.271
r6303g	0.306	0.333	0.355
r41703a	0.333	0.335	0.365
r51403a	0.343	0.358	0.372

Table 6.2: Table of estimated and measured values (g/dl) for representative erythrocyte samples containing various amounts of hemoglobin. The calculated values generally fall between the two measured values with a few exceptions.

A perfect corroboration would be represented by a 45° line passing through the origin. The separation of the two best-fit lines is related to the systematic offset of the Drabkin's assay and the Serono-Baker discussed earlier in the chapter (Figures 6.2 and 6.3). Table 6.2 offers an abbreviated look at some representative values plotted in Figure 6.8. The estimated (calculated) values largely fall between the two measured values with a few exceptions, indicating a general consistency in the results of the model. Interestingly, both measured data sets in Figure 6.8 show an increased scatter in the points as the

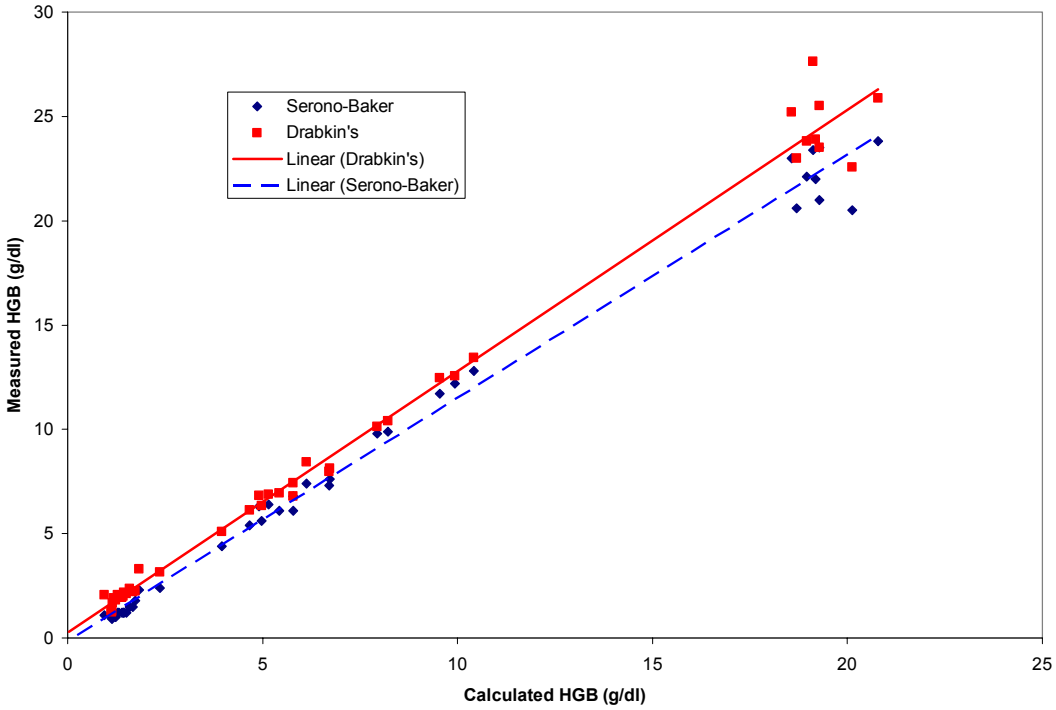

Figure 6.9: Comparison of the calculated hemoglobin concentration (HGB) to the HGB values measured by the hematology analyzer and the manual Drabkin's assay. The scatter plots were fitted with a linear regression curve. Both methods show a higher level of corroboration to the estimated values than the MCHC data. The separation of the two lines is attributed to the systematic offset inherent between the two methods of measurement.

hemoglobin values become larger. However, the same trend is seen in the direct comparison between the two physical methods in Figure 6.3 hence the increased scatter at the high hemoglobin concentrations is a result of measurement variability.

A similar comparison was made in terms of the total hemoglobin concentration (HGB) expressed in g/dl. This term represents the hemoglobin concentration quantified as the cells in suspension were lysed and the hemoglobin was diluted into solution.[47] The Drabkin's assay was the standardized method for the acquisition of this parameter. The hematology analyzer used a modified Drabkin's assay to collect the same information. The plot (Figure 6.9) illustrates a linear regression for both methods, each of which shows a high correlation with the calculated values. Consistent with the MCHC data, there is more scatter at the higher values than the low range. The tighter distribution of the points in Figure 6.8 is suggestive of the HGB parameter's unprocessed nature whereas MCHC is a value calculated from HGB and hematocrit (HCT) with an implied propagation of error. **Importantly, the estimation successfully accounted for the hemoglobin mass balance without the implementation of any correction for molecular hypochromism.**

Furthermore, comparisons were made between measured and calculated sizes of the cells, both expressed as equivalent sphere diameter and volume. The hematology analyzer provided the validation for the estimated sizes. The equivalent sphere diameters estimated by the interpretation model seemed to be reasonable estimates of the measured values for a large proportion (43/59) of samples (Figure 6.10). The calculated values for particle were close to or in the range of physiological values (5.35 – 5.76 μm). Greater

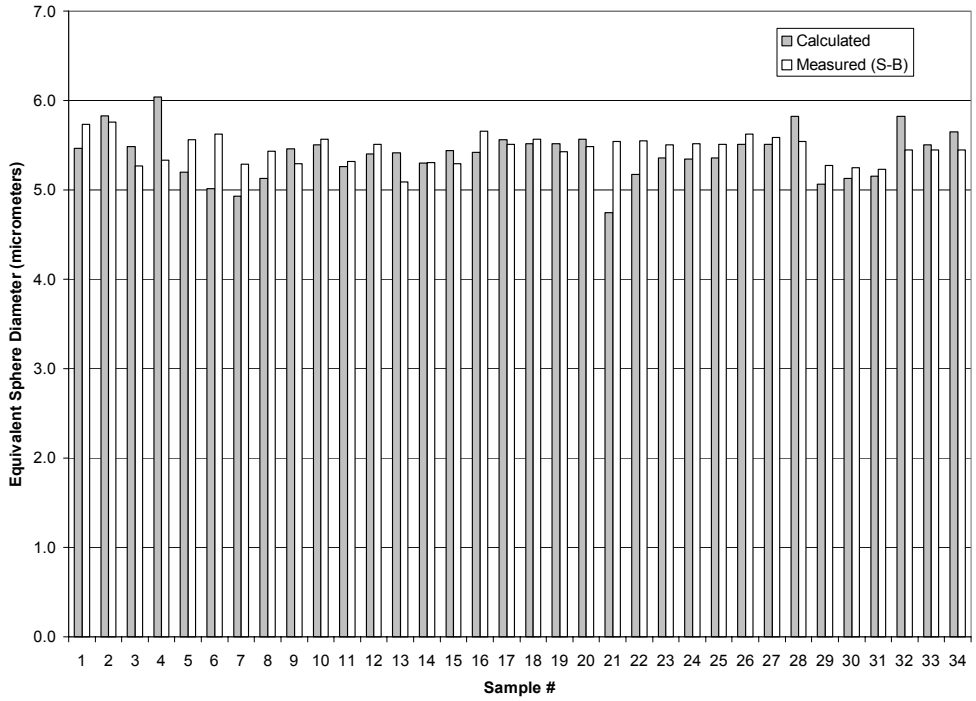

Figure 6.10: Calculated vs measured equivalent sphere diameters. The measured values were obtained from the Serono-Baker hematology analyzer and the calculated values were estimated by the interpretation model.

than 90% of the calculated estimates were within a 10% error of their measured counterparts. When these values were translated into volumes, even small differences were magnified due to the exponent in the spherical volume equation (Figure 6.11). Nevertheless, the differences between the calculated and measured MCVs are proportionate to their counterparts reported in Figure 6.10. Moreover, the phase contrast micrographs (Chapter 4) indicated that the sizes were consistent with both measured and estimated values. Hence it can be generally stated that the estimated volumes for a majority of our 59 experimental samples are in or approaching the physiological range of the erythrocytes.

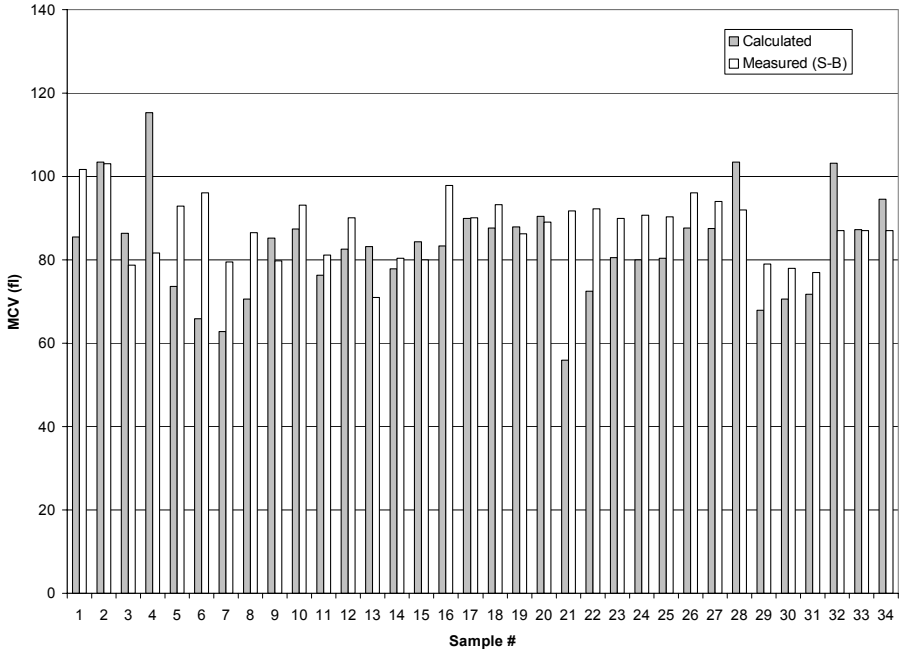

Figure 6.11: Calculated vs measured cell volumes. The measured values were obtained from the Serono-Baker hematology analyzer and the calculated values were estimated by the interpretation model.

Figure 6.12 illustrates the comparison between calculated and measured cell counts of purified and modified red cells. Although some of the smaller counts show significant variability, there are many samples that show very good agreement similar to the comparisons of cell volume in the previous figure. Of the 34 samples analyzed, the estimated values of approximately 70% of the samples were within 20% error of the measured values. It is important to note that the measured MCV and the cell counts have instrument-associated error as defined in Table 4.2 (Chapter 4). Moreover, the calculated values can fluctuate within the limits of acceptable solution sets as indicated previously in Figure 6.5.

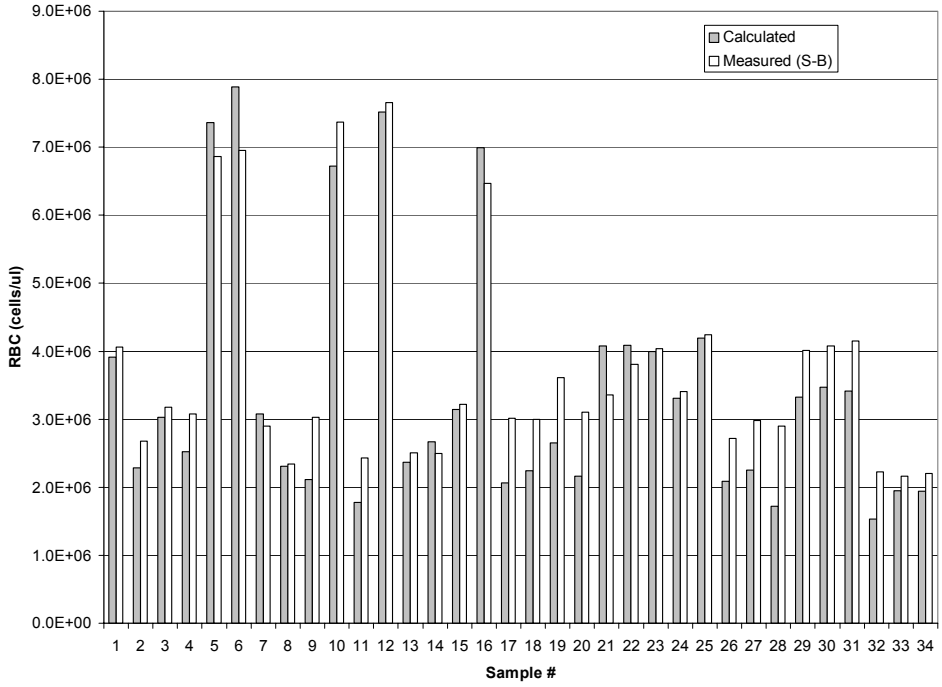

Figure 6.12: Calculated vs measured cell counts. The measured values were obtained from the Serono-Baker hematology analyzer and the calculated values were estimated by the interpretation model.

To further explore the variability of the measured values of cell count and cell size in comparison to the calculated numbers, a Coulter Z2 counter was used. Although the counts were obtained using electrical impedence measurements like the Serono-Baker hematology analyzer, it still provided another level of corroboration to validate the interpreted numbers. The counter is reported to give reproducible RBC counts within 5% and has an upper linearity limit of 8×10^6 cells/µl.[124] Tables 6.3 presents counts for six resealed cell samples measured on the Coulter and the Serono-Baker, and their calculated counterparts. Samples 1 – 3 were replicate samples of resealed cells prepared in parallel as were samples 4 – 6. Within each sample set, the

counts and sizes were relatively consistent for each instrument. Interestingly however, there were constant systematic offsets between the two impedance counters for each set of parameters. The calculated values obtained from the interpretation model generally fell close to the range of both measured values, but the precision appeared sample-related. The first sample set (1 – 3) yielded calculated values for both parameters that were closer to the measured values than the second sample set (4 – 6). The calculated equivalent sphere diameters (Table 6.4) showed better agreement to the experimental values.

	Coulter (10^6/μl)	Serono-Baker (10^6/μl)	Calculated (10^6/μl)
Sample 1	3.21	4.01	3.30
Sample 2	3.59	4.08	3.38
Sample 3	3.64	4.15	3.28
Sample 4	1.73	2.23	2.74
Sample 5	1.69	2.16	3.60
Sample 6	1.60	2.20	3.52

Table 6.3: Comparison of cell counts of resealed cells between measured (Coulter Z2 and Serono-Baker 9110) and calculated values.

	Coulter (μm)	Serono-Baker(μm)	Calculated(μm)
Sample 1	5.18	5.27	5.06
Sample 2	5.18	5.25	5.13
Sample 3	5.32	5.23	5.16
Sample 4	5.58	5.44	5.82
Sample 5	5.58	5.44	5.50
Sample 6	5.59	5.44	5.65

Table 6.4: Comparison of the equivalent sphere diameter (μm) of resealed cells between measured (Coulter Z2 and Serono-Baker 9110) and calculated values.

6.3 Discussion

It has long been debated over the last 50 years whether or not molecular hypochromism plays a role in the optical characteristics of encapsulated systems such as red blood cells and chloroplasts.[6,85] Considering the success of the interpretation model, however, it can be stated with confidence that molecular hypochromism is insignificant in the spectral analysis of red blood cells, and most probably in similar systems. The extension of Mie theory to accurately quantify the total hemoglobin concentration in a suspension of red cells is a large contribution to both fundamental and applied science. Moreover, the success in estimating other important red cell parameters including cell count, MCHC, MCV, and cell diameter strengthens the validity of the interpretation model.

When the interpretation model was subjected to multiple evaluations of the same red cell data, the algorithm consistently returned the same HGB value, although the MCHC and MCV fluctuated slightly and dependently between trials. This can be explained by examining how the interpretation model calculates these values. Consider the relationship

$$HGB = N_p\left(\frac{\pi D^3}{6}\right)\rho f_{Hb}$$

where the middle term in parentheses is the volume of a sphere, ρ is the density of the cell, and f_{Hb} is the mass fraction of hemoglobin. The interpretation program first attempts to fit a normalized spectrum, hence the particle concentration (N_p) is eliminated from the equation. Therefore, the two estimated values are D and f_{Hb}. These two parameters

fluctuate in accordance with each other to give a consistent HGB value that correlated well with the measured value.

Furthermore, the success of the estimated parameters was accompanied by good estimated fits of the measured spectra. The fits were best across the entire wavelength range (the data was fitted from 240 to 900 nm) for the low MCHC values (~0.05 – 0.10 mass fraction). This could be a result of one or more combined effects. First, the resealed cells appeared to take on a more spherical shape as evident in the phase contrast micrographs, thus approaching the spherical approximation used in Mie theory. Second, and perhaps more important, the lower contrast of resealed cells to medium due to the low hemoglobin concentration decreased whole particle scattering characteristics, simplifying the interpretation of the spectrum. As the MCHC increased, the scattering component increased adding to the complexity of the spectrum. At the wavelengths > 600 nm where mainly the scattering component is represented, a good overlap between the measured and calculated spectra is seen. At the low wavelengths, a combination of scattering and absorption components are represented. Here, there are differences in estimated and calculated spectra, however, the areas under the curves are similar. This appears to reflect a compensation for variations in spectral match that allows us to achieve relevant values for red cells. The experimental spectrum of the high MCHC (Figure 6.7) shows a smoothed curve compared to the estimated spectrum. This effect may be the result of distribution of cell orientations since it has been shown that a broadening of the distribution causes curve smoothening (unpublished work).[69] Thus accounting for cell shape and orientation in the calculations should further improve the

interpretation model, which is already providing good estimates of red cell parameters. Additionally, there are other distributions that merit consideration. The particle size distribution for the resealed cells could be slightly irregular compared to that of the unmodified red cells. Microscopy pictures suggest that the sizes range in the approximate diameters from 4 to 8 μm. In some cases, the distribution could be bimodal. Moreover, the MCHC distribution in the resealed cell samples could be heterogeneous, but to what degree remains to be seen. Examination of such issues should further improve upon an already satisfactory interpretation model. To conclude, in spite of the fact that we are using a simplified spherical approximation, the fact that there is good agreement between spectroscopy-based estimates and standard measurement strongly suggests that improvement of the scattering model is the right direction in completing the interpretation of the red blood cell.

Chapter 7: Conclusions

Multiwavelength UV-visible spectrophotometry is a versatile method for the characterization of suspended particles of various sizes. Optical analysis of particles such as red blood cells have been attempted on different levels (single wavelength or small wavelength range) and problems such as photometer design and the possibility of hypochromism have been identified. However, this is the first body of work that addresses the full array of fundamental questions associated with macroscopic particle characterization and successfully implements a reliable interpretation model for the quantification of the important parameters of red blood cells. The contributions are listed as follows.

- The concept of hypochromicity was revised in the context of obtaining precise estimates of hemoglobin concentration in red blood cells from spectroscopic measurements. Hypochromism (a decrease in the absorption spectrum with the increase in the concentration of a strong chromophore) in the past had only been defined as a phenomenon cause by electronic molecular interactions. In order to characterize red blood cells using the light scattering theory, it was necessary to adjust the perception of hypochromicity.
- Two levels of hypochromicity were established to better describe the optical behavior of macroscopic particles. Molecular hypochromicity is the aforementioned effect due

to particle interactions on the molecular level. Macroscopic hypochromicity is the attenuation of the absorption component as a result of increased light scattering as the refractive index of the particle increases. Red blood cells with high physiological concentrations of hemoglobin exhibit a particularly pronounced macroscopic hypochromicity.

- Instrumental configuration was shown to have a significant effect on the spectrum and the way it is interpreted. In previous studies,[6,7] the effect of photometer design (with respect to the angle of acceptance) on macroscopic particle spectra has been confused with molecular hypochromism. This study examined the importance of the acceptance angle on the red cell spectrum and in the process, we established that a small angle transmission spectrum contained the best balance of absorption and scattering information.
- A modified protocol for the hypotonic modification of red blood cells was developed, with the ability to control the resulting encapsulated hemoglobin concentration. The resealed cells were essential in the investigation of the optical behavior of red cells as the refractive index and the size of the particles changed.
- The light scattering theory of electromagnetic radiation was used to successfully account for the scattering and absorption components of red cell spectra. The capability to analyze both the scattering and absorption components of a large particle suspension allowed for the close examination of the two types of hypochromicity.
- In the context of light scattering theory, the Mie theory was implemented and extended to account for chemical composition across the entire wavelength range

(190 – 1100 nm). Although the theory assumes spherical particles, results showed its capability to reliably interpret red blood cell spectra in physiological and modified states.

- Using the Mie theory, trends and features of experimental red cell spectra were successfully simulated. Simulations were helpful in predicting the outcomes of experiments, and also to suggest the direction of future experiments.
- The interpretation model based on the Mie theory yielded realistic values of MCHC, MCV, N_p, and HGB for purified and resealed red cell samples.
- The success of the interpretation model in giving reasonable values for the hematologic parameters, particularly the total hemoglobin concentration (HGB) indicated that there was no significant molecular hypochromic effect as suggested in previous studies.

The implications of this work encompass the understanding of fundamental light scattering concepts and the possibilities of a rapid, inexpensive and reliable analysis of whole blood in a clinical setting. Since the contributions of red blood cells dominate a spectrum of whole blood, a good characterization of red cells was necessary in order to examine the effects of lesser optical contributors such as platelets and leukocytes. Furthermore, since the basic ideas are in place, multiwavelength light scattering analysis can be applied to encapsulated particle systems similar to red blood cells.

Future Work

The spherical restriction of the Mie theory may have been the reason for our inability to perfectly fit all of the features of the red cell spectrum, particularly for the cells containing a high concentration of hemoglobin. At high refractive indices of red cells, the scattering becomes more dominant and parameters such as shape and orientation could become important to the features of the spectrum. Current work involves other members of the research group attempting to incorporate form factors into the analysis to examine the effects of shape and orientation on the spectrum.[69,125]

Moreover, with regards to the characterization of resealed cells, there were physical details of the cells that were not accounted for by inspecting the sample with the hematology analyzer. For example, when the cells were permeabilized and resealed, the resulting MCHC most probably did not represent a uniform distribution of hemoglobin concentration across the entire population. The Serono-Baker reports an average value and is incapable of accounting for multiple populations. Simulations can be used to determine the impact of hypothetical distributions of hemoglobin concentrations. If the calculated model suggests that it is significant, then the resealed cells could be subjected to density separations to better characterize the cell spectra.

Experimental model systems can be used to further validate the results of the resealed cells. Liposomes were proposed in our studies as an alternative system, but results showed difficulty in producing unilamellar vesicles (Appendix C). A different protocol should be chosen to refine the quality of the liposomes to facilitate their characterization. Moreover, aggregation of proteins using high salt media provides

possibilities of mimicking encapsulated systems. Preliminary work with the aggregation of serum albumin and hemoglobin (Appendix H) showed drastic spectral changes when comparing pre- and post-aggregation. If the density and the size of the aggregates can be characterized, their spectra can be quantified.

References

[1] Garcia-Rubio, L. H. and Ro, N. Detailed copolymer characterization using ultraviolet spectroscopy. (1985) *Can J Chem*. 63 (1): 253-63.

[2] Garcia-Rubio, L. H. Characterization of proteins during aggregation using turbidimetry. (1989) *Chem Eng Commun.* 80 : 193-210.

[3] Elicabe, Guillermo E. and Garcia-Rubio, Luis H. The selection of the regularization parameter in inverse problems: estimation of particle size distribution from turbidimetry. (1988) *Polymeric Materials Science and Engineering*. 59 : 165-8.

[4] Brandolin, A., Garcia-Rubio, L. H., Provder, T., Koehler, M. E., and Kuo, C. Latex particle size distribution from turbidimetry using inversion techniques; experimental validation. (1990) *Polymeric Materials Science and Engineering*. 62 : 306-11.

[5] Weissbluth M. Hypochromism. (1971) *Quart Rev Biophys*. 4 (1): 1-34.

[6] Vekshin, N. L. Screening hypochromism in molecular aggregates and biopolymers. (1999) *J Biol Phys*. 25 (4): 339-354.

[7] MacRae, Robert A., McClure, Joseph A., and Latimer, Paul. Spectral transmission and scattering properties of red blood cells. (1961) *J. Opt. Soc. Am.* 51 : 1366-72.

[8] Bohren, C. F. and Huffman, D. R. Absorption and Scattering of Light by Small Particles. (1983) New York, NY: John Wiley and Sons, Inc.

[9] Mattley, Y., Leparc, G., Potter, R., and Garcia-Rubio, L. Light scattering and absorption model for the quantitative interpretation of human blood platelet spectral data. (2000) *Photochem Photobiol*. 71 (5): 610-619.

[10] Alupoaei, Catalina E., Olivares, Jose A., and Garcia-Rubio, Luis H. Quantitative spectroscopy analysis of prokaryotic cells: vegetative cells and spores. (2004) *Biosensors & Bioelectronics*. 19 (8): 893-903.

[11] McKenzie, S. B. Textbook of hematology. (1996) Baltimore, MD: Williams and Wilkins.

[12] Alkire K. and Collingwood J. Physiology of blood and bone marrow. (1990) *Seminars in Oncology Nursing*. 6 (2): 99-108.

[13] Alberts. B, Bray, D, Lewis, J, Raff, M, Roberts, K, and Watson, J. D. Molecular biology of the cell. (1989) New York, NY: Garland Publishing, Inc.

[14] Beutler, E., Lichtman, M. A., Coller, B. S., and Kipps, T. J. Williams Hematology, Sixth ed. (2001) New York, NY: McGraw-Hill, Inc.

[15] Harmening, D. M. Clinical hematology and fundamentals of hemostasis. (1997) Philadelphia, PA: F. A. Davis Co.

[16] Hoffman, R., Benz, Jr. E. J., Shattil, S. J., Furie, B., and Cohen, H. J. Hematology: Basic principles and practice. (1991) New York, NY: Churchill Livingstone Inc.

[17] Lee, G. R., Bithell, T. C., Foerster, J., Athens, J. W., and Lukens, J. N. Wintrobe's Clinical Hematology, Volume 1. (1992) Philadelphia, PA: Lea and Febiger.

[18] Besa, E. C., Catalano, P. M., Kant, J. A., and Jefferies, L. C. Hematology. (1992) Malvern, PA: Harwal Publishing Company.

[19] Dailey, J. F. Dailey's notes on blood. (1991) Somerville, MA: Medical Consulting Group.

[20] Kragh-Hansen, Ulrich. Structure and ligand binding properties of human serum albumin. (1990) *Dan. Med. Bull.* 37 (1): 57-84.

[21] Meloun, B., Moravek, L., and Kostka, V. Complete amini acid sequence of human serum albumin. (1975) *FEBS Lett.* 58 (1): 134-137.

[22] Schreiber, G. Synthesis, processing and secretion of plasma proteins by the liver and other organs and their regulation. In: Putnam, F. W. editor.The plasma proteins: Structure, function and genetic control. (1987) Orlando, FL: Academic Press, Inc.

[23] Ueno, A., Hong, Y. M., Arakaki, N., and Takeda, Y. Insulin-stimulating peptide from a tryptic digest of bovine serum albumin: Purification and characterization. (1985) *J. Biochem.* 98 : 269-278.

[24] Narayanan, S. Aggregation and structural changes in biological systems; An ultraviolet visible spectroscopic approach for analysis of blood cell aggregation and protein conformation. Ph.D. dissertation. (1999) Department of Chemistry, University of South Florida.

[25] Ness, P. M. and Stengle, J. M. Historical introduction. Editor: Surgenor, D. M.The Red Blood Cell. Second edition. (1974) New York, NY: Academic Press.

[26] Hillman, R. S. and Finch, C. A.Red cell manual, 7th Ed. (1996) Philadelphia, PA: F. A. Davis Co.

[27] Steck, T. L. The organization of proteins in the human red blood cell membrane. A review. (1974) *J Cell Biol*. 62 (1): 1-19.

[28] Voet, D.; Voet, J. G., and Pratt, C. W. Fundamentals of Biochemistry. Upgrade ed. (2002) New York, NY: John Wiley and Sons, Inc.

[29] Winkelmann, J. C. and Forget, B. G. Erythroid and nonerythroid spectrins. (1993) *Blood*. 81 (12): 3173-85.

[30] Marchesi, V. T. Structure and function of the erythrocyte membrane skeleton. Editors: Kruckeberg, W. C., Eaton, J. W., Aster, J., and Brewer, G. J. Erythrocyte membranes 3: Recent clinical and experimental advances. (1983) New York, NY: Alan R. Liss, Inc.

[31] Agre, P., Smith, B. L., Saboori, A. M., and Asimos, A. The red cell membrane skeleton: A model with general biological relevance but pathological significance for blood. Gunn, R. and Parker, J. C., Editors. Cell Physiology of Blood. (1988) New York, NY: Rockefeller University Press

[32] Liu, S. C. and Derick, L. H. Molecular anatomy of the red blood cell membrane skeleton: structure- function relationships. (1992) *Semin Hematol*. 29 (4): 231-43.

[33] Peters, L. L. and Lux, S. E. Ankyrins: structure and function in normal cells and hereditary spherocytes. (1993) *Semin Hematol*. 30 (2): 85-118.

[34] Brewer, George J. General red cell metaolism. Surgenor, D. M., Editor. The Red Blood Cell, 2nd Ed. (1974) 1: 387-433.

[35] Weinstein, R. S. The morphology of adult red cells. Surgenor, D. M., Editor. The Red Blood Cell, 2nd Ed. (1974) 1 : 213-268.

[36] Voet, D. and Voet, J. G. Biochemistry: Biomolecules, mechanisms of enzyme action, and metabolism. Vol. 1. Third ed. (2004) New York, NY: John Wiley and Sons, Inc.

[37] Antonini, Eraldo and Brunori, Maurizio. Hemoglobin and Myoglobin in their Reactions with Ligands (Frontiers of Biology, Vol. 21). (1971) New York, NY: American Elsevier.

[38] Devlin, T. M. Textbook of Biochemistry with Clinical Correlations. Fourth ed. (1997) New York, NY: John Wiley and Sons, Inc.

[39] Kaplan, L. A. and Pesce, A. J. Clinical Chemistry: Theory, Analysis, and Correlation. Third ed. (1996) St. Louis, MO: Mosby.

[40] Stryer, L. Biochemistry, Fourth ed. (1995) New York, NY: W. H. Freeman.

[41] Baldwin, Joyce and Chothia, Cyrus. Hemoglobin: the structural changes related to ligand binding and its allosteric mechanism. (1979) *J Mol Biol*. 129 (2): 175-220.

[42] Zwart, A., Van Kampen, E. J., and Zijlstra, W. G. Results of routine determination of clinically significant hemoglobin derivatives by multicomponent analysis. (1986) *Clin Chem*. 32 (6): 972-8.

[43] Petragnani, Nicola, Nogueira, Otilia C., and Raw, Isaias. Methemoglobin reduction through cytochrome b5. (1959) *Nature*. 184 (Suppl. No. 21): 1651.

[44] Mrvos, R. The spectrophotometric measurement of methemoglobin. (1997) *Clin Lab Sci*. 10 (3): 119-121.

[45] Gordy, Edwin, Drabkin, David L., and Marsh, Julian B. Spectrophotometric studies. XVI. Determination of the oxygen saturation of blood by a simplified technique, applicable to standard equipment. (1957) *J Biol Chem*. 227 : 285-99.

[46] International Committee for Standardization in Haematology. Recommendations for haemoglobinometry in human blood. (1967) *Br J Haematol*. 13 : 71-5.

[47] International Committee for Standardization in Haematology. Recommendations for reference method for haemoglobinometry in human blood (ICSH standard EP 6/2: 1977) and specifications for international haemiglobincyanide reference preparation (ICSH standard EP 6/3: 1977). (1978) *J Clin Pathol*. 31 (2): 139-43.

[48] Senozan, N. M. and Devore, J. A. Carbon monoxide poisoning: some surprising aspects of the equilibrium between hemoglobin, carbon monoxide, and oxygen. (1996) *J Chem Ed*. 73 (8): 767-770.

[49] Cox C J, Habermann T M, Payne B A, Klee G G, and Pierre R V. Evaluation of the Coulter Counter model S-Plus IV. (1985) *Am J Clin Pathol*. 84 (3): 297-306.

[50] Mayer K, Chin B, and Baisley A. Evaluation of the S-Plus IV. (1985) *Am J Clin Pathol*. 83 (1): 40-6.

[51] Wintrobe, M. M. The size and hemoglobin content of the erythrocyte. Methods of determination and clinical application. (1932) *J Lab Clin Med.* 17 : 899-912.

[52] Narayanan, S., Orton, S., Leparc, G. F., Garcia-Rubio, L. H., and Potter, R. L. Ultraviolet and visible light spectrophotometric approach to blood typing: objective analysis by agglutination index. (1999) *Transfusion.* 39 (10): 1051-1059.

[53] Narayanan, S., Galloway, L., Nonoyama, A., Leparc, G. F., Garcia-Rubio, L. H., and Potter, R. L. UV-visible spectrophotometric approach to blood typing II: Phenotyping of subtype A2 and weak D and whole blood analysis. (2002) *Transfusion*. 42 (5): 619-626.

[54] Lane, T. A.; Anderson, K. C.; Goodnough, L. T.; Durtz, S.; Moroff, Gary; Pisciotto, Patricia T.; Sayers, Merlin, and Silberstein, Leslie E. Leukocyte Reduction in Blood Component Therapy. (1992) *Ann Int Med*. 117: 151-162.

[55] Raftos, J. E., Stewart, I. M., and Lovric, V. A. Supernatant hemoglobin determinations after prolonged blood storage. (1986) *Pathology*. 18 (1): 123-6.

[56] Tinoco, I. Jr. Hypochromism in polynucleotides. (1960) *J Am Chem Soc*. 82 : 4785-90.

[57] Heiz, C., Raedler, U., and Luisi, P. L. Spectroscopy and Recognition Chemistry of Micelles from Monoalkyl Phosphoryl Nucleosides. (1998) *J Phys Chem B*. 102 (44): 8686-8691.

[58] Latimer, P. The deconvulation of absorption spectra of green plant material-improved corrections for the sieve effect. (1983) *Photochem Photobiol*. 38 (6): 731-734.

[59] Silverstein, R. M., Bassler, G. C., and Morrill, T. C. Spectrometric Identification of Organic Compounds, Fifth Ed. (1991) New York, NY: John Wiley and Sons, Inc. pp. 289-315.

[60] Christian, G. D. Analytical Chemistry, Sixth Ed. (2004) Hoboken, NJ: John Wiley and Sons, Inc.: 457-521.

[61] http://micro.magnet.fsu.edu/primer/java/electromagnetic/

[62] Garcia-Rubio, L. H. Refractive index effects on the absorption spectra of macromolecules. (1992) *Macromolecules*. 25 (10): 2608-13.

[63] Tinoco, I., Sauer, K., Wang, J. C., and Puglisi, J. D. Physical Chemistry: Principles and Applications in Biological Systems. (2002) Upper Saddle River, NJ.: Prentice Hall, Inc.

[64] Levine, Rodney L. and Federici, M. Marcia. Quantitation of aromatic residues in proteins: model compounds for second-derivative spectroscopy. (1982) *Biochem*. 21 (11): 2600-6.

[65] Ichikawa, Tetsuo and Terada, Hiroshi. Second derivative spectrophotometry as an effective tool for examining phenylalanine residues in proteins. (1977) *Biochim Biophys Acta*. 494 (1): 267-70.

[66] Wetlaufer, D. B. Ultraviolet spectra of proteins and amino acids. (1962) *Advan. Protein Chem.* 17 : 303-90 .

[67] Creighton, T. E. Proteins: Structures and Molecular Properties, Second Ed. (1993) New York, NY: W. H. Freeman and Company.

[68] Latimer, P., Brunsting, A., Pyle, B. E., and Moore, C. Effects of asphericity on single particle scattering. (1978) *Appl Opt*. 17 (19): 3152-3158.

[69] Personal communication with Prof. Luis H. Garcia-Rubio, College of Marine Science, University of South Florida, St. Petersburg, FL.

[70] Reynolds, L. O. Optical Diffuse Reflectance and Transmittance from an Anisotropically Scattering Finite Blood Medium. (1957) Ph.D. Dissertation, University of Washington.

[71] Kerker, M. The scattering of light and other electromagnetic radiation. (1969) New York, NY: Academic Press.

[72] van de Hulst, H. C. Light Scattering by Small Particles. (1981) New York, NY.: Dover Publications, Inc.

[73] Garcia-Rubio, L. H. Refractive index effects on the absorption spectra of macromolecules. (1992) *Macromolecules*. 25 (10): 2608-13.

[74] Garcia-Rubio, L. H., Lopez-Menacho, C. A., and Grossman, S. Characterization of proteins during aggregation. II. Use of model molecules for spectroscopy analysis. (1993) *Chem Eng Commun*. 122 : 85-101.

[75] Alupoaei, C. E. Modeling of the transmission spectra of microorganisms. M.S. Thesis. (2001) Department of Chemical Engineering, University of South Florida.

[76] Yaroslavsky, A. N., Priezzhev, A. V., Rodriguez, J., Yaroslavsky, I. V., and Battarbee, H. Optics of blood. Tuchin, V. V., Editor. Handbook of Optical Biomedical Diagnostics. (2002) Bellingham, WA: SPIE Press. pp. 169-216.

[77] Jay, Alfred W. L. and Canham, Peter B. Sedimentation of single human red blood cells. Differences between normal and glutaraldehyde fixed cells. (1972) *J Cell Physiol*. 80 (3): 367-72.

[78] Smallwood R H, Tindale W B, and Trowbridge E A. The physics of red cell sedimentation. *Physics Med Biol*. 30 (2): 125-37.

[79] Steinke, J. M. and Shepherd, A. P. Comparison of Mie theory and the light scattering of red blood cells. (1988) *Appl Opt*. 27 (19): 4027-4033.

[80] Hammer, M., Schweitzer, D., Michel, B., Thamm, E., and Kolb, A. Single scattering by red blood cells. (1998) *Appl Opt*. 37 (31): 7410-7418.

[81] Tycko, D. H., Metz, M. H., Epstein, E. A., and Grinbaum, A. Flow-cytometric light scattering measurement of red blood cell volume and hemoglobin concentration. (1985) *Appl Opt*. 24 (9): 1355-65.

[82] Latimer, P. The influence of photometer design on optical-conformational changes. (1975) *J Theor Biol*. 51 (1): 1-12.

[83] UV Atlas of Organic Compounds, Volume II. (1966) New York: Plenum Press.

[84] Latimer, P. The deconvulation of absorption spectra of green plant material-improved corrections for the sieve effect. (1983) *Photochem Photobiol*. 38 (6): 731-734.

[85] Duysens, L. N. M. Flattening of the absorption spectrum of suspensions, as compared to that of solutions. (1956) *Biochim Biophys Acta*. 19 : 1-12.

[86] Tinoco, I. Jr. Hypochromism in polynucleotides. (1960) *J Am Chem Soc*. 82 : 4785-90.

[87] Vekshin, N. L. Screening hypochromism of biological macromolecules and suspensions. (1989) *J Photochem Photobiol, B: Biology*. 3 (4): 625-30.

[88] Lawley, P. D. Interaction studies with deoxyribonucleic acid. III. Effect of changes in sodium-ion concentration, pH, and temperature on the ultraviolet absorption spectrum of sodium thymonucleate. (1956) *Biochim Biophys Acta*. 21 : 481-8.

[89] Vekshin, N. L. Screening hypochromism of chromophores in macromolecular biostructures. (1999) *Biofizika*. 44 (1): 45-55.

[90] Vekshin, N. L. Screening hypochromism stacked chromophores. (1987) *Opt Spectrosk*. 63 (3): 517-19.

[91] Bateman, J. B., Hsu, S. S., Knudsen, J. P., and Yudowitch, K. L. Hemoglobin spacing in erythrocytes. (1953) *Arch Biochem Biophys*. 45 : 411-22.

[92] Garcia-Rubio, L. H. The effect of the molecular size on the absorption spectra of macromolecules. (1987) *Macromolecules*. 20 (12): 3070-5.

[93] Kramer, Kurt, Elam, James O., Saxton, Geo. A., Elam, Wm. N. Jr., and Heob, Dorothy. Influence of oxygen saturation, erythrocyte concentration, and optical depth upon the red and near-infrared light transmittance of whole blood. (1951) *Am J Physiol*. 165 : 229-46.

[94] Anderson, N. M. and Sekelj, P. Light-absorbing and scattering properties of nonhaemolysed blood. (1967) *Phys Med Biol*. 12 (2): 173-84.

[95] Latimer, P. The influence of photometer design on optical-conformational changes. (1975) *J Theoret Biol*. 51 (1): 1-12.

[96] Borovoi, A. G., Naats, E. I., and Oppen, U. G. Scattering of light by a red blood cell. (1998) *J Biomed Opt*. 3 (3): 364-372.

[97] Amesz, J., Duysens, L. N. M., and Brandt, D. C. Methods for measuring and correcting the absorption spectrum of scattering suspensions. (1961) *J Theoret Biol.* 1 : 59-74.

[98] Leach, S. J. and Scheraga, H. A. Effect of light scattering on ultraviolet difference spectra. (1960) *J Am Chem Soc*. 82 : 4790-2.

[99] Whitaker, T. R., Sartiano, G. P., Hamelly, L. J. Jr., Scott, W. L., and Glew, R. H. Hypotonic exchange loading of human erythrocytes with iron-59-labeled rabbit hemoglobin. (1974) *J Lab Clin Med*. 84 (6): 879-88.

[100] Marsden, N. V. B. and Ostling, S. G. Accumulation of dextran in human red cells after hemolysis. (1959) *Nature*. 184 (Suppl. No. 10): 723-4.

[101] Sartiano, G. P. and Hayes, R. L. Hypotonic exchange-loading of erythrocytes. II. introduction of hemoglobins S and C into normal red cells. (1977) *J Lab Clin Med*. 89 (1): 30-40.

[102] Ihler, G. M., Glew, R. H., and Schnure, F. W. Enzyme loading of erythrocytes. (1973) *Proc Natl Acad Sci U S A*. 70 (9): 2663-6.

[103] Baker, R. F. Entry of ferritin into human red cells during hypotonic hemolysis. (1967) *Nature*. 215 (5099): 424-5.

[104] Seeman, P. Transient holes in the erythrocyte membrane during hypotonic hemolysis and stable holes in the membrane after lysis by saponin and lysolecithin. (1967) *J Cell Biol*. 32 (1): 55-70.

[105] Agilent 8453 UV-visible Spectroscopy System: Operator's Manual. (2002) Agilent Technologies.

[106] Hematology Analyzer 9110+ Operator's Manual. Serono-Baker, PA.

[107] Jones, O. T., Earnest, J. P., and McNamee, M. G. Solubilization and reconstitution of membrane proteins. Findlay, J. B. C. and Evans, W. H. Editors. Biological Membranes: A Practical Approach. (1987) Washington DC: IRL Press Ltd. pp. 139-177.

[108] Norbert P. Zemankiewicz (1995), University of South Florida, Tampa.

[109] Personal communication with Dr. Yvette Mattley, Tampa, FL.

[110] High concentrations of mannitol and dextrose maximize preservation. Brochure. Baxter Healthcare Corp, Fenwal Division, Deerfield, IL.

[111] Prihoda, L. A., Kelley, A., and Shah, C. Comparison of leukocyte reduction filters for red blood cells. (1997) *Transfus*. 37 (Suppl): 17S.

[112] Lane T A, Anderson K C, Goodnough L T, Kurtz S, Moroff G, Pisciotto P T, Sayers M, and Silberstein L E. Leukocyte reduction in blood component therapy. (1992) *Ann Int Med*. 117 (2): 151-62.

[113] Bodemann, H. and Passow, H. Factors controlling the resealing of the membrane of human erythrocyte ghosts after hypotonic hemolysis. (1972) *J Membr Biol*. 8 (1): 1-26.

[114] Hoffman J. F. Physiological characteristics of human red blood cell ghosts. (1958) *J. Gen. Physiol*. 42 (1): 9-28.

[115] Latimer, P. and Eubanks, C. A. H. Absorption spectrophotometry of turbid suspensions: a method of correcting for large systematic distortions. (1962) *Arch Biochem Biophys*. 98 : 274-85.

[116] Thormaehlen, I., Straub, J., and Grigull, U. Refractive index of water and its dependence on wavelength, temperature, and density. (1985) *Journal of Physical and Chemical Reference Data*. 14 (4): 933-45.

[117] Mattley, Y. D. An investigation of the spectroscopic properties of platelets during activation and storage: Implementation of a new interpretation model. Ph.D. Dissertation (2000) Department of Chemistry, University of South Florida.

[118] Narayanan, S. Aggregation and structural changes in biological systems: An ultraviolet visible spectroscopic approach for analysis of blood cell aggregation and protein conformation. Ph.D. Dissertation (1999) Department of Chemistry, University of South Florida.

[119] Elicabe, G. E. and Garcia-Rubio, L. H. Latex particle size distribution from turbidimetry using inversion techniques. (1989) *J Colloid Interf Sci*. 129 (1): 192-200.

[120] Elicabe, G. E. and Garcia-Rubio, L. H. Latex particle size distribution from turbidimetric measurements combining regularization and generalized cross-validation techniques. (1990) *Adv Chem Ser*. 227 : 83-104.

[121] Golub, G. H., Heath, M., and Wahba, G. Generalized cross-validation as a method for choosing a good Ridge parameter. (1979) *Technometrics*. 21 (2): 215-223.

[122] Personal communication with Dr. German Leparc, Florida Blood Services, Tampa, FL.

[123] Personal communication with Dr. Debbie Huffman, College of Marine Science, University of South Florida, St. Petersburg, FL.

[124] Coulter Z Series particle count and size analysers. User Manual #9914591-C. (1997) Beckman Coulter Inc., CA.

[125] Personal communication with Alicia Garcia-Lopez. (2004).

[126] New, R. R. C. Liposomes: A Practical Approach. (1990) New York: IRL Press.

[127] Monnard, P.-A., Oberholzer, T., and Luisi, P. Entrapment of nucleic acids in liposomes. (1997) *Biochim Biophys Acta*. 1329 (1): 39-50.

[128] Djordjevich, L. and Miller, I. F. Synthetic erythrocytes from lipid encapsulated hemoglobin. (1980) *Exp Hemat*. 8 (5): 584-92.

[129] Hunt C. A. and Burnette R R. Lipid microencapsulation of hemoglobin. *Appl Biochem Biotech*. 10 : 147-9.

[130] Domokos, G., Jopski, B., and Schmidt, K. H. Preparation, properties and biological function of liposome-encapsulated hemoglobin. (1992) *Biomat Art Cells Immob Biotech*. 20 (2-4): 345-54.

[131] Mobed, M., Nishiya, T., and Chang, T. M. S. Purification and characterization of liposomes encapsulating hemoglobin as potential blood substitutes. (1992) *Biomat Art Cells Immob Biotech*. 20 (1): 53-70.

[132] Dimitriadis, G. J. Entrapment of ribonucleic acids in liposomes. (1978) *FEBS Letters*. 86 (2): 289-93.

[133] Brochu, H., Polidori, A., Pucci, B., and Vermette, P. Drug delivery systems using immobilized intact liposomes: A comparative and critical review. (2004) *Current Drug Delivery*. 1 (3): 299-312.

[134] Ohki, N., Kimura, T., and Ogata, Y. The reduction of methemoglobin in Neo Red Cell. (1998) *Art Cells Blood Subs Immob Biotech*. 26 (5 & 6): 477-485.

[135] Szebeni, J., Di Iorio, E. E., Hauser, H., and Winterhalter, K. H. Encapsulation of hemoglobin in phospholipid liposomes: characterization and stability. (1985) *Biochemistry*. 24 (12): 2827-32.

[136] Shew, R. L. and Deamer, D. W. A novel method for encapsulation of macromolecules in liposomes. (1985) *Biochim Biophys Acta*. 816 (1): 1-8.

[137] Liu L and Yonetani T. Preparation and characterization of liposome-encapsulated haemoglobin by a freeze-thaw method. *J Microencapsulation*. 11 (4): 409-21.

[138] Gregoriadis, G. Liposome Technology: Liposome Preparation and Related Techniques. Vol. 1. (1993) Boca Raton: CRC Press.

[139] Schurtenberger, P. and Hauser, H. Characterization of the size distribution of unilamellar vesicles by gel filtration, quasi-elastic light scattering and electron microscopy. (1984) *Biochim Biophys Acta*. 778 (3): 470-80.

[140] Ostrowsky, N. Liposome size measurements by photon correlation spectroscopy. (1993) *Chemistry and Physics of Lipids*. 64 (1-3): 45-56.

[141] Deutscher, M. P. Methods in Enzymology, Vol 182: Guide to Protein Purification. (1990) New York: Academic Press, Inc.

[142] Scopes, R. K. Protein Purification: Principles and Practice, Third Ed. (1994) New York: Springer-Verlag Inc.

Appendices

Appendix A: Mie Theory Formulae

It has been established that the Mie efficiency coefficient[8,71,72] for extinction (Q_{ext}) is related to the optical density with the turbidity equation revisited below,

$$\tau = N_p \int_0^\infty \frac{\pi}{4} D^2 Q_{sca}(\alpha, m(\lambda)) f(D) dD + N_p \int_0^\infty \frac{\pi}{4} D^2 Q_{abs}(\alpha, m(\lambda)) f(D) dD$$

where $Q_{ext} = Q_{sca} + Q_{abs}$ thus the turbidity equation is divided into its scattering and absorption components. Other important parameters of the equation include the particle number (N_p), the equivalent sphere diameter (D), the size distribution function (f(d)), the size parameter (α) and the complex refractive index (m). The latter two parameters were defined in Chapter 3 as

$$\alpha = \frac{\pi D}{\lambda}, \qquad m(\lambda) = \frac{n(\lambda)}{n_0(\lambda)} + i\frac{\kappa(\lambda)}{n_0(\lambda)}$$

Q_{sca} and Q_{ext} are defined as

$$Q_{sca} = \frac{2}{\alpha^2} \sum_{n=1}^{\infty} (2n+1)\{|a_n|^2 + |b_n|^2\}$$

$$Q_{ext} = \frac{2}{\alpha^2} \sum_{n=1}^{\infty} (2n+1)\{\mathrm{Re}(a_n + b_n)\}$$

where Q_{abs} can be inferred from these two know values. Mie scattering coefficients, a_n and b_n are

$$a_n = \frac{m\psi_n(m\alpha)\psi'_n(\alpha) - \psi_n(\alpha)\psi'_n(m\alpha)}{m\psi_n(m\alpha)\xi'_n(\alpha) - \xi_n(\alpha)\psi'_n(m\alpha)}$$

$$b_n = \frac{\psi_n(m\alpha)\psi'_n(\alpha) - m\psi_n(\alpha)\psi'_n(m\alpha)}{\psi_n(m\alpha)\xi'_n(\alpha) - m\xi_n(\alpha)\psi'_n(m\alpha)}$$

$\xi_n(z)$, $\xi'_n(z)$, $\psi_n(z)$, and $\psi'_n(z)$ are Riccati-Bessel functions defined in terms of Bessel functions (J_n),

$$\xi_n(z)\left(\frac{\pi z}{2}\right)^{\frac{1}{2}}\left[J_{n+\frac{1}{2}}(z) + i(-1)^{n+1}J_{-\left(n+\frac{1}{2}\right)}(z)\right]$$

$$\xi'_n(z) = \xi_{n-1}(z) - \frac{n\psi}{\alpha}$$

$$\psi_n(z) = \left(\frac{\pi z}{2}\right)^{\frac{1}{2}} J_{n+\frac{1}{2}}(z)$$

$$\psi'_n(z) = \psi_{n-1}(z) - \frac{n\psi}{\alpha}$$

Appendix B: Concentration-Related Instrumental Limitations of Hemoglobin and Erythrocytes

It is important to understand and to operate within the limitations of the instrument (Agilent 8453 UV-vis spectrophotometer) when analyzing data. Two major concerns that required attention were both related to the concentration of the erythrocytes in the suspension: linearity of the instrument and multiple scattering. The former can be discussed in terms of the absorbance equation, $A = \log (I_0/I_t)$. If the recovered transmitted light is only 5% of the incident light intensity due to absorption, the value for A would be 1.3. At 1% recovery, A would be 2. Thus as absorption increases, the sensitivity of the detector is tested due to the decreasing light transmission. We have chosen a conservative 1.2 optical density units as our upper limit to ensure the reliability of our data. Figure B1 demonstrates the linearity of the optical density measurements as a function of concentration for a hemoglobin solution taken with a 1 cm pathlength cuvette. The small peak at 540 nm stays below an OD of one and thus maintains good linearity over the observed concentrations. The hemoglobin Soret band at 417 nm keeps linearity at higher OD and it can be inferred by the plot that the linearity breaks down between 2.5 and 3.0 OD. Therefore, it can be seen that our self-imposed limit of 1.2 OD is well within the linear limits and will give reliable data. Due to the high extinction coefficient of hemoglobin, the 417 nm band reaches and OD of 1.2 at a concentration of ~1.3 mg/ml and the 540 nm band at a concentration of ~14 mg/ml. These values are not remotely close to physiological encapsulated hemoglobin concentrations of 330 mg/ml. Thus it is easy to see the difficulty in examining the effect of molecular hypochromism in a free hemoglobin solution approaching physiological concentrations. For suspensions of

red cells, it was determined experimentally that a concentration of 4000 cells/μl gives an OD of ~1.2.

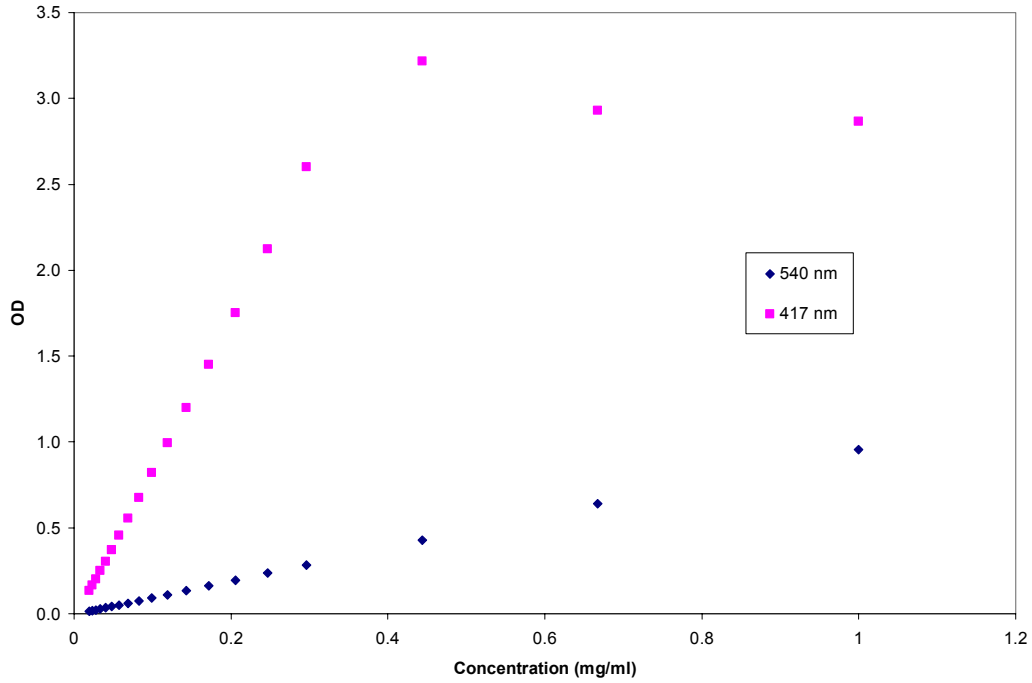

Figure B1: Assessment of the optical density linearity limits of the Agilent 8453 spectrophotometer as a function of hemoglobin (solution) concentration. The 540 nm band maintains linearity due to its low optical density over the observed concentrations. The 417 nm band, however, loses its linearity between OD of 2.5 and 3.0.

Multiple scattering effects also need to be considered in a particle suspension. The Mie theory predicts light scattered by a single particle. If the cells are concentrated enough to scatter light by multiple particles, the task of interpreting the spectra becomes complex. Figure B2 examines if there are any multiple scattering effects at the working sample dilution of 4000 cells/μl with serial dilutions of whole blood. The presence of

multiple scattering would manifest itself by deviating from linearity as the cell concentration increases. According to our observations, the measurement at approximately 4000 cells/µl shows negligible deviations at wavelengths of 417 and 540 nm. Thus it can be concluded that multiple scattering effects are not a factor in our simulations and interpretations of spectra based on the Mie theory.

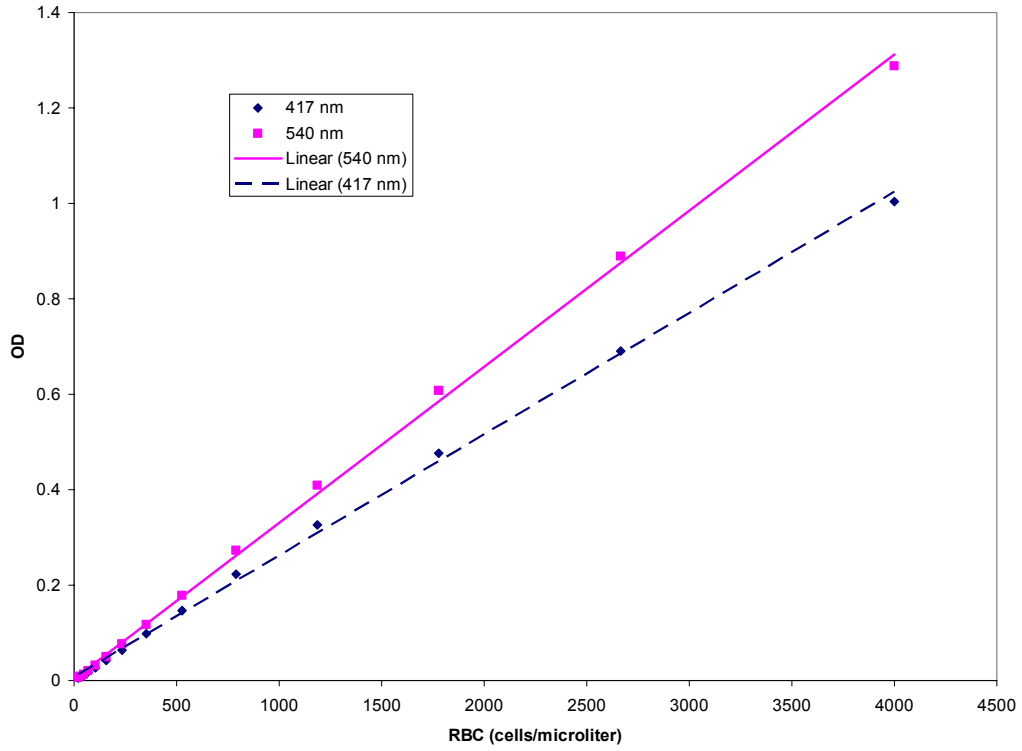

Figure B2: Serial dilutions of whole blood for the examination of multiple scattering. The linearity of the spectrum at wavelengths of 417 and 540 nm imply negligible multiple scattering effects at 4000 cells/µl.

Appendix C: Spectral Characterization of a Liposome Model System

Multiwavelength spectra of modified red blood cells were successfully characterized and interpreted in this dissertation. As an alternate experimental model system parallel to the red cells, liposomes were used to encapsulate hemoglobin (hemosomes) and other model proteins. The advantages to a good liposome model system are that they are easy to manipulate, a variety of model molecules can be encapsulated within the membrane, and their spherical nature fits well in the Mie framework.

Liposomes are lipid vesicles that enclose an aqueous volume. When lipids are introduced to aqueous media at the appropriate concentrations, they form spontaneously into vesicles with the membrane in a bilayer structure similar to those of biological cells (Figure C1).[126] Liposomes are typically made with common phospholipids such as phosphatidylcholine, phosphatidylserine and sphingomyelin in combination with cholesterol (~ 1:1 molar ratio of lipid:cholesterol). The physical structure of the liposomes membranes can be unilamellar or multilamellar (multiple concentric membranes within the same liposome) depending on the manner in which they are prepared.[126,127] Moreover, sizes of the liposomes can vary in the range of 0.02 – 20 μm in diameter.[126,128] Liposome systems have different clinical and experimental applications such as artificial red blood cell substitutes,[128,129,130,131] nucleic acid carriers,[127,132] drug delivery systems,[133] and systems observing enzymatic activity under encapsulated conditions.[134]

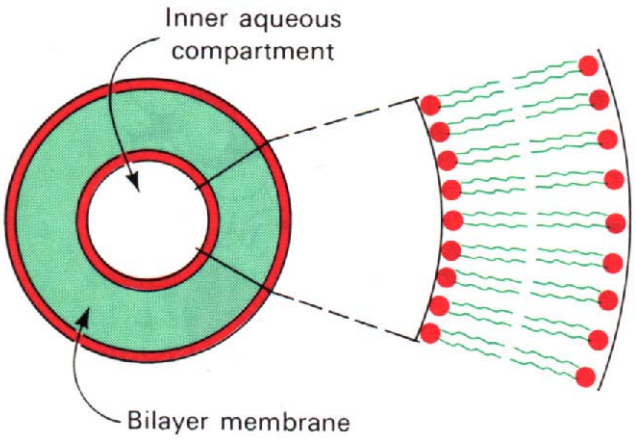

Figure C1: Diagram of a liposome. Like biological phospholipids bilayers, the membranes adopt tail-to-tail configuration and encapsulate an aqueous volume.

The objective of this research was to perform a multiwavelength UV-vis spectral analysis/chararacterization of liposomes encapsulating hemoglobin (hemosomes) to parallel our studies of the modified red cells. Given that the properties of the hemosomes are accurately elucidated, it should be possible to interprete the spectra of the hemosomes, considering the success the modified red cell characterization. The liposomes vary greatly in size, however this should not pose a problem with the interpretation since there are no size restrictions with the Mie theory. Moreover, liposomes encapsulating albumin were examined due to the accessibility of the model protein.

Materials and Methods:

For the preparation of the protein-encapsulated liposomes, a commonly described thin film method was used.[128,135] Lyophilized egg yolk phosphatidylcholine (PC) (Sigma-Aldrich, MO) was reconstituted to a stock solution of

100 mg/ml with chloroform. Using an approximate molecular weight of the PC (MW ~768 Da) given by the manufacturer, a 1:1 molar ration of PC:cholesterol was calculated. In a 250 ml round-bottom flask, 200 ml of PC stock solution and 10 mg of cholesterol were measured and dissolved in approximately 3 ml of chloroform. The flask was fitted to a rotary evaporator (Buchi Rotovapor R-3000 with a Buchi 461 water bath) and subjected to a vacuum with the water bath set to approximately 55^{o}C, slightly lower than the boiling point of chloroform (61.5^{o}C). The flask was rotated until the chloroform was completely evaporated and a thin layer of lipid/cholesterol was distributed evenly on the bottom of the flask.

The proteins encapsulated were bovine serum albumin (Sigma-Aldrich MO) (typically ~ 5% concentration was used), and hemoglobin harvested from red blood cells (Figure C2). For the hemoglobin, whole blood samples were obtained from the Florida Blood Services (St. Petersburg, FL). The whole blood sample was washed by centrifugation in three cycles with isotonic PBS as previously described in Chapter 4. The washed cell sample was then lysed by a freeze-thaw method. The cells were frozen in a -80^{o}C freezer for approximately 10 minutes, then immediately thawed in a 56^{o}C water bath. The process was repeated three times until inversion of the sample in its holding tube no longer showed any turbidity of intact cells. The sample was then centrifuged at 100,000 x *g* in a Beckman Optima TL ultracentrifuge with a TLA-100.4 rotor to rid the suspension of cell debris. The resulting hemoglobin solution was assayed for concentration using the Drabkin's assay (Chapter 4).

Next, the hemoglobin solution diluted to a desired concentration was measured (~10 ml) into the round-bottom flask containing the thin lipid/cholesterol layer and the mixture was sonicated for approximately 15 minutes at a frequency of 47 KHz (Branson 5120 sonicator) (Figure C3). The resulting liposomes were washed three times by centrifugation and resuspended with PBS to approximately 2 ml. A spectrum of the

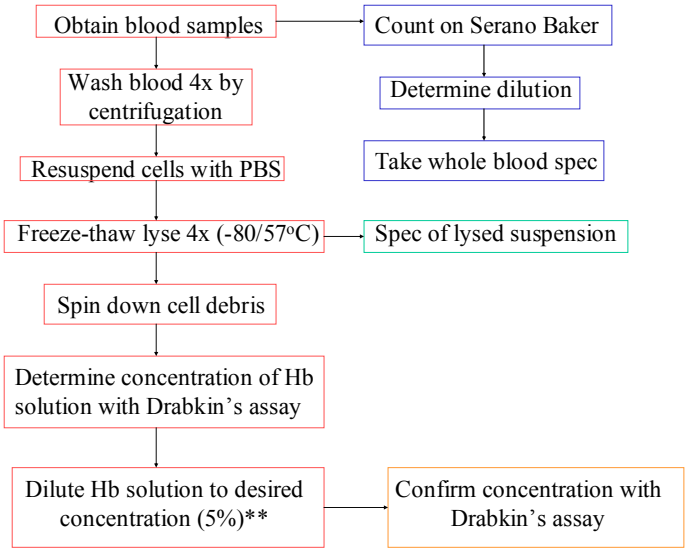

Figure C2: Flowchart of the method for hemoglobin harvesting prior to the production of hemoglobin-encapsulated liposomes (hemosomes).

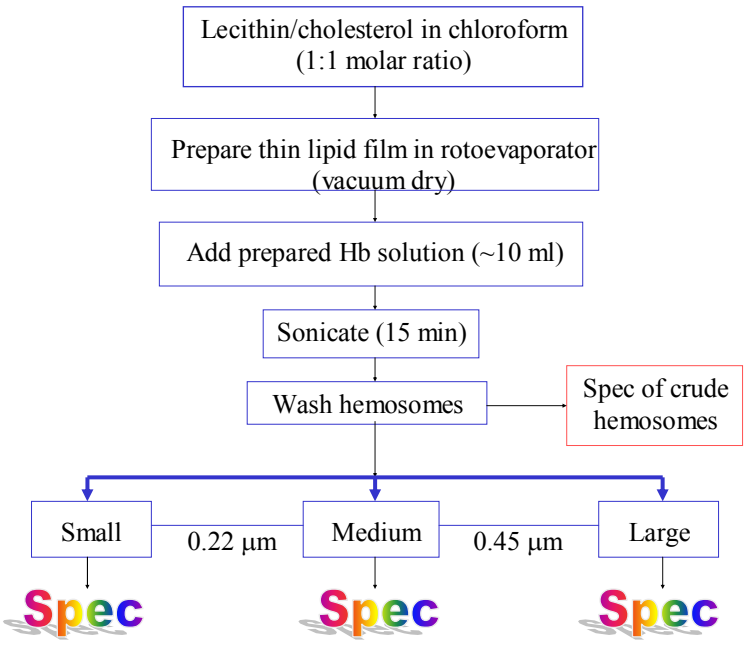

Figure C3: Protocol for the generation of hemoglobin-encapsulated liposomes (hemosomes). Other model proteins such as albumin can be substituted for hemoglobin.

crude sample suspension was obtained. The suspension was then mechanically extruded with syringe filters (Whatman polyethersulfone disc filters for low protein adsorption) with pore sizes of 0.22 and 0.45 µm to narrow the size ranges of the liposomes for analysis. Spectra were obtained for each size range.

Results and Discussion

Figure C4 shows normalized spectra of the crude, filtered and free albumin spectra from a representative albumin liposome experiment. The spectrum of the free albumin solution shows a clearly defined Soret band at ~280 nm but in contrast, none of

the liposome spectra show this peak. This effect is a scattering-related effect comparable to the one seen with hemoglobin and red cells. The crude sample, which represents the

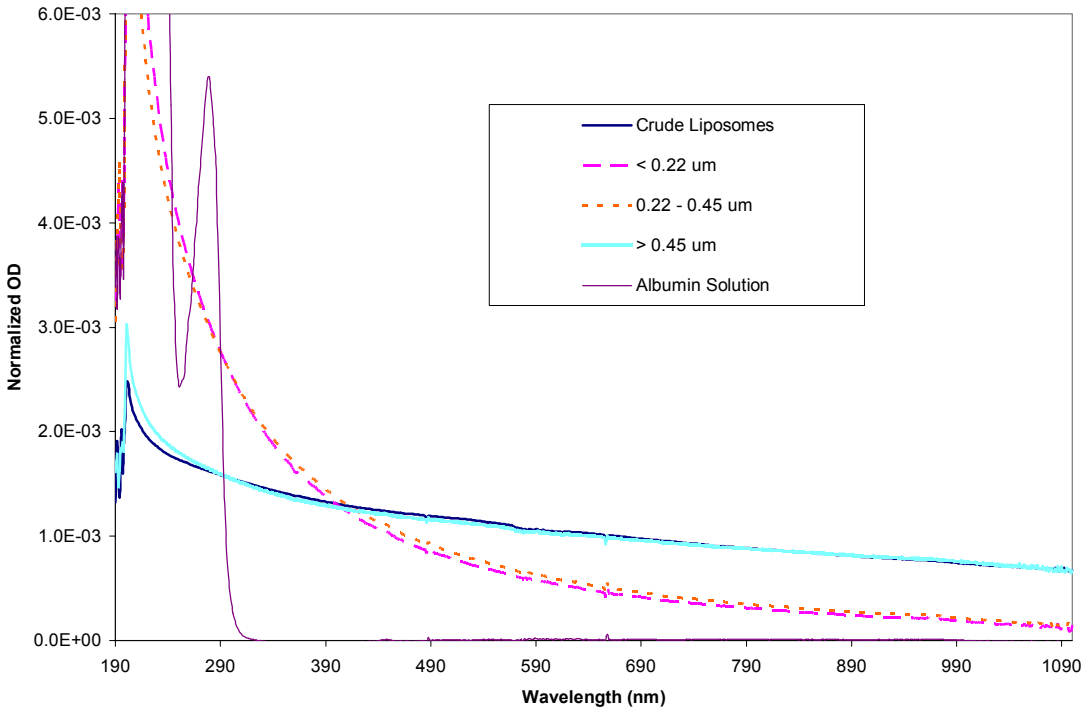

Figure C4: Normalized spectra of crude and filtered albumin liposomes compared to a spectrum of free albumin in solution.

unfiltered liposomes, the spectrum seems to be dominated by the scattering properties of the larger liposomes, judging from the flattened spectrum. This conjecture is further supported by the similarities of the crude spectrum to the that of the filtered liposomes containing sizes above 0.45 μm. The low (< 0.22 μm) and medium (0.22 – 0.45 μm)

range sizes of liposomes show spectra that nearly overlap. The small differences in the two spectra reflect a trend resulting from size disparities, consistent with our results from red cells. That is, as the size increases, a region of the small wavelengths (< 300 nm) decreases and the spectral intensity increases at the larger wavelengths (> 300 nm).

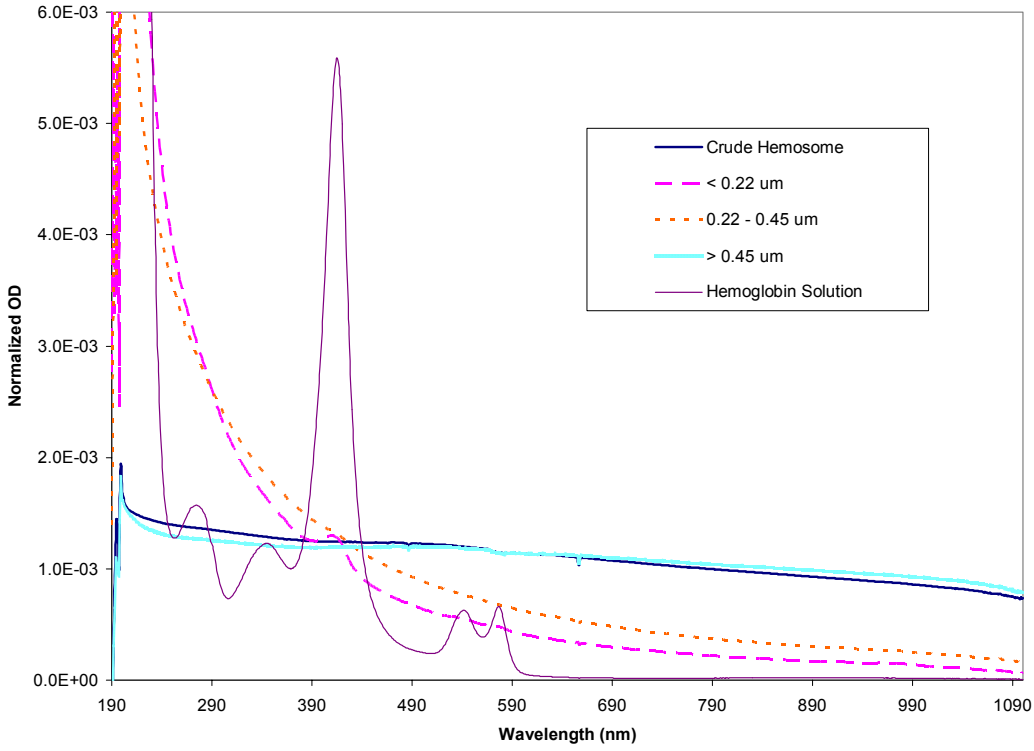

Figure C5: Normalized spectra of crude and filtered hemosomes compared to a spectrum of free hemoglobin in solution.

Figure C5 shows normalized spectra of crude and filtered hemosomes and free hemoglobin in solution. The hemosomes were prepared using a hemoglobin solution with a concentration of ~10%. The spectral characteristics of each of the samples are similar to those of the albumin-containing liposomes. The spectrum for the low size

range (< 0.22 μm) showed a characteristic hemoglobin band at 417 nm. This could be an indication of encapsulated hemoglobin, or free hemoglobin in solution outside the liposomes. The latter case is more probable considering that if the hemoglobin were encapsulated, the 417 nm peak would be visible in the other filtered fractions to some degree as well. For future reference, an additional step of centrifugation and inspection of the supernatant would verify this suspicion.

Both the albumin liposomes and hemosomes showed similar spectral qualities and trends. Visual examination of the liposomes using light microscopy showed large variations in particle size. Additionally, it was noted that the liposomes were multilamellar to varying degrees and tended to aggregate (Figure C6). The lamellarity of the vesicles would change the optical properties of the particles in the context of spectral analysis. It was therefore no surprise when the interpretation model did not give reasonable values for size and protein concentration for the albumin liposomes and the hemosomes. In order to achieve a good characterization of the liposome system, a few issues must be considered: 1) lamellarity of the liposomes, 2) the particle size distribution, 3) how much of the protein was encapsulated.

Recommendations for future work in this area should start with the refinement of the protocol to make liposomes. Different methods have been reported that control the characteristics of the liposomes during production, such as lipid dispersion in water,[136] freeze-thaw method[137] and emulsification.[138] Furthermore, corroboration of particle

characteristics require analytical methods, such as electron microscopy[139] and photon correlation spectroscopy.[140]

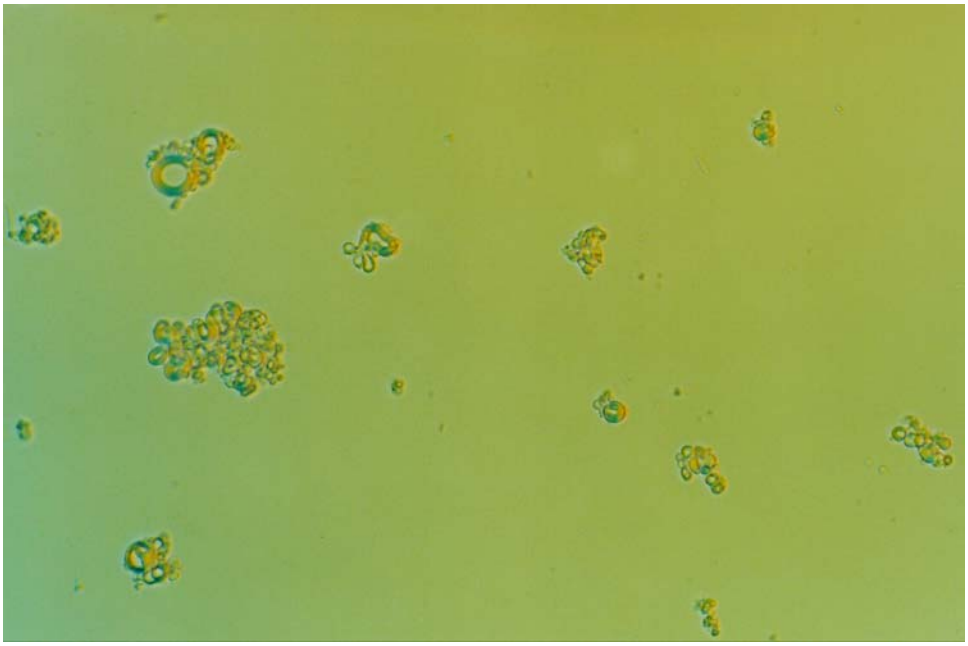

Figure C6: Light microscope picture of albumin liposomes magnified to 400x. Many of the liposomes are multilamellar and tend to aggregate. Hemosome showed similar qualities.

Appendix D: RBC Swelling

Under physiological conditions, red blood cells typically exist as biconcave disks. Changes in ionic strength can cause the cells to undergo morphological changes such as swelling, shrinking or crenating. UV-visible spectrophotometry was used to examine whole blood in varying medium tonicities to observe how these changes are represented in the spectra. Although whole blood was used, the red cells in particular act as the osmometers thus any changes in the spectra would reflect the changes in the red cells.

Materials and Methods

Whole blood samples were obtained from the Florida Blood Services, Tampa, FL and the sample was diluted to a concentration of ~4000 cells/μl as described in Chapter 4. Two dilutions were performed with the first being a 1:50 using 0.9% PBS. For the second dilution needed to achieve the final cell concentration, the ionic strengths of the media were varied. The different tonicities of media were obtained by diluting the 0.9% stock PBS accordingly to obtain concentrations of 0.7%, 0.5%, and 0.4%. When mixed with the blood cell sample, the final saline concentrations were calculated to be 0.899%, 0.707%, 0.515%, and 0.419%. OD spectra of the mixture was obtained as previously described.

Results and Discussion

Figure D1 illustrates normalized spectra of red cells in the various tonicities of saline each after a 15 minute incubation time where decreasing the decreasing tonicity of

the PBS medium causes the cells to swell, and eventually burst. The differences between the 0.899% and 0.707% curves are subtle. The small changes are a result of the swelling of the cells in the 0.707% medium reflecting a slight increase in the volume (size) coupled with a small decrease in the hemoglobin concentration. As the ionic strength of the medium is decreased to 0.515%, the slope of the linear portion of the spectrum (> 600 nm) changes, denoting larger alterations in size. Also, the emergence of a peak at 417 nm denotes the lysis of a small population of cells and the presence of free hemoglobin in the medium. Saline with a tonicity of 0.417% causes a more significant bursting of the

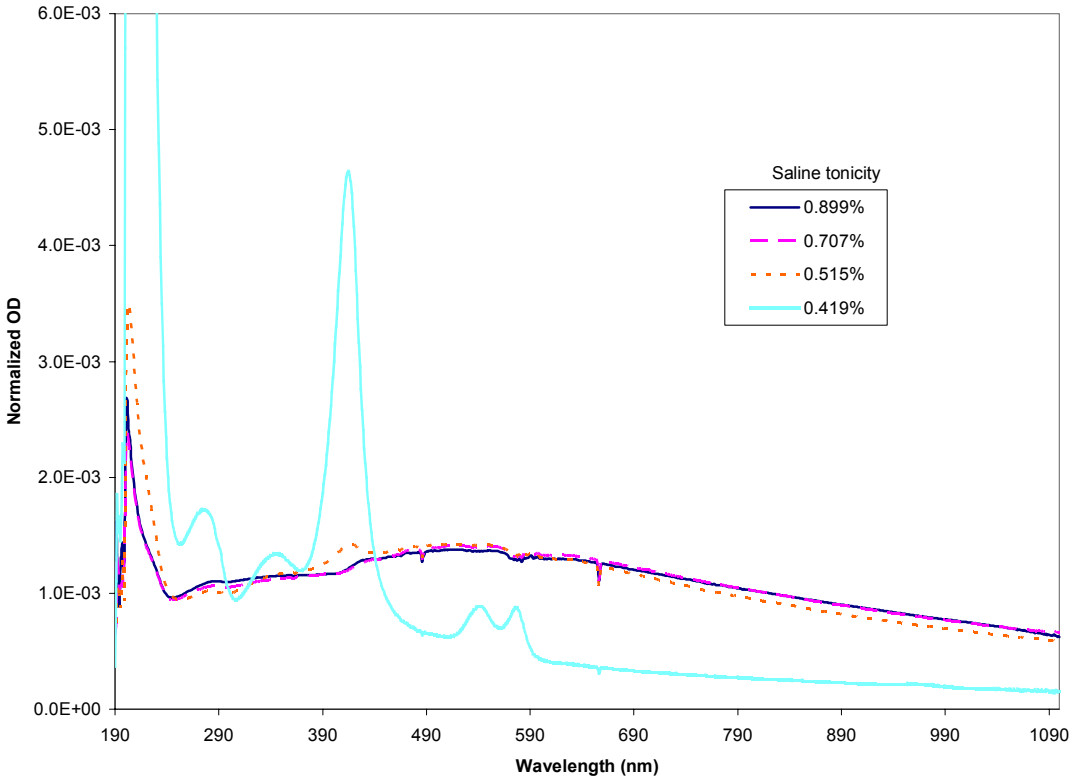

Figure D1: Spectra of red cells in varying tonicities of PBS media. As the tonicity decreases, the cells swell, eventually bursting and releasing hemoglobin into solution (0.419% curve).

cells. This is evident as the spectrum is dominated mainly by the hemoglobin absorption spectrum. There is indication of a population of intact cells because the spectrum is significantly elevated from the baseline across the entire wavelength range. Thus it can be concluded that subtle changes in the swelling of the red cells can be detected experimentally. This supports the swelling simulations shown in Chapter 5. Moreover, UV-visible spectroscopic measurements can detect lysis of cells. Further work should allow for the quantification of lysed cells, an application useful in clinical settings.

Appendix E: Spiking Red Cell Suspensions with Hemoglobin

Within the scope of this study, it has become evident that free hemoglobin in the medium of the red cell suspension is detectable in the multiwavelength spectrum. The spectral manifestation of the free hemoglobin in the suspension is most profound at the 417 nm Soret band. As a clinical application, simple spectroscopic detection can prove useful for the detection of disorders such as hemolytic anemia[14] and the quantification of blood substitutes like polymerized hemoglobin.[14] Herein, we show a preliminary study of free hemoglobin in a red cell suspension by artificial hemoglobin spiking and how it is spectrally represented.

Materials and Methods

Human hemoglobin A_0 was obtained from Sigma (cat. # H-0267) and it was reconstituted in PBS for a final concentration of approximately 0.5 g/dl. A sample of purified red blood cells was diluted 1:50 (2.45 ml PBS, 0.05 ml cell suspension), then a second dilution was performed (2.95 ml PBS, 0.05 ml 1:50 suspension) to achieve an OD maximum of approximately 0.5. To the 3 ml suspension, 10 µl of stock Hb solution was added and a spectrum was taken. A subsequent spectrum was taken after the addition of another 10 µl of stock Hb. The suspension was centrifuged for 10 minutes at 1500 x *g* and the supernatant was spectrophotometrically analyzed in an attempt to retrieve the 20 µl of Hb added to the suspension. As a control, 10 ml of hemoglobin stock was added twice to 3 ml of PBS and a spectrum was taken at each step. The same procedure was

performed with a sample of resealed cells. The hemoglobin concentrations were estimated using $\varepsilon_{417} = 7786\ cm^2/g$.

Results

Figure E1 shows the control samples of free hemoglobin in 3 ml of PBS. The addition of 10 µl and 20 µl of stock Hb to the PBS was quantified by the Drabkin's assay to be 0.0178 mg/ml and 0.0365 mg/ml. Figure E2 illustrates spectra of purified red blood cells spiked with the same volumes of stock hemoglobin solution as the control.

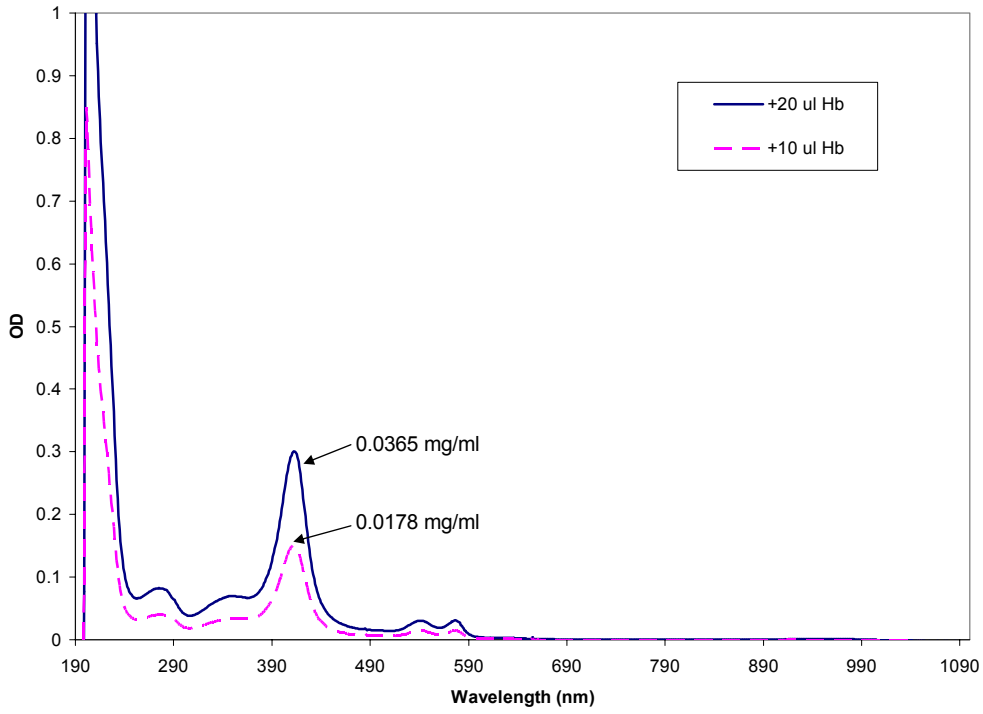

Figure E1: Spectrum of the control PBS spiked with two volumes of free hemoglobin. The concentrations were estimated using the extinction coefficient at 417 nm.

The increasing amounts of hemoglobin is represented with an increase in the intensity of the 417 nm peak. The absorption characteristics of the free hemoglobin largely changes the spectrum in the absorption region < 600 nm. The scattering region >600 nm shows a slight change. Since this wavelength range is mostly affected by size and refractive index changes, perhaps there is some surface adsorption of the free hemoglobin on the outside of the cells, affecting the refractive index of the particle to a small extent. Quantification of the Hb concentration in the supernatant gave a result of 0.0352 mg/ml, a value that is close to that of the control.

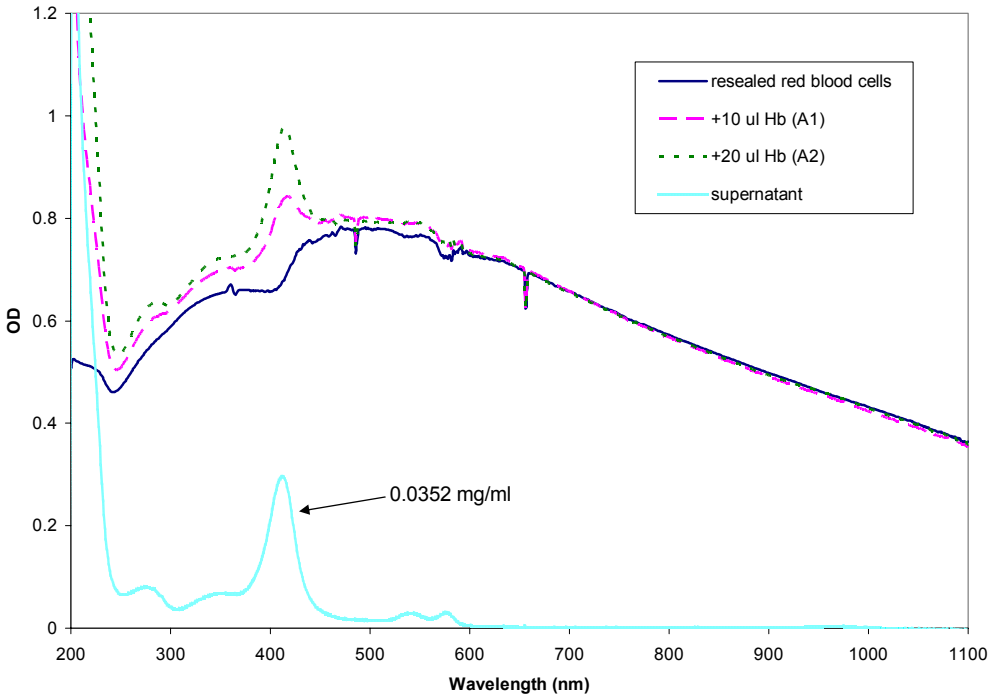

Figure E2: Spectrum of a purified red cell suspension spiked with free hemoglobin. The presence of the free hemoglobin is represented by the peak at 417. The spectrum of the supernatant of the spiked cell sample was quantified for concentration using the extinction coefficient at 417 nm.

Similar results are shown for a spiked resealed cell sample (Figure E3). The MCHC of the resealed sample was reported to be 0.215 mass fraction (Serono-Baker). Once again, the 417 nm peak significantly increased with increasing free hemoglobin. The supernatant was quantified to be 0.0348 mg/ml, a value that is extremely close to that of the spiking experiment of the purified red cells above. Both values are slightly smaller than the control, a fact that supports the hypothesis of surface adsorption.

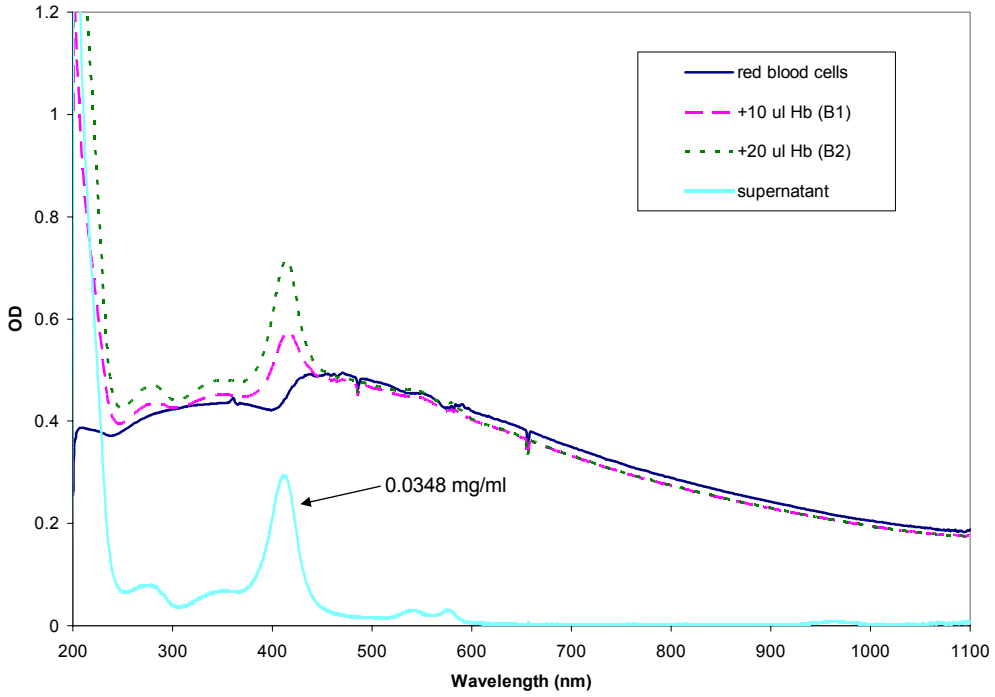

Figure E3: Spectrum of a resealed cell suspension spiked with free hemoglobin. The presence of the free hemoglobin is represented by the peak at 417. The spectrum of the supernatant of the spiked cell sample was quantified for concentration using the extinction coefficient at 417 nm.

Attempts to quantify the free hemoglobin for these samples using RBCHb02a.exe interpretation model (which takes into account free Hb) is covered in Appendix F.

Appendix F: Detailed Examination of Experimental and Simulated Spectra of Resealed Cells

Chapter 5 showed a comparison of data between measured and simulated spectra of resealed red blood cells. In this comparison, the simulation model proved to be successful at reproducing features and trends of the spectrum with changing MCHC and MCV. This appendix further examines the effectiveness of the simulations in predicting the features and trends of measured spectra that are grouped into narrower MCHC ranges.

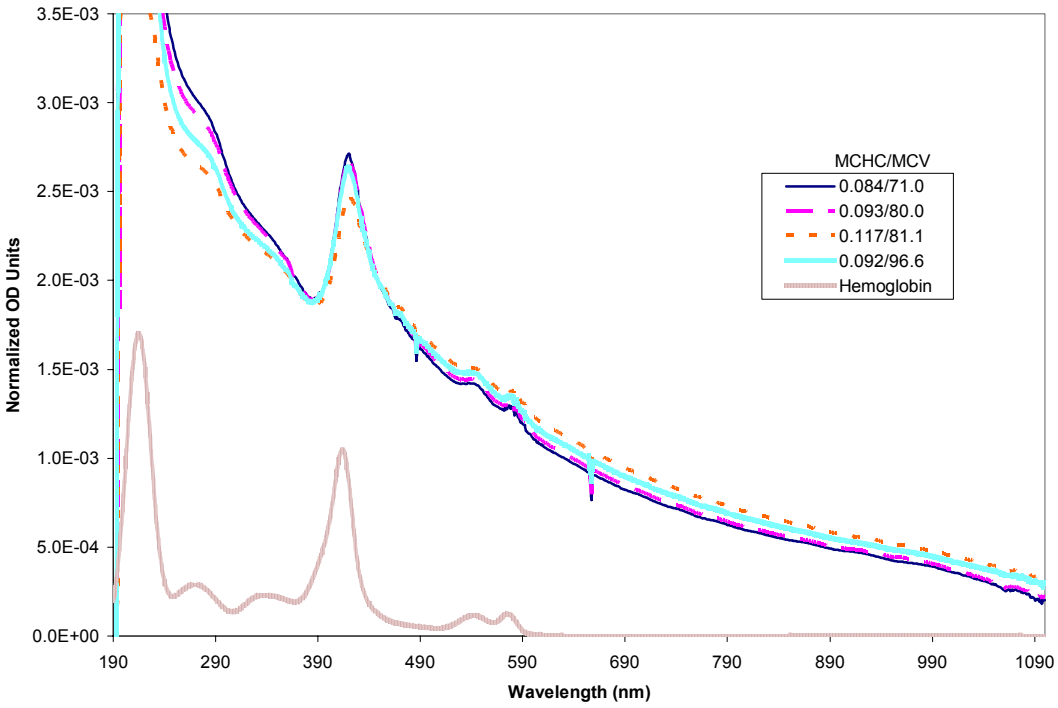

Figure F1: Experimental data set of resealed red cells in the low MCHC range with varying MCV values. The data set is normalized in the 230-900 nm range using the area under the curve method. The MCHC is expressed in mass fractions and the MCV in fl. The free hemoglobin solution spectrum is included as a reference.

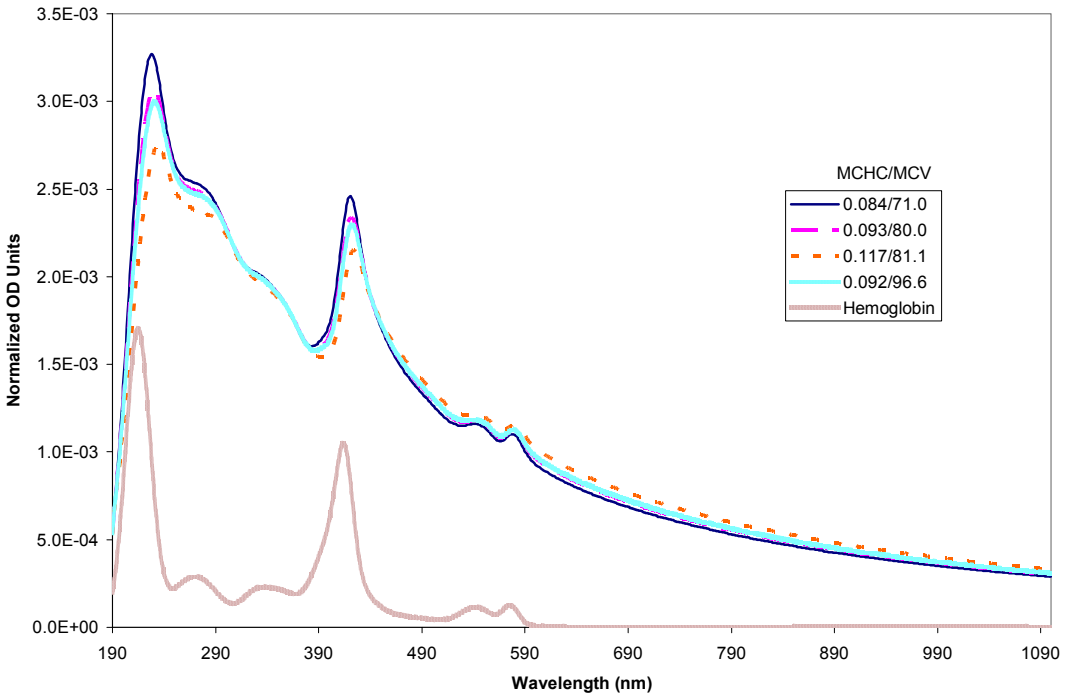

Figure F2: Simulated spectra of the low MCHC range data set normalized on a per cell basis. The MCHC is expressed in mass fractions and the MCV in fl. The free hemoglobin solution spectrum is included as a reference.

Figures F1 and F2 are measured and simulated spectra respectively of resealed red cells. Here, the theoretical model simulates the trends well. The sample with the highest MCHC (0.117 mass fraction) shows the lowest 417 nm hemoglobin band and the lowest MCHC (0.084) has the highest 417 nm peak in both figures. Although the samples vary in both MCHC and MCV, it has been shown in the simulations in Chapter 5 that the effect of MCHC changes is a more dominant one.

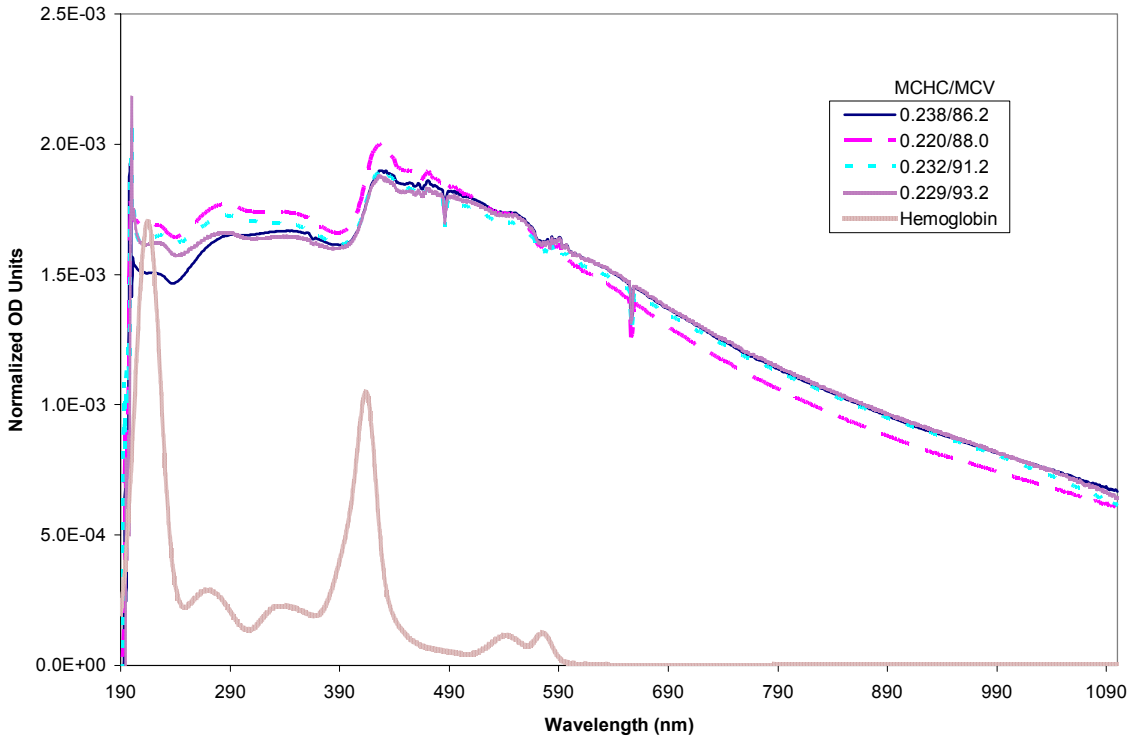

Figure F3: Experimental data set of resealed red cells in the medium MCHC range with varying MCV values. The data set is normalized in the 230-900 nm range using the area under the curve method. The MCHC is expressed in mass fractions and the MCV in fl. The free hemoglobin solution spectrum is included as a reference.

Figures F3 and F4 represent measured and simulated data respectively for a medium range of MCHCs. The calculated spectral features and trends in Figure F4 agree well with the experimental spectra from Figure F3. The lowest MCHC (0.220 mass fraction) exhibits the highest spectral intensity at the lower wavelengths (<600 nm), a trend that is consistent in both figures. There are small discrepancies in the features of

the measured and calculated spectra, however it must be noted that the simulation model does not take into account some details of the experimental red cell sample. For example,

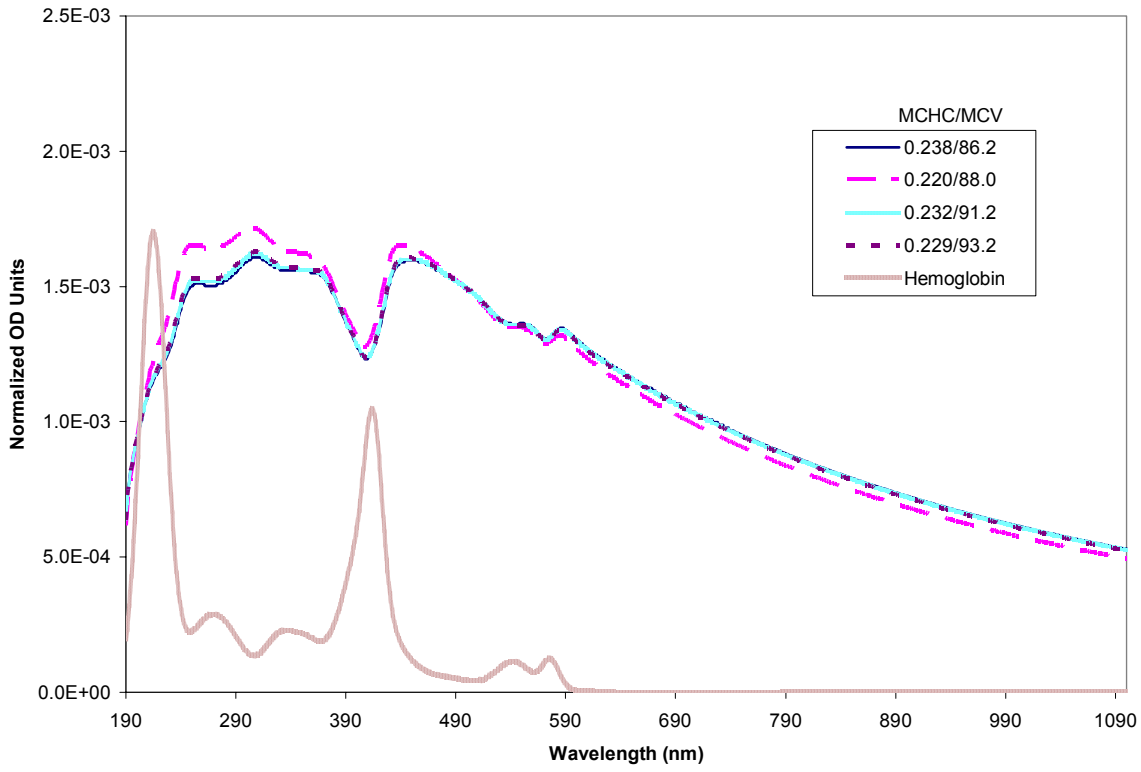

Figure F4: Simulated spectra of the medium MCHC range data set normalized on a per cell basis. The MCHC is expressed in mass fractions and the MCV in fl. The free hemoglobin solution spectrum is included as a reference.

the spherical approximation may pose limits on the simulation of the measured data. Furthermore, when the cells reseal, we are assuming a homogeneous distribution of MCHC which is probably not the case. Despite such unanswered questions, the model

does a good job simulating spectra based on known parameters of the particle suspension (i.e. MCHC and MCV).

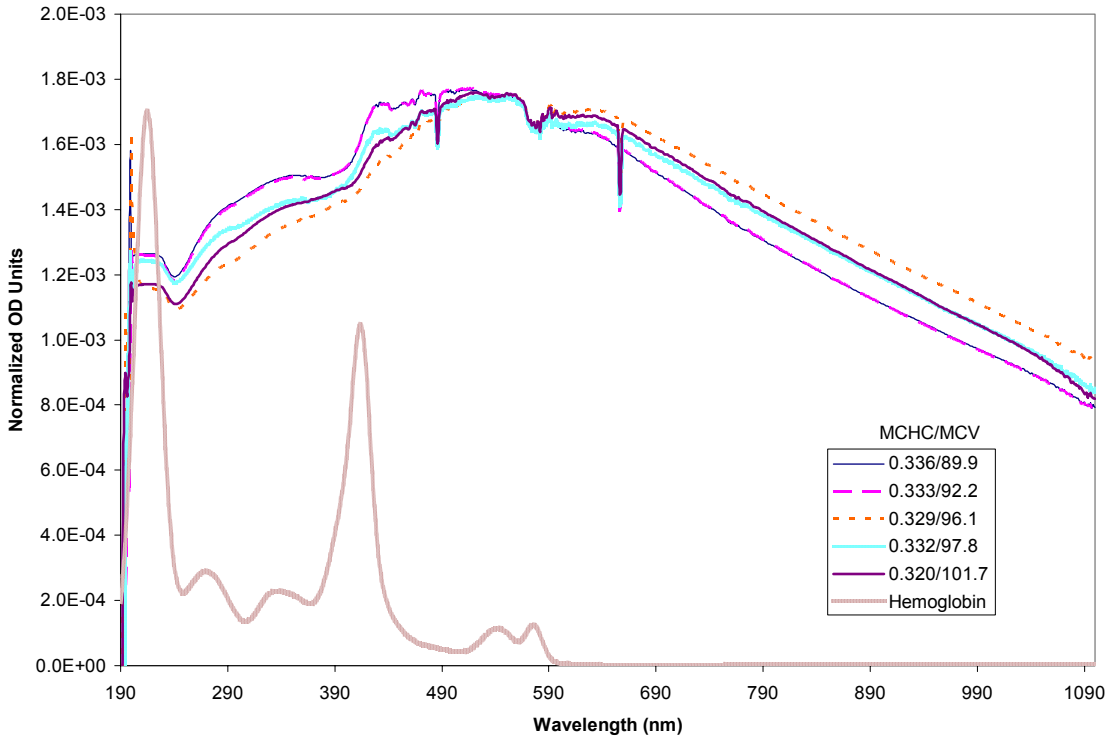

Figure F5: Experimental data set of resealed red cells in the high MCHC range with varying MCV values. The data set is normalized in the 230-900 nm range using the area under the curve method. The MCHC is expressed in mass fractions and the MCV in fl. The free hemoglobin solution spectrum is included as a reference.

Figures F5 and F6 show measured and simulated spectra respectively in the high MCHC range. Here, the simulated values show small changes in the spectra compared to the experimental spectra. This can be attributed to the above mentioned issues of the spherical approximation, or the assumption of hemoglobin homogeneity. At higher

hemoglobin concentrations, the refractive index of the particle increases, and scattering becomes prominent enough to exacerbate the effects of factors (such as shape) that may not have been a problem at lower refractive indices of the particle.

One peculiar sample in Figures F5 and F6 was the spectrum with an MCHC of 0.329. Upon close examination of experimental notes, it was evident that the sample used was approximately 10 days old. This was in stark contrast to the rest of the samples (50+ samples) which were used within 24-48 hours post-donation. It has been

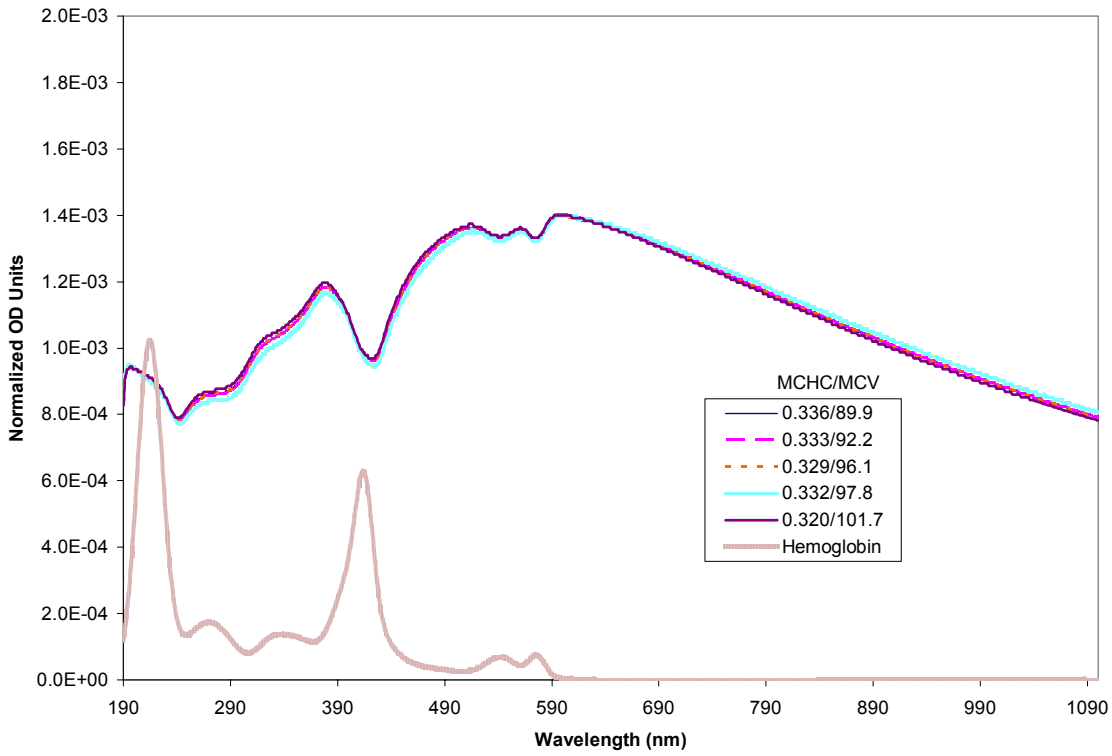

Figure F6: Simulated spectra of the high MCHC range data set normalized on a per cell basis. The MCHC is expressed in mass fractions and the MCV in fl. The free hemoglobin solution spectrum is included as a reference.

demonstrated by another project member that the aging of red cells in storage resulted in morphologic changes that translated into significant alterations of spectral features (unpublished data).[108] Over time, the morphology of the cells turned into a spherical crenated form. An examination of the sample under a light microscope at 100x magnification did indeed reveal a significant population of crenated cells. Such alterations manifested in the spectra could explain the irregularity of this particular sample.

Appendix G: Alternate Versions of the Interpretation Model

In Chapter 6, two alternate versions of the interpretation model were introduced: RBCHb01b and RBCHb02a. The kernels of both models are identical to that of RBCHb01a (the version used for the main analysis in this work), all functioning on the basis of the Mie theory-based turbidity calculations. Small alterations in the program design allow RBCHb01b to account for the presence of two derivatives of hemoglobin (typically oxyhemoglobin and methemoglobin in the case of resealed cells), and RBCHb02a introduces the capability to quantify any free hemoglobin existing in the medium outside the cells. The main scheme of this investigation used an interpretation model that did not consider such details included in the alternate versions because the simplified interpretation model generally yielded good results. However, when scrutinized on an individual basis, some samples were identified that were better suited to be interpreted using the alternate versions. Some examples are cited in this appendix.

A comparison of the results of RBCHb01a and RBCHb01b generally yielded similar results in the values of parameters such as cell number, cell size and cell hemoglobin concentration. However, there were a few select samples where the interpreted values improved with the use of RBCHb01b, accounting for the presence of methemoglobin. The inputs for this version were similar to those of RBCHb01a (as described in Chapter 6) with the major difference being the designation of the optical properties file of a second hemoglobin derivative (ophbfe3.01 file containing the complex refractive index of methemoglobin and the refractive index of water). In an example of a comparison of the two versions, Figure G1 shows a resealed cell with low MCHC

evaluated with RBCHb01a. The MCHC is estimated well, however, the cell counts and the MCV values do not agree well with the measured. The same data interpreted with RBCHb01b (incorporating methemoglobin) shows improved estimations of both counts and MCV (Figure G2). The sample containing a low MCHC could very well have elevated amounts of oxidized hemoglobin compared to those of higher MCHC considering the manner in which it is prepared. After permeabilizing the cells by way of hypotonic shock, the

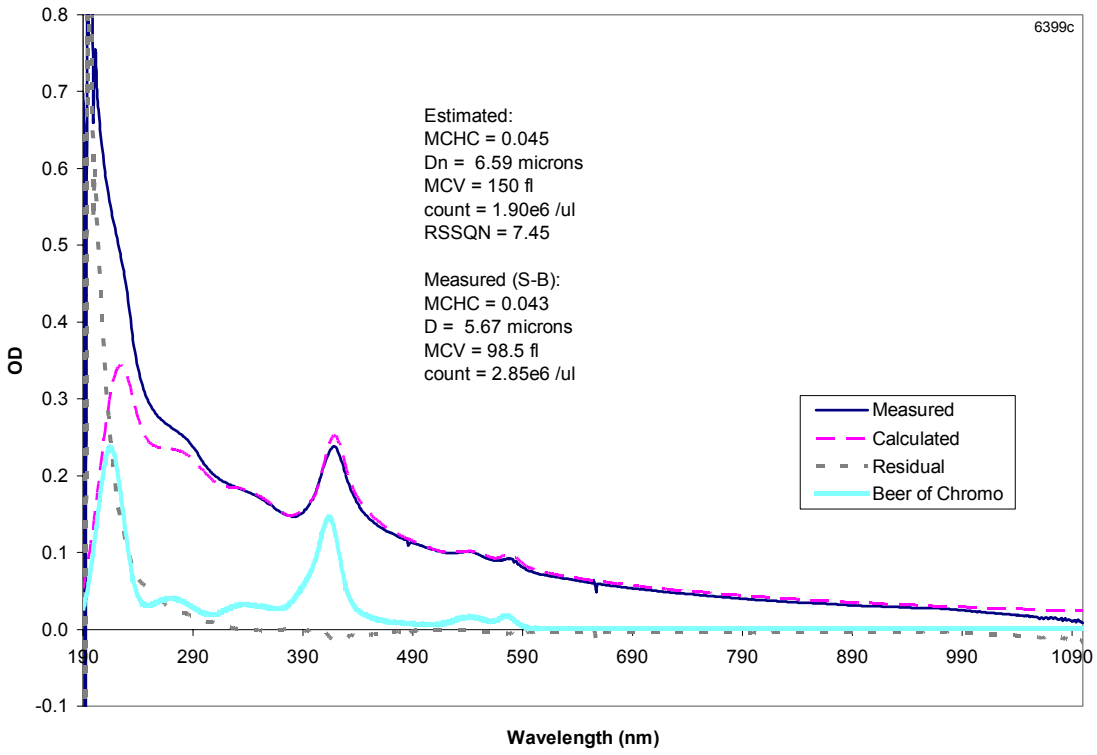

Figure G1: Resealed cell data interpreted using RBCHb01a interpretation model. The MCV is estimated to be substantially higher than the measured value.

suspension is equilibrated for an extended period before restoration (see Chapter 4 for details). This subjects the oxyhemoglobin to a highly oxygenated medium increasing the chances of conversion to methemoglobin.

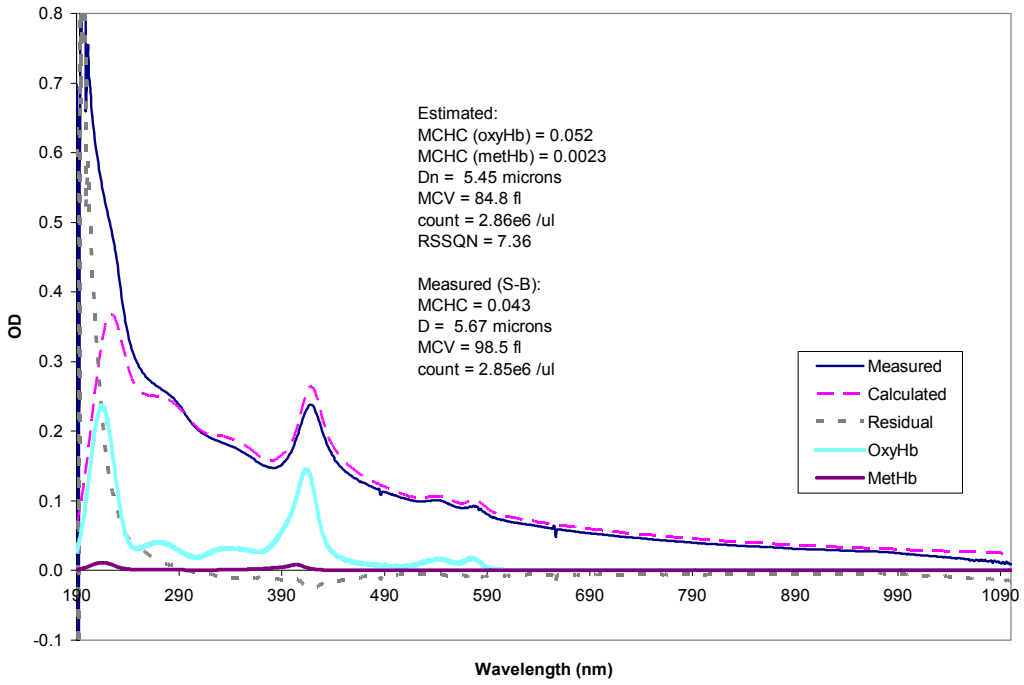

Figure G2: Data of same resealed sample as Figure A1 interpreted with RBCHb01b, accounting for the presence of methemoglobin. The MCV and cell count estimations are closer to the measured values.

Analysis of data using RBCHb02a is a work in progress. This version of the interpretation model accounts for any free hemoglobin in the medium, outside of the red cells. The test sample is a suspension of purified red cells spiked with a known amount of free hemoglobin (as described in Appendix E). Figure G3 shows that the estimated fit of the spectrum is not accurate although the estimated values are relatively close to the

measured values. The calculated spectrum also does not reflect the large amount of free hemoglobin with a peak at 417 nm. The data shown represents work that has not been completed, and further improvement of this model will provide us with the capability to detect small amounts of lysis in red cell suspensions and whole blood.

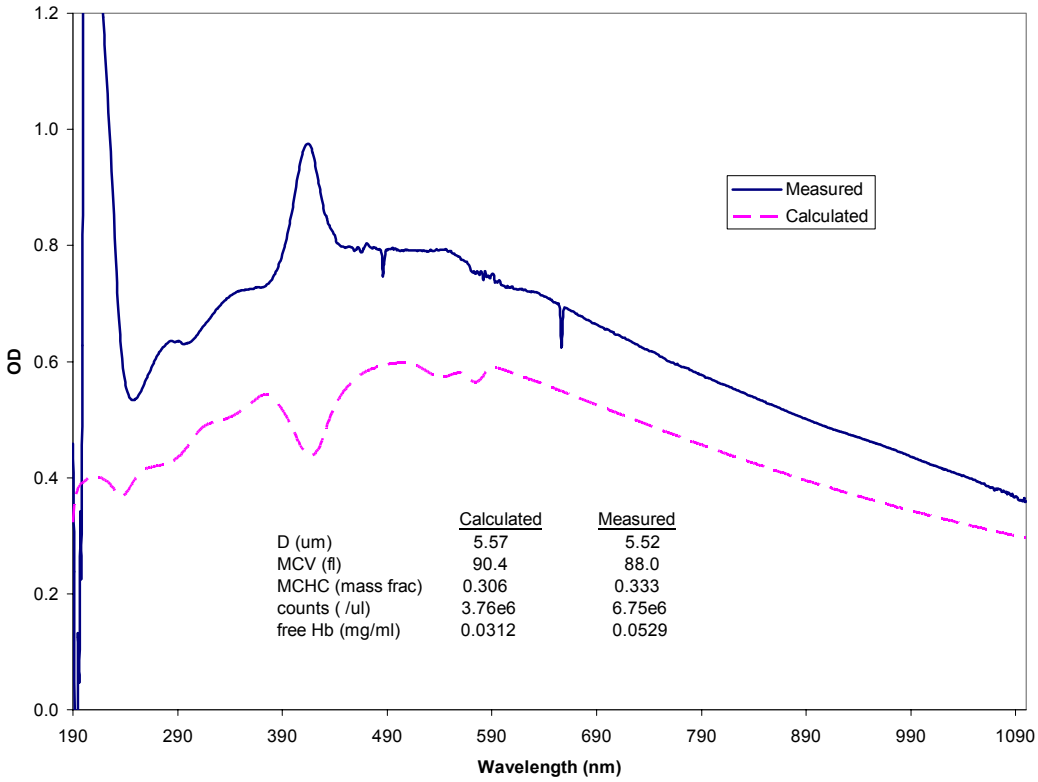

Figure G3: An RBCHb02a interpretation of a purified red cell suspension spiked with free hemoglobin. The fit of the curve is not good although the estimated values compare well with the measured values.

Appendix H: UV-Visible Analysis of Molecular Aggregates

The focus of the encapsulated systems mentioned in this work (resealed red cells, liposomes) was to achieve a spectral understanding of the effects of changing chemical composition. A similar model system for the optical characterization of macroscopic particles is molecular aggregates. For example, a comparison of hemoglobin in solution and hemoglobin in an aggregated state should show drastic changes in the spectral profile. Light scattering characteristics of the aggregated form should approach the optical properties of encapsulated systems containing similar concentrations of hemoglobin. Provided that there are good corroborative methods of analyzing the physical properties of the aggregates, a reliable interpretation of the spectral data is sure to be achieved.

Large molecules on the order of proteins can be salted out at high salt concentrations by taking advantage of their hydrophobicity.[141,142] At low salt concentrations, water molecules become ordered around hydrophobic patches on the protein, a thermodynamically unstable situation. With the addition of a salt, the hydrated ions of the salt disrupt the ordered water molecules, exposing the hydrophobic patches and allowing the proteins to aggregate. The concentration of salt required to salt out a protein depends on the amount of hydrophobic residues residing on the protein of interest. The most effective salts are ones containing multivalent anions and possess a high solubility, such as ammonium sulfate [$(NH_4)_2SO_4$].[142] Alternate precipitation methods use water miscible organic solvents (ethanol, actone) or a soluble high molecular weight organic polymer (polyethylene glycol) to decrease the solvation power of the water thereby aggregating the protein.

Our preliminary studies on protein aggregation were performed on purified human hemoglobin A_0 (Sigma-Aldrich) and bovine serum albumin (Sigma-Aldrich). The latter was chosen because it was readily available and it had been previously characterized spectrally. Ammonium sulfate was used as the precipitating agent and the concentrations (percent saturation) required to aggregate the proteins were experimentally determined. The spectral characteristics of the proteins were compared in their dissolved and precipitated states for any detectable differences.

Materials and Methods

The buffer used in these experiments was a standard 0.2 M phosphate recipe.[141] The ionic strength of the buffer is not much of an issue here as it is when preparing the hypotonic shock phosphate buffer (0.007 M) for the resealing experiments. Briefly, 100 ml of 0.2 M solutions of monobasic sodium phosphate and dibasic sodium phosphate were prepared separately. To obtain a final pH of 7.4, 19.0 ml of the monobasic and 81.0 ml of the dibasic solutions were combined and the final volume was brought up to 200 ml.

For the preparation of the ammonium sulfate solutions, the % saturation was calculated by the equation

$$g = \frac{533(S_2 - S_1)}{100 - 0.3S_2}$$

where S_1 and S_2 are the initial and final saturation percentages and g is grams of ammonium sulfate to be added to 1 L of water or buffer at 20° C.[142] Different saturation levels of the ammonium sulfate were test at 10% increments to determine the

concentration at which hemoglobin and albumin aggregated. Incubation times were typically around 2 minutes. The concentration of the stock solution of the commercial hemoglobin sample was 20 mg/ml and the albumin stock was 10 mg/ml with both proteins being reconstituted with phosphate buffer.

An example of concentration calculations for the hemoglobin sample is as follows (with albumin concentrations being calculated in the same manner). Here, the desired concentration for the sample to be measured was 0.1 mg/ml hemoglobin in 80% saturated ammonium sulfate. With the final sample volume to be 2 ml, 0.01 ml of the 20 mg/ml stock solution was added to 1.99 ml of 80% phosphate buffered ammonium sulfate solution (PB/AMS). If the PB/AMS was 80% saturated at the time of addition, the final saturation would be 79.6%, which is a negligible difference for our purposes.

Results

For both albumin and hemoglobin, it was determined that 90% ammonium sulfate saturation was needed to maximize precipitation of the proteins. Figure H1 shows a precipitation experiment of a 0.2 mg/ml albumin solution. The dashed line represents the albumin solution prior to aggregation. The spectrum shows a characteristic peak at 280 nm with a low baseline at the wavelengths > 300 nm indicating a lack of macroscopic scattering. When the albumin is subjected to a 90% AMS solution, there is an appreciable elevation in the entire wavelength range suggesting the formation of

aggregates. Centrifugation (15,000 x *g*) to isolate the supernatant shows no significant presence of free albumin as evident by the lack of a 280 nm peak.

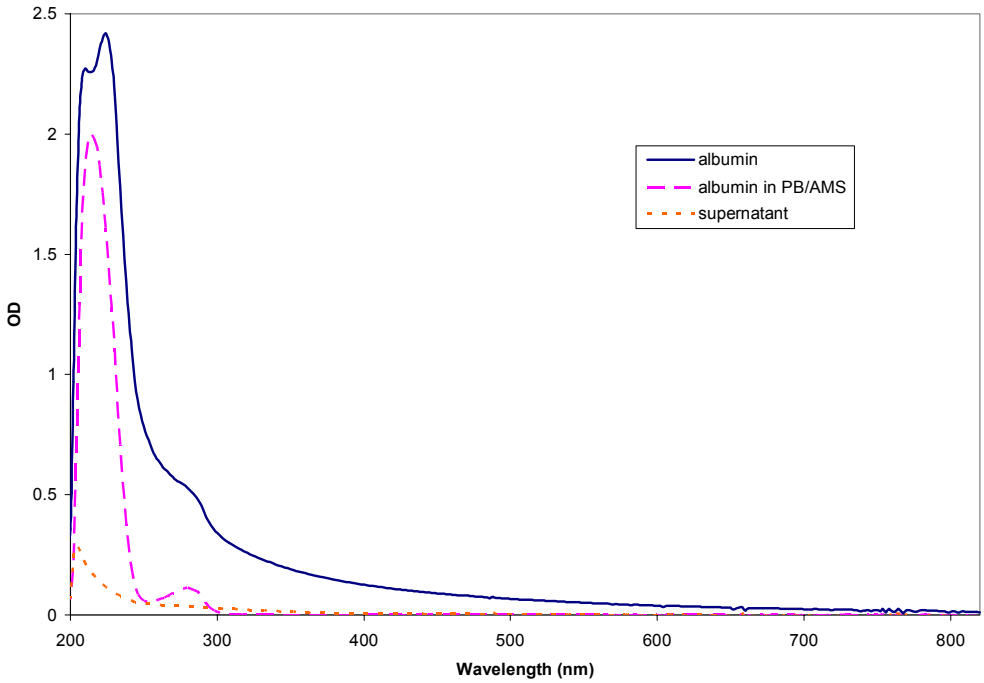

Figure H1: Ammonium sulfate precipitation of bovine serum albumin. There is a noticeable difference in the spectra between free albumin and aggregated albumin. The aggregated suspension shows considerable scattering with an elevated OD spectrum. The supernatant spectrum after centrifugation shows no indication of an albumin peak, indicating the absence of a significant amount of non-aggretated albumin.

Figure H2 shows a precipitation of a 0.10 mg/ml solution of hemoglobin. Much like the encapsulated form of hemoglobin, the aggregated form exhibits significant scattering elements marked by the elevation of the OD spectrum. The preliminary data indicates that an aggregated system can be used as another model system to support the results of the resealed cells. Contrary to the liposomes, there is no need to worry about

multiple membrane layers changing the refractive index of the aggregates, since there is no membrane. Hence it seems that the interpretation model could be successfully implemented as it was with the resealed cells. It will however be necessary to corroborate the size distribution and hemoglobin content of the aggregates.

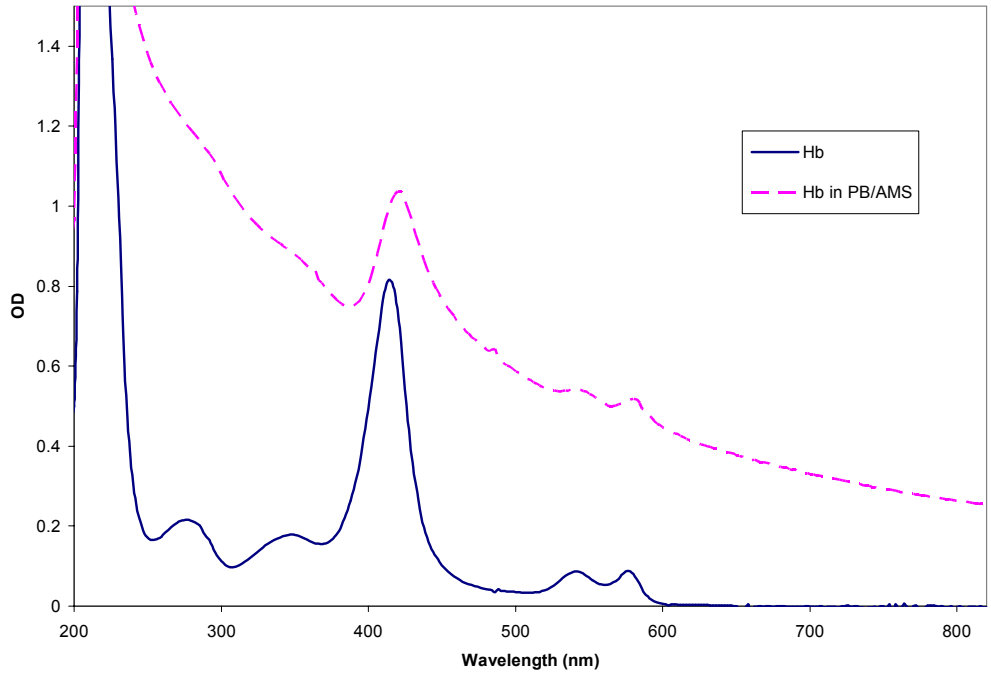

Figure H2: Ammonium sulfate precipitation of 0.10 mg/ml hemoglobin. Upon aggregation, the spectrum shows larger scattering elements.

About the Author

Akihisa Nonoyama received his Bachelor's degree in Chemistry from Case Western Reserve University in Cleveland, OH. During his undergraduate years, he gained laboratory experience doing research in the Molecular and Microbiology Department at the CWRU School of Medicine. There, he learned skills such as DNA mutagenesis and sequencing. He entered the graduate program in Chemistry at the University of South Florida in 1995 where he began work on a multi-disciplinary project characterizing red blood cells using multiwavelength UV-visible spectroscopy. During his tenure as a graduate student, he held a position as a Teaching Assistant for General Chemistry, Organic Chemsitry, and Biochemistry laboratories.